An evaluation of tailored magnetic nanoparticles in the induction of stem cell differentiation

---

Sandhya Moise

Doctor of Philosophy

June 2016

Keele University

Abstract

Improving the differentiation capacity of stem cells by defining the ideal physico-chemical and spatial parameters will enhance the efficiency of stem cell-based clinical therapies. In this thesis the hypothesis that heat shock (elevated temperatures) could positively influence osteogenic differentiation was investigated. A methodology was developed to employ magnetic nanoparticle-based local heating (magnetic hyperthermia) to spatially control temperature distribution at the cellular level. For this purpose, bacterially synthesized zinc and cobalt doped iron oxide nanoparticles with tuned physical and magnetic properties were assessed for their interaction with cells, and their magnetic response and heating properties when in a cellular milieu. Nanoparticles with moderate levels of zinc doping showed strong heating effects and minimal cytotoxicity, proving to be promising candidates for cellular applications.

The effects of mild and severe heat stress were assessed by heating cells using conventional techniques such as water baths (bulk heat shock); using localised heating with extracellular nanoparticle suspensions; or by targeting different cellular regions with nanoparticles. The effect of the heat shock treatment on the osteogenic differentiation was assessed in primary bone marrow-derived human mesenchymal stem cells and a cancerous osteoblastic cell line, MG-63. With both bulk and nanoparticle-mediated extracellular mild heat shock (~42^0C), very little evidence for a positive effect on osteogenic differentiation was found in both cell types. On the other hand, severe heat shock treatments (>50^0C) showed differentiation enhancement though this also negatively impacted cell viability. Further experimentation can shed light on the optimum temperature range within which the

differentiation behaviour of cells can be influenced without compromising viability. The nanoparticle-based methodology developed here to apply heat shock to different cellular components, could lead to further work investigating how intracellular pathways translate the heat stimulus into a cellular response for stem-cell based applications.

Contents

List of figures vii
List of tables xi
List of associated publications xi
List of associated presentations xii
Acknowledgements xiii
CHAPTER 1 Introduction 1
1.1 Behaviour of stem cells 2
1.1.1 Introduction to stem cells 2
1.1.2 Differentiation of Stem Cells 2
1.1.3 Effect of Heat Shock on Stem Cell Behaviour 6
Evidence for Role of Heat Shock in Controlling Stem Cell Fate 6
Possible Mechanisms for Heat Shock Regulation of Cellular Behaviour 9
1.2 Magnetic nanoparticles for remote manipulation of stem cells 13
1.2.1 Magnetic and Functional Properties of Biomedical MNPs 14
1.2.2 Bacterially synthesized iron oxides 18
1.2.3 Substituted iron oxides 20
1.2.4 Magnetic nanoparticle-mediated heating 22
Néel and Brownian relaxation 23
AC susceptibility (ACS) 24
Specific loss power 28
1.2.5 Assessing biocompatibility of doped nanoparticles 29
1.3 Magnetic Nanoparticles for Stem Cell Differentiation 34
1.3.1 Mechanotransduction 34
1.3.2 MNPs for localized elevation of temperature in cells 37
1.4 Thesis Aims and Objectives 40
CHAPTER 2 Materials and methods 42
2.1 Nanoparticle preparation 43
2.1.1 Preparation of stable suspensions of MNPs by citric acid coating 43
2.1.2 RGD biofunctionalization 44
2.2 Nanoparticle characterization 45
2.2.1 Size and Zeta potential measurements 45
2.2.2 Prussian blue staining 45

2.2.3 Characterizing magnetic properties: AC Magnetic Susceptibility 46
2.3 Iron quantification methods 46
2.3.1 Gravimetric analysis.....46
2.3.2 Ferrozine assay.....47
2.4 Cell Culture 47
2.4.1 hMSC isolation 48
2.4.2 Determination of cell numbers.....48
2.4.3 Chemical stimulation of differentiation 49
2.5 Characterization of the hMSCs 50
2.5.1 Trilineage differentiation potential 50
2.5.2 Expression of CD markers 50
2.6 Assessment of cellular behaviour: differentiation, viability and mitochondrial metabolic activity.....51
2.6.1 Alizarin red staining for osteogenesis.....51
2.6.2 Oil red 'O' for adipogenesis.....51
2.6.3 Alcian blue for chondrogenesis.....52
2.6.4 Alkaline phosphatase (ALP) assay.....52
2.6.5 Picrogreen assay for DNA Quantification 53
2.6.6 XTT assay for quantifying mitochondrial metabolic activity of cells 54
2.7 Assessing interaction of cells and MNPs microscopically 55
2.7.1 Fluorescent staining of cellular proteins (Immunocytochemistry) 55
2.7.2 Transmission electron microscopy (TEM) for assessing cellular uptake of MNPs 56
2.7.3 Time lapse imaging.....57
2.8 Statistics 57
CHAPTER 3 Assessing cell-nanoparticles interactions 58
3.1 Introduction.....59
3.2 Materials and methods 61
3.2.1 Magnetic nanoparticle suspensions.....61
3.2.2 Cell culture.....61
3.2.3 Cellular uptake studies 62
3.2.4 Cytotoxicity studies.....63
Microscopy.....63
Flow cytometry quantification 64
3.2.5 AC Susceptibility 65

3.3 Results 66
3.3.1 Cellular uptake of Magnetic Nanoparticles 66
3.3.2 Cellular biocompatibility of magnetic nanoparticles 73
3.3.2 Effect of cellular internalization on the magnetic response of nanoparticles 89
3.3 Discussion 92
CHAPTER 4 Effect of bulk heat shock on stem cell behaviour 97
4.1 Introduction 98
4.2 Materials and methods 99
4.2.1 Cell culture 99
4.2.2 Heat shock treatments 99
4.2.3 Differentiation studies 101
4.2.4 Assessing heat shock protein expression 101
4.3 Results 103
4.3.1 Targeted and actual temperature during heat shock 103
4.3.2 Effect of a single mild heat shock exposure on cellular behaviour 105
4.3.3 Effect of multiple heat shock treatments and of temperature on cellular behaviour 110
4.3.4 Assessing heat shock protein expression and its role in osteogenesis 121
4.4 Discussion 124
4.5 Conclusions and implications for future work 128
CHAPTER 5 Effect of magnetic nanoparticle mediated heat stress on cellular behaviour 129
5.1 Introduction 130
Electrical-cell impedance sensing- Theory 132
5.2 Materials and methods 136
5.2.1 Nanoparticle characterization 136
5.2.2 RGD biofunctionalization of MNPS and assessment of cell membrane binding 137
5.2.3 Measurement and application of magnetic hyperthermia 138
5.2.4 Electrical-Cell substrate Impedance Measurements 140
5.2.5 Cellular heat shock experiments using magnetic hyperthermia 140
5.3 Results 145
5.3.1 Nanoparticle characterization for magnetic field heating experiments 145
5.3.2 Strategies for cellular level scale targeting of MNPs 151
5.3.3 ECIS for monitoring changes in cellular behaviour 155

5.3.4 Effect of MNP-mediated heat shock on cellular behaviour 167
Intracellular Heat Shock Experiments 167
Extracellular Heat shock Experiments 171
5.4 Discussion 187
5.5 Conclusions 189
CHAPTER 6 Conclusions and future work 191
REFERENCES 197
APPENDIX 213
Characterization of primary bone marrow-derived human mesenchymal stem cells (hMSCs) 214

List of figures

1.1.1 Schematic of a hypothetical stem cell niche *4*

1.1.2 Signalling pathways implicated in osteogenic differentiation of stem cells *11*

1.1.3 TREK activation via various physical and chemical stimuli *12*

1.2.1 Alignment of spins in different magnetic materials *15*

1.2.2 Comparison of the magnetic behaviour of ferromagnets and SPMs *16*

1.2.3 TEM images of bacterially synthesized doped iron oxide MNPs *21*

1.2.4 Dependence of magnetic properties of MNPs on the type and level of dopant *21*

1.2.5 Magnetization vs external applied field *23*

1.2.6 Simplified schematic of relaxation mechanisms *24*

1.2.7 ACS data for an aqueous solution of blocked spherical magnetic particles *25*

1.2.8 ACS simulation plots for MNP populations with varying anisotropy values *27*

1.2.9 Calcein staining of live cells *32*

1.2.10 Fluorescence dot plot of ungated Calcein vs. propidium iodide stained K562 cells *33*

1.2.11 Change in side scatter with MNP interaction *34*

1.3.1 Mechanical activation of membrane receptors using MNPs *37*

1.3.2 Biomedical applications of MNPs *37*

1.3.3 Remote activation of membrane ion channels using MNP technology *39*

2.6.1 Fluorescence intensity vs 4-MU concentration plots for standard solutions of 4-MU with a hyperbolic fit *53*

2.6.2 Fluorescence intensity vs DNA concentration plots for standard DNA solution fitted with a linear trend line *54*

3.2.1 Defining populations in flow cytometry samples *65*

3.3.1 Prussian blue staining for iron to detect MNPs *66*

3.3.2 Time lapse imaging of cell-MNP interactions *68*

3.3.3 Time lapse imaging of a single cell-MNP interactions *69*

3.3.4 Bright field image of cells with MNPs *70*

3.3.5 Fluorescent micrograph of cells with MNPs *71*

3.3.6 Electron micrographs of cells with MNPs *72*

3.3.7 Bright field images of MG-63 cells exposed to varying concentrations of *74*

synthetic magnetite
3.3.8 Live/Dead staining of MG-63 cells exposed to different concentrations of synthetic magnetite *75*
3.3.9 Bright field images of hMSCs with varying concentrations of synthetic magnetite and $Co_{1.0}$ MNPs *77*
3.3.10 Calcein-AM staining of hMSCs exposed to synthetic magnetite and $Co_{1.0}$ *79*
3.3.11 EthD staining of hMSCs exposed to synthetic magnetite and $Co_{1.0}$ *80*
3.3.12 Flow cytometric quantification of synthetic Fe_3O_4 and $Co_{1.0}$ cytotoxicity in MG-63 cells *81*
3.3.13 FL1 vs FL3 scatter plots of MG-63 cells exposed to different concentrations of synthetic Fe_3O_4, $Co_{1.0}$ and $CoCl_2$ *82*
3.3.14 Change in FS and SS values of cells with MNP uptake *83*
3.3.15 FL1 vs FL3 scatter plots of MG-63 cells exposed to different cobalt doped MNPs *84*
3.3.16 Flow cytometric quantification of the cytotoxicity of different cobalt MNPs in MG-63 cells *84*
3.3.17 Effect of zinc-doped MNPs on calcein fluorescence *86*
3.3.18 Flow cytometric quantification of the cytotoxicity of different zinc MNPs in MG-63 cells *87*
3.3.19 Flow cytometric quantification of the cytotoxicity of different zinc and cobalt doped MNPs in hMSCs *88*
3.3.20 Effect of MNPs on the osteogenic differentiation potential of hMSCs *88*
3.3.21 ACS curves of stable aqueous suspensions of MNPs *90*
3.3.22 ACS curves of MNPs associated with MG-63 cells *92*
4.2.1 Checking for non-specific binding for HSP70 staining *103*
4.3.1 Temperature measurement during a single bulk heat shock of hMSCs at 40^0C for 30min (Experiment 01 and 02) *104*
4.3.2 Temperature measurement during multiple bulk heat shock treatments of hMSCs at 40-41^0C for 60min (Experiment 03) *104*
4.3.3 Temperature measurement during mild and severe bulk heat shock of hMSCs and MG-63 cells (Experiment 04 and 05) *105*
4.3.4 Effect of mild bulk HS on osteogenesis of hMSCs with initial low seeding density *106*

4.3.5 Effect of mild bulk HS on osteogenesis of hMSCs with high initial seeding density *107*
4.3.6 Effect of mild bulk HS on mineralization of hMSCs *109*
4.3.7 Effect of mild HS on osteogenic differentiation of MG-63 cells (Experiment 03) *111*
4.3.8 Bright field images of hMSCs exposed to multiple HS treatments (Experiment 04) cultured in expansion medium *113*
4.3.9 Bright field images of hMSCs exposed to multiple HS treatments (Experiment 04) cultured in osteogenic medium *114*
4.3.10 Bright field images of MG-63 cells exposed to multiple HS treatments (Experiment 05) cultured in expansion medium *116*
4.3.11 Bright field images of MG-63 cells exposed to multiple HS treatments (Experiment 05) cultured in osteogenic medium *117*
4.3.12 Effect of mild HS on cell numbers and ALP production of hMSCs (Experiment 04) *118*
4.3.13 Effect of mild HS on cell numbers and ALP production of MG-63 cells (Experiment 04) *119*
4.3.14 Effect of passage number on the HSP70 production capacity in hMSCs *122*
4.3.15 Effect of bulk heat shock on HSP70 protein production in hMSCs *123*
5.1.1 Schematic explaining theory behind ECIS measurements *134*
5.1.2 ECIS array types *135*
5.2.1 Rate of heating for an aqueous suspension of $Zn_{0.2}$ at a set frequency of 165kHz and varying voltages *139*
5.2.2 Schematic showing the set-up for applying magnetic hyperthermia to cells *141*
5.3.1 Stability of citric acid coated MNPs with time in cell-culture medium *145*
5.3.2 Comparison of the magnetic behaviour of MNPs in different biological environments *147*
5.3.3 Comparing ACS behaviour between different Zn-doped MNPs *149*
5.3.4 Predicting the resonant frequency for MNPs *149*
5.3.5 Heating power of Zn-doped MNPs under different magnetic field conditions *150*
5.3.6 Heating rates of solutions with and without MNPs (Experiment 03) *152*
5.3.7 Changes in ACS signal with bio-functionalization *152*
5.3.8 Effect of RGD coating and time on cell-membrane association of MNPs *154*

5.3.9 MG-63 cells attached to different ECIS arrays *156*
5.3.10 Cells on 8W1E and 8W10E+ arrays at 10E3 cells/cm^2 seeding density immediately following attachment *157*
5.3.11 Bright field images of cells on ECIS well plates *159*
5.3.12 Identification of optimum frequency of measurement *160*
5.3.13 ECIS measurements for detecting osteogenesis in hMSCs *162*
5.3.14 ECIS measurements for detecting osteogenesis in MG-63 cells *164*
5.3.15 ECIS measurements during later stages of osteogenesis in both cell types *166*
5.3.16 Effect of MNP-mediated heat shock on cellular morphology (Experiment 01) *168*
5.3.17 Morphology and cellular viability of MG-63 cells exposed to MNP-mediated heat shock (Experiment 02) *169*
5.3.18 Mitochondrial metabolic activity and cellular viability of MG-63 cells exposed to MNP-mediated heat shock (Experiment 02) *170*
5.3.19 Effect of MNP-mediated severe heat shock on cellular morphology (Experiment 03) *172*
5.3.20 Temperature measurements during extracellular MNP-mediated heating of cells (Experiment 04) *173*
5.3.21 Effect of MNP-mediated mild HS on DNA content and ALP production of hMSCs (Experiment 04) *173*
5.3.22 Mineralization of hMSCs exposed to $Zn_{0.4}$ - MNP mediated heat shock (Experiment 04) *174*
5.3.23 Temperature measurements during extracellular MNP-mediated heating of hMSCs (Experiment 05) *175*
5.3.24 Effect of MNP-mediated heat treatment on morphology hMSCs (Experiment 05) *176*
5.3.25 Temperature measurements during extracellular MNP-mediated heating of hMSCs (Experiment 06) *177*
5.3.26 Effect of MNP-mediated heat shock on hMSC morphology (Experiment 06) *178*
5.3.27 ECIS measurements showing the effect of MNP-mediated heat shock on hMSCs *180*
5.3.28 Effect of MNP-mediated mild HS on DNA content and ALP production of *181*

hMSCs (Experiment 06)
5.3.29 Temperature measurement during extracellular MNP-mediated heating of hMSCs (Experiment 07) *182*
5.3.30 Effect of MNP-mediated heat shock hMSC morphology (Experiment 07) *183*
5.3.31 ECIS measurements showing the effect of MNP-mediated HS on cellular behaviour (Experiment 07) *185*
5.3.32 Effect of MNP-mediated HS on DNA content and ALP production of hMSCs (Experiment 07) *186*
A1: hMSC staining for CD markers *214*
A2: Quantification of CD marker expression in hMSCs *215*
A3: Quantification of CD marker expression in hMSCs *216*
A4 Multilineage potential of hMSCs *218*

List of tables

1.1 Summary of Cytotoxicity assays, the dyes used and the cellular property tested to assess viability *31*
2.1 Chemical supplements for preparation of differentiation media *49*
2.2 Antibodies used for immunocytochemistry *56*
3.1 Details of the various magnetic nanoparticles used in this study *61*
4.1 Details of the various bulk heat shock experiments. *100*
5.1 Coil-capacitor combinations available in the magnetic hyperthermia device *139*
5.2 List of the different samples for extracellular the heat shock experiments and the conditions of treatment *143*
5.3 Details of the various MNP-mediated heat shock experiments *144*

List of associated publications

Moise, S., Céspedes, E., Soukup, D., Byrne, J. M., Haj, A. E., & Telling, N. D. Biocompatibility and cellular magnetic response of biogenic zinc and cobalt doped magnetite nanoparticles. Target: Nanoscale, Status: (To be submitted)

Soukup, D., **Moise, S**., Céspedes, E., Dobson, J., & Telling, N. D. (2015). In Situ Measurement of Magnetization Relaxation of Internalized Nanoparticles in Live Cells. *ACS Nano*. doi:10.1021/nn503888j

Céspedes, E., Byrne, J. M., Farrow, N., **Moise, S**., Coker, V. S., Bencsik, M., Lloyd, J.R., Telling, N. D. (2014). Bacterially synthesized ferrite nanoparticles for magnetic hyperthermia applications. *Nanoscale*, *6*(21), 12958–70.

Byrne, J. M., Coker, V. S., **Moise, S**., Wincott, P. L., Vaughan, D. J., Tuna, F., Arenholz, E., van der Laan, G., Pattrick, R.A., Lloyd, J.R., Telling, N. D. (2013). Controlled cobalt doping in biogenic magnetite nanoparticles. *Journal of the Royal Society, Interface / the Royal Society*, *10*(83), 20130134.

List of associated presentations

Exploring suitability of biogenic zinc and cobalt doped magnetite nanoparticles for cellular biomedical applications, **Frontiers in Biomagnetic Particles,** Telluride, USA, June 2015 (Oral)

A study of the cellular-nanoparticle interactions and assessment of the magnetic response of novel bacterially synthesized substituted ferrites, **Faraday Discussion 175: Physical Chemistry of Functional Biomedical Nanoparticles**, Bristol, United Kingdom, September 2014 (Oral)

Cell-nanoparticle interactions: Magnetic response and biocompatibility of bacterially synthesized zinc and cobalt magnetite nanoparticles, **10th International Conference on the Scientific and Clinical Applications of Magnetic Carriers**, Dresden, Germany, June 2014 (Poster)

Cytotoxicity of Biogenic Cobalt Doped Magnetite Nanoparticles, **Symposium on nanoparticle-based technologies for cell tracking**, Liverpool, United Kingdom, July 2013 (Poster)

Assessing Cytotoxicity of Biogenic Magnetic Nanoparticles, **TERMIS EU**, Istanbul, Turkey, June 2013 (Oral)

Acknowledgements

As Buckminster Fuller points out in his 1969 essay 'Operating manual for spaceship earth',[1] 'Of course, our failures are a consequence of many factors, but possibly one of the most important is the fact that society operates on the theory that specialization is the key to success, not realizing that specialization precludes comprehensive thinking.' Science is rapidly changing this paradigm and I am extremely lucky to be working on a topic sitting at the cusp of the two traditional fields of physics and biology. Of course, this would not have been possible without the help and guidance of my supervisors, Neil Telling and Alicia El Haj. Without their drive, commitment and guidance, my doctoral training or dissertation would not have been nearly as good. During this three year period, I learned a lot from them and I am still trying to learn more. Heartfelt thanks again to Neil for investing so much time and effort in me for shaping me as scientist. Trained as a physicist, his success in the field of biological engineering is a deep source of inspiration for me and gives me courage to take-on new fields of research especially those of a multi-disciplinary nature. I am also very much indebted to my advisor Paul Roach for all the scientific and career related advice he has given me over the years which helped me grow as a scholar. I am most grateful for all this generous support. This dissertation would not have been possible without the financial support from EPSRC, and Keele University

My Ph.D. friends and colleagues also deserve special mention for sharing their thoughts and interests with me. Special thanks to Mike, James, Eva, Kaarjh, Dali and Neil Farrow who've trained and advised me on various techniques. Thanks to all my friends and colleagues at ISTM for being a strong support to lean on in hard times, especially the crazy turks Berrin and Hati, my housemate Dr.-to.be Yanny, friends Fazia ji, Anto, Ranga, Arch, Yams, Gav, Divs, Matt (esp. for proofreading my thesis), Lanxin (esp. for help with printing), Mohammad, my friend and mentor Anand Pandyan. I also wish to extend my gratitude to Jan-Herman Kuiper, Karen Walker, Neil Grazier for help with various techniques. Thanks to Joachim Wegener and all his students for their support in teaching me the ECIS technique. Thanks to all my teachers who inspired my passion for learning.

Biggest thanks to my amma and appa for not curbing my spirit at any point, for all the monitory and emotional support to go abroad, pursue my ambitions, to petheepu for making me love science. Finally, thank you mamakutty for being so understanding of my phd-related mood swings, odd working hours, for all the food you cooked and pushes you gave when I felt low.

Neil Telling has thoroughly read and commented on all parts of the dissertation. Numerous debaters have commented on parts of the dissertation during an international conference in the USA and at two annual Ph.D. student conferences organised by the EPSRC Doctoral Training Centre network for Regenerative medicine. All remaining errors are my own.

Sandhya Moise

12 Dec 2015

CHAPTER 1 Introduction

1.1 Behaviour of stem cells

1.1.1 Introduction to stem cells

Stem cells have a vast therapeutic potential to repair, replace and regenerate damaged or diseased tissues[2]. In the field of regenerative medicine typically endogenous or transplanted stem cells are used to reconstruct injured tissues. This is due to their unique properties to unalterably self-renew as well as form more specialised cells, a process known as differentiation.[2] Stem cells can be derived from various sources including embryos, umbilical cord, or from adult tissues. Adult stem cells reside within specialised niches in different tissues such as the skin,[3] bone marrow,[4] adipose tissue,[5] brain[6] and teeth[7] from where they can be isolated.

Of the various adult stem cells types, the mesenchymal stem cells (MSCs) are one of the most extensively studied for their therapeutic properties and applications. These cells are of particular interest for regenerative medicine applications as they can be isolated from easily accessible sources, including bone marrow aspirate[4] or adipose tissue[8] and can be expanded *in vitro* to get higher cell numbers. Also, being multipotent, they can differentiate into cells belonging to the mesodermal lineage,[9] namely bone, cartilage, fat, tendon and muscle cells. MSCs repair or remodel tissue *in vivo* by responding to a myriad of environmental stimuli. By providing the right conditions as would be found in native tissue *in vivo*, MSCs can be guided to differentiate along a certain lineage *in vitro*.

1.1.2 Differentiation of Stem Cells

Stem cells have been used in cell-based clinical therapies for more than a decade.[10] Their ability to home to the site of inflammation, to differentiate into specialized cells, and to

exhibit anti-inflammatory properties help wound healing and hence regeneration.[11] Although being excellent candidates for cell-based therapies, their efficiency depends on their capacity to be expanded and differentiated both *in vivo* and *ex vivo*. This in turn depends on many factors like the age of and presence of any disease conditions in the donor,[12] and a better understanding of these factors can help improve their efficiency.

To achieve efficient *in vitro* differentiation, it is best to mimic *in vivo* conditions in terms of the chemical signalling molecules, architecture and physical forces cells would experience (Fig 1.1.1). With this in mind, various triggers of stem cells differentiation *in vitro* and *in vivo* are being developed and compared. Chemical supplements added to the cell-culture media efficiently stimulate *in vitro* osteogenic (bone cells),[13] chondrogenic (cartilage cells),[14] and adipogenic (fat cells)[15] lineage differentiations. 2D and 3D scaffold materials are being extensively studied to exemplify the tissue architecture and spatial cues found *in vivo.* Scaffolds mimicking the extracellular matrix (ECM) environment in terms of geometry, ligands and their mechanical properties have shown potential to guide stem cell differentiation. In a study by Murphy *et al*.,[16] MSCs were grown on modified collagen-glycosaminoglycan scaffolds of different stiffness values: 0.5, 1 and 1.5 kPa in the absence of chemical differentiation supplements. They found that on the scaffold with the lowest stiffness (0.5 kPa), there was a significant up-regulation of SOX9 gene expression indicating chondrogenesis whereas the greatest level of RUNX2 protein expression (indicating osteogenesis) was found in the stiffest scaffolds (1.5 kPa).[16]

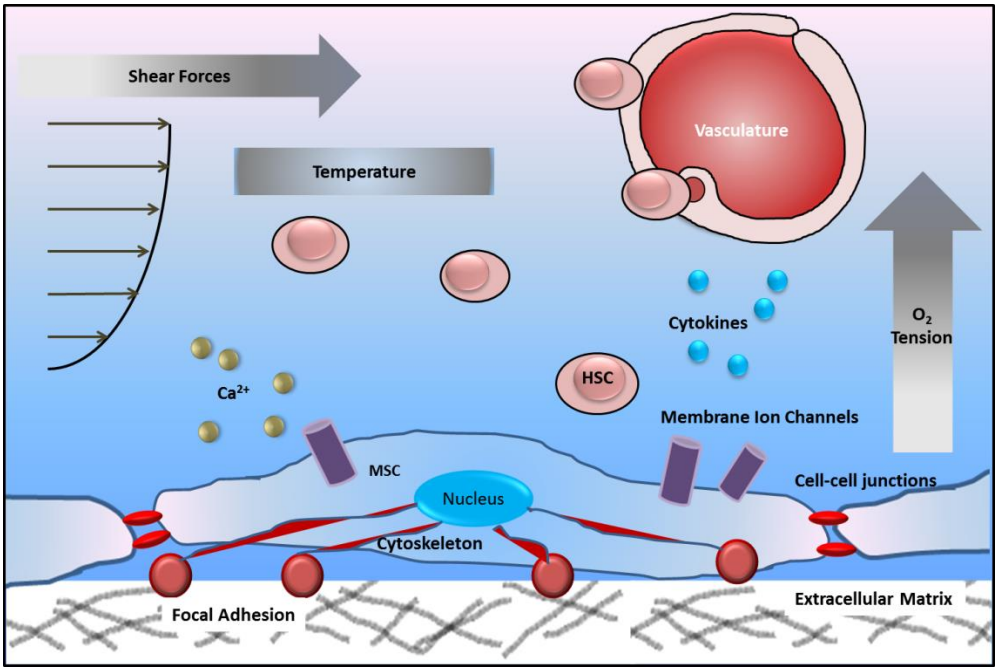

Fig 1.1.1 Schematic of a hypothetical stem cell niche: Different cell populations, soluble signalling factors, extracellular matrix components and other physical parameters are shown that together play a role in dictating stem cell fate in vitro. Physical signals in the form of matrix stiffness, fluid shear stress and temperature are shown. These are sensed via the mechanosensitive membrane ion channels, focal adhesions, cytoskeleton and cell-cell adhesions. (HSC: Hematopoietic stem cells and MSC: Mesenchymal stem cells; Adapted from Sun et al. 2012[17] and Wang et al. 2011[18])

Physical triggers have also been shown to affect cellular behaviour.[17–19] In the body, cells are constantly being exposed to various types of physical stimuli and being the sensors of the tissue, adapt the tissue properties in response to the stimuli. For example, changes in shear stress due to blood flow are sensed by the endothelial cells lining the blood vessel. These cells signal this information to the neighbouring cells to remodel the blood vessel architecture to adapt to the new forces.[18,20,21] Similarly, changes in the strain experienced by the bone tissue causes extracellular fluid flow and is sensed by the osteocytes. [22,23] They in turn trigger remodelling of the bone tissue by signalling to bone marrow stem cells and osteoclasts so as to adapt to the new strain profile.[24] Cells sense these external physical stimuli via a multitude of cellular components. There are receptors on the cell membrane responsive to stress, referred to as mechanosensitive ion channels.[25,26] *In vivo* these are

activated typically in response to extracellular fluid shear stress triggering intracellular signalling cascades and downstream gene expression. The cellular cytoskeleton has been implicated in sensing the stiffness of the ECM.[27] Such physical stimuli cause behavioural changes in cells such as growth, differentiation, migration or apoptosis. These in turn remodel the tissue's architecture to adapt to the forces it is exposed to.[19,24]

Although in a simple *in vitro* 2D or 3D system, differentiation has been induced using any of the different stimulation methods (physical, chemical or spatial), a more efficient induction could result from using a combination of them.[28,29] The closer the physico-chemical conditions are to those found *in vivo*, the higher the efficiency of inducing differentiation. The stem cell niche consists of various components such as other cell populations (mesenchymal, vascular, neuronal, inflammatory), paracrine and membrane associated signalling molecules, spatial and physical parameters such as the matrix architecture, stiffness and temperature (Fig 1.1.1).[30] For example, in the work by Mauney *et al*.,[31] a combination of chemical, spatial and physical stimuli were provided to human bone marrow MSCs. Cells grown on partially demineralized bone scaffolds in the presence of four point bending loads and 10nM dexamethasone were found to show improved osteogenesis compared to static or dexamethasone-free controls.

Currently, extensive work is being done on studying the influence of the various chemical signalling molecules, scaffold designs and types of mechanical stimuli needed for differentiation promotion.[32,33] On the other hand, the effect of heat on stem cell fate has not been explored extensively with little understood on the role of temperature and its mechanism of action. It could be a missing piece in the puzzle for designing the ideal *ex vivo* stem cell niche.

1.1.3 Effect of Heat Shock on Stem Cell Behaviour

Evidence for Role of Heat Shock in Controlling Stem Cell Fate

Cells are exposed to various types of stresses. Even during early stages of development, cells within the embryo are exposed to transient stresses within the maternal milieu due to maternal hormones, local infection and inflammation, hypoxia or heat shock. These stresses reduce proliferation but can promote differentiation of stem cells in the embryo.[34–36]

One of the common types of stress cells are exposed to is elevations in temperature also referred to as heat shock. This may be due to environmental factors or a local occurrence during inflammation. Stem cells in general are found to have a higher tolerance for stress than their more specialised counterparts.[37–39] In fact, this has been used to enrich stem cells within mixed cell populations by exposing the population to elevated temperatures.[38] During-infection led pyrexia (fever) the elevated whole body temperature besides killing foreign bodies also damages native tissues in the body. Since stem cells aid healing of the body tissue during pyrexia an increased tolerance to heat stress would be a desirable quality for stem cells. Also, under such conditions, the temperature elevation itself could possibly be a trigger to activate the usually quiescent stem cells[40,41] into proliferation or differentiation.[42]

The effect of heat shock (HS) on human embryonic stem cells (hESCs) was studied by exposing the cells to 42^0C and 46^0C for durations of 30min, 1h and 2h.[36] There was no significant cell death in all the different treatments. On the other hand, the heat shock factor (HSF), a transcription factor for heat shock proteins (HSPs), negatively regulated the

expression of OCT-4 gene, a core self-renewal regulator. This triggered the switching of the embryonic stem cells from self-renewal to differentiation mode as evidenced by the upregulation of various differentiation related genes.

Numerous studies in adult stem cells have also found evidence of mild heat shock affecting cellular proliferation and differentiation.[43–46] Both single and repetitive HS treatments were found to be effective in influencing cellular behaviour. In the work by Nørgaard et al,[47] bone marrow-derived hMSCs were established into a telomerase-immortalized cell line (hMSC-TERT). These cells were exposed to temperatures of 41, 42.5 or 44^0C for 1h in a temperature controlled water bath, as a single treatment. HS was found to enhance the production of the enzyme alkaline phosphatase (ALP). Although ALP has been found to be a marker for embryonic stem cells it is not a universal marker for all stem cell types.[48,49] Specifically for hMSCs, they indicate commitment to the osteogenic lineage[48] and are involved in aiding mineralization of the extracellular matrix (ECM).[50] Apart from upregulating ALP production on day 8, it was also found to upregulate mineralized matrix formation compared to cells cultured in proliferation medium or untreated cells in osteogenic medium. Maximum upregulation was found for the 42.5^0C, 1h treatment condition. In another experiment, effect of HS and cold shock treatments on the osteogenic differentiation of bone marrow derived hMSCs and the osteoblast-like osteosarcoma (bone cancer) cell line MG-63 were studied.[44] Multiple exposure times were compared including a single 1h treatment, a long continuous treatment of 96h and a repeated treatment of 1h every third day. Overall, a continuous cold shock of 33^0C for 96h decreased DNA synthesis and ALP production in both cell types. DNA synthesis also decreased at temperatures higher than 42.5^0C in both cell types (with MG-63s being more sensitive). However, ALP production per cell linearly increased with temperature for both the single

short and long exposure treatments for both cell types. Mineralization at 21 days was either unaffected or inhibited at 33^0C whilst HS at 39^0C increased mineralization in hMSCs. Adipose-derived hMSCs also conformed to the enhanced osteogenic behaviour upon HS. Repeated mild heat shock of 42^0C for 1h weekly not only improved osteogenesis, but also adipogenesis for cells grown in the specific induction medium as well as their proliferation rates in expansion medium. [43]

Apart from osteogenesis and adipogenesis, there is evidence for HS playing a role in other differentiation pathways.[32,46] Periodic mild HS of 41^0C for 1 h weekly enhanced osteo- (2D and 3D)[45] or chondrogenic (3D)[46] differentiation of bone marrow hMSCs compared to untreated cells, both cultured in the specific induction media.[45,46] Dental follicle-derived cell populations showed improved adipogenesis and neurosphere formation upon continuous mild HS (between 40 to 41.5^0C for 5 days).[38] HS has also shown promise for inducing cardiomyogenic differentiation. Mild HS was found to enhance expression of transforming growth factor beta (TGF-β) *in vitro* 12-48h post-HS in cultured rat cardio fibroblasts (41.5^0C for 2h) and *in vivo* 48- 72h post-HS in hearts of rats (41.5^0C core temperature for 15min).[51] TGF-β is a potent inducer of cardiomyogenic differentiation[52] and HS could be employed to trigger and direct cardiomyogenic differentiation of stem cells.

Heat shock, apart from being a promising stimulus for improving cellular proliferation and differentiation, is also found to be a favourable pre-transplantation treatment. Cells exposed to mild HS prior to introduction into a site of injury *in vivo*, showed a higher survival rate.[53,54]

Possible Mechanisms for Heat Shock Regulation of Cellular Behaviour

The influence HS has on cells could be mediated primarily via two modes: (1) heat shock proteins (HSP) and heat shock factors (transcription factors' of HSPs) and (2) heat-sensitive membrane ion channels.

Exposing cells or whole organisms to elevated temperatures causes synthesis of a family of proteins known as the heat shock proteins (HSPs). These proteins are highly conserved and universally expressed in animals, plants and even archaebacteria, attesting their importance. These proteins play a primary protective role, with other types of stress also affecting their expression.[55] Depending on the type of cell or organism in which they are expressed, HSPs regulate their response, demonstrating the versatility of their biological function and their evolutionary adaptation.

The heat shock response was first discovered in the fruit fly, *Drosophila busckii* in 1962.[56] For *in vitro* studies, *Drosophila* cells are normally grown at 25^0C. When the cells were elevated to greater than 4^0C above optimum growth temperature (29 - 38^0C), HSP expression was observed. The protein expression peaked at 36-37^0C.[57] Also, when the cells were under the heat shock, all other gene transcription and RNA translation were found to be suspended.[58,59] In other organisms, the threshold temperature for maximum HSP induction varied depending on the normal physiological temperature of the organism, typically occurring at 10-15^0C above the optimum growth temperature.[55] In addition, depending on the intensity of the heat shock, the response was a sustained or transient one. The response is usually transient at moderate temperatures and cells are capable of normal functioning following the heat shock. In contrast, at extreme temperatures where the response is sustained, cells eventually die. The moderate temperature range is organism

dependant. For example, in *Escherichia coli* (gram negative bacteria) grown at 30-37^{0}C, it was found that while at 42^{0}C, HSP expression was transient, and upon raising the temperature to 45-50^{0}C it was a sustained response.[60–62] The response is also influenced by the metabolic state of the cells. For instance, in *Saccharomyces cerevisiae* (yeast), fermenting cells grown at 25^{0}C have a transient response at 36^{0}C and sustained response at 40^{0}C. On the other hand, if the cells are respiring, the response is transient at 34^{0}C and sustained at 36^{0}C instead.[63] HSP expression is also a function of previous exposure temperatures. A single step increase in temperature of *E.coli* cells to higher temperatures shows maximum response at 37^{0}C and none at 39^{0}C. On the contrary, with a more gradual rise in temperature the response occurs at higher temperatures. The functional role of heat shock proteins is not only to protect the cell from the toxicity of thermal or other forms of stress but could also be to develop cellular tolerance towards extreme temperatures (thermotolerance). Stability of HSPs developed following heat shock (41^{0}C) in Chinese hamster fibroblasts correlated well with the persistence of the thermotolerance behaviour which lasted up to 36h post-HS.[64]

HS has shown evidence of upregulation of differentiation of mesenchymal stem cells.[15,47,65] It also causes expression of HSP. There is evidence to show the concurrent upregulation of differentiation marker genes and HSP genes with HS.[45,46,66] Whether there is a direct role for HSPs in triggering or enhancing differentiation or their expression is purely to increase tolerance of cells to stress is unclear. One possible route of HSP affecting differentiation pathways was constructed by Hronik-Tupaj *et al.*[65] as shown in Fig 1.1.2.

Fig 1.1.2 Signalling pathways implicated in osteogenic differentiation of stem cells: (a) osteogenic differentiation pathway, (b) crosstalk between osteogenic differentiation pathway and stress response to an alternating current electric field. [65]

In the proposed model, HSP70 affects RunX2, one of the main transcription factors implicated in early onset of osteogenic differentiation, via other downstream signalling molecules. Runx2/Cbfa1 upregulates the expression of other osteogenic markers including ALP, collagen 1, osteocalcin and osteopontin. Another possible route is the role HSPs play in stabilising the Raf protein.[67] Raf is an integral part of the ERK pathway, a signalling pathway implicated in differentiation of mesenchymal stem cells.[68] Based on these hypothesis and other studies there is evidence to show the role of HSPs in affecting differentiation of adult stem cells, though further studies are required to confirm this.

The other possible route for HS to modulate stem cell differentiation is via heat-sensitive ion channels. Ion channels are membrane proteins that form pores traversing the width of the lipid bilayer. They play a role in maintaining the membrane potential, creating action potentials and other electrical signals by facilitating the passive transport of ions across the

plasma membrane. They are present in the membrane of all cells and some intracellular organelles. Ion channels are classified based on what triggers the opening of the channel or based on what ions they facilitate passage of. The most common ion channels are voltage gated and sense changes in voltage gradients across the membrane. Mechanosensitive ion channels respond to mechanical stimuli such as stretch or shear forces. Heat sensitive ion channels respond to changes in temperature and are activated above or below a certain threshold temperature value. Some ion channels are responsive to more than one stimulus depending on the cell type they are expressed in, for instance, TREK and TRPV channels apart from being mechano- and osmosensors can act as thermosensors (Fig 1.1.3).[69,70]

<*copyrighted image*>

Fig 1.1.3 TREK activation via various physical and chemical stimuli[69]

As the name suggests, heat-sensitive ion channels are activated by temperature changes and are found in various human cell types. They comprise the potassium ion channel TREK-1 and the transient receptor potential (TRP) family of ion channels.[71,72] The ion channels are activated when temperature rises or falls below a threshold value and this threshold varies between the different ion channels. For example, TRPV1 is activated above 43^0C and TRPV2 above 53^0C.[72] TRPV3 is active over a wide range of temperatures (between 23 to 35^0C)[73–75] and TRPV4 is active above 24 or 34^0C.[76,77] TREK-1 is active at

physiological temperatures[78] as its threshold temperature is 32^0C while TRPM8, another vanilloid family ion channel, is a cold sensor and is activated when temperature falls below 22^0C.[74,79]

TRP channels also have a direct effect on stem cell functioning. TRPV4 has been shown to direct chondrogenic differentiation of chondrogenic cell line ATDC5 and the murine mesenchymal stem cell line C3H10T1/2 cells upon chemical activation.[80] Chemical activation of TRPV1 has been shown to play a role in mineralization and desorption of bone tissue[81] and it would be interesting to study its role as a heat sensitive ion channel in osteogenesis. TREK-1 has been extensively studied as a mechanically activated inducer of osteogenic differentiation[82] and its potential as a heat activator of osteogenesis could also be investigated using hyperthermia. Heat sensitive ion channel TRPV1 has been found to modify HSP expression proteins and through them could be indirectly regulating stem cell differentiation.[83]

1.2 Magnetic nanoparticles for remote manipulation of stem cells

Magnetic nanoparticles are nano-scale (1 nanometer=10^{-9}m) particles made of metal or metal oxide cores that are responsive to an external magnetic field. Under the influence of an external magnetic field they can physically move, dissipate heat or affect the magnetic field around them. These properties have been exploited for various biomedical applications: for hyperthermia in cancer therapy, for site specific drug delivery and as contrast agents in magnetic resonance imaging.[84,85] Their small sizes are comparable to that of macro-biomolecules such as proteins (5-50nm), genes (10-100nm) allowing efficient binding of these molecules on the surface of the nanoparticles (Biofunctionalization).[86] This allows binding to cells, targeting cells expressing specific

membrane receptors, activation of these receptors to trigger intracellular signalling process to control cellular behaviour. These properties of the MNPS coupled with advances in development of biocompatible surface coatings have made them versatile candidates for both therapeutic and diagnostic (theranostic) applications in the biomedical field.[86]

1.2.1 Magnetic and Functional Properties of Biomedical MNPs

All materials give a magnetic response when placed in an external magnetic field. The response depends on the electronic configuration of the material as the spin and orbital moments of the electrons determine the magnetic properties of the material. Depending on the response to an external field, materials are classified as diamagnetic, paramagnetic, ferromagnetic, ferrimagnetic, antiferromagnetic and superparamagnetic. In diamagnets, the magnetic behaviour is dictated solely by the orbital moment of the electrons and these materials are repulsed when placed in a magnetic field, that is, they have a weak negative magnetic susceptibility. In contrast, all the other types have uncompensated spin moments and hence their magnetic behaviour is governed by the spin motion of their electrons. Paramagnets are attracted in a magnetic field and hence have a positive susceptibility, though this is weak and they lose their magnetization once the field is removed. Antiferromagnets have coupled anti-parallel spins of equal magnitude that cancel each other out and hence have zero susceptibility (Fig 1.2.1a). Ferromagnets have coupled parallel spins such that the material displays a strong positive susceptibility. Ferrimagnets are similar to antiferromagnets and have coupled anti-parallel spins but of unequal magnitude resulting in a net positive susceptibility (Fig 1.2.1b). Most iron oxide materials are ferrimagnets and all magnetic materials described henceforth and used in this work, are ferrimagnetic at the macro-scale. An example of a ferrimagnetic material, magnetite given by the formula Fe_3O_4, is shown in Fig 1.2.1c. In this material, iron is present in both its 2+

and 3+ oxidation state and occupies tetrahedral and octahedral sites (Fig 1.2.1c) in an antiparallel configuration.

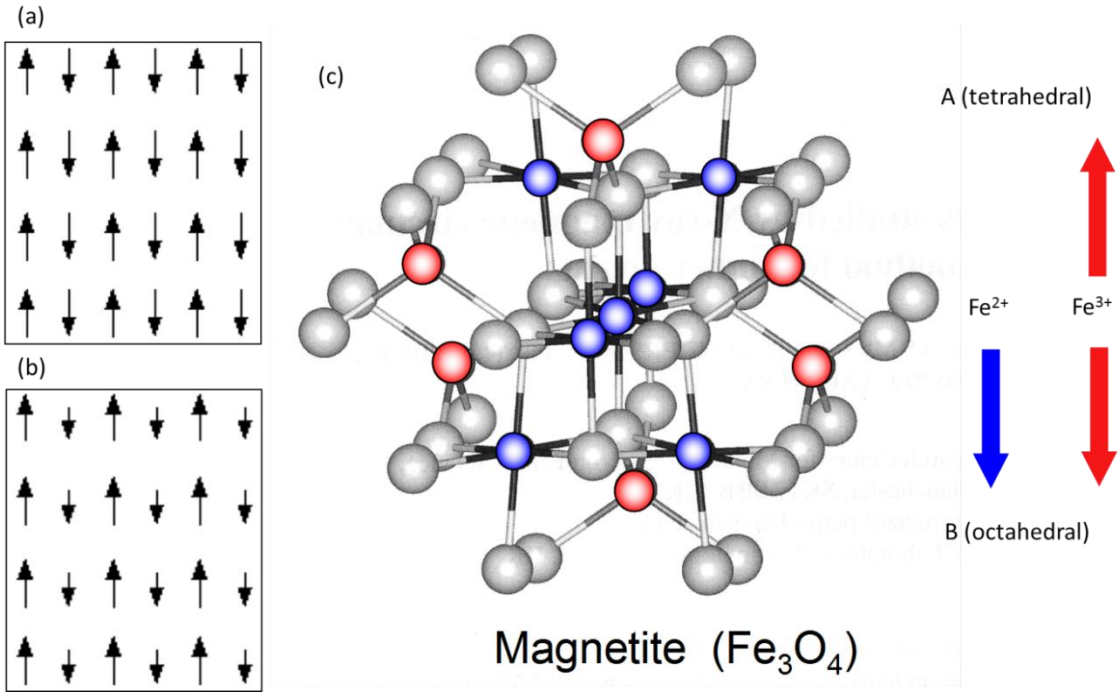

Fig 1.2.1 Alignment of spins in different magnetic materials: Antiparallel alignment of equal magnitude spins in antiferromagnets (a) and unequal spins in ferrimagnets (b) are shown. (c) A schematic of the crystal structure of the ferrimagnetic material magnetite showing the opposing alignment of the spins of iron ions depending on their position within the lattice (tetrahedral or octahedral).

At the bulk scale, in a ferrimagnetic material, the magnetic moment of the material divides into domains containing coupled spins with a net magnetisation. When ferrimagnets are placed under an external magnetic field, the field energy facilitates alignment of all the domains along the field direction. Removal of the field does not result in restoration of the original domain arrangements and a residual magnetization remains. A coercive field H_C, in the opposite direction is necessary to decrease the magnetization of the material to zero, a phenomenon referred to as hysteresis (Fig 1.2.2a-FM). Ferrimagnets, due to hysteresis losses, generate heat when placed in an oscillating external field.

< *copyrighted image* >

Fig 1.2.2 Comparison of the magnetic behaviour of ferromagnets and SPMs: (a) Multi-domain configuration of macroscopic ferromagnetic materials (FM) and their Hysteresis plots compared with nano- scale superparamagnetic (SPM) spheres.[86] *(b) Plot of particle diameter against the coercive field (Hc) showing the transition of ferrimagnetic materials into the single domain and superparamagnetic region with decreasing particle size.(Adapted from Jun et al. 2008)* [87]

At the nano- scale, ferrimagnets (<100nm, depending on the composition) reach sub-domain dimensions and all the magnetic spins are aligned in a single direction (Fig 1.2.2a-SPM, b). Further reduction in size, below a critical diameter (Fig 1.2.2b), pushes the particles into the superparamagnetic (SPM) regime. Similar to ferrimagnets, electron spins are coupled and hence SPMs show a strong magnetic response. On the other hand, as the name describes SPM particles show a paramagnetic behaviour, that is they do not retains any remanent magnetization (zero remanence as Hc=0; Fig 1.2.2b) unlike multi-domain ferrimagnets. This is because in SPMs, thermal energy, in the absence of an external magnetic field, causes constant flipping of the particle magnetization between the energy minima axes resulting in zero net magnetization.

SPM nanoparticles have zero remanence and hence do not agglomerate due to inter-particular magnetic attraction unlike larger ferrimagnetic particles which could agglomerate and potentially block blood vessels[88] . Also, their small sizes allow them to

efficiently evade the body's immune system making SPM nanoparticles suitable candidates for *in vivo* application. The magnetic structures can therefore be used for various *in vivo* applications and suitably functionalized with receptor specific ligands or other proteins to selectively bind/ interact with particular targets on the cell.

Magnetic nanoparticles to be used for cellular applications are prepared as stable colloidal suspensions in water.[89] For this purpose, the MNPs are coated with surfactants containing charged surface groups or with bulky polymers such as polyethylene imine[90] which circumvent agglomeration due to electrostatic repulsion or steric hindrance. Suitable coatings also help reduce the interaction of MNPs with their vicinity and hence any possible leaching of metal ions into the cellular milieu. The type of interaction between the coating material and the MNP can be covalent or electrostatic in nature and the coated MNPs can further be functionalized through introduction of 'linker' molecules that can in turn bind to biomolecules such as ligands, antibodies and other proteins. The biomolecule attachment confers the MNP with application specific usability and site targeting capacity.

Iron oxides occur naturally within the human body. Iron stored in the human body is in the form of ferrihydrite ($5Fe_2O_3.9H_2O$) whilst magnetite (Fe_3O_4) can be found in the human brain.[91] Hence, iron oxide ferrofluids, especially magnetite and maghemite (Fe_2O_3) are the natural choice of MNPs for cellular applications owing to their biocompatibility. In terms of magnetic properties, as ferrofluids, iron oxide nanoparticles have a strong magnetic response. But for cellular applications, especially for *in vivo* clinical applications, it is beneficial to be able to elicit an optimum magnetic response with the weakest external magnetic field conditions possible. A stronger response also allows a lower therapeutic dosage to get the necessary effect.

1.2.2 Bacterially synthesized iron oxides

Magnetic nanoparticles can be synthesized by chemical, physical or biogenic means. The chemical method is the most common mode of synthesis as it is relatively cheaper and simpler in comparison to the other methods. Most commercially available MNPs are chemically synthesized. Physical methods of synthesis, such as lithography, deliver MNP batches with the most uniform and excellent magnetic properties. However, in spite of the level of precision achievable in terms of the atomic arrangement and crystal structure, it can be a very expensive route of synthesis.

In the biogenic mode, iron-reducing bacteria can be used to synthesize the MNPs.[92,93]Magnetotactic bacteria, gram negative prokaryotes, have the unique ability to produce intracellular phospholipid membrane bound ferrimagnetic particles of magnetite (Fe_3O_4) or greigite (Fe_3S_4), with diameters ranging around 50-100nm, called magnetosomes.[93] The presence of these magnetosomes cause the organisms to align and travel along the earth's magnetic field lines.[94,95]

The biogenic mode of synthesis combines the advantages of physical and chemical routes in the sense that it is a simple and inexpensive approach producing MNPs with excellent physical and magnetic properties. Organisms that produce magnetic particles fabricate them atom by atom to produce particles of extremely well defined magnetic and physical properties.[96] These characteristics of biogenic MNPs make them potentially better candidates for ferrofluid based applications than their chemically synthesized counterparts. The better performance of biogenic MNPs over chemically derived MNPs has been reported in various instances. Some examples include applications such as recovery of DNA using dendrimer-modified biogenic MNPs which have a six fold higher efficiency

than their synthetic counterparts[97], oligo nucleotide modified magnetosomes for mRNA isolation[98] and magnetic microarray for various cyanobacterial identification.[99] In addition, the bacteria can be genetically engineered to express ligands as a fusion protein with the magnetosome membrane.[100,101] These magnetosomes can then be targeted towards cells of interest that express the receptors that the ligands are specific for. In addition, the biogenic route is environmentally benign and is easily scalable making it an attractive route of synthesis.

The magnetic properties of the MNPs affect the nanoparticle response to an external magnetic field. For instance, modifying the magnetic moment of the nanoparticles alters their efficiency as contrast agents in magnetic resonance imaging (MRI), whilst their magnetic anisotropy (directional dependence of a material's magnetic properties) determines whether they are in a superparamagnetic state at physiological temperature (37°C). A variety of factors influence the magnetic properties of iron oxide MNPs including the size, shape and composition. By tuning these parameters, MNPs can be tailored to have application specific magnetic behaviour. For instance, in magnetic hyperthermia applications a better design of the MNP would be able to ensure a high but not toxic level of heat generation within clinically relevant external field conditions. The upper limit to the field strength and frequency that is safe for human exposure was defined experimentally by Brezovich[102] as the product of field frequency and strength not exceeding $4.85 \times 10^{8} Am^{-1}s^{-1}$. Recently, a more relaxed limit of 5×10^{9} $Am^{-1}s^{-1}$ is being widely reported as safe especially when exposing smaller diameter regions of the body and also considering the seriousness of the illness being treated.[103,104] When designing magnetic nanostructures for magnetic hyperthermia applications, they should be able to cause a sufficient temperature rise within these field conditions.

1.2.3 Substituted iron oxides

Substituting (used interchangeably with the term 'doping') iron ions within the iron oxide core with other divalent cations from the transition metal series affects the magnetic moment, magnetic anisotropy and hence magnetic behaviour of the MNPs[105,106]. In ferrimagnetic magnetite, as seen earlier (Fig 1.2.1c) the Fe^{3+} ions in the tetrahedral and octahedral sites are antiparallel and cancel out each other with the net magnetization only due to the Fe^{2+} ions. Hence, when other divalent transition metals replace the Fe^{2+} or Fe^{3+} cations, the net magnetization of the MNP is modified affecting its magnetic properties.[92,107] For instance, in the work by Tung *et al,*[105] doping of cobalt was found to increase the magnetic anisotropy of chemically synthesized iron oxide cores. This affected the relaxation rate of their magnetic moment following the removal of an external magnetic field (see Chapter 1 section 1.2.4 AC susceptibility). Hence, the increase in anisotropy due to the doping allows the use of smaller sized MNPs for eliciting the same response compared to pure iron oxides. This margin to reduce the size is advantageous for *in vivo* applications as it would have a higher circulation time and hence higher bioavailability, necessitating a lower therapeutic dose.[108]

In the work by Bryne *et al.,*[109,110] iron reducing bacterium *Geobacter sulfurreducens* was used to synthesize cobalt and zinc doped magnetite cores. The MNPs have the general formula $Fe_{3-x}M_xO_4$ where M = Co or Zn and x was increased from 0 up to 1. The magnetic as well as the physical properties of the MNPs were found to be dependent on the type and extent of doping (Fig 1.2.3 and 1.2.4). Variation of size with doping is seen in the TEM images of the substituted particles in Fig 1.2.3. The size falls with increase in doping levels and smaller sizes imply a higher surface to volume ratio. The high surface to volume ratio

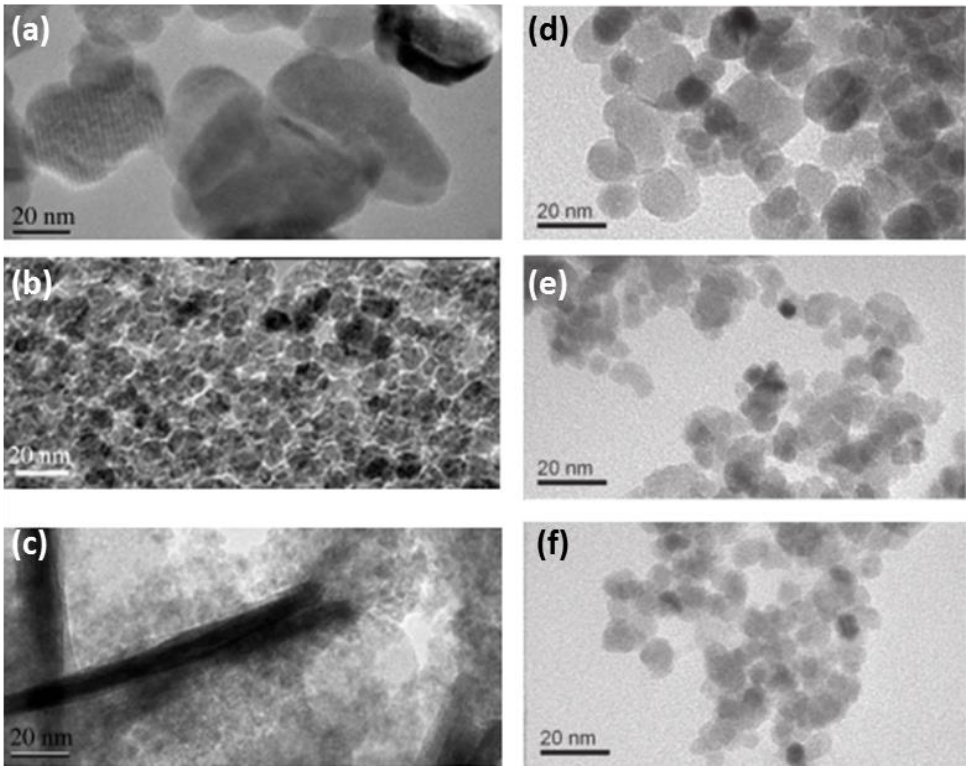

Fig 1.2.3 TEM images of bacterially synthesized doped iron oxide MNPs: Ultramicrographs showing the change in size of MNPs with type and level of doping: (a) $Co_0Fe_3O_4$, (b) $Co_{0.42}Fe_{2.58}O_4$ (c) $Co_{1.01}Fe_{1.99}O_4$ (d) $Zn_0Fe_3O_4$ (e) $Zn_{0.42}Fe_{2.58}O_4$ (f) $Zn_{0.92}Fe_{2.08}O_4$[109,110]

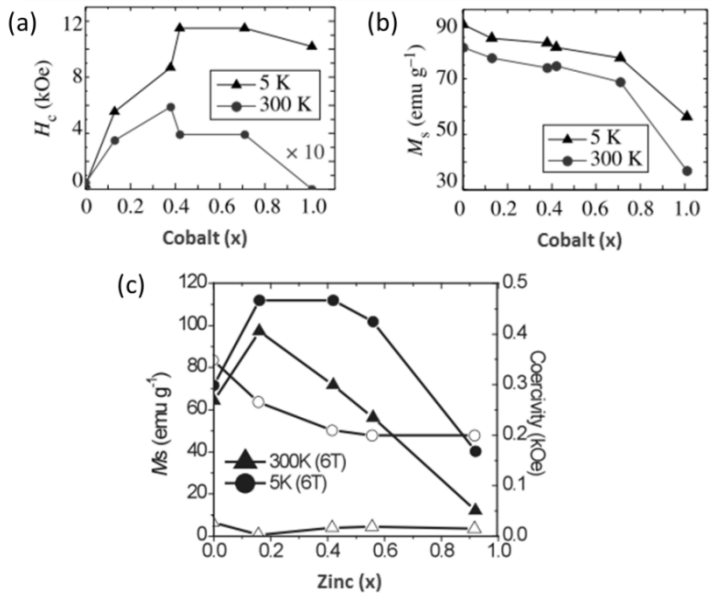

Fig 1.2.4 Dependence of magnetic properties of MNPs on the type and level of dopant: Plots show the change in coercivity (a) and saturation magnetization (b) of MNPs on level of Co (II) and for Zn (II) (c) at T=5K and 300K.[109,110]

increases the surface reactivity, and this could be an advantage when trying to surface-functionalize the particles with biocompatible materials and other biomolecules.

In these biogenic MNPs, Co (II) doping has a significant impact on the magnetic anisotropy (H_c, coercivity is a function of magnetic anisotropy) of the MNP up to mid-levels of doping (Fig 1.2.4a). With further increase, anisotropy falls to zero (at 300K) for x=1.01. The saturation magnetization (M_s) is maintained until x<1 (Fig 1.2.4b). Similarly, the effects of zinc doping on saturation magnetization and coercivity of MNPs are shown in Fig 1.2.4c. At 300K, for $Zn_{0.16}$, there is an increase in M_s and further doping decreases the M_s with $Zn_{0.92}$ being almost non-magnetic. Magnetic anisotropy, in contrast to cobalt doping, decreases with zinc doping. So it can be seen that depending on the type and extent of substitution, the magnetic properties of the MNPs can be altered. While high levels of doping cause the loss of magnetism in the MNPs, at lower levels, doping offers the opportunity to control two important magnetic properties, the saturation magnetization and the coercivity, allowing tailoring of the magnetic properties of nanoparticles for different applications.

1.2.4 Magnetic nanoparticle-mediated heating

Magnetic nanoparticles when exposed to an external oscillating electromagnetic field can transduce the field energy into heat. The magnetization, B of the MNPs lags behind the applied field, H as shown in Fig 1.2.5 and the area inside this loop corresponds to the energy dissipated. For one cycle, the net energy gained by the MNPs is a product of the volume of the magnetic material and the area inside the loop. Thus a high frequency field can generate proportionally higher levels of heating. This heating, referred to as the specific loss power (SLP; Units: W/g) can be defined as

$$SLP = energy\ per\ cycle \times applied\ field\ frequency \quad [1.1]$$

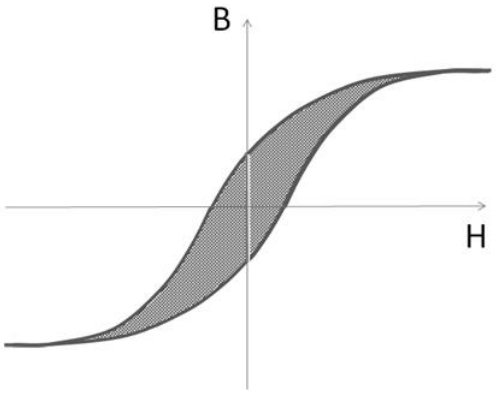

Fig 1.2.5 Magnetization vs external applied field: Plot showing the change in the magnetization of MNPs (B) with the applied field (H). The area inside the loop (shaded region) is a measure of the energy dissipated as heat, per cycle of the magnetic field.

Néel and Brownian relaxation

When placed in an oscillating field, MNPs in stable suspension respond by trying to align their magnetic moments along the direction of the external field. Upon field removal, the impact of the molecules in the suspension on the particle can cause random movement of the MNPs perturbing their orientation status (Fig 1.2.6a), a process referred to as Brownian relaxation.[111] In another mode of relaxation, known as Néel relaxation,[112] the MNPs do not physically move but only their internal moments are perturbed by thermal energy (1.2.6b). Depending on the field conditions and the particle's physical and magnetic properties, one mode of relaxation dominates over the other.

The Brownian relaxation time is given by the expression $\tau_B = 3\eta V_H/kT$ and it depends on the viscosity (η) of the solvent in which the particles are distributed, the hydrodynamic volume (V_H) of the particle and the ambient temperature (T). The product of k, the Boltzmann constant, and temperature T represents the thermal energy available to the

particle. The Néel relaxation time is given by the expression $\tau_N = \tau_0 e^{K_A V/kT}$ where K_A is the anisotropy constant (dependent on the magnetic core composition and shape) and V is the volume of the magnetic core. τ_0, the time constant is usually in the order of ~ 10^{-9}s. Comparing the expressions, it can be seen that unlike Brownian relaxation, the Néel relaxation is independent of the environmental parameters and depends purely on the core magnetic properties of the MNPs. From the expression for the net relaxation time (τ), $1/\tau = 1/\tau_B + 1/\tau_N$, it can be seen that the quicker relaxation is the predominant mode of energy dissipation.

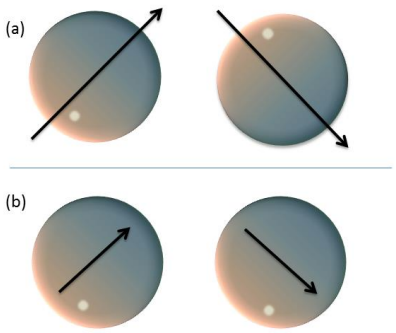

Fig 1.2.6 Simplified schematic of relaxation mechanisms: The schematic shows the movement of the entire particle during Brownian relaxation (a) and movement of only the internal magnetic moments during Néel relaxation (b) while the particle is stationary.

AC susceptibility (ACS)

The magnetic relaxation behaviour of MNPs can be assessed by measuring their alternating current (AC) magnetic susceptibility. When magnetic nanoparticles are placed under the influence of an oscillating magnetic field developed by an alternating current, their magnetic response or magnetic susceptibility changes with frequency. By studying this frequency dependant variation, information about the particle size, particle cluster size, magnetic behaviour in aqueous suspension, in cell-culture media and in cells, can be derived. When placed in an oscillating magnetic field, the relaxation process causes

dissipation of heat due to a phase lag between the external field and the magnetic moment of the MNPs. ACS measurements provide information about the phase lag of MNP populations and is a very good tool to identify optimum conditions for gaining maximum magnetic response from a population of MNPs.

For a stable aqueous suspension of magnetite nanoparticles exposed to an alternating magnetic field, the magnetization response can be described by the complex term $\chi = \chi' + i\chi''$, where χ is the AC magnetic susceptibility of the solution. χ' is the component of magnetic susceptibility that is in phase with the applied field and χ" is the 90^0 out-of-phase (quadrature) component. A typical susceptibility curve for blocked magnetite nanoparticle solution (particles that only show a single relaxation, in this case Brownian) is shown in Fig 1.2.7.

<< *copyrighted image* >

Fig 1.2.7 ACS data for an aqueous solution of blocked spherical magnetic particles: ACS measurements for MNPs at 20^0C having hydrodynamic radii of 75nm±7.5nm showing the in-phase component χ' and the quadrature component χ" of magnetic susceptibility.[113]

At the lower frequency end, the magnitude of χ' can be an indication of the amount of magnetic material present as it is the degree of the magnetization response for material exposed to a magnetic field. It decreases as the relaxation frequency is approached while the quadrature component peaks when $\omega\tau = 1$, where τ is relaxation time and ω the angular

frequency of the oscillating field (Fig 1.2.7). The relaxation frequency is the frequency at which the particle's magnetic moment is 45^0 out of phase with the external field direction (where the quadrature component peaks) and corresponds to frequency above which maximum energy is dissipated in the form of heat. From ACS measurements the relaxation frequency can be identified and the appropriate field parameters for magnetic hyperthermia can be estimated.

When Brownian relaxation dominates, the hydrodynamic sizes of the MNPs can be calculated by identifying the frequency f at which the quadrature component of the ACS, peaks. Using the expression for Brownian relaxation time, $\tau_B = 4\pi\eta {r_H}^3/kT = 1/2\pi f$ (Boltzmann constant, k=1.38x10^{-23} kg.m.s^{-2}.K^{-1}) the hydrodynamic radius (r_H) can be calculated. Brownian relaxation is a low energy process compared to the Néel relaxation process. This is because, for the internal oscillation of the magnetic moment (Néel relaxation), the thermal energy should be higher than the energy barrier due to the anisotropy of the particle. Hence, the Néel relaxation peak for ACS is usually observed at higher frequencies than for Brownian. This is also the reason why MNPs with high anisotropy, like the cobalt doped MNPs, cannot show Néel relaxation. Their high anisotropy results in a high energy barrier that usually cannot be superseded by thermal energy at ambient conditions.

The frequency-dependent ACS for a polydisperse MNP population comprising of clusters of individual nanoparticles, can be modelled with varying anisotropy constants (K), as shown in Fig 1.2.8.[114] When the anisotropy is very low or too high, a symmetrical χ" peak at either low frequency corresponding to Brownian (Fig 1.2.8f) or high frequency corresponding to Néel (Fig 1.2.8a) relaxation is observed. The frequency at which the Brownian peak occurs corresponds to the mean cluster diameter while that of the Néel

peak corresponds to the mean particle diameter. For intermediate anisotropies, a part of the population is large enough to relax by the Brownian mode while the smaller part of the population relaxes via the Néel mode. Hence for these cases, asymmetrical peaks having a contribution from both Brownian and Néel are observed.

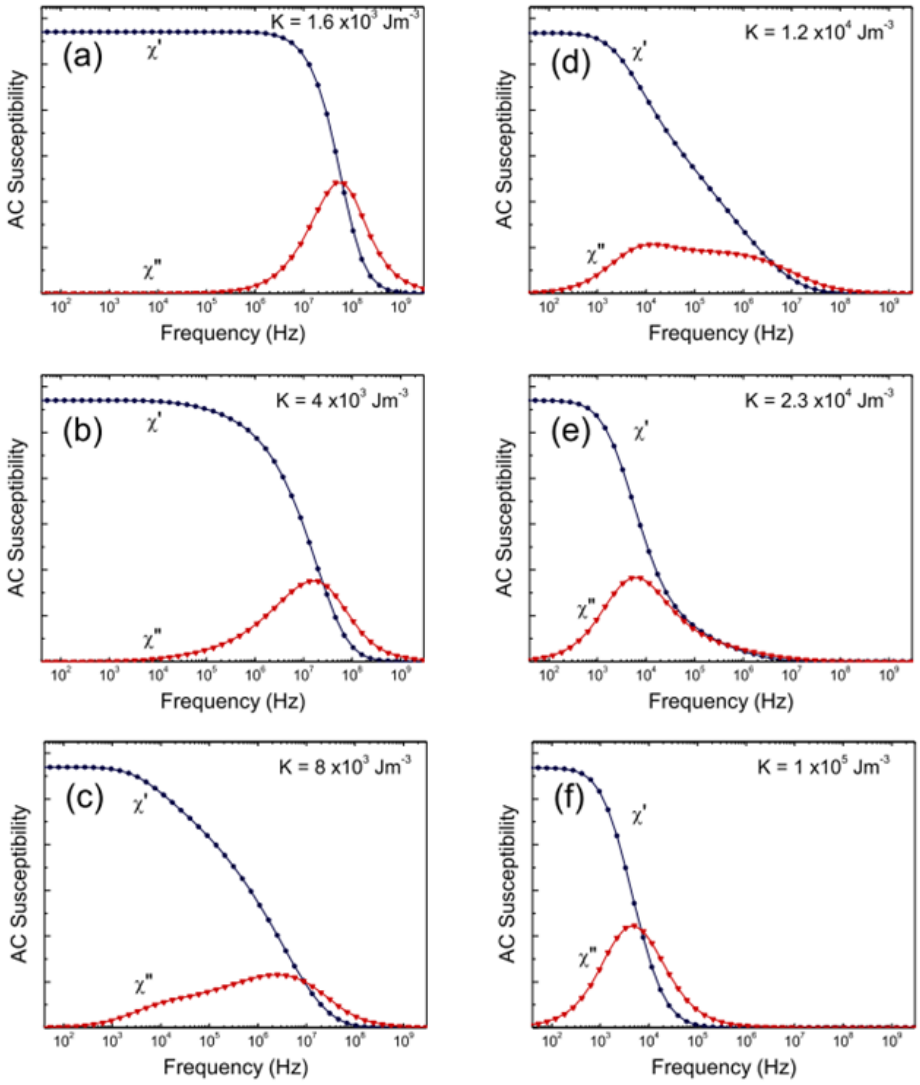

Fig 1.2.8 ACS simulation plots for MNP populations with varying anisotropy values: Samples showing pure Néel (a), combinations of Néel and Brownian (b-e) and pure Brownian (f) relaxations. Modelling parameters include particle core diameter, D= 15.5 nm and polydispersity, σ(D) = 0.2 with cluster diameter D_H = 40 nm and σ(DH) = 0.30 dispersed in water at 310 K (η = 7 x 10-4 Pa s).[114]

As seen earlier, the particle diameter affects the mode of relaxation and hence determines the optimum frequency for relaxation as detected by ACS measurements.[115] Hence ACS has found applications in biosensing to detect the interaction of biomolecules with MNPs.[113,116] Shifts in the peak frequency can be used to detect and estimate the change in the hydrodynamic size due to binding of biomolecules. ACS measurements can also give information about the way MNPs interact with cells and the degree of immobilization and clustering of the MNP cores in a cellular environment.

Specific loss power

When placed in an oscillating magnetic field, nanoparticles can transduce a part of the external energy into thermal energy. If the magnetisation relaxation processes discussed previously are dominant (which is more likely for weaker magnetic fields), the SLP is a function of the magnetic field strength (H) and the effective relaxation time (τ). For low external field parameters (where B is linear with H), at the resonant frequency, the SLP is due to relaxation (either Néel or Brownian). At stronger field conditions (beyond the linear range), and for frequencies above the Néel relaxation frequency, the MNPs can also dissipate heat due to hysteresis losses (Fig 1.2.5).[117] ACS measurements can help predict the frequency beyond which MNPs can show very high thermal energy losses during magnetic hyperthermia.

For clinical applications, due to the limit on the magnetic field conditions that can be used, particles that can show heating effects within these limits are desired (see Chapter 1 section 1.2.2 for more details). Therefore doping with divalent cations, which affects the magnetic properties of the MNPs, can be used to tune the relaxation frequency and hence show better heating efficiency than pure iron oxides.

1.2.5 Assessing biocompatibility of doped nanoparticles

As discussed in the previous section, the magnetic properties of iron oxides can be tuned to suit the end application by altering their composition. Elements from the transition series such as cobalt and zinc are being investigated for their effects on the magnetic properties of iron oxide cores upon doping (refer Section 1.2.3 –Substituted iron oxides). When doping iron oxide cores with other elements, the doped element replaces iron atoms in the crystal lattice. Depending on the ability of the doped material to interact with cells in its ionic form, either by dissolution or due to exposure of the surface atoms, it could alter the biocompatibility of the MNPs as these metals could be cytotoxic in their ionic form. It is essential to ensure the biocompatibility of doped nanoparticles prior to employing them for cellular and clinical applications.

Cobalt doping of magnetite alters the nanoparticles' magnetization and depending on the level of substitution can enhance the heating power of the nanoparticle suspension. However, cobalt in its ionic form is a known cytotoxic agent.[118,119] Cobalt's cytotoxicity has been studied to determine the safety of cobalt alloys in implanted orthopaedic prosthetics and the cytotoxicity of metal particles were compared to that of a cobalt chloride salt.[120] Clear signs of loss in cellular viability were observed for the cells exposed to its salt where cobalt is available freely in its ionic form. The cobalt chromium alloy particles also showed strong cytotoxicity which was attributed to their relatively high solubility (4µmol/l after 7 day incubation). In foetal rat dermis-derived fibroblasts, it was found that 5µg Co2+/ ml (~85µM) is almost 100% cytotoxic at 48 hours and it was proposed that cobalt ions exerted toxicity by having an effect on the respiratory mechanism of the cells.[119] Cobalt chloride is highly toxic to human synovial fibroblasts at 500 µM after 72 hours of exposure.[120] The concentration at which cells undergo complete necrosis

depends on the cell type, and the high concentrations of the salt form can be set as the positive control when assessing the cytotoxicity of cobalt-doped nanoparticles.

A number of cytotoxicity or cell viability assays are available to assess biocompatibility of nanoparticles. Each assay estimates cytotoxicity by measuring some aspect of cell death. It is important to use the right assay for the particular toxic agent being studied depending on the mode of cytotoxicity. In a work done by Yang *et al.*,[121] four different nanoparticles were investigated for their cytotoxicity, genotoxicity and oxidative effects. Based on the methyl thiazolyl tetrazolium (MTT) assay and water-soluble tetrazolium assay (WST), they found that zinc oxide nanoparticles (ZnO) exerted a higher cytotoxic effect compared to single wall carbon nanotubes, carbon black and silicon dioxide nanostructures. Carbon nanotubes caused more DNA damage (genotoxicity) than cytotoxic effects which was quantified by measuring the amount of breaks in the DNA strand through the comet assay. Assessing intracellular oxidative stress by measuring glutathione depletion, malondialdehyde production, superoxide dismutase inhibition and reactive oxygen species generation showed that it was the primary mechanism of cytotoxicity for all four nanostructures tested.

A detailed comparison of nine different cytotoxicity assays for five different nanomaterials was done by Monteiro-Riviere *et al.*[122] Table 1.1 gives a summary of the cytotoxicity assays compared. The MTT and Alamar blue assays work by measuring mitochondrial metabolic activity. In the MTT assay, active mitochondrial enzymes in viable cells convert the tetrazolium salt to purple formazan which is then measured colorimetrically whereas in the Alamar blue assay, the mitochondrial metabolic activity reduces a blue coloured redox indicator, resazurin into a red fluorescent dye, resorufin.

Assay number	Assay	Stain/Dye	Action
01	Trypan blue	Blue dye stains dead cells	Cell membrane integrity
02	Calcein-AM	Green fluorescent dye stains live cells	Enzymatic activity
03	Live/Dead®	Green fluorescent dye stains live cells; Red fluorescent dye stains compromised cells	Enzymatic activity and cell membrane integrity
04	Neutral red	Lysosomal uptake in live cells	Lysosomal membrane
05	MTT	Tetrazolium conversion to insoluble purple formazan in live cells	Mitochondrial etabolic activity
06	CellTiter 96® AQueous One	MTS conversion to soluble purple formazan in live cells	Mitochondrial metabolic activity
07	Alamar Blue®	Resazurin reduction to red fluorescent dye resorufin by live cells	Mitochondrial metabolic activity
08	CytoTox One™ Homogeneous Membrane Integrity	LDH enzymatically reduces resazurin into resorufin	Cell membrane integrity

Table 1.1 Summary of Cytotoxicity assays, the dyes used and the cellular property tested to assess viability (Adapted from Monteiro-Riviere et al. 2009[122]*)*

The lactate dehydrogenase (LDH) and the trypan blue assays work on the principle that dying or dead cells have compromised cellular membranes. In the LDH assay, cells with compromised membranes leak the enzyme LDH into the culture medium which converts the assay reagent into a fluorescent dye which is then measured fluorimetrically. In the Trypan blue assay, the trypan blue dye is membrane impermeable and is taken up only by dying or dead cells with compromised plasma membranes. Live cells are not stained and cell count under a light microscope is used for quantification. The method suffers from drawbacks of variability arising due to manual counting and the fact that it is time consuming can lead to false positives due to cell death during the assay. Hence trypan blue, in spite of being an inexpensive and quick method to assess cell viability, fails in accuracy for assessing large sample numbers. It could be used as a perfunctory estimate for

experiments with larger number of samples and other fluorimetric or colorimetric based assays could be used along with the trypan blue method to increase the confidence of the results.

In the calcein-AM assay, the acetomethoxy (AM) derivate of calcein, calcein-AM, a neutral membrane permeable non-fluorescent molecule, is taken up non-specifically by both live and dead cells. Active esterase enzymes, found only in viable cells, remove the acetomethoxy group generating the highly negative membrane impermeable fluorescent molecule calcein that stains live cells green (Fig 1.2.9). Live/Dead® assays use calcein AM for staining viable cells and ethidium homodimer (EthD) or propidium iodide (PI) to stain dead cells. EthD and PI have very low fluorescence and are membrane impermeable. Their fluorescence increases many-fold when they chelate with DNA strands upon non-specific uptake by non-viable cells. The Live/Dead® assay employs both the loss of membrane integrity in dead cells and presence of active enzymes in viable cells to assess cytotoxicity and hence provides more confidence in the quantification. The level of staining can be quantified both by fluorimetry and by flow cytometry.[123]

<*copyrighted image*>

Fig 1.2.9 Calcein staining of live cells: HEK cells exposed to 0.1mg/ml carbon nanomaterials (CNM) for 24h (arrows point to CNM aggregates). Viable cells are stained bright green. Bar = 680µm.[122]

In the Live/Dead® assay, two fluorescent dyes are used and different detectors in the flow cytometer quantify the intensity of the emitted fluorescence as well as the fraction of population stained for each dye. A dot plot of the live stain channels fluorescence against that of the dead dye can be divided into four quadrants (Fig 1.2.10). Cells stained high for the individual dyes give information about the completely viable and compromised populations. Cells staining high for both the dyes are cells thought to be intermediate between healthy and compromised cells.

< *copyrighted image* >

Fig 1.2.10 Fluorescence dot plot of ungated Calcein vs. propidium iodide stained K562 cells after 4 days in culture. Quadrants are marked to indicate live, dead and hurt (intermediate between live and dead) populations. The single parameter histograms are shown along the axes. [123]

The advantage of using flow cytometry is that, apart from giving information about cytotoxicity, the side versus forward scatter plots can be used to assess MNP uptake. The side scatter is a measure of the roughness or granularity of the cell. Cells exposed to MNPs show an increase in granularity and this can be used as a measure of MNP uptake (Fig 1.2.11).[124]

Studying cytotoxicity using well established cytotoxicity assays that have provided accurate results for classical toxicology studies, in the case of nanomaterials, gives variable

and sometimes even contradictory results[122]. This is predominantly due to the fact that the assay does not measure cytotoxicity as imparted by the toxic agent. It is important to understand the mechanism of toxicity imparted by the nanoparticles to choose the appropriate assay when measuring cell viability. Equally important is performing preliminary studies to establish cell parameters within which the assays are linear and setting up the necessary controls to remove artifacts and other assay related errors.

< *copyrighted image* >

Fig 1.2.11 Change in side scatter (SS) with MNP interaction: Increase in the side scatter (SS) of cells is observed when the nanoparticle concentration added to cells is increased.[124]

1.3 Magnetic Nanoparticles for Stem Cell Differentiation

1.3.1 Mechanotransduction

As seen earlier (Fig 1.1.1), cells are constantly exposed to various types of physical forces which in turn influence their behaviours. A fine example is the bone tissue, one of the most load bearing components of the body. It is constantly exposed to various types of loads that cause remodelling of the tissue architecture so as to adapt to the changing stress and strain conditions it is subject to.[125] Cells in the bone act as sensors of these mechanical forces to elicit an adaptive response[23,126] Many different types of cells such as osteoprogenitor cells, MSCs are found in the bone tissue that can give rise to bone cells known as osteoblasts, which in turn secrete the ECM of the bone tissue.

Mechanical conditioning of MSCs *in vitro* has been shown to trigger differentiation of the cells. Macro-level applications of mechanical forces use direct compression/ tensile force systems or fluid-flow induced shear stress systems. These techniques, although having a significant effect on the differentiation behaviour of stem cells, suffer from disadvantages. The most prominent one is the inhomogeneous application of force especially in 3D systems such as cell-seeded scaffolds. Also, depending on the type and level of force being applied, the right choice of scaffold strength and shape need to be chosen which instead should be dependent on the tissue type being developed.

One of the primary mechanosensors in cells is the integrin molecule. Integrins are transmembrane proteins which associate with matrix components through their extracellular domain while inside the cell they interact with cytoskeletal components via focal adhesion proteins. They transmit extracellular mechanical signals to the cell by modifying the cytoskeleton which in turn regulates cellular processes.[127,128] The other important cellular-level mechanosensors are the stretch sensitive membrane cation channels where the mechano-actuation of these channels causes an inward current. This increases intracellular cation concentrations to directly promotes gene expression or depolarizes the membrane to activate voltage-gated membrane channels and thereby promote gene expression.[129]

A direct method of stimulating the mechanosensitive machinery of the cells is by using magnetic nanoparticles. Nanoparticles can attach to specific cell surface receptors when suitably functionalized with biomolecules such as membrane receptor ligands (Fig 1.3.1). The force applied via magnetic nanostructures is higher, more homogenous and controlled than bulk application of forces such as via fluid flow, compressive or tensile forces applied to cell seeded scaffolds. Some of the first experiments using magnetic nanoparticles to

apply mechanical forces on membrane components studied changes in the properties of the cytoplasm under an applied stress. In the work by Wang and Ingber,[130] ferromagnetic microbeads, suitably coated with ligands specific for integrins, such as fibronectin or collagen (Fig 1.3.1a) were first magnetically blocked by a strong field pulse. Upon applying a second rotating magnetic field, it was possible to apply a torque which caused the beads to show a twisting motion (Fig 1.3.1b). By gauging the force necessary to twist the particles, the mechanical properties of the cytoskeleton could be investigated. Another type of magnetic mechanical force can be applied by exposing superparamagnetic (not magnetically blocked) particles to a gradient field. The magnetic particles exhibit translational motion (Fig 1.3.1c) that stimulates nearby mechanosensitive ion channels.[131–134]

Magnetic actuation of mechanosensitive ion channels was found to trigger osteoprogenitor cells to differentiate down the osteogenic lineage.[135] Silica coated 250nm magnetite or maghemite particles were used to mechanically stimulate encapsulated or monolayers of human bone marrow stromal cells (HBMSCs), *in vitro* and *in vivo*. The MNPs were covalently functionalized with anti-TREK antibody to target the extracellular domain of the mechanosensitive TREK channels, which are known to play a role in osteogenesis[82] or RGD (arginine–glycine–aspartic acid) peptides that bind integrin molecules (Fig 1.3.2A). The cells were grown as monolayers and in 3D encapsulated within alginate/ chitosan capsules *in vitro* and by subcutaneous implantation in MF-1 nu/nu immunodeficient mice *in vivo* (Fig 1.3.2B- D). Mechanical stimulus as a cyclic load was applied by exposing MNP bound cells to a 1Hz frequency field for 1 hour every alternate day. Monolayers were treated for a 7 day period while encapsulated cells were exposed to the loading regime for a 21 day period. Results showed that MNPs had low cytotoxic effects on both cells grown

< copyrighted image >

Fig 1.3.1 Mechanical activation of membrane receptors using MNPs: (A) MNPs can be bound to various biomolecules specific to different cell surface receptors; (B) Magnetic twisting cytometry: MNPs apply mechanical torque to the membrane receptor when exposed to an external magnetic field perpendicular to the particle's magnetic dipole moment (μ). The shear stress thus imparted activates the stretch activated calcium channels (SAC) and integrin molecules. (C) MNPs displaying translational motion when exposed to a magnetic field gradient. It is reported that up to 10nN forces can be applied in this technique.[129]

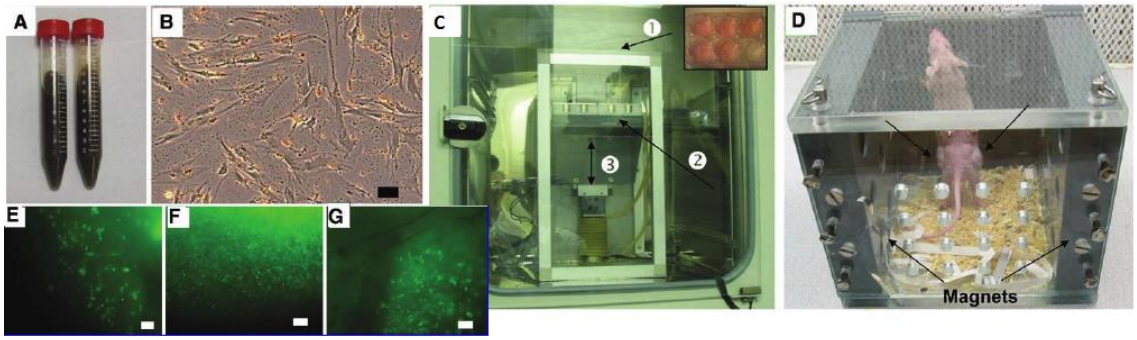

Fig 1.3.2 Biomedical applications of MNPs: (A) Colloidal suspensions of 250nm MNPs coated with silica and bound to anti-TREK-1 antibody (100ug/ml) or RGD. (B) HBMSCs labeled with MNPs (5-15 particles/ cell). (C) Magnetic bioreactor treating six-well plate MNP labeled cells seeded in alginate/ chitosan scaffolds exposed to a pulsed magnetic field which moves up and down. (D) Magnetic box containing mice subcutaneously implanted with MNP-labeled cell seeded capsules exposed to magnetic field conditions for 21 days. Cell viability was estimated by the cell tracker green/ ethidium homodimer-1 staining for HBMSCs seeded scaffolds (E) and capsules with the HBMSCs+TREK-1 particles (F) and HBMSCs-RGD particles (G) at 21 days from the treated mice. Scale bars: B- 50 mm; E–G-100 mm.[135]

in monolayer and in 3D (Fig 1.3.2E-G) as observed by CellTracker™ Green and ethidium homodimer staining. Increase in the expression of osteogenesis and chondrogenesis marker genes osteopontin and Cbfa1, respectively was observed in the monolayers, whereas in the encapsulated cells, there was increased synthesis of proteoglycans, collagen

type 1 and 2. Other similar studies have shown elevated expression of the osteogenic genes and proteins including alkaline phosphatase upon mechanical conditioning of bone marrow-derived stem cells.[136,137]

1.3.2 MNPs for localized elevation of temperature in cells

As mentioned earlier, MNPs dissipate heat energy when placed under the influence of an alternating field. This property can be used to provide the necessary thermal stimuli to activate heat sensitive ion channels in a fashion similar to mechanostimulation of stem cell differentiation. In the work by Huang *et al.*[138] and Stanley *et al.*[139] neuronal cells expressing heat sensitive ion channel TRPV1 were remotely manipulated using a radio frequency field. Superparamagnetic manganese ferrite nanoparticles ($MnFe_2O_4$, φ=6nm) were functionalized with streptavidin and coated with fluorophore DyLight549 to target genetically engineered neuronal cells expressing biotinylated transmembrane proteins also tagged with a fluorophore, cyan fluorescent protein (CFP).[140] Upon exposure to a radio-frequency (RF) field (40MHz, 0.84mT), the MNPs generated a highly localized temperature rise (0.62^0C/s) resulting in the activation of the cation channels TRPV1 (Fig 1.3.3 b-d). The field conditions used exceed the safe limits for *in vivo* applications[103,104] but the results give a proof of concept to show that magnetic hyperthermia-mediated stimulation of heat sensitive ion channels is possible and can be extrapolated to remotely control stem cell behaviour for regenerative medicine purposes.

< *copyrighted image* >

Fig 1.3.3 Remote activation of membrane ion channels using MNP technology: MNPs can be functionalized to bind heat sensitive ion channel TRPV1 directly (a) or to nearby membrane channels (b and c). Upon exposure to an alternating field B, the MNPs generate heat and activate TRPV1 (a and c) and cause influx of Ca^{2+} *ions triggering intracellular signaling pathways and finally gene expression. (d) Highly localized nature of the heating effect is shown by a spike in the temperature at the position of the MNP which falls linearly with distance along the plasma membrane.*[138,139]

Enhancing proliferation and differentiation potential along a specific lineage would improve success of stem cell-based regenerative therapies. Magnetic nanoparticles allow precise application of localized mechanical forces or thermal energy directly to the cell's sensory machinery, namely the mechanosensitive and heat sensitive ion channels. This allows a much higher degree of control over the consequent cellular response. Another advantage of using MNPs is the ability to localize them to different regions of the cells including the membrane for targeting ion channels or intracellularly following endocytosis which could lead to more enhanced HSP response. With the ability to target different regions, there is an opportunity to investigate and understand the different cellular components playing a role in heat stimulated regulation of stem cell differentiation. Hence,

this could lead to the development of a more efficient approach to stimulate stem cell differentiation.

1.4 Thesis Aims and Objectives

From the available scientific literature it appears that a mild heat shock can positively influence the behaviour of cells, including their osteogenic differentiation. The literature also suggests that magnetic nanoparticles can be used to provide the thermal stimulus. However, the relation between heat and cellular behaviour has not been clearly established, especially in terms of the cellular mechanisms underlying the translation of the stimulus to a response. To fill this gap, in this thesis, it is aimed to investigate the effect of elevated temperature on the differentiation behaviour of cells using magnetic nanoparticles. To achieve this, the key objectives defined are as follows:

- To investigate the role of heat shock applied using conventional methods on the viability and osteogenic differentiation behaviour of cells
- To investigate the suitability of bacterially synthesized doped magnetic nanoparticles for cellular heating applications
- To develop magnetic nanoparticle based approaches to apply heat shock in different subcellular regions and thereby investigate the role of different cellular components involved in translating the heat stimulus.

Two different cell types were employed in this study: the primary stem cell hMSCs and cancerous cell line, MG-63s. Cell lines and primary cells act as suitable models for understanding responses to external stimuli on cellular behaviour. hMSCs are multipotent stem cells which have shown promise in treating connective tissue injuries[141] and MNPs

have been used in stem cell based therapies to trigger osteogenic differentiation as well as for stem cell tracking *in vivo*. Hence hMSCs are good candidates for evaluating the suitability of the doped MNPs for cellular applications. Cell lines, being easy to culture and having a high turnover rate are a time and cost effective alternative to primary cells. In particular, MG-63 cells are a good model for studying osteogenic differentiation as they mimic the bone precursor cell phenotype. Also being a bone cancerous cell line, the behaviour of MG-63 cells is also important from the aspect of understanding the response of transformed cells to physical stimuli.

It is hoped that the finding in this thesis will help further our understanding of the role of temperature in dictating cell behaviour. Also, the magnetic nanoparticle based approach could emerge as a more efficient and targeted alternative to conventional heating techniques. In addition, it can provide information on the role of various cellular components in translating the thermal stimuli into a cellular response.

CHAPTER 2 Materials and methods

2.1 Nanoparticle preparation

Commercially available magnetite nanoparticles (MNPs), prepared via chemical routes of synthesis, were obtained from Sigma, UK. They are referred to as 'synthetic magnetite' in the rest of the sections. Bacterially synthesized (referred to as biogenic) nanoparticles were obtained from collaborators in the School of Earth, Atmospheric and Environmental Sciences (SEAS), Manchester University, UK. These nanoparticles were produced using iron reducing bacteria *Geobacter sulfurreducens* according to the method described in the work by Byrne *et al*.[109,110] The chemical (composition of the magnetic cores), physical (size and polydispersity) and magnetic properties of these particles have been thoroughly assessed previously.[109,110]

2.1.1 Preparation of stable suspensions of MNPs by citric acid coating

Stable colloidal suspensions of citric acid coated synthetic magnetite, biogenic undoped magnetite, zinc and cobalt doped magnetite were prepared. Dry powders of the nanoparticles were weighed and made up with water to final concentrations of 20mg/ml. The pH was adjusted to ~2 where the particles had a higher zeta potential (surface charge) of ~ +20mV that would help prevent particles from aggregating due to electrostatic repulsion. The suspension was sonicated for 2 minutes to break down large clusters. Citric acid powder was added to this suspension to get a final concentration of 15mg/ml. The pH was adjusted to 5.2 as at this pH two out of the three carboxyl groups on the citric acid moiety are present as COO^- and can interact with the surface of the MNP electrostatically. This solution was heated at 80^0C for 30min with intermediate sonication to facilitate further breaking down of clusters and hence better coating. Following the heating step, the excess citric acid was removed by magnetic decantation, the MNPs were washed with

acetone to remove excess citric acid and resuspended in de-ionized water at pH >9 (zeta potential of the coated MNPs was measured to be ~ -40mV at pH 9). To break down the clusters even further and remove the large unstable clusters, the suspensions were subject to a combination of centrifugation (5min at 4000rpm), sonication (2min) and vortexing (30s). Large clusters were pulled out of suspension using a magnet resulting in stable suspensions of MNPs.

The coating technique was able to successfully break the large clusters that uncoated particles are usually present as and to coat them resulting in stable colloidal suspensions of the nanoparticles. Following the coating procedure, the suspensions were filter sterilized using 0.2μm filters to make them suitable for cellular experiments and also with an aim to remove any large nanoparticle clusters still left in the suspensions.

2.1.2 RGD biofunctionalization

For functionalizing the MNPs with the RGD peptide the following protocol was adopted. 0.1-1mg (0.3ml) of sterile citric acid coated MNP solution was mixed with a fresh sterile solution of 31mM N-(3-Dimethylaminopropyl)-N′-ethylcarbodiimide hydrochloride (EDC; Sigma, UK) and 0.1mM N-Hydroxysuccinimide (NHS; Sigma, UK) in 0.5M MES (2-(N-morpholino)ethanesulfonic acid; Sigma UK) buffer, pH 6.3. For 1mg (0.1ml) of MNP solution, 20μl of EDC/NHS solution was added. The EDC/NHS system acts as the activator molecule. Following the activation step (incubation for 1h at room temperature) the excess EDC/NHS was washed off with 0.1M MES, pH 6.3. The MNPs were magnetically separated for the washing steps. For every 1mg of MNP, 25μg of RGD was added in 0.3ml of 0.1M MES buffer and mixed gently by pipetting up and down. Samples were mixed overnight at 4^0C to enable RGD binding. Following incubation, excess RGD

was washed off with 0.1M MES buffer and the functionalized MNPs were resuspended in sterile water. The entire process is carried out with sterile solutions in a sterile environment.

2.2 Nanoparticle characterization

2.2.1 Size and Zeta potential measurements

The Dynamic light scattering technique was used to measure size of MNPs in a Zetasizer (Malvern, UK) instrument. Size measurements were done at a scattering angle of 90^0 and at temperatures of 25^0C and 37^0C. The samples were diluted in distilled water to concentrations below 0.1mg/ml where the counts per second were within the valid range (50-200kcps) for particle size measurements. Zeta potential measurements were carried out in the Zetasizer (Malvern, UK) with similar temperature conditions and concentrations as the size measurements.

2.2.2 Prussian blue staining

The Prussian blue staining technique was used to stain for iron and hence detect presence of MNPs. The ferric ions (3+) in the sample (MNPs) react with the ferrocyanide in the stain to form a ferric ferrocyanide complex that is blue in colour. Cells were first fixed with 95% methanol (15min at room temperature) following which they were treated with acidic solution of 5% potassium ferrocyanide. This solution was prepared fresh by mixing 20% aqueous solution of Hydrochloric acid (v/v) and 10% aqueous solution of potassium ferrocyanide (w/v) and incubated with cells at room temperature for 20min. After excess stain was washed off, the cellular nuclei were counterstained with Nuclear fast red (Sigma, UK). After removing excess stains by repeated washing with de-ionized water, bright field

images of the cells were taken using the LAS imagining software on a Leica DMIL microscope fitted with a camera. All reagents were obtained from Sigma, UK.

2.2.3 Characterizing magnetic properties: AC Magnetic Susceptibility

200µl of nanoparticle suspensions in water or cell-culture media were exposed to a band of frequencies ranging from 10 to 10^6 Hz and their magnetic susceptibility measured. For cellular uptake studies, cells incubated with the nanoparticles for 72h, washed and resuspended in culture media were used. To measure immobilized nanoparticles, MNPs were resuspended in glycerol, due to its high viscosity.

The frequency f, at which the susceptibility peaks for particle clusters of a few nanometer dimensions within the frequency range tested, corresponds to Brownian relaxation. The hydrodynamic radius can hence be calculated using the expression $\tau_B = 4\pi\eta {r_H}^3/kT = 1/2\pi f$ where η is the viscosity of the solvent (water, η= 1 x 10^{-3} Pa.s at room temperature), k, the Boltzmann constant (k=1.38x10^{-23} kg.m.s^{-2}.K^{-1}) and T, the temperature (room temperature, 298K).

2.3 Iron quantification methods

2.3.1 Gravimetric analysis

Sample concentrations were measured via gravimetric methods by drying out 1ml of the sample at ~80^0C overnight (weight did not reduce with further evaporation) and weighing the powder.

2.3.2 Ferrozine assay

MNP samples (200µl) were digested with acid (100µl of 6M Nitric acid) at temperatures >60^{0}C overnight to release iron in its ionic form. Following this, the 150µl of the sample was treated with equal volumes of reducing agent, 6.6M hydroxylamine hydrochloride for 2.5h at room temperature. This reduces Fe^{3+} to Fe^{2+} as the Ferrozine assay is specific for the latter. 100µl of the reduced sample was then treated with 700µl of 2mM Ferrozine reagent (0.1g Ferrozine+ 5ml HEPES buffer made up to a 100ml with distilled water). Ferrozine binds to the Fe (II) ions to form a complex that strongly absorbs at 562nm. Absorbance was read at 562nm on a Biotek synergy2 plate-reader using the GEN 1.05 software. Standard curves were plotted using Fe^{2+} and Fe^{3+} standard salts/ solutions.

2.4 Cell Culture

MG-63, an osteosarcoma cell line (up to passage 100; Lonza, USA) and human bone marrow derived primary mesenchymal stem cells (hMSCs, up to passage 5; Lonza, USA) were cultured under sterile conditions within class II biological safety cabinets. Cells were seeded in expansion medium consisting of 4.5gL^{-1} glucose Dulbecco's Modified Eagle's medium (DMEM; Lonza, UK) supplemented with 10% Fetal bovine serum (FBS), 1% Penicillin/ Streptomycin (antibiotics and antimycotics) and 1% L-glutamine (referred to as expansion media). They were grown in sterile T-flasks or well plates at 37^{0}C in a CO_2-regulated incubator and the cell-culture medium was changed once every 3 days. The old medium was aspirated and pre-warmed (37^{0}C) expansion medium was added to the cell-culture flasks. When the flasks reached ~90% confluency, the cells were trypsinized (see section 2.4.2), their numbers counted (see section 2.4.2) and re-seeded at 5000 cells/cm^2 in sterile T75 flasks with ~15ml expansion media. hMSCs were not used beyond passage 5.

2.4.1 hMSC isolation

hMSCs were isolated from commercially available bone-marrow aspirates (Lonza, USA) from young male donors by selecting for adhesion.[142,143] The aspirates were seeded in T75 flasks in 15ml of cell isolation medium (1mg/ml glucose DMEM with 10% FBS, 1% Penicillin/ Streptomycin and 1% L-glutamine) and cultured for 7 days. Following this, a 50 % media change with hMSC isolation medium was performed and another 7 days later a 100 % media change to expansion medium. Cells that had adhered to the tissue culture plastic after 14 days in culture were identified as hMSCs. Adherent hMSCs were stored for future use in cryopreservation media consisting of 10% FBS with 90% sterile Dimethyl sulfoxide (DMSO; Sigma, UK) in liquid nitrogen.

2.4.2 Determination of cell numbers

The cell-culture medium was aspirated and cells washed with sterile phosphate buffer saline (PBS; Sigma, UK). Following the washing, 1x Trypsin-EDTA (Lonza, UK) enzyme diluted in PBS solution was added to the cells at volumes sufficient to cover the monolayer. The cells were incubated with the Trypsin for 3-5min at 37^0C. The flask was tapped gently to detach the cells and cell detachment was confirmed microscopically. Cell-culture medium was added at 3 times the volume of Trypsin to deactivate the enzyme. The cells were completely detached by pipetting the solution up and down and then were transferred to centrifuge tubes. Cells were pelleted by centrifuging the sample at 1000rpm for 3min. Lower speeds of 800rpm were used for cells associated with MNPs to reduce risk of cellular damage due shearing by the MNPs. The supernatant was removed and the cell pellet resuspended in fresh media (1-5ml). 11µl of the cell suspension is mixed with equal volumes of Trypan blue (Sigma, UK) and incubated for 1min.The mixture is loaded onto a haemocytometer at 10µl per chamber of the haemocytometer. Cells were counted manually

in a bright field microscope. Unstained cells were considered viable and trypan blue stained cells dead. The cell count was calculated by taking into consideration the dilution factor for trypan blue addition.

2.4.3 Chemical stimulation of differentiation

For triggering differentiation in cells chemically, the expansion medium was supplemented with chemicals specific to each type of differentiation as shown in table 2.1.

Media and Supplements	**Concentration**
Osteogenesis	
Dexamethasone	0.1 μM
Ascorbic Acid	50 μM
B-Glycerophosphate	50 mM
Adipogenesis	
3-Isobutyl-1-methylxanthine	0.5 mM
Dexamethasone	0.5 μM
Insulin	10 μg/ml
Indomethecin	100 μM
Chondrogenesis	
Insulin, Transferin, Sellenium Prefix	1% v/v
Dexamethasone	0.1 μM
Ascorbic Acid	50 μM
L-proline	40 μg/ml
Sodium Pyruvate	1% v/v
Transforming growth factor-β3 (Peprotech, UK,)	10 ng/ml
FBS	1% v/v

Table 2.1 Chemical supplements for preparation of differentiation media: Osteogenic and adipogenic media were prepared in expansion medium with 10% FBS while chondrogenic mediium was prepared in expansion medium containing 1% FBS. All reagents were obtained from Sigma, UK unless otherwise specified.

2.5 Characterization of the hMSCs

2.5.1 Trilineage differentiation potential

The multilineage potential of hMSCs to differentiate into osteocytes, chondrocytes and adipocytes was confirmed. Cells were seeded into 24 well plates and cultured in expansion medium or the relevant differentiation media (Table 2.1) for 21 days. Following this, the cells were fixed with 95% ice-cold methanol (Fisher Scientific, UK) at room temperature for 15min for cells in expansion, osteo- and chondrogenic media whilst for cells in adipogenic medium 4% paraformaldehyde was used (for all experiments). The fixed cells were stained histologically using Alizarin red for confirming osteogenesis (section 2.6.1), oil red 'O' for adipogenesis (section 2.6.2) and Alcian blue for chondrogenesis (section 2.6.3).

The CD marker expression prolife of hMSCs was also analysed via fluorescent staining for the receptors followed by imagining and flow cytometry. Following expansion, cells were resuspended at 10^6 cells/ml and incubated with the blocking solution of 2% Bovine serum albumin (BSA) in Phosphate buffered saline (PBS) for 1h at 4^0C. Following this, the cells were split into 5ml aliquots of 80,000 cells and incubated with the directly conjugated antibody or the respective isotype control solutions (in 2%BSA in PBS) for 30min at 4^0C on a plate shaker. Finally, the cells were washed twice before resuspension in a final volume of 200µl of 2% BSA/PBS for further analysis.

2.5.2 Expression of CD markers

The following CD markers and isotype controls were used at the described concentrations in 2% BSA/PBS. CD markers (dilutions and clone numbers) include: CD 14 (1:50; TÜK4),

CD 19 (1:50; not available), CD 34 (1:100; AC136), CD 45 (1:200; 5B1), CD 105 (1:50; 43A4E1), CD 73 (1:20; AD2), CD 90 (1:200; DG3). Isotype control antibodies include: Anti-HLA–DR (1:200; AC122), IgG1 (1:50; 1SF-21F5) and IgG2a (1:50; S43.10). All reagents were obtained from MACS Miltenyi Biotec, UK. Propidium iodide staining to detect dead cells was not included.

Flow cytometry was performed on a Becton Dickinson FACScan flow cytometer. Cell suspensions in 2%BSA/PBS were analysed by collecting 100,000 counts per sample. Using controls the data were gated in the forward vs side scatter plots to exclude cell debris. Data were analysed using the CellQuestPro software (Becton Dickinson, UK).

2.6 Assessment of cellular behaviour: differentiation, viability and mitochondrial metabolic activity

2.6.1 Alizarin red staining for osteogenesis

Deposition of mineralized matrix in hMSCs committed to the osteogenic lineage was assessed using alizarin red staining. The stain is specific for calcium ions and stains the extracellular calcium present in the mineralized matrix. 2% (w/v) aqueous Alizarin red stain was added in sufficient amounts to cover a monolayer of fixed cells and incubated for 5 min at room temperature in the dark. Excess stain was completely removed by multiple washes using deionized water. Bright field images were taken using the LAS imaging software on a Leica DMIL microscope fitted with a camera.

2.6.2 Oil red ‘O’ for adipogenesis

Cells undergoing adipogenesis produce intracellular lipid droplets. To detect this, fixed cells were stained with Oil red ‘O’ that stains these lipid droplets. The stain was prepared

at 0.18% in 60% isopropyl alcohol. The fixed cells were washed with 60% isopropyl alcohol prior to staining. Following this, cells were incubated with oil red 'O' for 15min at room temperature. Excess stain was completely removed by multiple washes using deionized water until. Bright field images were taken using the LAS imaging software on a Leica DMIL microscope fitted with a camera.

2.6.3 Alcian blue for chondrogenesis

Fixed cells were stained with Alcian blue that detects sulphated glycosaminoglycans associated with chondrogenesis. Aqueous Alcian blue stain (Sigma, UK) was prepared and its pH set to 1.5 using 3% acetic acid. Cells were incubated with the stain overnight at room temperature. Excess stain was completely removed by multiple washes using deionized water. Bright field images were taken using the LAS imaging software on a Leica DMIL microscope fitted with a camera.

2.6.4 Alkaline phosphatase (ALP) assay

Cells were lysed using 0.1% Triton-X (Sigma, UK) in water to release the nuclear DNA or by repeated cycles (3x) of freezing and thawing of cells in water. 50µl of cell lysate was incubated with 50µl of 4- methylumbelliferyl phosphate (4-MUP; Sigma, UK) in alkaline conditions by the addition of 50µl of diethanolamine buffer (pH 9.8; DEA). ALP cleaves the 4-MUP in alkaline conditions to release the fluorescent product 4-MU. After an incubation of 90 min at 37^0C in the dark, the sample fluorescence was read on a Biotek synergy2 plate reader. The fluorescence was read using the GEN 1.05 software at excitation/emission wavelengths of 360nm/440nm (optics position was set to 'Bottom' and sensitivity adjusted based on measurements of empty wells). 100µl of the buffer with 4-MUP was used as blank. Standard curves were plotted using 100µl of 4-MU (Sigma, UK)

in 50µl of DEA solution at different concentrations (Fig 2.6.1a). For the first two heat shock experiments in Chapter 4 (Experiment 01 and 02), the DEA buffer was not used and a separate standard curve of 4-MU without DEA was also plotted (Fig 2.6.1 b). A hyperbolic curve was fitted through the points and the expression derived was used for calculating ALP in terms of the amount of 4-MU (µg/ml).

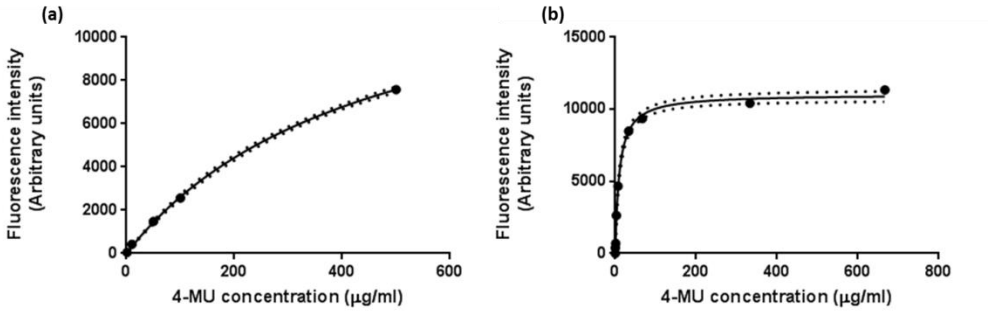

Fig 2.6.1 Fluorescence intensity vs 4-MU concentration plots for standard solutions of 4-MU with a hyperbolic fit without DEA buffer (a) and with DEA buffer (b).

Expression for hyperbolic fit: $Y = B_{max} * x/(Kd + x)$

Values for plot (a): B_{max} = 14443; Kd = 452.8 (R^2=0.9996) and for (b) B_{max} = 11046; Kd = 10.07 (R^2= 0.9975)

2.6.5 Picrogreen assay for DNA Quantification

Cells were lysed using 0.1% Triton-X in water to release the nuclear DNA (if samples for different time points were cultured in the same well plate) or by repeated cycles (3x) of freezing and thawing of cells in water. DNA concentration was quantified using the Quanti-iT™ Picogreen® dsDNA assay kit (ThermoFisher Scientific, UK). In brief, 20µl of cell lysate was mixed with 50µl of 1x Picogreen (PG) diluted in 1x TE buffer. Sample was incubated with PG for 5min at room temperature in the dark. The fluorescence of PG is

enhanced when bound to double stranded DNA. The fluorescence intensities of the samples following incubation were measured at excitation/emission wavelengths of 485nm/ 530nm on a Biotek synergy2 plate reader using the GEN 1.05 software (optics position was set to 'Bottom' and sensitivity adjusted based on measurements of empty wells). Standard DNA solution provided with the kit was used to plot a fluorescence intensity vs DNA concentration standard plot for every assay. The DNA was diluted to known concentrations in 1x TE buffer and 20µl was incubated with 50µl of PG (5min, dark, room temperature). An example standard curve is shown in Fig 2.6.2.

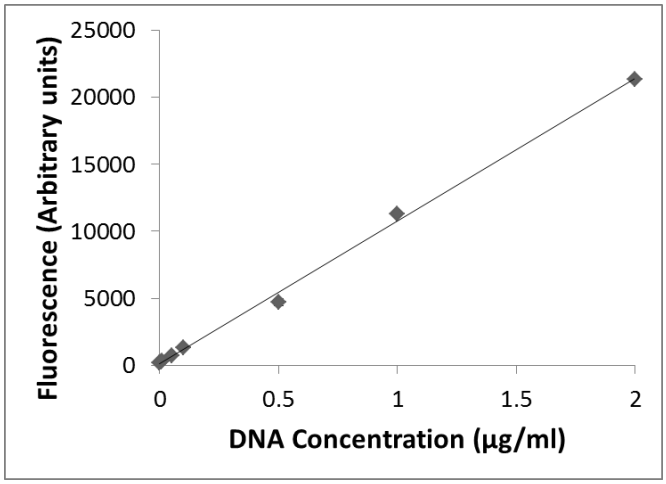

Fig 2.6.2 Fluorescence intensity vs DNA concentration plots for standard DNA solution fitted with a linear trend line obtained via the Picogreen assay.

2.6.6 XTT assay for quantifying mitochondrial metabolic activity of cells

The XTT kit from Roche, UK was used to study the mitochondrial metabolic activity of cells. Tetrazolium salts are cleaved to formazan by the succinate-tetrazolium reductase system in the mitochondria only in metabolically intact cells. The tetrazolium salt, XTT (sodium 3′-[1-(phenylaminocarbonyl) - 3, 4-tetrazolium]-bis (4-methoxy-6-nitro) benzene sulfonic acid hydrate) labelling reagent in RPMI 1640 (without phenol red) that is added to the culture medium is cleaved in the presence of an electron-coupling reagent. The

cleavage product, formazan is soluble in water. Briefly, XTT labelling reagent (5ml at 1mg/ml) was mixed with the electron-coupling reagent (0.1ml of PMS (N-methyl dibenzopyrazine methyl sulphate) at 0.383 mg/ml (1.25 mM), in phosphate buffered saline (PBS), filtered through 0.2μm pore size membrane) are mixed and pre-warmed to 37^0C. Fresh media with pre-warmed XTT reagent at 2:1 ratio were added to the cells and incubated for 4h at 37^0C in the dark. After the incubation, the media were transferred to a fresh well plate and absorbance read at 470nm with reference wavelength at 650nm. In the well with cells, fresh medium was added after the PBS wash.

2.7 Assessing interaction of cells and MNPs microscopically

2.7.1 Fluorescent staining of cellular proteins (Immunocytochemistry)

Cells were stained with various fluorescent antibodies to assess expression of proteins of interest. For this purpose, a monolayer of cells was grown on coverslips or in well plates. Following treatment, the cells were washed with PBS and fixed with the appropriate fixative (4% w/v paraformaldehyde; 70% v/v ice cold methanol or ethanol) for 10min at room temperature. Excess fixative was washed off and cells were permeabilized (if target protein was expressed intracellularly) using 0.1% Triton X-100 in PBS for 10min at room temperature. Excess detergent was removed by washing with PBS. The permeabilized samples were then blocked using 1% w/v BSA/ PBS for 30min to avoid non-specific binding of the antibodies. Excess solution was removed following incubation. The primary antibody was prepared at the required dilution in 1%BSA/PBS and added to the cell monolayer at volumes sufficient to cover the surface. Cells were incubated with the antibody overnight at 4^0C in a plate shaker. For samples where there is high protein expression the samples were incubated at room temperature for 1h. If the 1^0antibody is attached to a fluorophore the incubation steps were performed in the dark. Following

incubation, excess antibody was removed and the samples washed 3x 5min with PBS. For samples where a secondary antibody was used, it was added to the cells at the required concentration and incubated for 1h at room temperature in the dark. Excess antibody solution was removed and the samples washed with PBS. Finally, the nuclei were counterstained using DAPI (10μg/ml; Sigma, UK) for 10 min at room temperature. The coverslips are mounted on glass slides using mounting medium or in the case of well plate were directly observed in an Olympus IX83 confocal microscope fitted with a camera using the Fluorview 10 software.

Primary Antibody (1^0 Ab)	**Secondary Antibody (2^0 Ab)**	**Target organelle**	**Fluorescence Excitation /Emission wavelength (Colour)**	**Product name and manufacturer**
Anti-HSP70 [5A5]	Goat anti-Rabbit IgG (H+L) Secondary Antibody, DyLight 488 conjugate	Heat shock protein 70	495/519	1^0 Ab: Abcam, UK
Rabbit polyclonal Anti-LAMP1	Goat anti-Rabbit IgG (H+L) Secondary Antibody, DyLight 405 conjugate	Cell membrane. Endosome membrane. Lysosome membrane.	400/420	1^0 Ab: Abcam, UK 2^0 Ab: Thermo Scientific (Pierce Antibodies), UK
Alexa Fluor® 488 Phalloidin	-	Actin cytoskeleton	495/519	1^0 Ab: ThermoFisher SCIENTIFIC, UK

Table 2.2 Antibodies used for immunocytochemistry

2.7.2 Transmission electron microscopy (TEM) for assessing cellular uptake of MNPs

MG-63 cells were seeded on PLA films and incubated with synthetic magnetite (citric acid coated) for 72h. Following incubation, the samples were dehydrated by washing in

increasing concentration of aqueous ethanol (70, 80 90 100% and dry ethanol) and incubated at room temperature for 15min. The dehydrated samples were embedded in fresh aliphatic SPURR resin in planchettes. The embedded samples were sliced in cross section and stained with uranyl acetate. The stained samples were imaged using a camera-fitted JEOL1230 transmission electron microscope.

2.7.3 Time lapse imaging

Cells were seeded in well plates and allowed to attach overnight. After attachment, synthetic magnetite (citric acid coated) MNPs were added to cells at 100μM and the well plates were placed on the microscope stage within a temperature and gas controlled humidified chamber. Bright field images of different locations within the wells were captured at fixed intervals for a period of three days using an inverted Nikon Ti eclipse microscope fitter with a camera using the NIS Elements software .

2.8 Statistics

All experiments were set up with experimental replicates of n=3 (unless otherwise specified). Samples were statistically compared using the GraphPad Prism 6 software. Unpaired t-tests (two tailed) were used to compare between two groups and One-way ANOVA was used for comparison between three groups with the p-value set at 0.05. The sample variance was confirmed to be equal between the groups for ANOVA. The error bars in all graphs represent the standard error of the means.

CHAPTER 3 Assessing cell-nanoparticles interactions

3.1 Introduction

Prior to the use of magnetic nanoparticles for cellular applications, it is important to understand the interaction between cells and nanoparticles. This is necessary to identify the right particle types in terms of biocompatibility and dosages in order to obtain the most efficient magnetic response. The mechanism and degree of interaction, such as membrane binding and internalization, depend on the nanoparticle cluster size, surface coating and presence of biological ligands on the nanoparticle's surface (Biofunctionalization).[144–146] Since the bacterially synthesised MNPs used in this work are obtained as large clusters of particles without any surface coating, a custom protocol has been developed to coat them with citric acid (see section 2.1.1). The citric acid coating method reduces cluster size and provides a surface charge to gives rise to stable aqueous suspensions of the MNPs. In this chapter the cellular association of the citric acid coated synthetic iron oxides (chemically synthesized) and bacterially synthesized (biogenic) doped iron oxides will be studied using various techniques.

As discussed in section 1.2.3, the introduction of transition metal cations modifies the magnetic properties of iron oxide nanoparticles. By controlling the level of doping, the magnetic properties of the nanoparticles can be tuned to suit the end application. On the other hand, the modification of the core composition of the nanoparticle might alter its biocompatibility. Coated iron oxide nanoparticles in general have low levels of cytotoxicity and a few types have already been approved for clinical use.[147] The doping of MNPs with zinc or cobalt could considerably increase the cytotoxicity of the nanoparticles as these metals are cytotoxic in their ionic form[118,148–150]. This is especially true if cells

endocytically internalize the particles, as they will be localized within lysosomes, the highly acidic nature of which may corrode the nanoparticle coating and metal core releasing metal ions within the cell.[151,152] Previous studies have shown evidence of *in vitro* cytotoxicity for chemically synthesized doped magnetite nanoparticles, indicating that doping modifies the biocompatibility of the nanoparticles.[153–155] Apart from ensuring low cytotoxicity, it is necessary to assess the effect doped MNPs have on normal cellular functioning. For example, in the case of stem cells, it is critical that the MNPs do not interfere with cellular differentiation,[156–159] an essential property of the cells being exploited for clinical therapies.[160–163]

In this chapter, the suitability of biogenic doped MNPs for cellular applications will be assessed in terms of cytotoxicity. The MNPs of the form $M_xFe_{3-x}O_4$, where M=Co (x=0.1, 0.38, 0.4, 0.7, 1) or Zn (x=0.2, 0.4, 0.6, 0.9) were synthesized using the iron(III) reducing bacteria *Geobacter sulfurreducens.*[92,109,110,164] For comparison, undoped (zero cobalt or zinc doping) magnetite nanoparticles produced both bacterially and by traditional chemical synthesis (commercially available) will be examined.

Besides the effect of nanoparticles on cells, the cellular environment also influences the magnetic behaviour of the particles. [165–167] The effect of the changes in the physiochemical conditions in a cellular environment, on the magnetic response of MNPs can be assessed using AC susceptibility (ACS) measurements.[168,169] ACS is an effective technique to non-invasively probe the magnetic response of nanoparticles in live cells.[114,170] In this chapter, the ACS technique will be used for determining the magnetic response of MNPs, both as aqueous suspensions and following interaction with cells. The effect of nanoparticle association will be explored on two different cell types: primary human bone marrow

derived mesenchymal stem cells (hMSCs), and human osteosarcoma derived cells (MG-63s) (See Chapter 1 section 1.4 for more details).

3.2 Materials and methods

3.2.1 Magnetic nanoparticle suspensions

All nanoparticles used in this chapter were coated with citric acid to form stable aqueous suspensions (see Chapter 2 section 2.1.1). The suspensions were sterilized using 0.2μm filters prior to use in cellular experiments. Nanoparticle suspension concentrations were measured using the Ferrozine assay for total iron following complete digestion by concentrated nitric acid (70%) at high temperatures (> 60^0C) overnight. A list of all the MNPs discussed in this chapter is given in the table 3.1.

Chemical Formula	Notation	Synthesis route
Fe_3O_4	Synthetic magnetite	Chemical
Fe_3O_4	Biogenic magnetite	Bacterial
$Co_{0.4}Fe_{2.6}O_4$	$Co_{0.4}$	Bacterial
$Co_{0.7}Fe_{2.4}O_4$	$Co_{0.7}$	Bacterial
$CoFe_2O_4$	$Co_{1.0}$	Bacterial
$Zn_{0.4}Fe_{2.6}O_4$	$Zn_{0.4}$	Bacterial
$Zn_{0.6}Fe_{2.4}O_4$	$Zn_{0.6}$	Bacterial
$Zn_{0.9}Fe_{2.1}O_4$	$Zn_{0.9}$	Bacterial

Table 3.1 Details of the various magnetic nanoparticles used in this study

3.2.2 Cell culture

MG-63, an osteosarcoma cell line (Lonza, UK) and human bone marrow derived primary mesenchymal stem cells (less than 5 passages) (Lonza, UK) were seeded in expansion

medium consisting of 4.5gL^{-1} glucose Dulbecco's Modified Eagle's medium (Lonza, UK) supplemented with 10% Fetal bovine serum, 1% Penicillin/ Streptomycin (antibiotics and antimycotics) and 1% L-glutamine in well plates at ~80% confluency and allowed to attach overnight before addition of nanoparticle suspensions.

For cytotoxicity studies, MG-63 cells were seeded in well plates (for imaging) at 40-50,000 cells/cm^2 to have sufficient numbers for flow cytometry. MNPs were added at the required concentrations by diluting in sterile water. They were added at 10% (v/v) of the media and in the case of untreated controls (no MNP added) water was added at 10% v/v.

3.2.3 Cellular uptake studies

MG-63 cells and hMSCs were incubated with citric acid coated MNPs for 72h (unless otherwise specified) for studying the MNP's cellular interaction and uptake. The procedure for Prussian blue staining (see chapter 2 section 2.2.2), immunocytochemistry (see chapter 2 section 2.7.1), time-lapse imaging (see Chapter 2 section 2.7.3) and sample preparation for transmission electron microscopy (see chapter 2.7.2 section 2.2.2) are described in chapter 2. For immunocytochemistry investigating the lysosomal localization of internalized MNPs, cells incubated with MNPs for 72h, following the incubation were fixed with 4% PFA. The lysosomes were fluorescently stained with primary antibody rabbit polyclonal Anti-LAMP1 (Abcam, UK) and Goat anti-rabbit IgG (+L) DyLight 405 conjugate (Pierce Antibodies, UK) secondary antibody. The Anti-LAMP1 antibody targets the LAMP-1 protein (Lysosomal-associated membrane protein) on lysosomal membranes but also can shuttle between endosomal and plasma membranes. The cells were then counterstained for actin filaments using the Alexa Fluor 488 Phalloidin dye (ThermoFisher Scientific, UK). The bright field images showing the localization of the MNPs were

inverted and the contrast altered (using ImageJ) so that only the MNPs were visible. The bright field images were given a false blue colour and merged with the fluorescent images using ImageJ after adjusting the contrast. The colour of the other antibodies were also swapped (Actin was shown in red and LAMP1 in green) to get the best contrast.

3.2.4 Cytotoxicity studies

Control wells were treated with equivalent amount of sterile distilled water which was the negative control while cobalt chloride (Sigma- Aldrich, UK) at a concentration of 500μM was used as the positive control. The cation/MNP concentrations were maintained constant between comparisons (unless otherwise mentioned) and cells were incubated with the additives for 72h before being assessed for loss in viability.

Microscopy

The live dead dual staining kit for mammalian cells (Life Technologies, UK) was used to assess cell viability. 2μM of Calcein-AM (CAM) in phosphate buffered saline (PBS) was added to stain live cells green and 4μM of the nuclear stain ethidium homodimer (EthD) in PBS was added to stain compromised cells red. Cells were incubated with the dyes at 25°C in the dark for 30min. Following this, excess stain was washed off and fresh medium added. Cells were immediately imaged in the microscope under bright field and fluorescent conditions.

Flow cytometry quantification

For flow cytometry, cells were seeded in 24 well plates and tested similar to the fluorimetry samples. Staining was performed using 1μM CAM and 2μM EthD as these concentrations gave optimum levels of fluorescence in the cytometer. Incubation with the dyes was performed at 37°C for 15min. Incubation at higher temperatures caused the cells to lift off compared to incubation at room temperature and this helped obviate the trypsinization step during sample preparation circumventing any artefacts trypsinization might introduce. The cells were transferred to round-bottom tubes, washed and subsequently resuspended in flow cytometry buffer (1% bovine serum albumin in PBS). Five to ten thousand events gated on size (forward scatter) and granularity (side scatter) were analysed. A separate set of controls were prepared for every set of samples analysed and were used for setting the parameters and compensation values. It included live cells without any staining, stained only for CAM, only for EthD and for both the dyes. Identical sets of controls were prepared for the negative control where the cells were treated with 70% methanol. Data analysis was performed using the Cyflogic flow cytometry data analysis software.

The controls were analysed to set the gating limits. CAM fluorescence was measured using the FL1 gate in the flow cytometer while EthD fluorescence was measured in the FL3 region. Compensation for leakage of CAM into FL3 region was performed by matching the geometric mean of unstained cells' fluorescence in FL3 to that of live cells stained for only CAM. Similar compensation was performed for leakage of EthD fluorescence in the FL1 using unstained and compromised cells stained for EthD alone. 99% of the unstained live and dead cell populations were set to fall under the live staining background using FL1 v FL3 plots (Fig 3.2.1a). These setting were then used to filter the background fluorescence

for the actual samples in FL1 vs. FL3 log plot. Similarly, based on the live (Fig 3.2.1 b) and dead (Fig 3.2.1 c) controls stained for both dyes, the regions for viable and compromised cells were defined.

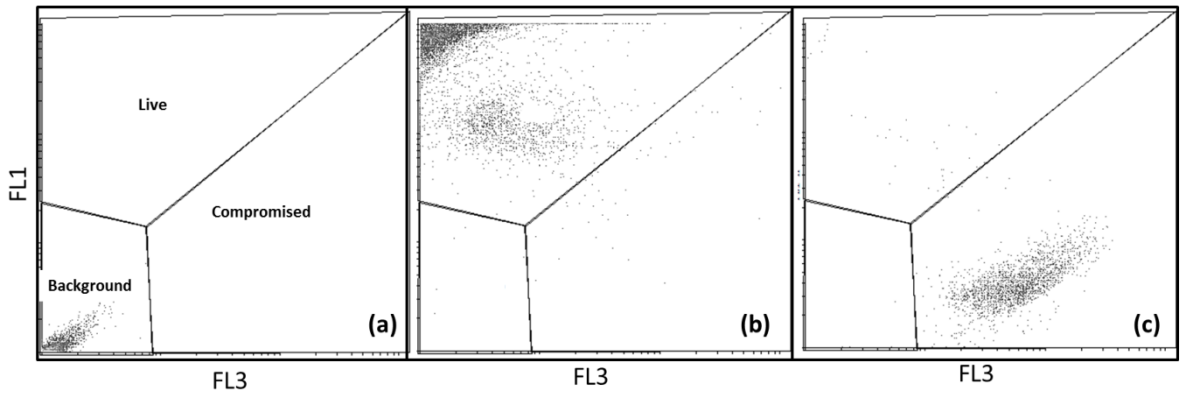

Fig 3.2.1 Defining populations in flow cytometry samples: FL1 Vs FL3 density plots for unstained live (a) cells, CAM stained live cells (b) and EthD stained dead (c) cells. Regions for live, compromised populations and the background were defined so as to encompass 99% of the respective control populations.

3.2.5 AC Susceptibility

The magnetic susceptibility was measured in a custom built AC susceptometer. The oscillating magnetic field performs a frequency sweep from 10 to 210 kHz. 200µl volume of sample is transferred to a glass sample holder that is placed at the centre of the coil of the custom-built AC susceptometer. For measurements of MNPs in cells, the cells were incubated with MNPs for 72h following which they were trypsinized. The trypsinized cells were resuspended in fresh medium and transferred to the glass vial for ACS measurements. The cell samples had low levels of magnetic material which fell below the detection limits of AC susceptometer at the higher frequency range. Hence, measurements from these samples were obtained only up to 10 kHz frequency. All susceptibility measurements were made at 37°C (310K) to maintain physiological temperature.

3.3 Results

3.3.1 Cellular uptake of Magnetic Nanoparticles

To understand the association of magnetic nanoparticles (MNPs) with cells a variety of imaging and other techniques were employed. Fig 3.3.1 shows Prussian blue staining for iron in MG-63 cells incubated with synthetic magnetite nanoparticles. Unlike the control samples (Fig 3.3.1 a, b) a strong blue stain corresponding to iron localization is observed for the cells with MNPs (Fig 3.3.1 c, d). By 72h, there is a strong association of MNPs to

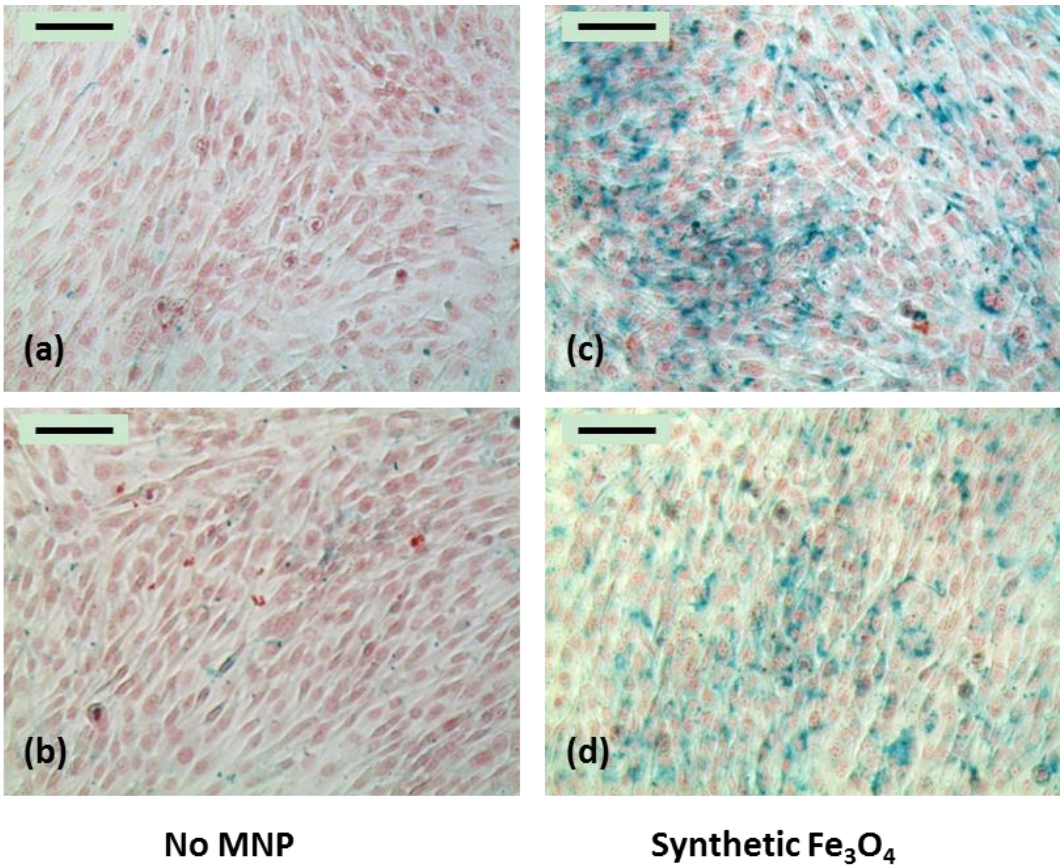

Fig 3.3.1 Prussian blue staining for iron to detect MNPs: MG-63 cells not exposed to nanoparticles (NO MNP; a, b) or incubated with 60μM synthetic magnetite (synthetic Fe_3O_4; c, d) for 72h are stained for iron using the Prussian blue stain with the nuclei counterstained for nuclear fast red. Samples were washed to ensure removal of unbound MNPs. (Scale bars represent 100μm)

cells. The distribution of the stain appears inhomogeneous indicating uneven cellular uptake or membrane association. This could probably be due to the differential activity of cells in terms of endocytosis or motility (where they move around to access the MNPs settled to the bottom of the well).

To better understand the dynamics of cell-nanoparticle interaction, MG-63 cells incubated with synthetic magnetite nanoparticles were monitored by time lapse imaging in bright field conditions (Fig 3.3.2). Initially, the cells and MNPs are in different planes of focus such that at the beginning of the time lapse imagining (t=0), only the MNPs are visible as dark spots. The distribution is quite homogenous and particle clusters are big enough to be visible. In culture media with serum, the MNP clusters were typically a few hundreds of nanometres (200-500nm based on dynamic light scattering measurements). Due to their size they settle within a few tens of minutes and were accessible to the cells at the well bottom. With time, the cells were delineated by the MNP and clear cellular forms are seen. The cells were constantly moving and scavenged the MNPs in their way and eventually MNPs in the intercellular spaces reduced considerably (by 45h). At this time point, there are hints to the cellular localization of the MNPs as well. The spread of the MNPs at the cell surface can discerned at 19h whilst by 32h the MNPs appear to be arranged in circular shapes. At later time points, this effect is more obvious as the MNPs appear to occupy the perinuclear region. This could be due to endocytosis followed by localization around the nucleus.

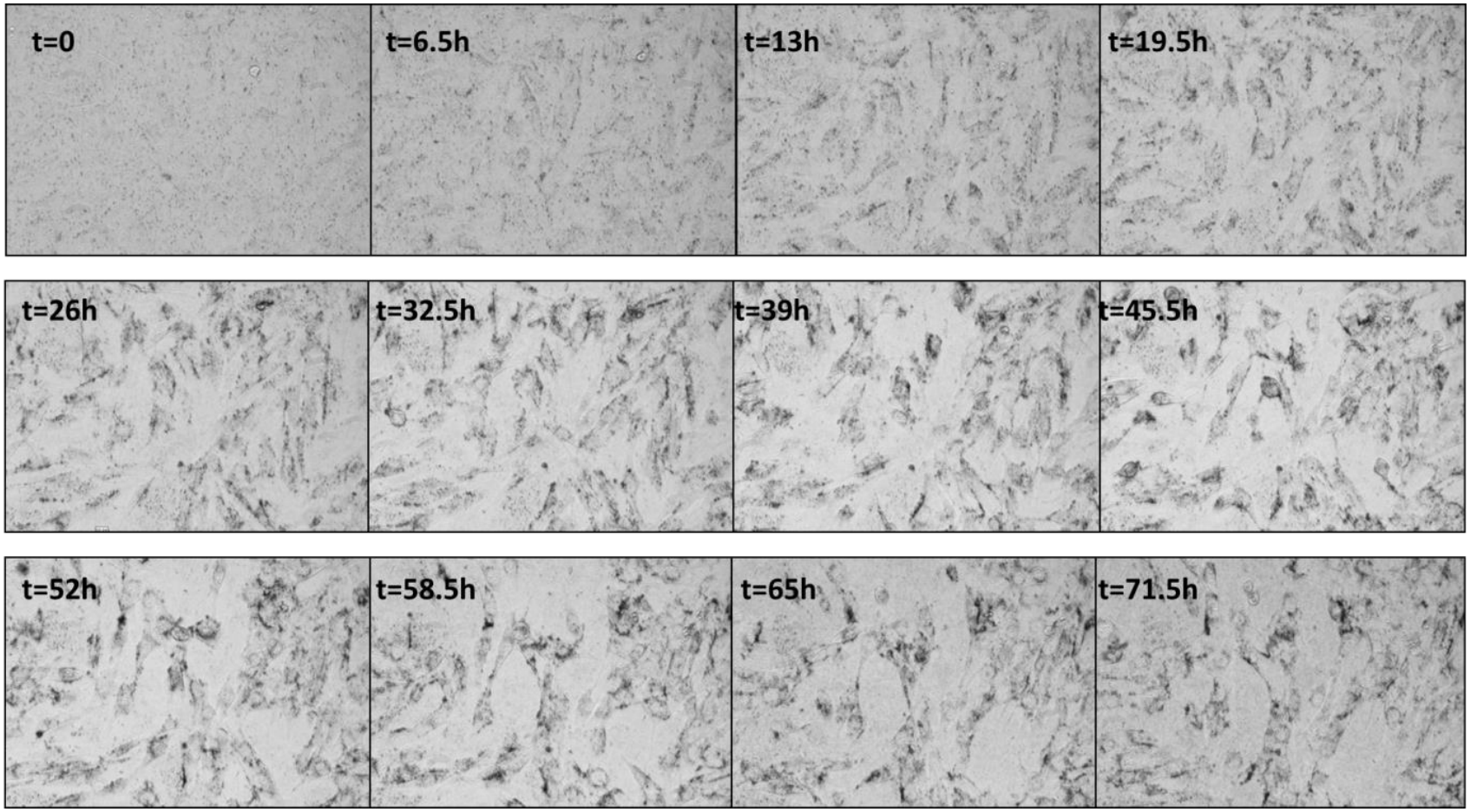

Fig 3.3.2 Time lapse imaging of cell-MNP interactions: Time lapse images of MG-63 cells incubated with synthetic magnetite MNPs over a period of 72h. Each image is a snapshot and t indicates the time (in hours) that it was obtained at. (Images are arranged in chronological order from top left to bottom right; Scale bars not available)

In Fig 3.3.3, a single cell is tracked over the course of time. At the initial time point (Fig 3.3.3.a), the cell does not appear to be associated with MNPs. However, MNP association can be seen as time progresses, as observed by the darkening of the cell boundaries. The movement of the cell is also observed in relation to its initial location (indicated by the *). Eventually, after detaching the cell rounds up (Fig 3.3.3 f) and divides into two daughter cells (Fig 3.3.3 g). It appears that the MNPs are equally distributed between the daughter cells (as seen by the equal levels of contrast imparted by the MNPs).

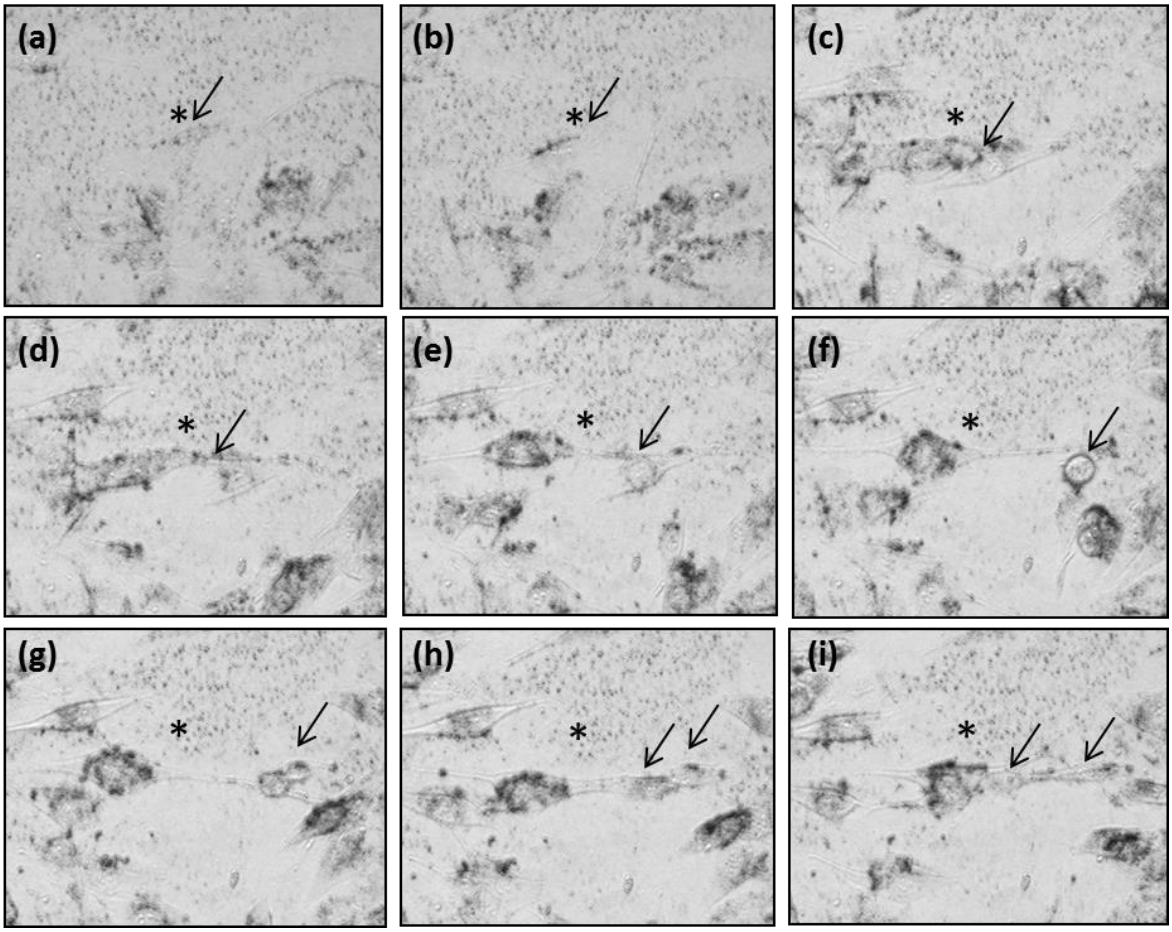

*Fig 3.3.3 Time lapse imaging of a single cell-MNP interaction: Snapshots tracking a single MG-63 cell incubated with synthetic magnetite MNPs over a period of 72h. Micrographs (a) through (i) show snapshots at consecutive time points with no specific fixed time interval. The * indicates the initial location of the cell of interest and arrow(s) indicates its (or daughter cells) position at that time point. (Images are arranged in chronological order from top left to bottom right; Scale bars not available)*

In a different experiment, the perinuclear localization of the MNPs can be seen clearly in Fig 3.3.4b for MG-63 cells incubated with synthetic magnetite nanoparticles for 72h. The dark circle of MNPs is absent for the control samples not exposed to nanoparticles (Fig 3.3.4a).

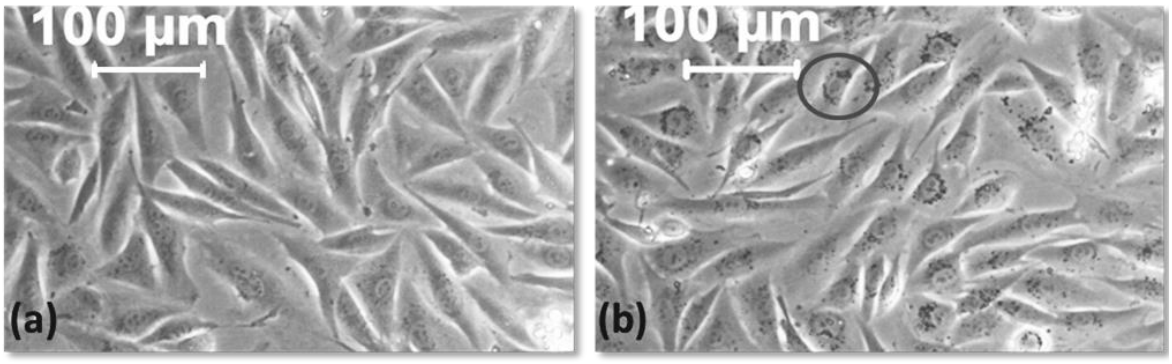

Fig 3.3.4 Bright field image of cells with MNPs: MG-63 cells without any nanoparticles (a) and incubated with synthetic magnetite MNPs for 72h (b). The perinuclear localization of the MNPs can be seen clearly (highlighted by the circle) for cells incubated with particles.

The MNPs, depending on their size, could be internalized via the endocytic pathway. When endocytosed, they are present within membrane bound vesicles such as early endosomes (during initial stages of endocytosis), late endosomes and finally lysosomes. To confirm the presence of the citric acid coated MNPS within vesicles, hMSCs incubated with synthetic magnetite MNPs were stained for lysosomes (Fig 3.3.5). The actin cytoskeletal staining (red) shows the presence of an almost confluent layer of cells. On the other hand, the MNPs (blue) and lysosomes (green) are seen only in certain regions and appear to overlap to a certain extent (seen as yellow staining). This indicates that the MNPs could be associated with lysosomes hence further studies were performed using transmission electron microscopy to explore this.

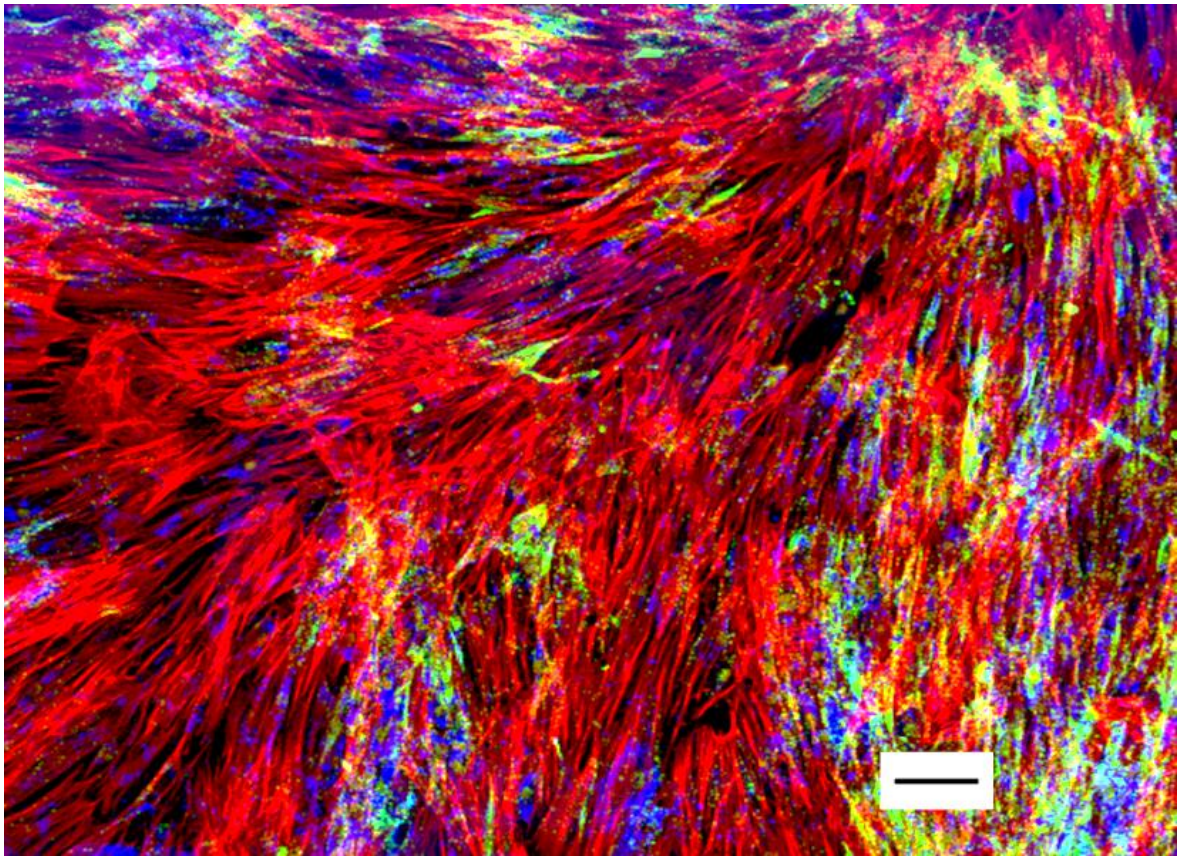

Fig 3.3.5 Fluorescent micrograph of cells with MNPs: MG-63 cells incubated with synthetic magnetite MNPs (72h) were stained for actin cytoskeleton (Phalloidin; red) and lysosomes (Anti-LAMP1; green). The nanoparticles are represented in blue following alteration of the bright field image. (Scale bar represents 100µm)

The intracellular location of MNPs was further investigated using transmission electron microscopy of cross section of cells grown on PLA films (Fig 3.3.6). Multi-layer of cells can be observed in Fig 3.3.6a and a decrease in the amount of internalized MNPs with the increasing depth of cells indicate the reduction in availability of MNPs to cells when present as multi-layers. In Fig 3.3.6b-d MNPs can be seen in membrane bound vesicles in the cytoplasm. It is interesting to note that the distribution of the MNPs within the vesicular structures is not uniform. In some they are sparse and are located just along the periphery (Fig 3.3.6b, c) while in others they have completely packed the vesicles (Fig 3.3.6b). The perinuclear localization can also be seen (Fig 3.3.6c, d) of the vesicles containing the MNPs around the nucleus.

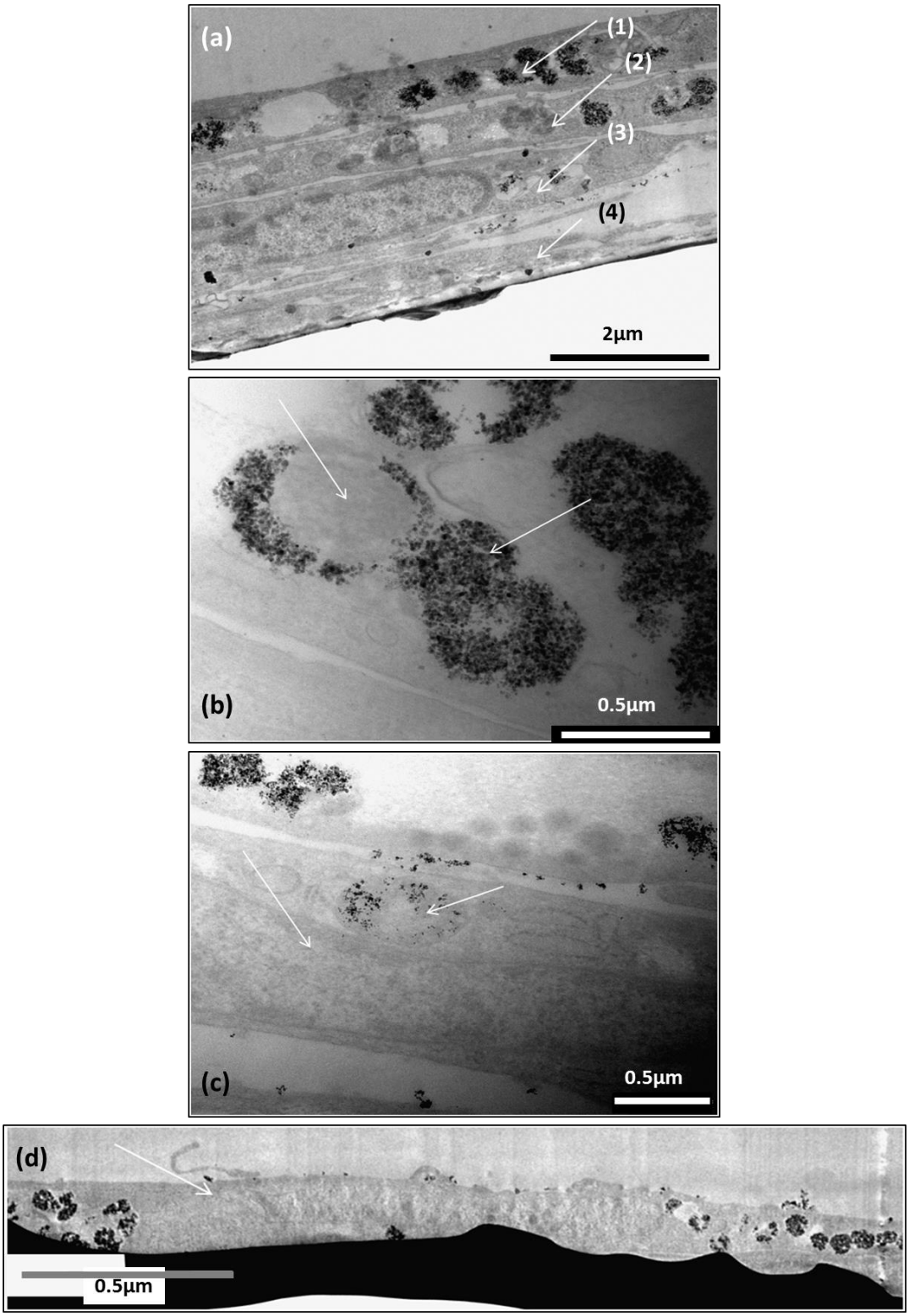

Fig 3.3.6 Electron micrographs of cells with MNPs: MG-63 cells incubated with synthetic magnetite MNPs (72h) were imaged in a transmission electron microscope. (a) Multi-layer of cells with decreasing concentration of MNPs (appear as dark spots) with increasing depth of the cell layer (arrow 1 indicates topmost layer through to arrow 4 indicating the deepest layer). (b) Differential loading of MNPs in cellular vesicles. (c, d)Peri-nuclear localization of the MNP-containing vesicle (white arrows pointing to the nucleus and the vesicle).

3.3.2 Cellular biocompatibility of magnetic nanoparticles

The cytotoxicity of different nanoparticles was assessed in hMSCs and MG-63 cells. Confluent layers of cells can be observed for the no nanoparticle control (0μM; Fig 3.3.7a) with the regular triangular morphology of viable MG-63 cells. For the cells exposed to different concentrations of synthetic magnetite (from 10-500μM; Fig 3.3.7 b-e), cells appear similar to the control and no obvious change in morphology is observed. The MNP clusters are not very visible for the lower concentrations but at 500μM, (Fig 3.3.7e), they appear as dark spots in the bright field images. Ionic Co (II) in its salt form ($CoCl_2$) has been used as a positive control for cytotoxicity. Equivalent concentrations of $CoCl_2$ to the MNPs were added for comparison. Whilst at the lower concentrations of up to 100μM (Fig 3.3.7 f-h), no significant change in cell number or morphology is observed, at the highest concentration of 500μM $CoCl_2$, cells have detached and rounded up (Fig 3.3.7i) indicating a complete loss in viability.

The cytotoxicity of various MNPs was investigated by staining cells with CAM/EthD dyes and measuring the degree of staining (Fig 3.3.8). Fluorescent micrographs show cells in the live controls (marked 'No MNP') largely stained only for Calcein (green) with minimal staining for EthD (Fig 3.3.8a). For cells exposed to $CoCl_2$ viability decreases with concentration and at 500μM, no live cells are present (Fig 3.3.8 b, c). Similar to the observations in the bright field images, there is very little loss in viability for the cells incubated with synthetic magnetite at all concentrations (Fig 3.3.8 d-g) indicating its low cytotoxicity.

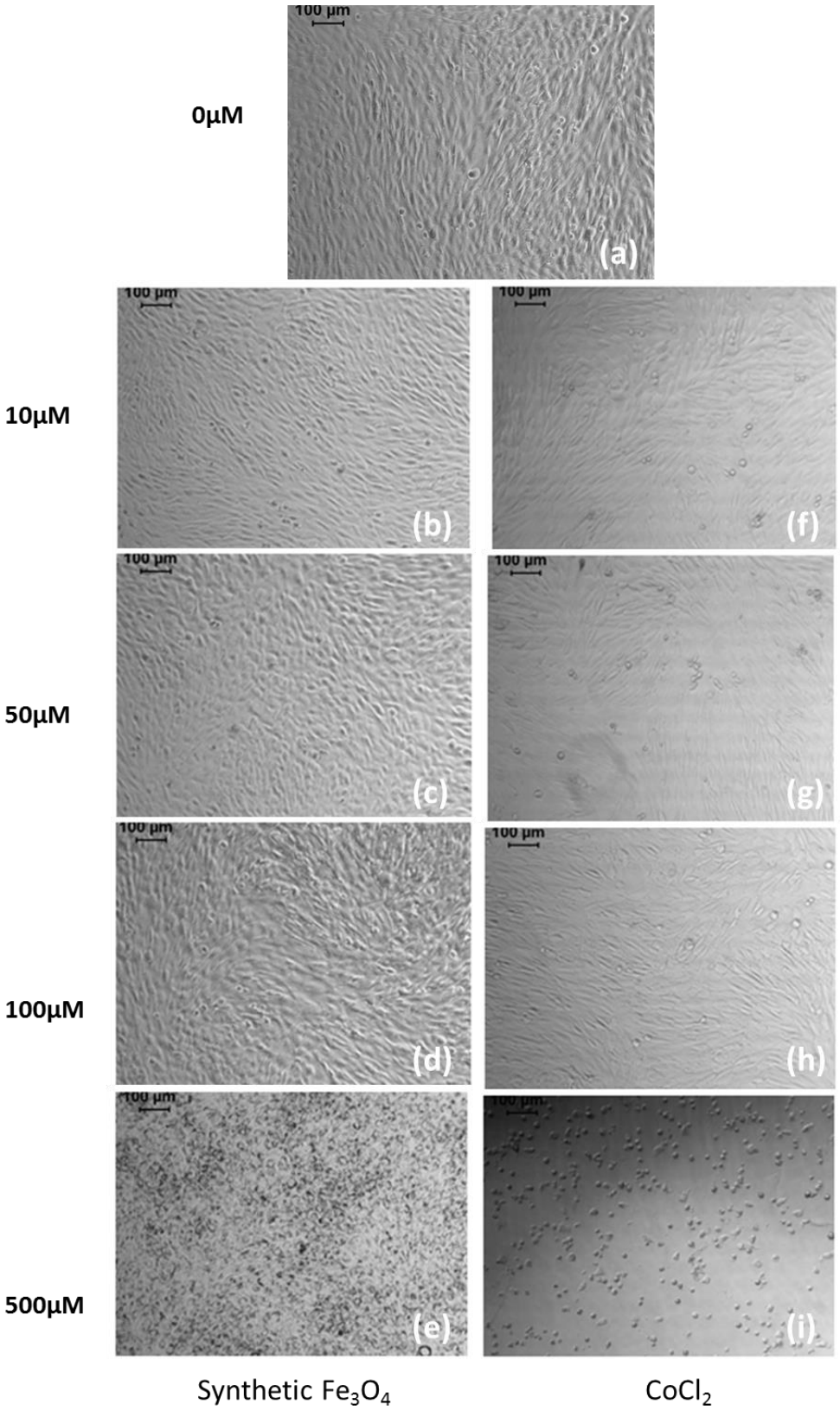

Fig 3.3.7 Bright field images of MG-63 cells exposed to varying concentrations of synthetic magnetite: MG-63 cells incubated with different concentrations of synthetic magnetite (10-500µM; b-e) compared to cells with no MNPs (a) and cells with equivalent cation concentrations of $CoCl_2$ (f-i) after 72h. Excess MNPs have not been washed away (Scale bars correspond to 100µm).

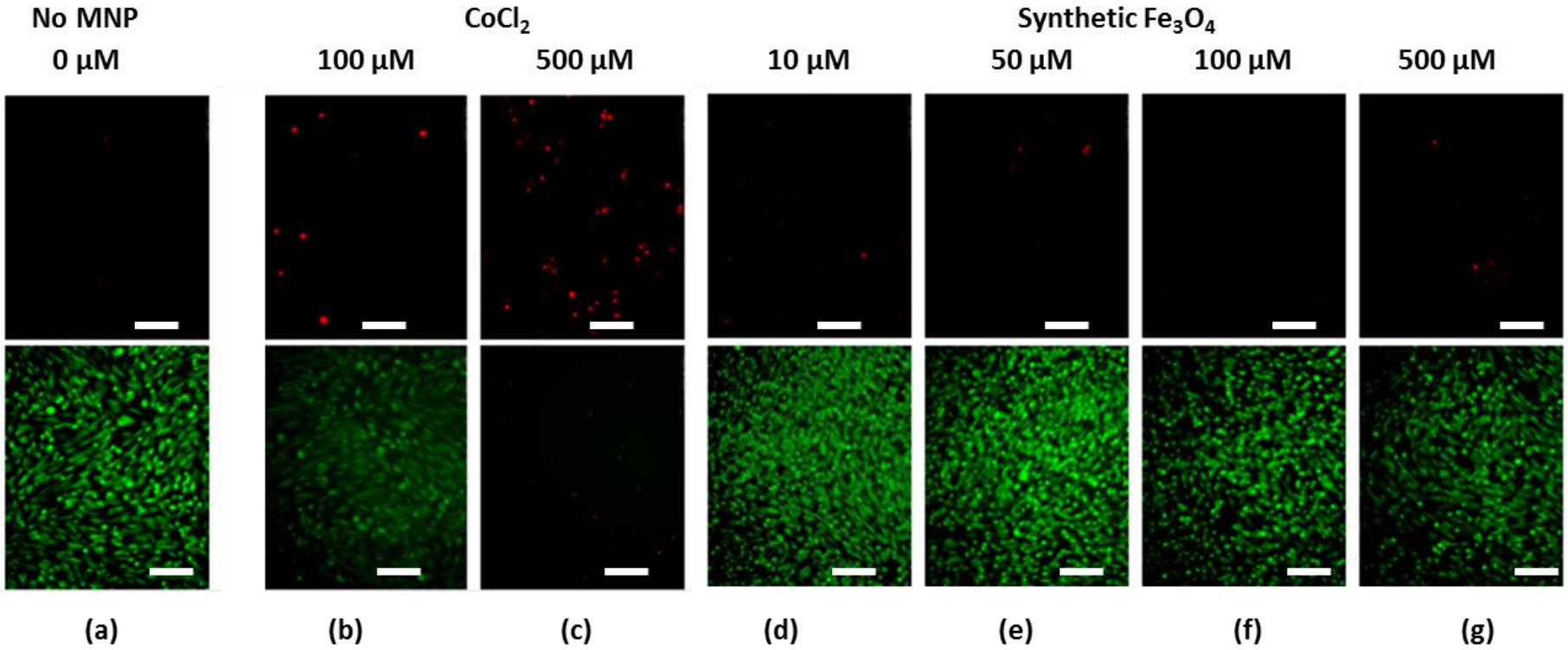

Fig 3.3.8 Live/Dead staining of MG-63 cells exposed to different concentrations of synthetic magnetite: MG-63 cells incubated with 10-500µM (d-g) of synthetic magnetite (Fe_3O_4) , compared to cells with no MNPs (a) and cells with equivalent cation concentrations of $CoCl_2$ (b, c) after 72h. Cells have been stained with EthD (top) for compromised cells and Calcein-AM (bottom row) for viable cells. (Scale bars correspond to 200µm).

To assess the effect of cobalt doping, bright field images for hMSCs incubated with synthetic magnetite, $Co_{1.0}$ MNPs and $CoCl_2$ are shown in Fig 3.3.9. Due to the sharp increase in cytotoxicity from 100 to 500μM in the case of MG-63s, an intermediate concentration of 250μM was assessed in hMSCs. Further, the cobalt doped MNP with the highest level of doping was also compared with pure iron oxide and the ionic form of cobalt ($CoCl_2$) all added in equivalent cation concentrations. Confluent layers of hMSCs with typical fibroblastic morphology (spindle-shaped) similar to the untreated controls (0μM; Fig 3.3.9 a) were observed for cells exposed to synthetic magnetite at all concentrations (Fig 3.3.9 b-d) indicating that these MNPs are not toxic to cells. The MNPs were localized in the perinuclear localization as observed by the circular shapes formed by the brown MNP clusters (Fig 3.3.9 c, d). For the $Co_{1.0}$ MNPs, at 10μM (Fig 3.3.9 f) cellular morphology was similar to the control sample, whereas at 250μM and 500μM cells appeared longer and thinner (Fig 3.3.9 g, h) indicating that at higher concentrations the $Co_{1.0}$ MNP was affecting cell viability. Unlike the synthetic magnetite particles, the $Co_{1.0}$ MNPs are not easily visible in bright field images. This could be due to the larger cluster sizes of magnetite (~123nm) compared to the smaller sizes for $Co_{1.0}$ (~80nm) as measured by the dynamic light scattering technique. Further clustering following internalization makes the synthetic magnetite nanoparticles clearly visible in the bright field images while this internalization-clustering might not be happening for the $Co_{1.0}$ possibly due to their effect on cell viability. In the case of $CoCl_2$, at 250μM (Fig 3.3.9 i) cells are sparse and appear more affected than for the $Co_{1.0}$. At 500μM, very few cells are left and appear completely compromised (Fig 3.3.9 j).

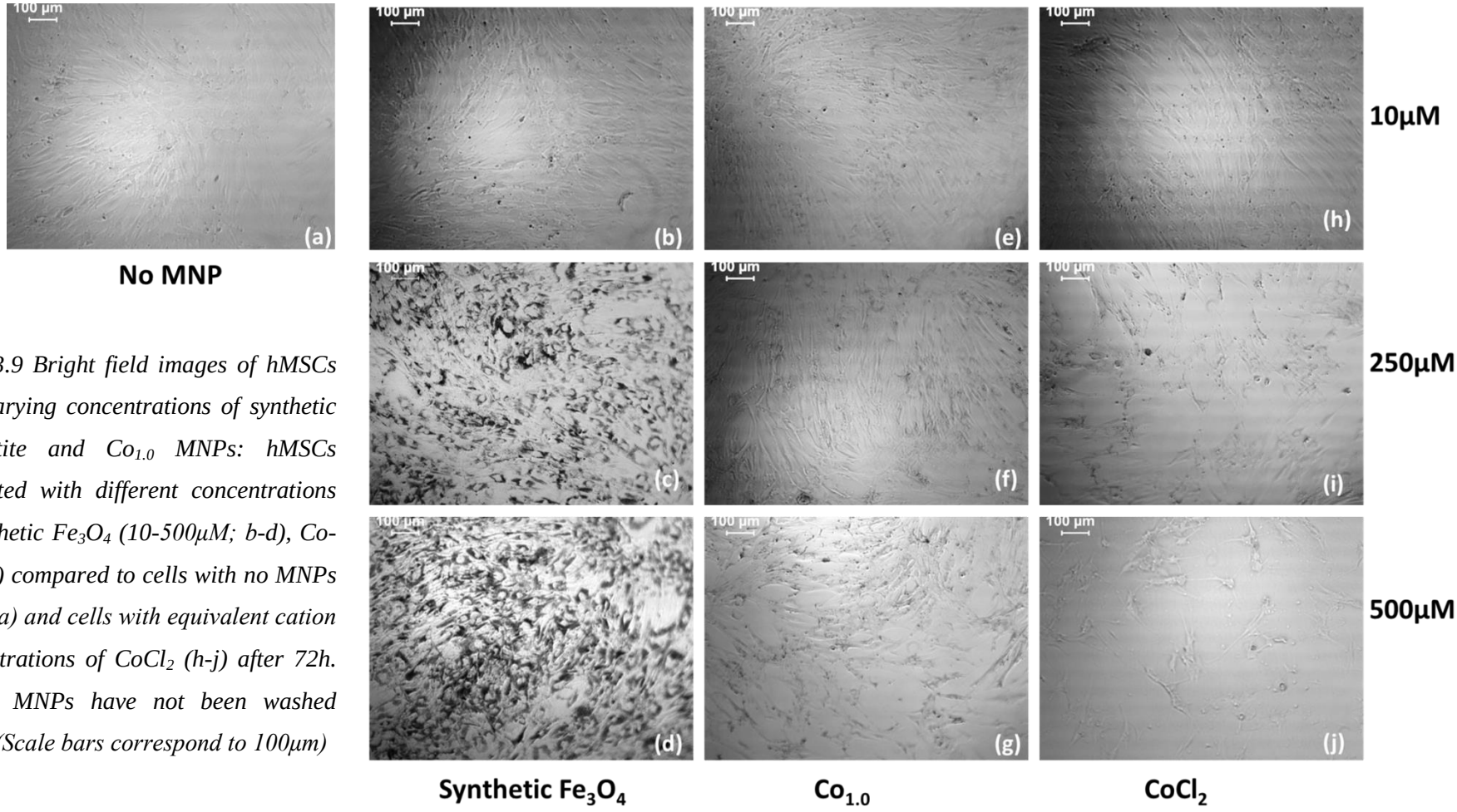

Fig 3.3.9 Bright field images of hMSCs with varying concentrations of synthetic magnetite and $Co_{1.0}$ MNPs: hMSCs incubated with different concentrations of synthetic Fe_3O_4 (10-500µM; b-d), $Co_{1.0}$ (e-g) compared to cells with no MNPs (0µM; a) and cells with equivalent cation concentrations of $CoCl_2$ (h-j) after 72h. Excess MNPs have not been washed away. (Scale bars correspond to 100µm)

Differential live/dead cellular staining for the hMSCs is shown in Fig 3.3.10-11. The viable confluent layer of hMSCs is stained green for the live-no nanoparticle control (Fig 3.3.10a) with very few red-stained dead cells (Fig 3.3.11a). On the other hand, the lysed cell sample (also with no nanoparticles) has no viable (green-stained cells; Fig 3.3.10b) and only dead cells (Fig 3.3.11b). Confluent layers of viable cells are observed for all concentrations of synthetic magnetite (Fig 3.3.10c-e). There is a slight increase in the number of red stained nuclei indicating a possible minor loss in cell viability with addition of the synthetic magnetite MNPs (Fig 3.3.10c-e). For the cells with $Co_{1.0}$, the number of viable cells decreases with increasing nanoparticle concentration (Fig 3.3.10f-h) while there is not a corresponding increase in the number of dead cells (Fig 3.3.1 f-h). This might be due to the fact that the dead cells have detached and have been washed off leaving fewer non-viable cells still attached to the well bottom. At 10μM, neither the $Co_{1.0}$ MNP nor the salt seem to affect viability (Fig 3.3.10f, i). At 250 and 500μM, while both reduce viability, the ionic form of Co (II) has a higher cytotoxicity with lower number of viable cells present (Fig 3.3.10-11 j, k) than its nanoparticle equivalent (Fig 3.3.10-11 g, h).

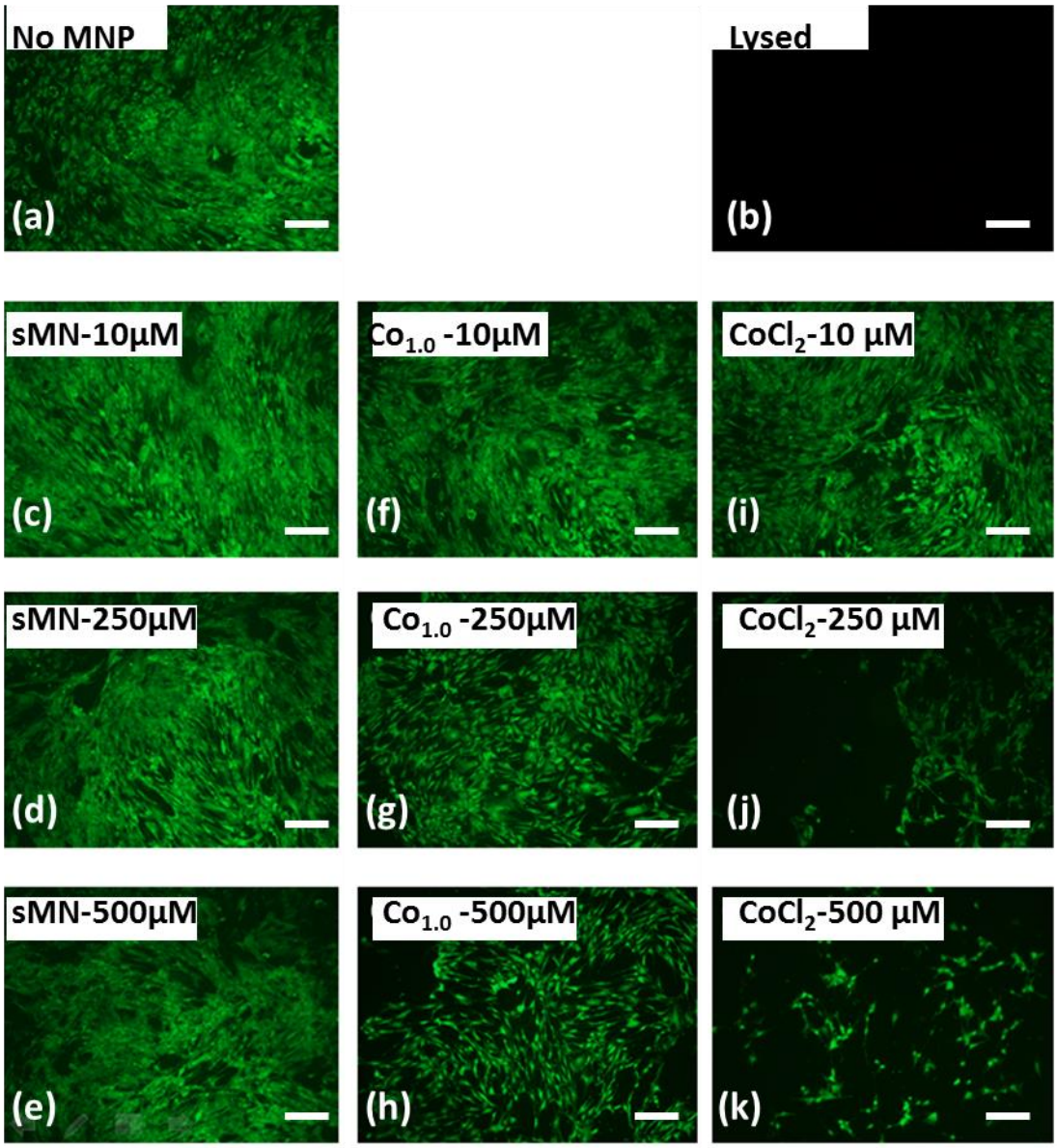

Fig 3.3.10 Calcein-AM staining of hMSCs exposed to synthetic magnetite and $Co_{1.0}$: hMSCs incubated with different concentrations of synthetic magnetite (10-500µM; c-e), $Co_{1.0}$ (f-h) compared to live cells with no MNPs (a) and dead cells with no MNPs (b) after 72h. Also, $CoCl_2$ was added to cells at equivalent cation concentrations (i-k). Cells have been stained with Calcein-AM specific for viable cells (Scale bars correspond to 200µm)

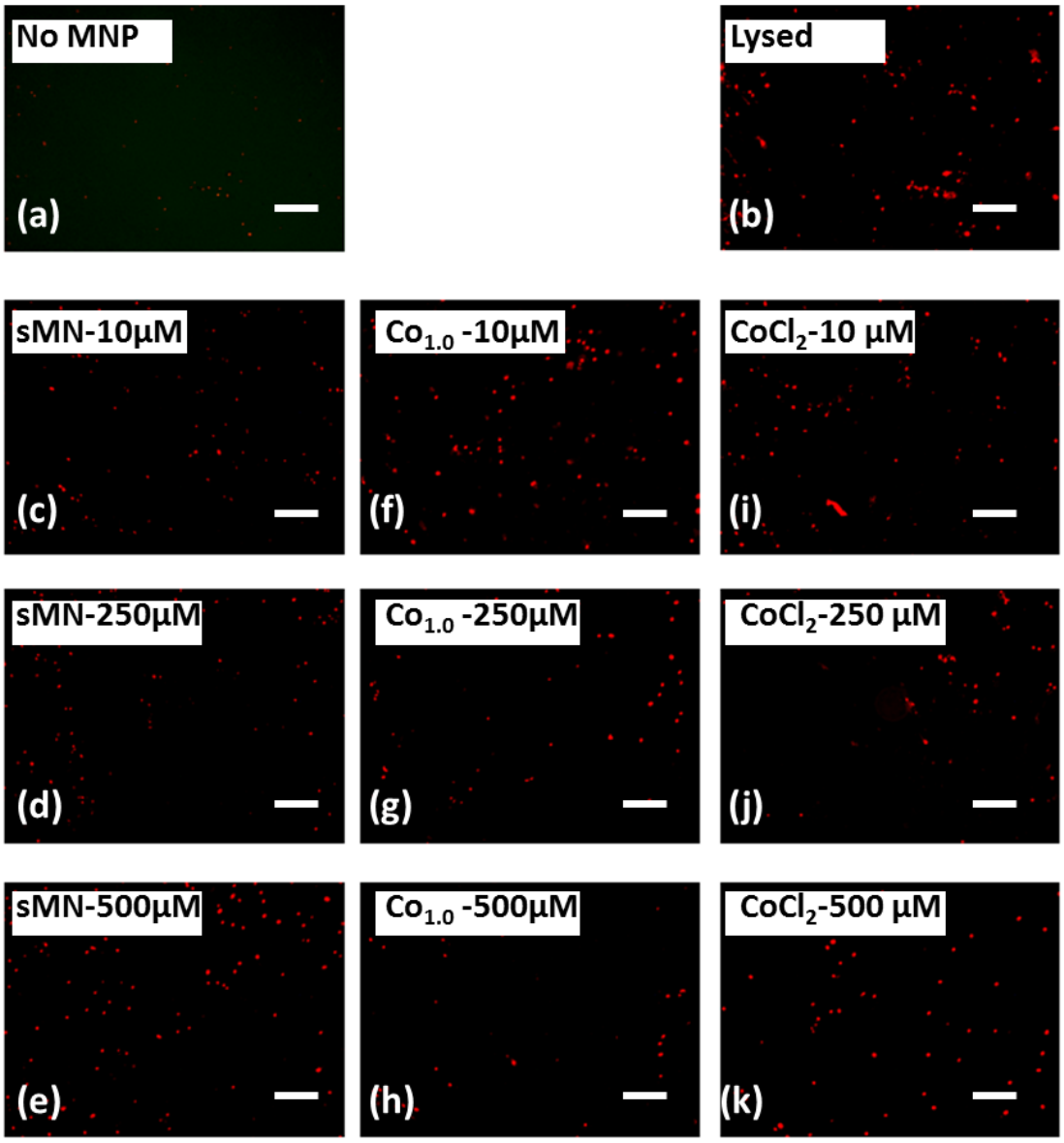

Fig 3.3.11 EthD staining of hMSCs exposed to synthetic magnetite and $Co_{1.0}$: hMSCs incubated with different concentrations of synthetic magnetite (10-500µM; c-e), $Co_{1.0}$ (f-h) compared to live cells with no MNPs (a) and dead cells with no MNPs (b) after 72h. Also, $CoCl_2$ was added to cells at equivalent cation concentrations (i-k). Cells have been stained with EthD specific for compromised cells (Scale bars correspond to 200µm)

The loss in viability, apart from qualitative assessment by fluorescence microscopy, was also quantitatively analysed using flow cytometry (Fig 3.3.12). In a separate experiment, MG-63 cells were incubated with synthetic magnetite, $Co_{1.0}$ and $CoCl_2$ at cation concentrations of 10, 100, 250 and 500µM for 72h. Synthetic magnetite and $Co_{1.0}$ have low cytotoxicity as observed by the similar levels of live (~100%) populations to the

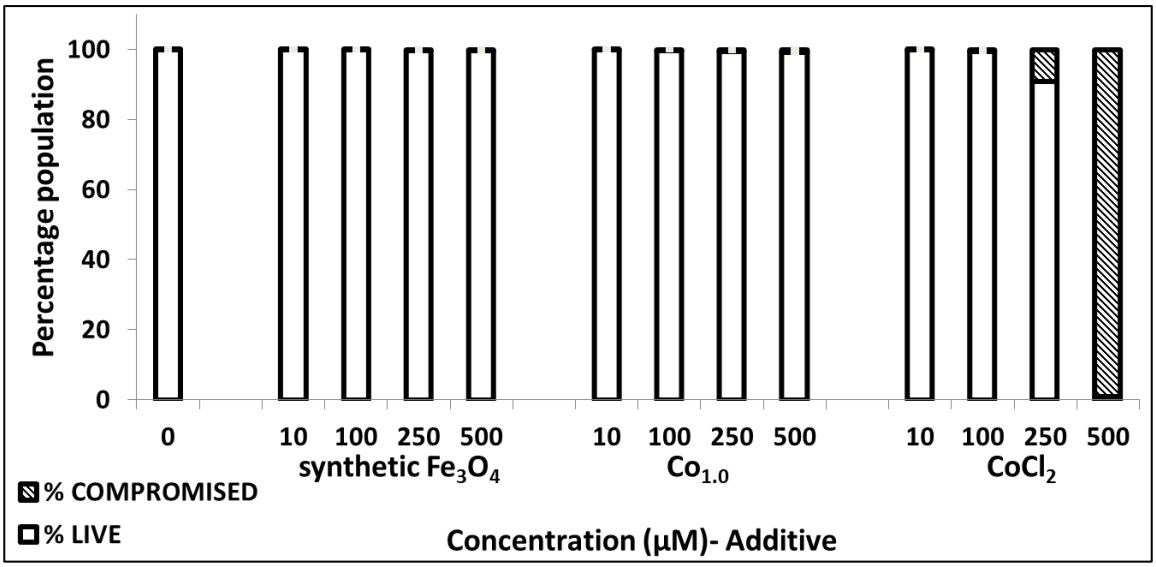

Fig 3.3.12 Flow cytometric quantification of synthetic Fe_3O_4 and $Co_{1.0}$ cytotoxicity in MG-63 cells: MG-63 cells were stained with Calcein-AM and EthD following 72h incubation with different concentrations of synthetic Fe_3O_4, $Co_{1.0}$, and equivalent cation concentrations of $CoCl_2$. The percentage populations of viable and compromised cells were quantified using the flow cytometry technique. Error bars represent the standard error of the means for n=3.

control sample without nanoparticles. The $Co_{1.0}$ nanoparticles are not toxic up to 100µM and at higher concentrations only show moderately higher cytotoxic effects relative to the synthetic magnetite samples of the same concentration. On the other hand, the ionic form of Co (II) has a stronger cytotoxic effect, especially at higher concentrations, with complete loss of viability at 500µM. The raw data FL1 vs FL3 plots (filter for Calcein vs. filter for Ethidium homodimer) are shown in Fig 3.3.13. While for the MNPs, there is no significant change in the population distribution, for the $CoCl_2$ salt treated cells, the shift from live to compromised regions is observed clearly at higher concentrations.

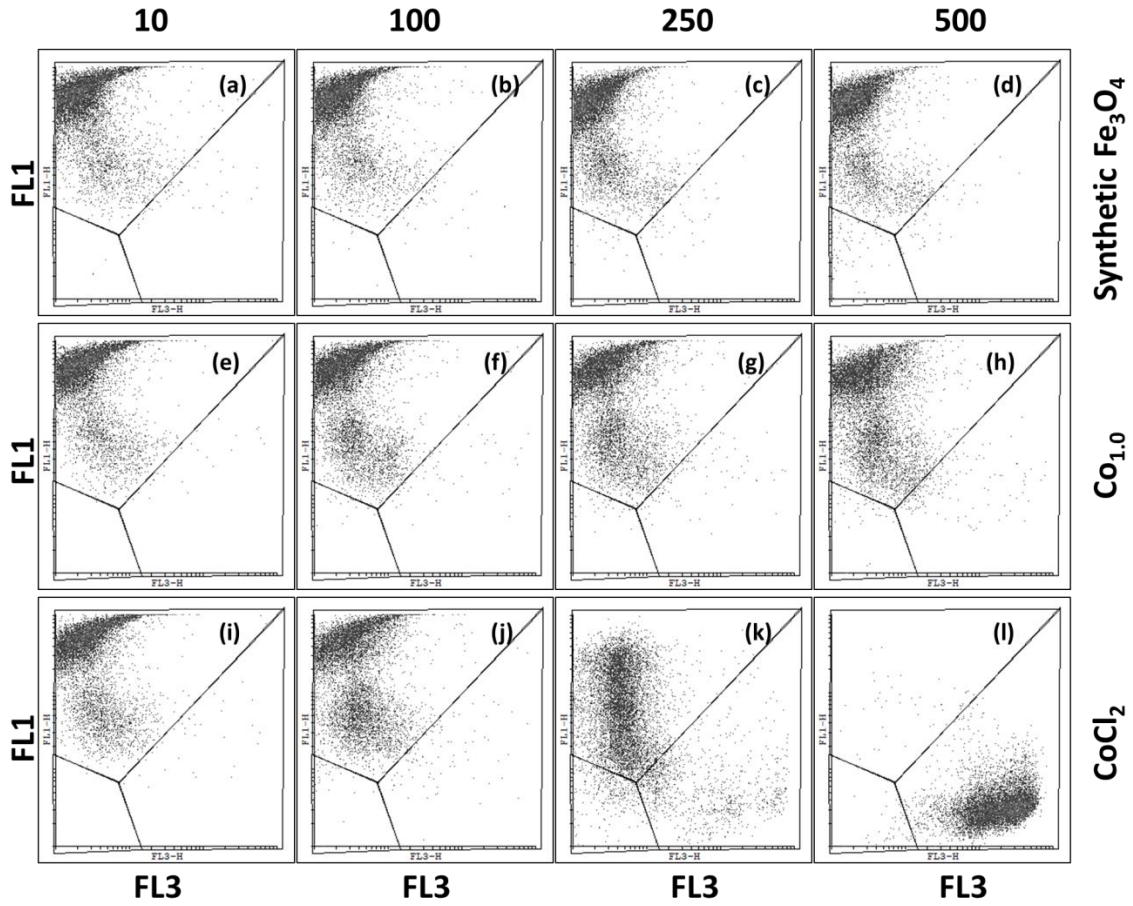

Fig 3.3.13 FL1 vs FL3 scatter plots of MG-63 cells exposed to different concentrations of synthetic Fe_3O_4, $Co_{1.0}$ and $CoCl_2$: MG-63s incubated for 72h with different concentrations of synthetic magnetite at 10 (a), 100 (b), 250 (c), 500μM (d), $Co_{1.0}$ at 10 (e), 100 (f), 250 (g), 500μM (h), and equivalent cation concentrations of $CoCl_2$ (10-i;, 100-j, 250-k, 500μM-l). Cells were stained with Calcein-AM (FL1 channel) and Ethidium Homodimer (FL3 channel).

Apart from giving information about the viability of cells, flow cytometry also provides a method to assess the level of MNP association with cells. The side scatter (SS) of cells indicates their granularity and is modified when cells are associated with MNPs.[124] The increase in the SS of MG-63 cells is observed with increase in the concentration of synthetic magnetite nanoparticles that they were exposed to (Fig 3.3.14) indicating a dose dependant increase in uptake. While at 10μM, no obvious difference to the no-MNP sample (0μM) is observed there is a slight increase for 100-250μM concentrations. At

500μM a sharp increase in the SS is observed. A minor decrease in the forward scatter (FS) values is observed with increasing association with MNPs.

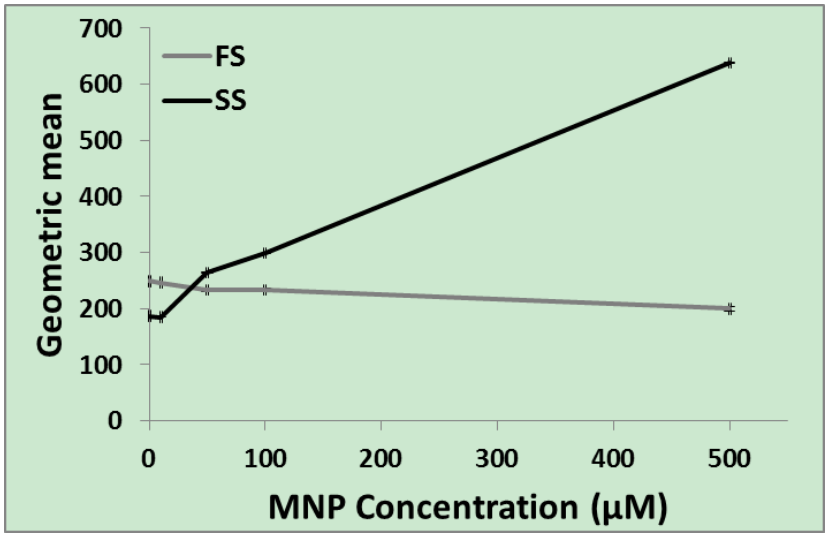

Fig 3.3.14 Change in FS and SS values of cells with MNP uptake: The forward (FS) and side scatter (SS) geometric mean values for MG-63 cells exposed to synthetic magnetite MNPs from 10 to 500μM concentration for 72h.

In the next experiment, the modification in cytotoxicity depending on the level of doping was assessed using cobalt doped nanoparticles in MG-63 cells. Between $Co_{0.4}$, $Co_{0.7}$ and $Co_{1.0}$, decrease in Calcein staining intensity is observed for increasing levels of cobalt doping (Fig 3.3.15 a, c and e respectively). However, they all are quite low for EthD staining indicating the cells are still viable. In this experiment, the Co^{2+} concentrations were equivalent between the nanoparticles and MNPs (and not the total cation concentration). In the cells exposed to the salt, a larger decrease in calcein staining intensity is observed with a concurrent increase in ethidium staining indicating loss in viability. From Fig 3.3.16 it is quite clear that the Co MNP toxicity is much lower than when present as free ions.

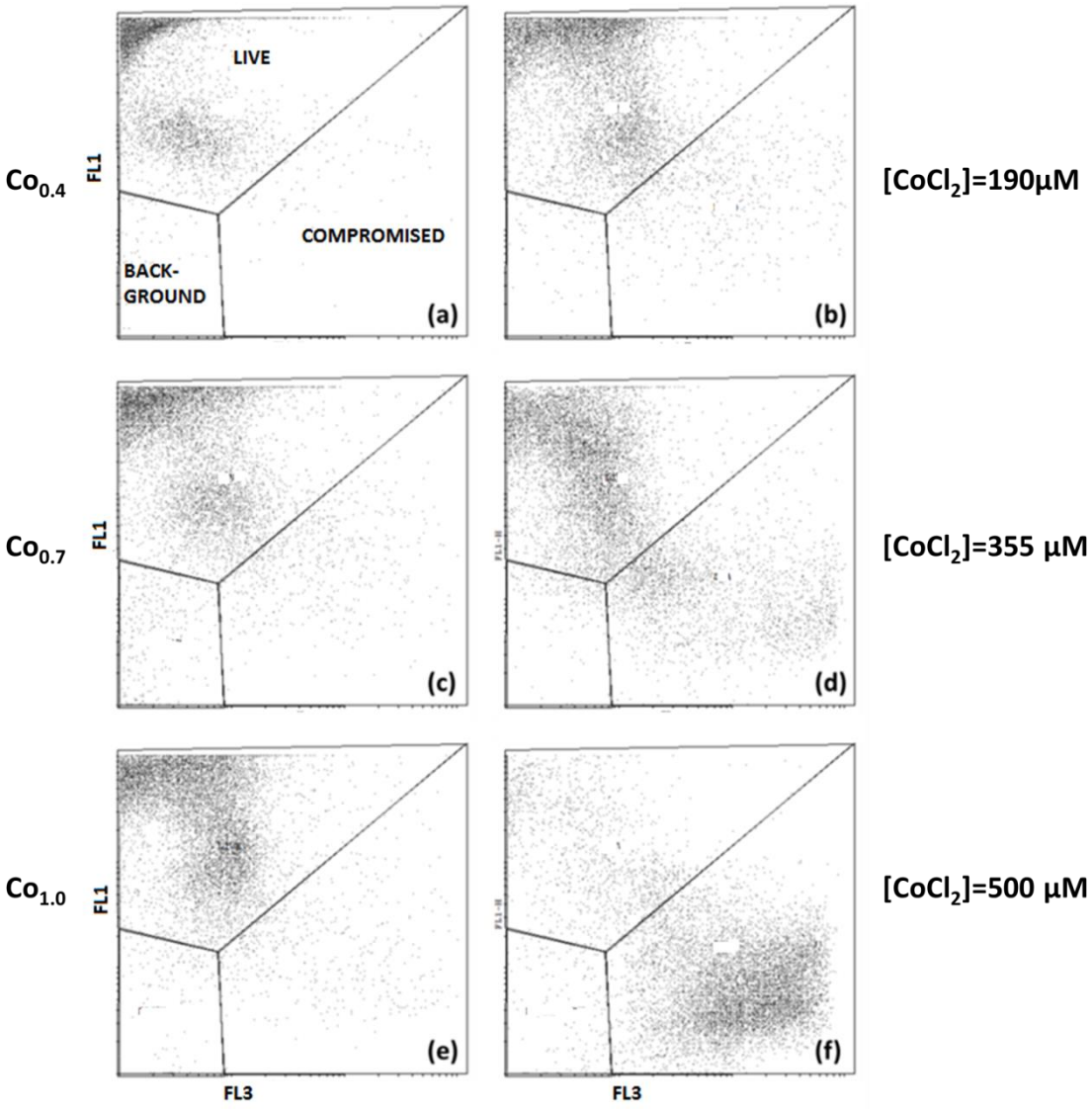

Fig 3.3.15 FL1 vs FL3 scatter plots of MG-63 cells exposed to different cobalt doped MNPs: MG-63 cells incubated with the following MNPs for 72h: $Co_{0.4}$ (a), $Co_{0.7}$ (c) and $Co_{1.0}$ (e) and equivalent Co^{2+} concentrations of $CoCl_2$: 190µM (b), 355µM (d) and 500µM (f) were stained with Calcein-AM (FL1 channel) and EthD (FL3 channel). Plots show cells distributed between the live (cells staining high for CAM), compromised (staining high for EthD) regions and any background (staining for neither dyes) (Regions are marked in plot (a)).

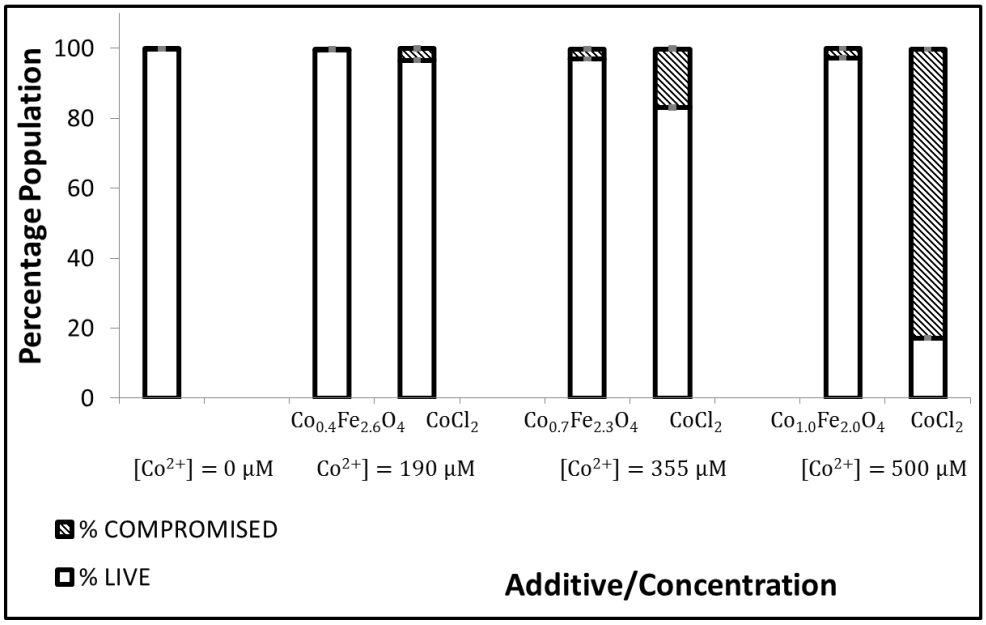

Fig 3.3.16 Flow cytometric quantification of the cytotoxicity of different cobalt MNPs in MG-63 cells: MG-63 cells were stained with Calcein-AM and EthD following 72h incubation with $Co_{0.4}$ (Co^{2+}=190µM), $Co_{0.7}$ (Co^{2+}=355µM) and $Co_{1.0}$ (Co^{2+}=500µM) and equivalent Co^{2+} concentrations of $CoCl_2$. The percentage populations of viable and compromised cells were quantified using the flow cytometry technique. Error bars represent the standard error of the means for n=3.

The effect of zinc doping was also assessed in MG-63s as shown in figs 3.3.17-18. In the case of $Zn_{0.4}$, three distinct populations staining differentially for the calcein dye were observed (FL1 channel measured calcein staining and FL3 the EthD staining; fig 3.3.17a). Comparing their side and forward scatter mean values showed that the side scatter was higher for the population showing lower calcein staining intensity (fig 3.3.17b, c). This increasing SS could probably be an indication of higher MNP uptake. It could be that the zinc-doped MNPs are interfering with calcein staining. Divalent cations such as Fe and Co are also known to interfere with calcein fluorescence[171] but this has not been observed in our experiments. To allow for this effect the gates for the live and compromised regions were re-defined ensuring that at least 95-99% of each population fell within the gated regions.

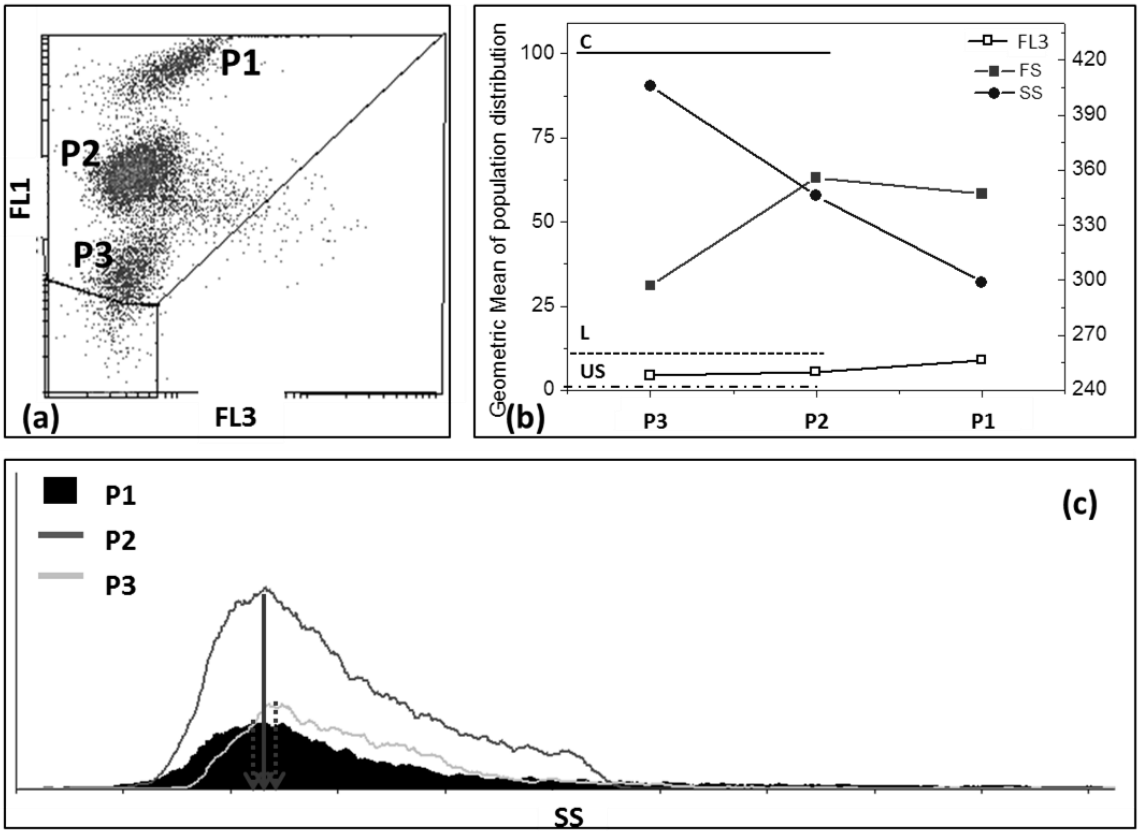

Fig 3.3.17 Effect of zinc-doped MNPs on calcein fluorescence: MG-63 cells incubated with different $Zn_{0.4}$MNPs (500μM) for 72h were stained with CAM and EthD, assessed via flow cytometry. (a) Three distinct populations marked P1-3 for CAM (FL1) fluorescence (with similar EthD/FL3 intensities) were observed. (b) The variation of CAM intensity (FL1), forward (FS) and side (SS) scatter for the three populations compared to the value of the control populations of live (L), compromised (C) and unstained (US) cells. (c) Histogram showing that the CAM staining decreasing with increase in side scatter (SS) for the three populations

As seen in Fig 3.3.18, synthetic magnetite (98% Live), $Zn_{0.4}$ (99% Live) and $Zn_{0.6}$ (97% Live) have negligible cytotoxicity with levels of viable cells similar to the population not exposed to nanoparticles (100% Live). The cells exposed to the $Zn_{0.9}$ sample show a higher cytotoxic effect with almost 40% of the population compromised.

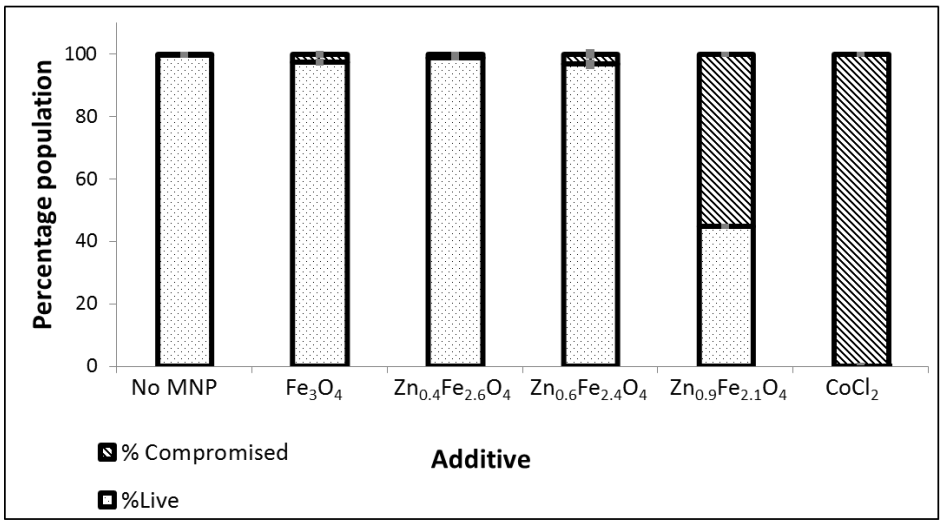

Fig 3.3.18 Flow cytometric quantification of the cytotoxicity of different zinc MNPs in MG-63 cells: MG-63s were stained with Calcein-AM and EthD following 72h incubation with 500μM of $Zn_{0.4}$, $Zn_{0.6}$ and $Zn_{0.9}$ and $CoCl_2$ at equivalent cation concentration. The percentage populations of viable and compromised cells were quantified using the flow cytometry technique. Error bars represent the standard error of the means for n=3.

The cytotoxicity of the MNPs was also assessed in hMSCs. Unlike in the case of MG-63s where an exhaustive study of different particle at different concentrations were carried out, in the hMSCs MNPs of interest at concentrations not toxic to MG-63s (100μM) were assessed to confirm their cellular biocompatibility in hMSCs as well (Fig 3.3.19). A similar trend to the MG-63s was present for the synthetic magnetite, $Zn_{0.4}$ and $Co_{0.4}$: very low levels of cytotoxicity. The percentage of viable population was similar to the cells not exposed to MNPs. The $CoCl_2$ at equivalent cation concentrations was significantly cytotoxic with the viable population lower than 30%.

Following cytotoxicity studies, the doped MNPs were assessed for possible effects on the differentiation potential of hMSCs. The osteogenic differentiation of hMSCs as measured via the alkaline phosphatase (ALP) assay[172] at day 7 and 14 is shown in Fig 3.3.20. Compared with the cells cultured in expansion media, cells cultured in osteogenic differentiation media show a significant up-regulation in the ALP production at day 7 and

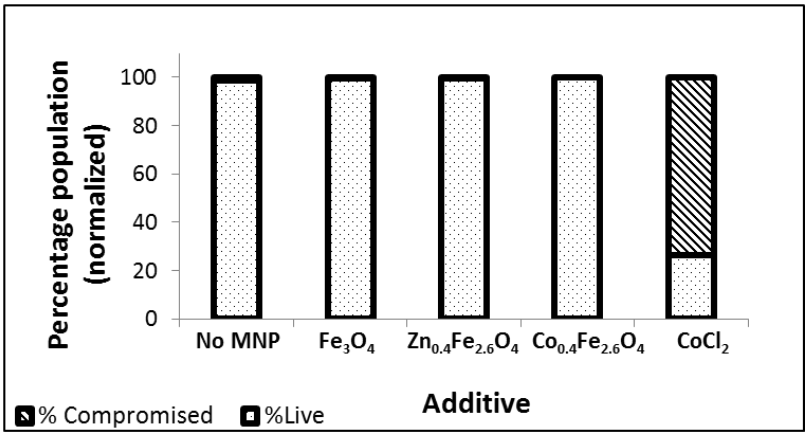

Fig 3.3.19 Flow cytometric quantification of the cytotoxicity of different zinc and cobalt doped MNPs in hMSCs: hMSCs were stained with Calcein-AM and EthD following 72h incubation with synthetic Fe_3O_4, $Zn_{0.4}$ and $Co_{0.4}$ at 100µM and equivalent cation concentrations of $CoCl_2$. The percentage populations of viable and compromised cells were quantified using the flow cytometry technique. Error bars represent the standard error of the means for n=3.

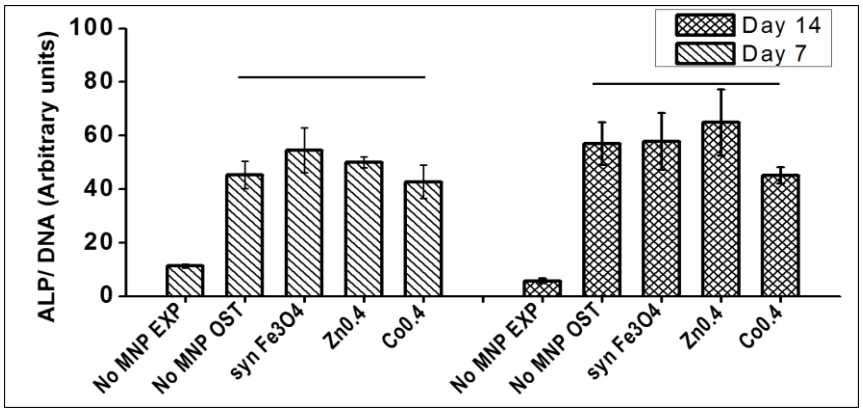

Fig 3.3.20 Effect of MNPs on the osteogenic differentiation potential of hMSCs: hMSCs were exposed to 100µM of synthetic Fe_3O_4 (syn Fe_3O_4), $Zn_{0.4}$ and $Co_{0.4}$ for 72h following which they were incubated in osteogenic (OST) media. Osteogenesis was measured through ALP production and normalized to cell number by measuring DNA content at day 7 and 14. ALP production was compared to cells not exposed to nanoparticles grown in expansion media (No MNP EXP) and osteogenic media (No MNP OST). Error bars represent standard error for n=3 and line over columns indicates groups that were not significantly different from each other (Tukey's HSD, $p< 0.05$)

day 14. However the ALP production of cells following internalization of synthetic Fe_3O_4, $Zn_{0.4}$ and $Co_{0.4}$, in osteogenic differentiation media, is not significantly different from the

control cells in the same media (Fig. 3.3.20). Thus it appears that osteogenic differentiation of the cells is unaffected by their uptake of the nanoparticles.

3.3.2 Effect of cellular internalization on the magnetic response of nanoparticles

The magnetic ACS measurements give information about the magnetic relaxation mechanisms of nanoparticles in the conditions tested. The ACS of citric acid coated stable aqueous suspensions (100μM) of chemically synthesized magnetite (synthetic magnetite) and various biogenic undoped and cobalt or zinc doped magnetite nanoparticles are shown in Fig 3.3.21. With increasing frequency, the χ' (the component in phase with the applied field) reduces while χ" (the out-of-phase component), depending on the sample type peaks at a certain frequency. These peaks in the χ" curves are typical of a Brownian magnetisation relaxation process, with the frequency position of this peak depending on the hydrodynamic size of the particles.[114] Between the different MNPs, the synthetic magnetite (Fig 3.3.21a), biogenic $Co_{0.4}$ (Fig 3.3.21c) and $Zn_{0.4}$ (Fig 3.3.21f) show the strongest signal (large χ' values at lower range of frequencies). Although the nanoparticle core sizes vary between samples depending on the level of doping,[109,110] the similar positions of the χ" peaks reveal comparable hydrodynamic particle/cluster sizes for all samples, being in the range 35-55nm. Despite the peak positions in the χ" curves being similar, distinct variations in the relative shapes of the ACS curves can be seen for the different particle types. For example, in $Co_{0.4}$ the overlap of the χ' and χ" curves are typical of MNPs relaxing via a single mechanism. Based on the low frequency (around 10 kHz) at which this is observed it can be said that the $Co_{0.4}$ MNPs are blocked MNPs showing pure Brownian relaxation (see Fig 1.4.5). The symmetry of χ" peak at (Fig. 3.3.21c) and a complete loss in the χ' signal beyond this value also confirm this observation. A similar

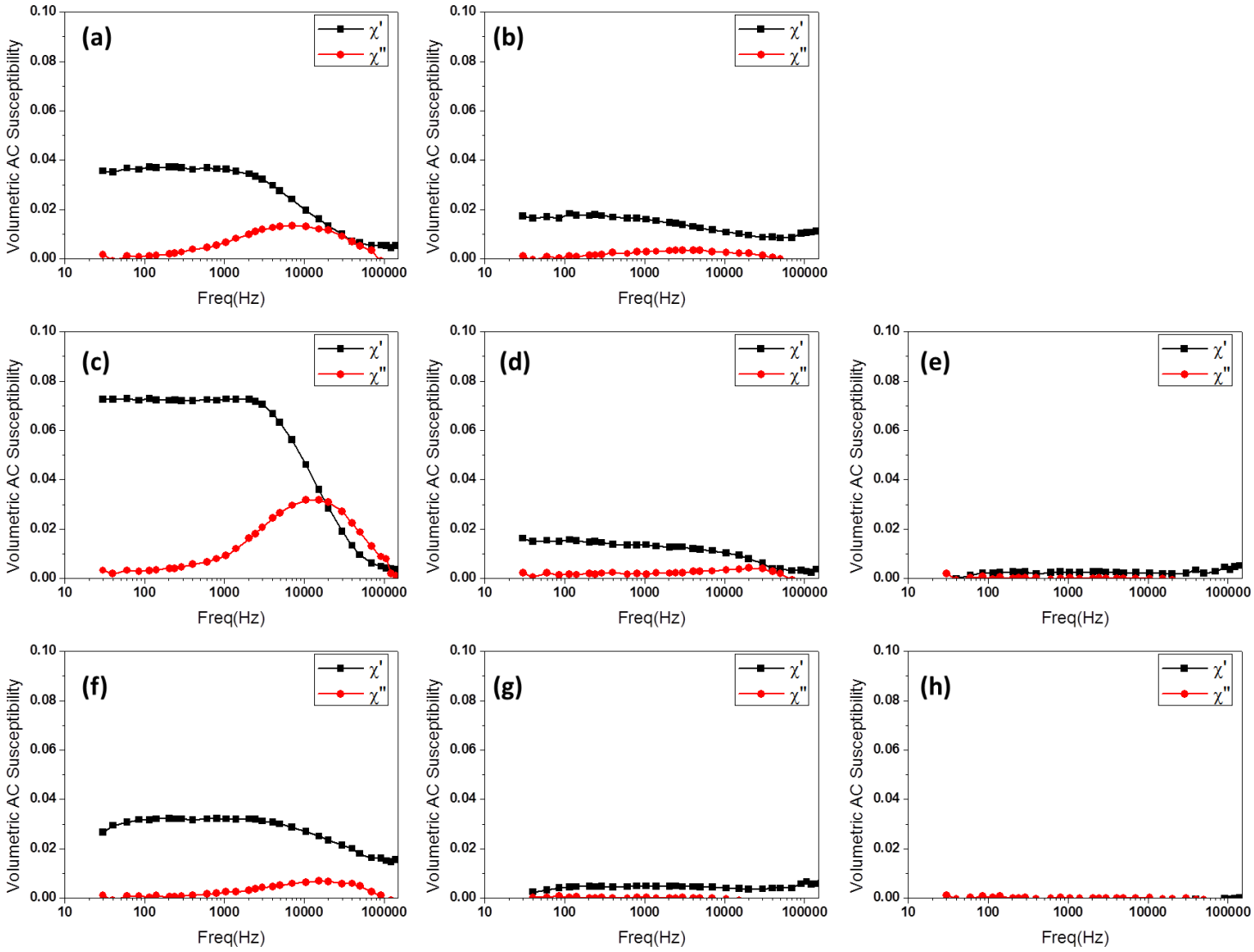

Fig 3.3.21 ACS curves of stable aqueous suspensions of MNPs: synthetic Fe_3O_4 (a), biogenic Fe_3O_4 (b), $Co_{0.4}$ (c), $Co_{0.7}$ (d), $Co_{1.0}$ (e), $Zn_{0.4}$ (f), $Zn_{0.6}$ (g) and $Zn_{0.9}$ (h).

trend is observed for $Co_{0.6}$ in terms of loss in signal beyond the very low peak observed at around 20 kHz (Fig 3.3.21d). This indicates a dominant Brownian mode of relaxation which is expected for the magnetically blocked cobalt MNPS due to their high anisotropy.[109,114] In contrast the undoped synthetic (Fig 3.3.21a) and biogenic magnetite (Fig 3.3.21b) as well as $Zn_{0.4}$ (Fig 3.3.21f) have an asymmetrical χ" peak and a real (χ') component that persists above zero at the higher frequencies. This is because these samples contain a fraction of particles that are superparamagnetic (small core size/ lower anisotropy) within the measured frequency range relaxing via the Neél mode which typically occurs at higher frequencies.[110,114,170] Higher levels of cobalt and zinc doping completely eliminate the magnetic properties of the MNPs as evidenced by the lack of ACS signal for $Co_{1.0}$ (Fig 3.3.21e), $Zn_{0.6}$ (Fig 3.3.21g) and $Zn_{0.9}$ (Fig 3.3.21h).

The MNPs showing the strongest ACS signal in water, namely synthetic magnetite, biogenic $Co_{0.4}$ and $Zn_{0.4}$ were further investigated for changes in magnetic properties when associated with cells. In cells, the magnitude of ACS is reduced by a factor of ~20 for synthetic Fe_3O_4 (Fig 3.3.22a) compared with a factor of ~10 for $Zn_{0.4}$ (Fig 3.3.22b). Most dramatically, the cobalt doped MNPs, which showed the strongest signal in water, give a negligible response in cells with almost zero susceptibility signal (Fig 3.3.22c). Further to this the peaks in the χ" component, associated with Brownian relaxation, are absent for all the particle types when in cells (Fig 3.3.21a, c, f and Fig 3.3.22). These results are entirely consistent with the complete removal of the Brownian relaxation from the ACS signal such that only the contribution from the MNPs relaxing via the Neél mode remains. As Brownian relaxation can only occur when the nanoparticles are mobile, this result suggests that the nanoparticles have lost mobility following their interaction with the cells. This could be due to binding of the nanoparticles with the plasma membrane or intracellular

membranes. Also, another possible reason could be due to aggregation of the nanoparticles upon internalization to form larger clusters with sizes greater than that detectable by the ACS instrument (the maximum hydrodynamic size detectable in water is ~350nm).

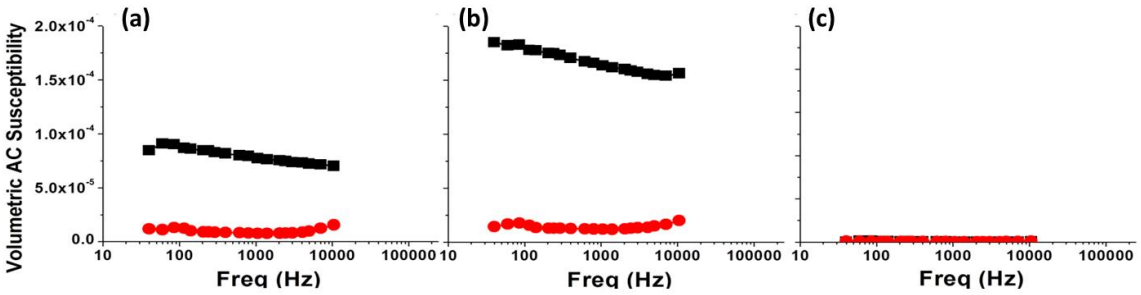

Fig 3.3.22 ACS curves of MNPs associated with MG-63 cells following 72 hours incubation for synthetic Fe_3O_4 (a), $Zn_{0.4}$ (b), and $Co_{0.4}$ (c). Black curves represent the χ' components and the red curves, the χ" components of ACS. (Data limited to lower frequencies as the samples were dilute)

3.3 Discussion

Understanding the interaction between cells and nanoparticles gives valuable information for choice of various parameters such as the particle type, dosage and incubation time in order to elicit the most efficient magnetic response for biological applications. In this chapter, synthetic and biogenic MNPs were investigated for their dynamics of uptake, cytotoxicity in cells as well as the effect cells have on the MNPs' magnetic behaviour. The citric acid coating on these particles is versatile as apart from being a preliminary surface coat for preparing stable aqueous suspensions, the free carboxyl groups[173] provide options for further coatings or attachment of biomolecules. They could be functionalized with ligands to target specific membrane proteins for applications needing membrane localization rather than internalization. On the other hand, the citric acid coating does not maintain the colloidal stability of the MNPs when introduced into cell-culture media and the MNPs cluster further. This clustering could be advantageous as it increases the settling

rate of the MNPs to the bottom of the wells thereby increasing their bioavailability to the cells. Also, the different MNPs investigated, due to the identical citric acid coating, cluster in a similar fashion irrespective of the metal core composition or size. The main MNP characteristics affecting their cellular uptake are the hydrodynamic size, shape and surface charge of the MNPs.[145,174] Having similar coating material and cluster sizes would allow similar levels and route of cellular uptake[175] between the different particle types under investigation making it easier to compare between them for the different assays. Also, similar cluster sizes would reduce disparities in the settling rate and obviate any dose-related changes in cytotoxicity.[174]

The internalization of MNPs within lysosomes could facilitate their rapid dissolution/ corrosion within the cytoplasm, especially due to their high surface to volume ratio and consequently large reactive surface, leading to the release of toxic ions. Uncoated ~30nm cobalt nanoparticles at concentrations as low as 2μM have previously been shown to significantly reduce the viability of human fibroblasts within 72h of exposure.[151] In our work, the dopant metals are present in the nanoparticles as tightly bound cations within the magnetite lattice.[92,109,110] This could minimise the leaching of cobalt or zinc ions compared to the pure metal or metal oxide nanoparticles and hence decrease their cytotoxicity. However the fact that we observe an increase in cytotoxicity that correlates with the level of dopant in the nanoparticles, suggests some leaching of the dopant may still occur. Also, the $Zn_{0.9}$ MNP had a higher cytotoxicity than cobalt MNP with equivalent cobalt concentrations ($Co_{1.0}$). This could be due to the higher solubility of zinc oxide nanoparticles in aqueous solutions and also because zinc ions are more cytotoxic than cobalt ions.[149] However, another possible explanation could be the interaction of the zinc with the citrate surface coating. It is known that the solubility of zinc oxide is enhanced in

the presence of citrate and that it depends on the core nanoparticle size irrespective of the cluster (hydrodynamic) sizes.[176] This, together with the higher levels of zinc doping, would explain the enhanced toxicity as the $Zn_{0.9}$ MNPs which have smaller core sizes and hence higher surface area in comparison to the lower doped zinc nanoparticles.[109,110] On the other hand, cobalt oxide solubility is not significantly affected by presence of citrate[177] and hence a gradual and minor increase in cytotoxicity is observed with increasing levels of cobalt doping. It is important to note that the MG-63 cells are different to hMSCs in their sensitivity to $CoCl_2$. While even at 190μM of $CoCl_2$ very low levels of cytotoxicity is observed in MG-63 cells, hMSCs are more affected even at 100μM (75% cell death). This clearly demonstrates the difference in sensitivity between cell types, in this case primary stem cells and a cancerous cell line, and the need to assess this carefully prior to cellular applications. Although *in vitro* experiments are not true indications of *in vivo* biocompatibility, they are valuable as pre-screening tests of cytotoxicity. Further studies looking at the genotoxicity for *in vitro* cellular applications as well as the short and long term biocompatibility *in vivo* studies need to be performed prior to use in clinical applications.

In terms of their magnetic properties, synthetic magnetite, biogenic $Co_{0.4}$ and $Zn_{0.4}$ showed the strongest magnetic response in water amongst all other MNPs. Apart from having low cytotoxicity in both cell types (MG-63 cells and hMSCs), they also did not interfere with the production of ALP in hMSCs and hence onset of osteogenesis. Generally, previous studies have shown that the effect on trilineage differentiation of stem cells seems to depend on the particle type and the lineage of differentiation. For instance while chitosan coated superparamagnetic iron oxide particles did not interfere with osteo-/adipo-/ chondrogenic differentiation of bone marrow derived hMSCs,[33] MRI contrast agent

nanoparticle Resovist/ Ferucarbotran was shown to affect differentiation.[33,34] While one study shows that Resovist particles inhibit only the chondrogenic differentiation[33] (not adipo- or osteogenic) another study[34] shows that the same nanoparticle does inhibit osteogenic differentiation[34] in the same cell type. Such contradicting results increase the need to thoroughly assess effects of all different nanoparticles on stem cell behaviour. Further studies are needed to ensure that the zinc and cobalt doped nanoparticles used in this study do not affect adipogenic and chondrogenic potential of hMSCs, but the results obtained here strengthen the biocompatible nature of these biogenic doped magnetites for cellular applications.

Despite the strong ACS response of synthetic magnetite, biogenic $Co_{0.4}$ and $Zn_{0.4}$ in water, due to immobilization in cells only $Zn_{0.4}$ gives a strong response due to its strong Néel relaxation component. This has implications for intracellular magnetic heating applications that utilise magnetisation relaxation mechanisms of MNPs. MNPs such as the cobalt doped particles, that show strong response in aqueous suspensions lose this property when immobilized in glycerol due to loss in their Brownian relaxation.[114] Unless strong magnetic field amplitudes are applied, a similar suppression of magnetic hyperthermia would be expected in cell based applications using cobalt doped nanoparticles. Conversely the survival of Néel relaxation for the zinc doped nanoparticles associated with cells, suggests cellular based magnetic hyperthermia might be possible with these particles even under clinically relevant magnetic field conditions.

In summary, the low levels of zinc-doped MNPs appear to be the best candidates for cellular hyperthermia applications. This is attributed to their low cytotoxicity and high magnetic response in a cellular milieu compared to the other particle types. The surface

coating could be modified or improved to further ensure cellular biocompatibility and for Biofunctionalization with proteins or ligands to target different sub-cellular regions.

CHAPTER 4 Effect of bulk heat shock on stem cell behaviour

4.1 Introduction

The behaviour of cells is dictated by the physical factors such as the mechanical forces they experience, oxygen tension, and temperature. In the case of stem cells, these factors affect their proliferation and differentiation and hence tissue organization and properties. Especially, the positive effect of mechanical parameters on the differentiation of human mesenchymal stem cells (hMSCs) is well established. For instance, four-point bending loads, compressive loads, translation and rotational strains increase osteogenesis,[31] chondrogenesis[178] and ligamentogenesis[179], respectively.

The influence of temperature on stem cells behaviour has not been thoroughly investigated. A few studies have shown that mild heat shock of up to 5^0C above the optimal temperature of 37^0C, has a positive effect on the differentiation potential of hMSCs.[43–46] The mechanism via which heat regulates changes in cellular behaviour is also not clear. It could possibly be via the production of heat shock proteins (HSPs) or via activation of heat sensitive membrane ion channels. Typically, maximum HSP expression is observed at 10-15^0C above optimal growth temperatures in most organisms while moderate temperature changes might give rise to a diminished and transient HSP expression. Their expression in turn might affect downstream gene expression and hence cellular behaviour. In the case of heat sensitive membrane ion channels, each type has a different threshold temperature above/below which the channel is activated triggering downstream signalling cascades. Both mechanisms are strongly dependant on the temperature of heat shock.

In this chapter, the effect of bulk heat shock in terms of temperatures, exposure times and frequencies on proliferation and osteogenic differentiation on cells will be explored. Bulk heat shock refers to the process where the cell system (cells cultured in well plates or T-

flasks with cell-culture media) is as a whole exposed to an elevated temperature. The effect will be investigated on two cell types, namely human mesenchymal stem cells and osteoblast-like cancer cell-line, MG-63s (see section 1.4 for more details). For these cells, osteogenesis will be studied by assessing expression of the early osteogenic-marker enzyme, alkaline phosphatase (ALP) and mineralization at later time points (> 20 days) via the Alizarin red staining technique. The investigations will help understand the effect of heat on cellular behaviour and identify optimum heating conditions to promote osteogenesis of cells.

4.2 Materials and methods

4.2.1 Cell culture

Primary bone marrow derived human mesenchymal stem cells below passage 5 were used for all experiments. MG-63 cells were used between passages 20-100. Stocks were recovered from liquid nitrogen and cultured in expansion medium consisting of high glucose Dulbecco's modified Eagle minimum essential medium (DMEM) (Sigma, UK) supplemented with 10% foetal bovine serum (FBS) (Sigma, UK), 1% antibiotics and antimycotics and 1% glutamine (Sigma, UK). For preparing the osteogenic differentiation medium, the expansion medium was supplemented with the following (all from Sigma, UK): 1% Non-essential amino acids, 0.1µM Dexamethasone in DMSO, 50µM ascorbic acid and 10mM β-glycerophosphate.

4.2.2 Heat shock treatments

Cells were seeded in 24 well plates at 6,000 cells/cm^2 (unless mentioned otherwise) for hMSCs and variable numbers for MG-63s. In the first experiment 20,000 cells/cm^2 MG-63 cells were used, but since they reached confluence rapidly, for future longer time period

experiments, a lower seeding density of 5,000 cells/cm^2 was used. Cells were counted in a haemocytometer following trypan blue staining. Mild heat shock is defined as temperatures not higher than 5^{0}C from the normal culture temperature of 37^{0}C and greater than 10^{0}C above 37^{0}C were defined as severe heat shock.

After 24h following seeding, cells were exposed to the heat shock treatments defined below (Table 4.1). Osteogenic assays were carried out at different time points as stated below.

Experiment number	**Achieved (Target) Temperature (^{0}C)**	**Duration (min)**	**Frequency (Heat shock application time point)**	**Cell Type and seeding density (cells/cm^2)**	**Assays and time points**
01	40 (42)	30	1x	hMSCs 2000	DNA and ALP Day 10, 20, 30
02	40 (42)	30	1x	hMSCs 6000	DNA and ALP Day 10, 20, 30
03	40 to 41 (42)	60	2x (Day 3, 5)	MG-63 20,000	DNA and ALP Day 4, 6
04	40 (42), >50 (55)	60	4X (Day 0, 3, 5, 7)	hMSCs 6,000	DNA and ALP Day 2, 4, 6, 8
05	40 (42), >50 (55)	60	4x (Day 0, 3, 5, 7)	MG-63 5,000	DNA and ALP Day 2, 4, 6, 8

Table 4.1 Details of the various bulk heat shock experiments.

All heat shock was provided in bulk. Cells grown in well plates or flasks were placed in water baths, incubators or fan ovens to achieve the required temperatures. An attempt to use media preheated to the required temperature did not work efficiently as the solution temperature fell to ambient temperature level before samples were transported to the heating chamber. Temperature was monitored using a K-type thermocouple connected to a data-logger. The thermocouple was immersed in cell-culture medium (same volume as in

the samples) in a separate well-plate or in some cases a cell-free well within the same well plate. The untreated controls were kept in the incubator at 37^0C. To compensate for the lack of CO_2 regulation in the treated samples, the untreated samples were covered with parafilm to prevent gas exchange within the incubator. In mild heat shock experiments, cell-culture medium was changed prior to and immediately following heat shock. The post-heat shock media change ensures that cells are immediately brought back to optimal temperatures and also compensates for any media lost due to evaporation (outer empty wells were filled with PBS and the whole plate covered with parafilm to reduce evaporation). In the case of severely heat shocked samples, where cells seemed on the verge of detachment, media change was avoided to circumvent loss of cells during the aspiration step. Following this, cell-culture medium was changed once every 3 days for the duration of the experiment.

4.2.3 Differentiation studies

Osteogenic differentiation was studied for cells at different time points by measuring ALP production and mineralization. The methodology for ALP and Alizarin red staining for mineralization are explained in detail in Chapter 2, sections 2.6.1 and 2.6.4. Cell numbers were quantified by measuring the DNA concentrations using the Picogreen assay (see Chapter 2, section 2.6.5 for further details).

4.2.4 Assessing heat shock protein expression

Cells exposed to bulk heat shock or to HSP70 (heat shock protein 70kDa) inducer, Geranylgeranylacetone (GGA; Sigma, UK) were stained for HSP70 protein using mouse monoclonal primary Anti-HSP70 antibody (Abcam, UK) targeting human HSP70. In brief, hMSCs at passage 1 and 5 were grown as monolayers on coverslips. They were incubated

with different concentrations of GGA (0-100μM) in PBS or exposed to bulk heat shock (42^0C) in a water bath for 1h. Following this media was changed in all wells. After 4h, cells were stained for HSP70 as follows. Cells were washed with PBS and fixed with 70% v/v ice cold methanol for 10min at room temperature. They were washed and permeabilized in 0.25% Triton-X in PBS (v/v). Following this they were washed and the proteins were blocked using 1% w/v bovine serum albumin (BSA) in PBS for 30min. The primary antibody at 1:100 dilutions in in PBS was added to cells and incubated overnight at 4^0C on a shaker. Following incubation, the excess primary antibody solution was washed off and cells were incubated with the Goat anti-Rabbit IgG (H+L) Secondary Antibody, DyLight 405 conjugate (1:1000 dilutions in 0.1% v/v BSA in PBS; Thermo Scientific, Pierce Antibodies, UK) at room temperature in the dark for 1h. After washing off the excess secondary antibody solution, cells were stained for DAPI (10μg/ml; Sigma, UK) for 10min at room temperature. Excess stain was washed off, coverslips were mounted on glass slides using mounting medium and observed under the fluorescence microscope. To assess levels of non-specific binding (binding of the secondary antibody to proteins other than the primary antibody non-specifically giving rise to false positives) a set of controls were incubated only with the secondary antibody (Fig 4.2.1) and not the primary. There was no staining which indicates low levels of non-specific binding of the secondary antibody.

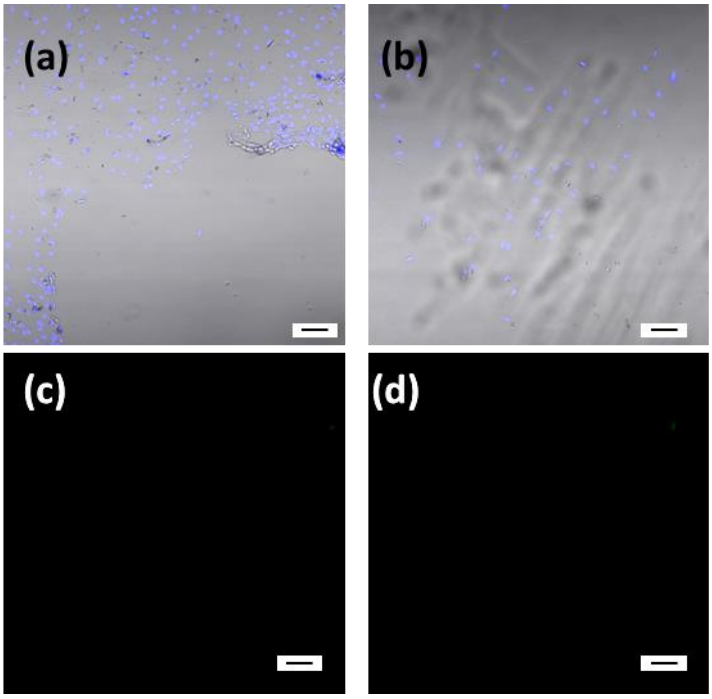

Fig 4.2.1 Checking for non-specific binding for HSP70 staining: Merged images of bright field and DAPI staining is shown in (a) and (b) (replicates) and the lack of non-specific staining for HSP70 protein in (c) and (d) (Scale bars correspond to 100μm)

4.3 Results

4.3.1 Targeted and actual temperature during heat shock

The temperature measurements for each heat shock treatment are shown below (Fig 4.3.1-3). The actual temperature of the medium in well plates was off by up to 2^0C from the targeted temperature for mild heat shock treatment (Fig 4.3.1-2). For the more severe heat shock treatments, cells were exposed to progressively increasing temperatures higher than 50^0C (Fig 4.3.3). The aim was to severely stress the cells at temperatures difference of greater than 10^0C from the optimum conditions of 37^0C. While mild-heat shock is expected to cause transient HSP expression, severe heat shock would cause maximum and sustained expression of HSP. [60–62]

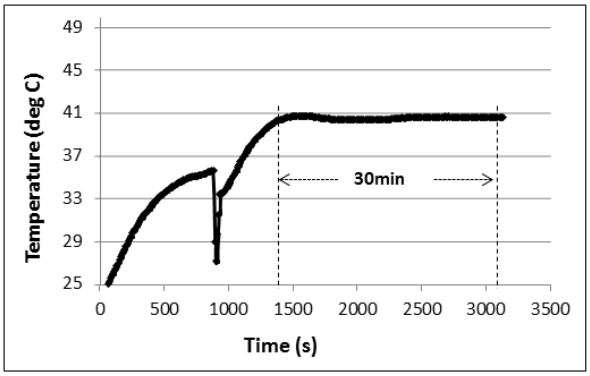

Fig 4.3.1 Temperature measurement during a single bulk heat shock of hMSCs at 40^0C for 30min (Experiment 01 and 02): Cells were placed in a fan-oven and the temperature measured in a separate well plate only containing cell-culture medium.

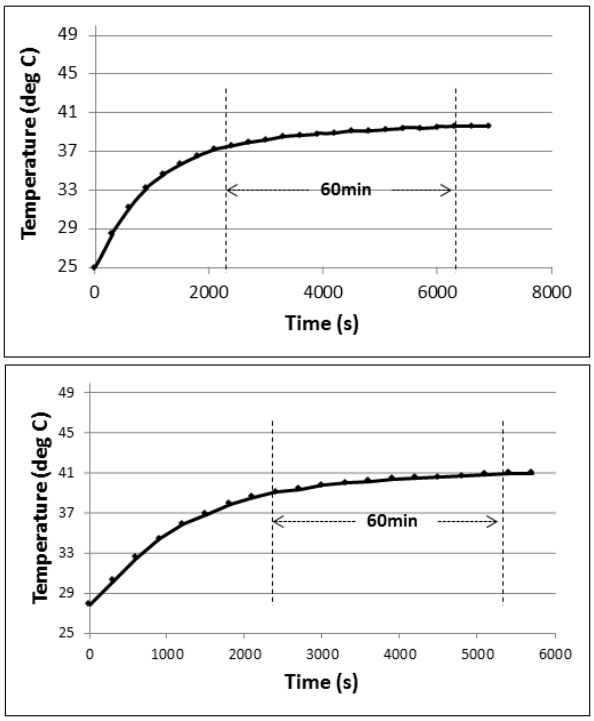

Fig 4.3.2 Temperature measurement during multiple bulk heat shock treatments of hMSCs at 40-41^0C for 60min (Experiment 03): Cells were placed in the incubator with temperature set at specified values on day0 (top) and day 3 (bottom). Temperature was measured in a separate well plate only containing cell-culture medium.

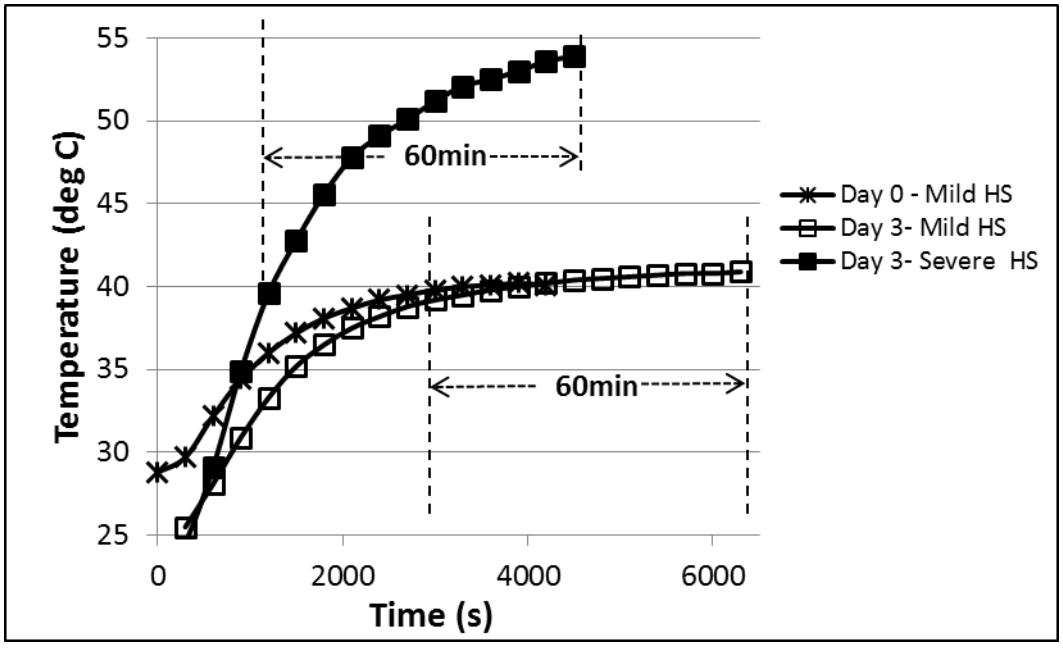

Fig 4.3.3 Temperature measurement during mild and severe bulk heat shock of hMSCs and MG-63s (Experiment 04 and 05): Cells were placed in an oven on day0 and day3 and the temperature measured in a separate well plate only containing cell-culture medium. Temperature was not measured for other time points (day 5 and 7).

4.3.2 Effect of a single mild heat shock exposure on cellular behaviour

Viability of cells exposed to mild heat shock (Experiment 01 and 02) is shown in Fig 4.3.4-5 parts (a), as inferred from Pico Green assay which measures total DNA content in cells (see Chapter 2, section 2.6.5). *In situ* temperature measurements during the heat shock treatment show that cells were at 40^0C rather than the aimed 42^0C (Fig 4.3.1). The effect of the initial cell seeding density was also compared to see if this affects differentiation. A significant increase in cell number (in terms of DNA content) is observed when cells are grown in osteogenic medium compared to expansion beyond day 10. This effect is evened out by day 30 for the sample with the higher seeding density. Mild heat shock does not affect cell viability as no reduction in DNA content was observed for either seeding densities at all time points assessed (Fig 4.3.4a, 5a). On the other hand, the mild-heat shock

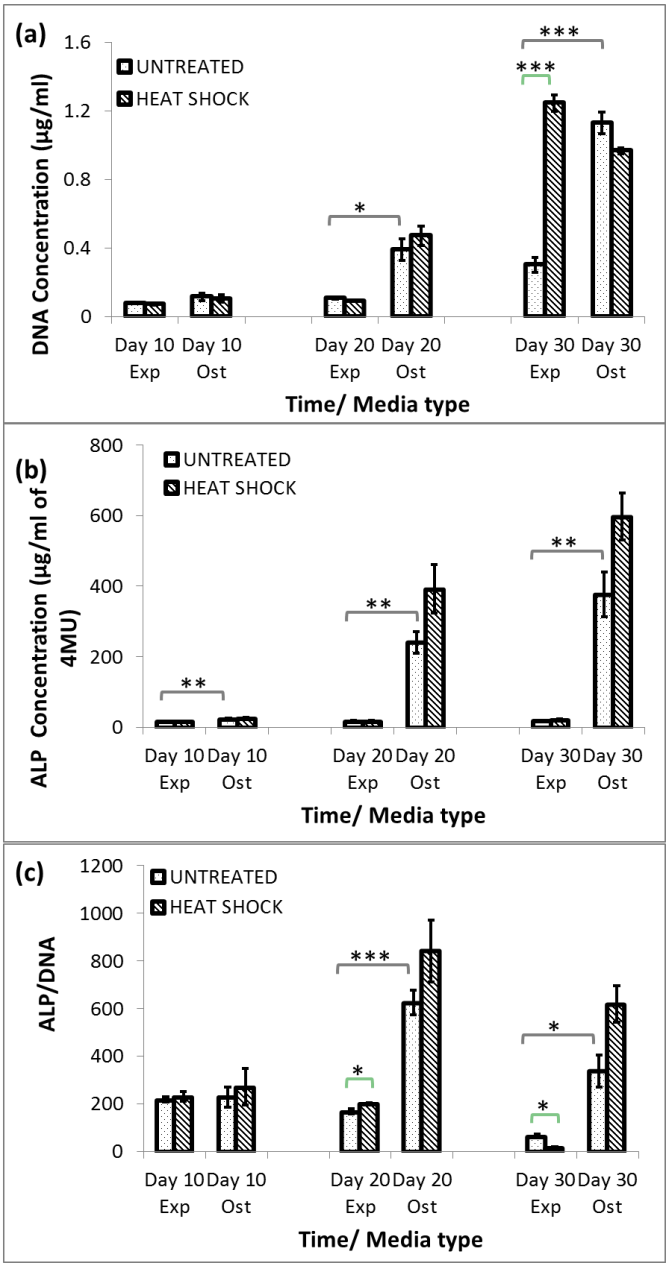

*Fig 4.3.4 Effect of mild bulk HS on osteogenesis of hMSCs with initial low seeding density: hMSCs were seeded at 2000 cells/ cm^2 and exposed to mild bulk HS (Experiment 01-02; 40^{0}C for 30min once; HEAT SHOCK). Controls were kept at 37^{0}C (UNTREATED). Their total DNA content (a), ALP content (b) and ALP/cell (normalized to DNA concentration) on day 10, 20 and 30 after heat shock in expansion (EXP) and osteogenic (OST) media is shown. Error bars represent standard error of the mean for n=3 and line over columns indicates groups that were significantly different from each other (unpaired student t-test between samples in the same media type and for untreated controls across media type. p< 0.05 with * indicating level of significance. No comparison was made between treated and untreated samples across media types or for any of the samples across different time points).*

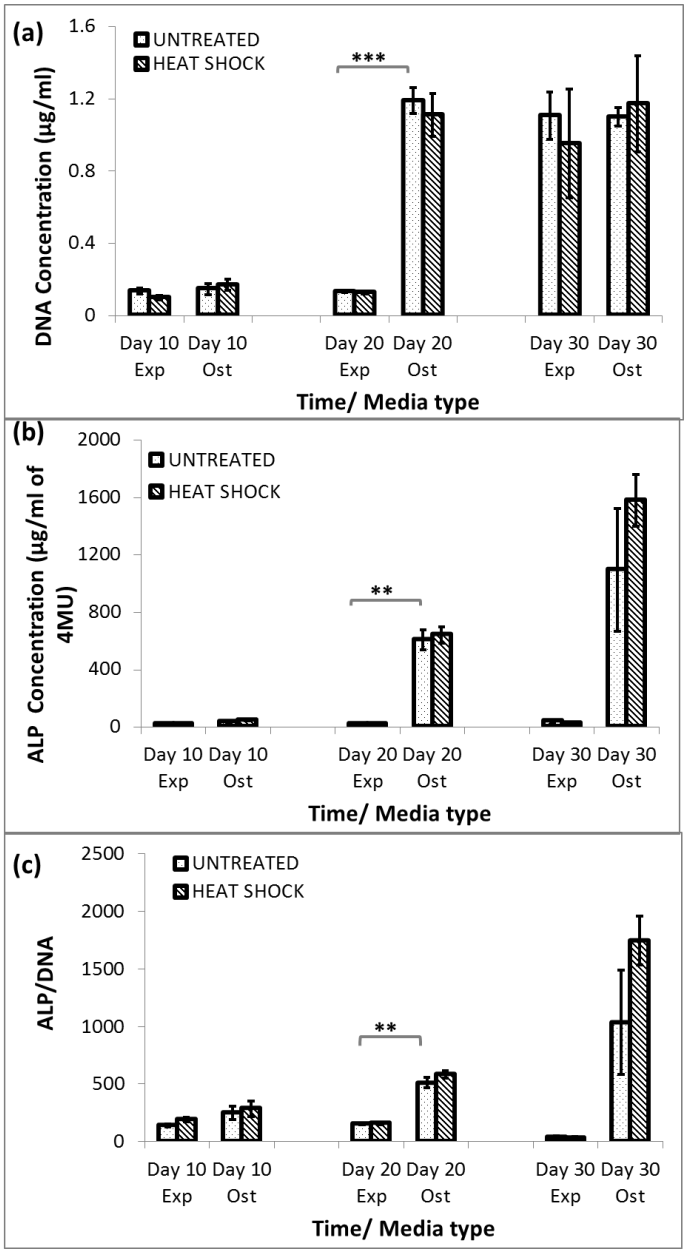

*Fig 4.3.5 Effect of mild bulk HS on osteogenesis of hMSCs with high initial seeding density: hMSCs were seeded at 6000 cells/ cm^2 and exposed to mild bulk HS (Experiment 01-02: 40^0C for 30min once; HEAT SHOCK). Controls were kept at 37^0C (UNTREATED). Their total DNA content (a), ALP content (b) and ALP/cell (normalized to DNA concentration) on day 10, 20 and 30 after heat shock in expansion (EXP) and osteogenic (OST) media is shown. Error bars represent standard error of the mean for n=3 and line over columns indicates groups that were significantly different from each other (unpaired student t-test between samples in the same media type and for untreated controls across media type. $p< 0.05$ with * indicating level of significance. No comparison was made between treated and untreated samples across media types or for any of the samples across different time points).*

treated sample in expansion medium has cell numbers higher than the untreated control in the same medium type (and comparable levels to untreated cells in osteogenic medium). The reason for this behaviour is not clear as it is a single time point event and it is not clear whether this is an anomalous behaviour of the expansion controls or if the treatment genuinely increased proliferation of cells.

The concentration of the early osteogenic marker, ALP (Alkaline phosphatase) was measured (Fig 4.3.4b, 5b) to assess differentiation. For the lower seeding density, there is a significant upregulation of the total ALP (at all time points; Fig 4.3.4b) and ALP/cell (beyond day 20; Fig 4.3.4c) in osteogenic medium compared to expansion medium. In the case of the higher seeding density samples, an increase in total ALP and ALP/cell content for cells in osteogenic medium compared to expansion medium is observed at all time points (Fig 4.3.5b) but is only significant at day 20. The data on day 30 has huge errors and cannot give accurate information about differences in ALP production.

These results confirm onset of osteogenesis for the hMSCs at both seeding densities investigated. The total ALP and ALP/cell are higher for the treated samples, especially in osteogenic medium but the difference is not significant in the lower as well as the higher seeding density samples (lower seeding density in Fig 4.3.4b, c and higher seeding density in Fig 4.3.5b, c). On the other hand, in expansion medium, these samples show a significant upregulation at day 20 for ALP/cell but downregulation by day 30. This could be a consequence of the temporal nature of ALP expression. One possibility is that, the ALP production might have peaked earlier (between days 10-20) due to the heat shock treatment. Hence, the values fall off earlier as well and could be the reason why ALP is lower at later time points (day 20 and 30) for the treated than the untreated sample. These results show some indications of heat shock affecting the ALP/cell production whilst the

seeding density gives rise to only subtle differences in response to the treatment. However the lower seeding density seems more promising in terms of the likelihood of detecting the effect of treatment.

Also, to study the changes in temporal expression of ALP, in all further experiments, shorter time points were studied. Staining for mineralization in the cells cultured in osteogenic medium showed significant areas of mineralised matrix, confirming cellular differentiation (Fig 4.3.6), regardless of whether the cells were exposed to heat shock or not.

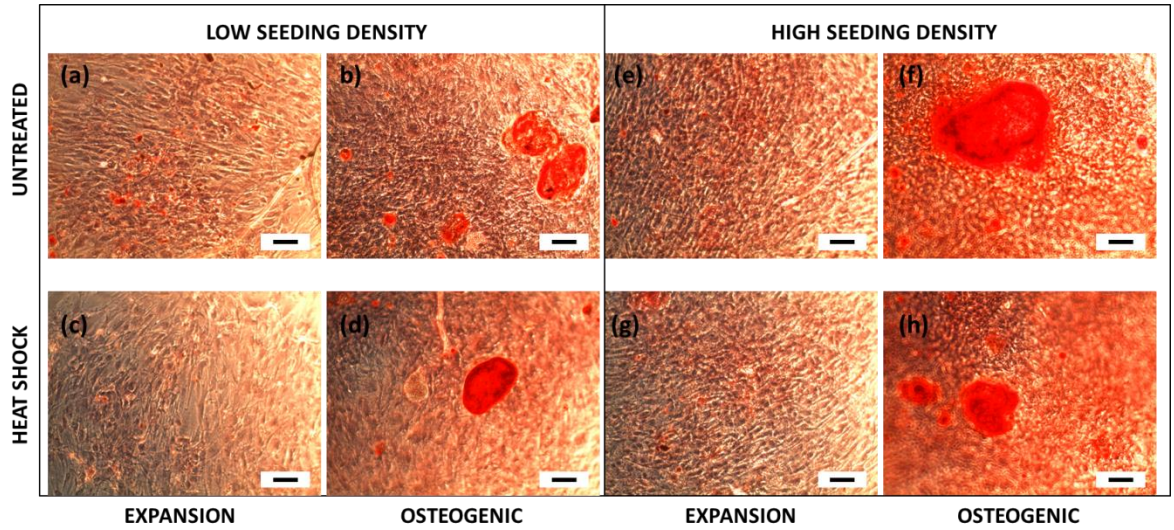

Fig 4.3.6 Effect of mild bulk HS on mineralization of hMSCs: Mineralization on day 30 (Alizarin Red staining) for hMSCs untreated in expansion (a, e) and osteogenic (b, f) media. The bulk heat shocked samples exposed to 40^0C for 30min once, were also cultured in expansion (c, g) and osteogenic medium (d, h). (Experiment 01: Low seeding density: a-d; Experiment 02: High seeding density e-h; Scale bars represent 100µm)

4.3.3 Effect of multiple heat shock treatments and of temperature on cellular behaviour

In this section, effects of multiple exposures for a longer duration of 60min were tested. Also, apart from the mild heat shock temperature of between 40-42^{0}C, the effect of a more severe heat shock was also tested in later experiments.

The effects of multiple and a longer treatment times on MG-63 cells are shown in Fig 4.3.7 (Experiment 03; Fig 4.3.2). The DNA content indicative of cell numbers is higher for the MG-63 cells in expansion medium compared to osteogenic medium both on day 4 and 6. Heat shock did not affect cell viability in either media type at day 4 or 6.

The total ALP expression (Fig 4.3.7b) and ALP/cell (Fig 4.3.7c) were higher for cells in osteogenic medium compared to expansion medium at day 4 and 6 confirming onset of osteogenesis. Compared to the hMSCs (at day 10), MG-63 cells had a higher upregulation of total ALP and ALP/cell with chemical induction (in osteogenic medium) even by day 4 indicating that onset of differentiation is more rapid in these osteoblast-like cells. While the total ALP and ALP/cell (on day 4) appear higher after the first heat treatment, they were reduced (on day 6) following the second treatment, especially in expansion medium (significance was only observed for total ALP on day 4 and ALP/Cell on day 6 in expansion medium). It could be that the cells were being stressed with repeated treatments and although cell numbers did not decrease their ALP production might have been mildly affected.

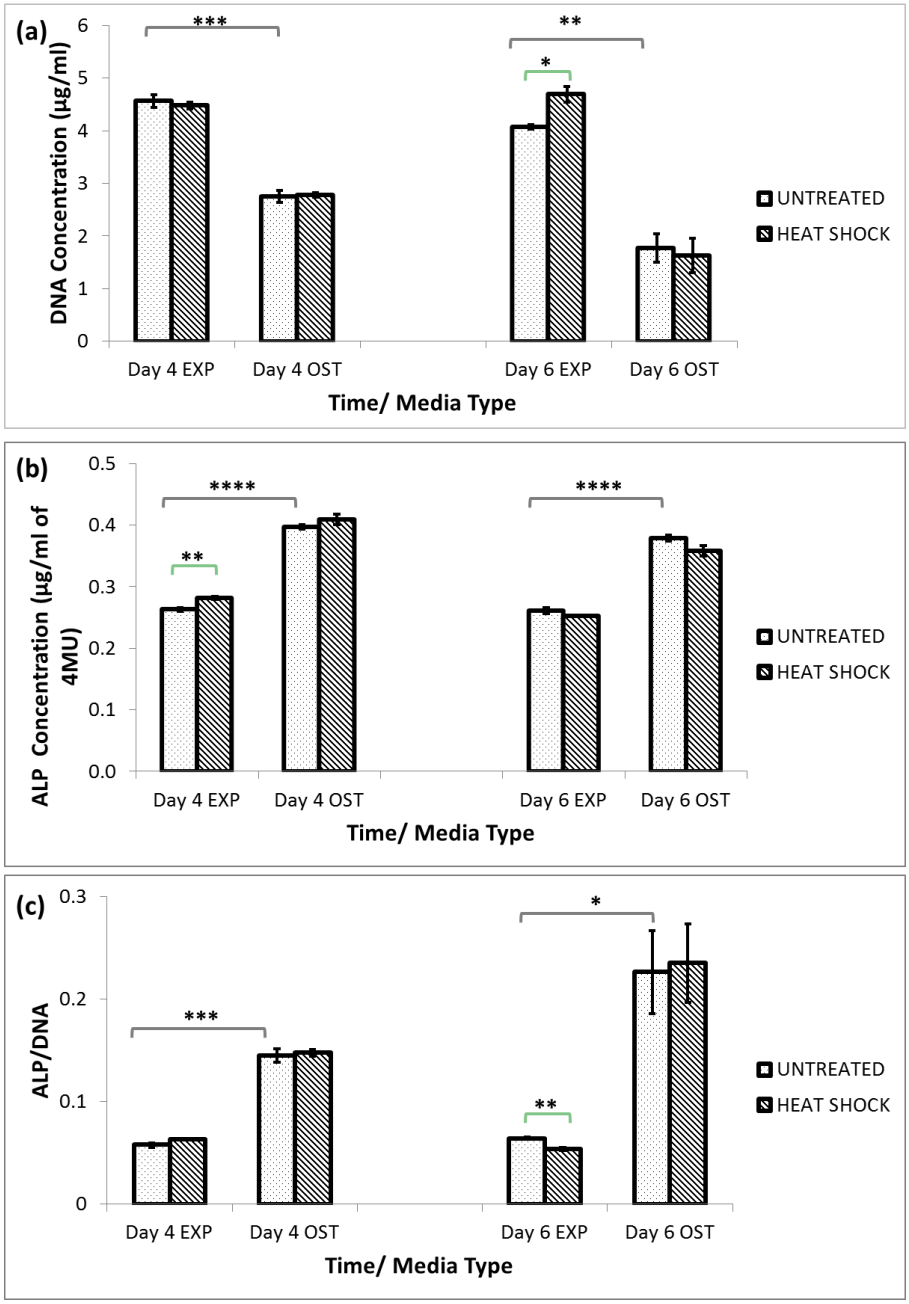

*Fig 4.3.7 Effect of mild HS on osteogenic differentiation of MG-63 cells (Experiment 03): Total DNA content (a), total ALP expression (b) and the ALP/ cell (Normalized to DNA content; c) of MG-63 cells exposed to mild heat shock (41^{0}C for 60min on day3 and 5) measured on day 4 and 6 in expansion (EXP) and osteogenic (OST) media. Error bars represent standard error of the mean for n=3 and line over columns indicates groups that were significantly different from each other (unpaired student t-test between samples in the same medium and for untreated controls across media types. p< 0.05 with * indicating level of significance. No comparison was made between treated and untreated samples across media types or for any of the samples across different time points).*

In the next attempt (Experiment 04, 05), in addition to mild-heat shock the effect of severe heat shock was assessed. Cells were exposed to multiple temperatures: mild heat shock at 41^0C and severe heat shock of $>50^0$C (Fig 4.3.3). It was aimed to have the cells maintained at the target temperature for 60min. Also, the cells were treated every alternate day and the ALP and DNA content measured 24 hours later. Fig 4.3.8-11 show bright field images of hMSCs and MG-63 cells exposed to the above defined heat shock treatments.

For the hMSCs cultured in expansion media, the mild heat shock sample (41^0C) was similar to the untreated (37^0C) control at all time points and their increased confluency was observed (Fig 4.3.8). The cells appeared to have the normal fibroblastic morphology of proliferating hMSCs. On the other hand, cells in the severely HS sample (55^0C) increasingly lost viability with subsequent treatments. A very similar trend was observed for hMSCs in osteogenic (Fig 4.3.9) medium and MG-63 cells in expansion (Fig 4.3.10) and osteogenic (Fig 4.3.10) media.

Apart from the severely HS sample, cell numbers progressively increased and in the case of hMSCs, a change in morphology (cuboidal) typical of osteogenesis, from spindle shaped to cuboidal, was observed in both the untreated and 41^0C heat shock treated cells (Fig 4.3.9, i, k: samples on day 8). No observable indication of osteogenesis-related morphology changes were observed for mild-heat shock treated cells in expansion medium (Fig. 4.3.8). For the cells exposed to $>50^0$C the severe heat shock treatment adversely affected cell viability. This loss in viability further increased with subsequent treatments. This can be seen from the emergence of a shrunken appearance in the case of hMSCs (see for e.g. Fig. 4.3.8j and Fig. 4.3.9i) and rounding up of cells in MG-63s (see for e.g. Fig. 4.3.10j and Fig. 4.3.11i), as well as a reduction in cells numbers and eventual cell-detachment in the case of MG-63s indicating cell death.

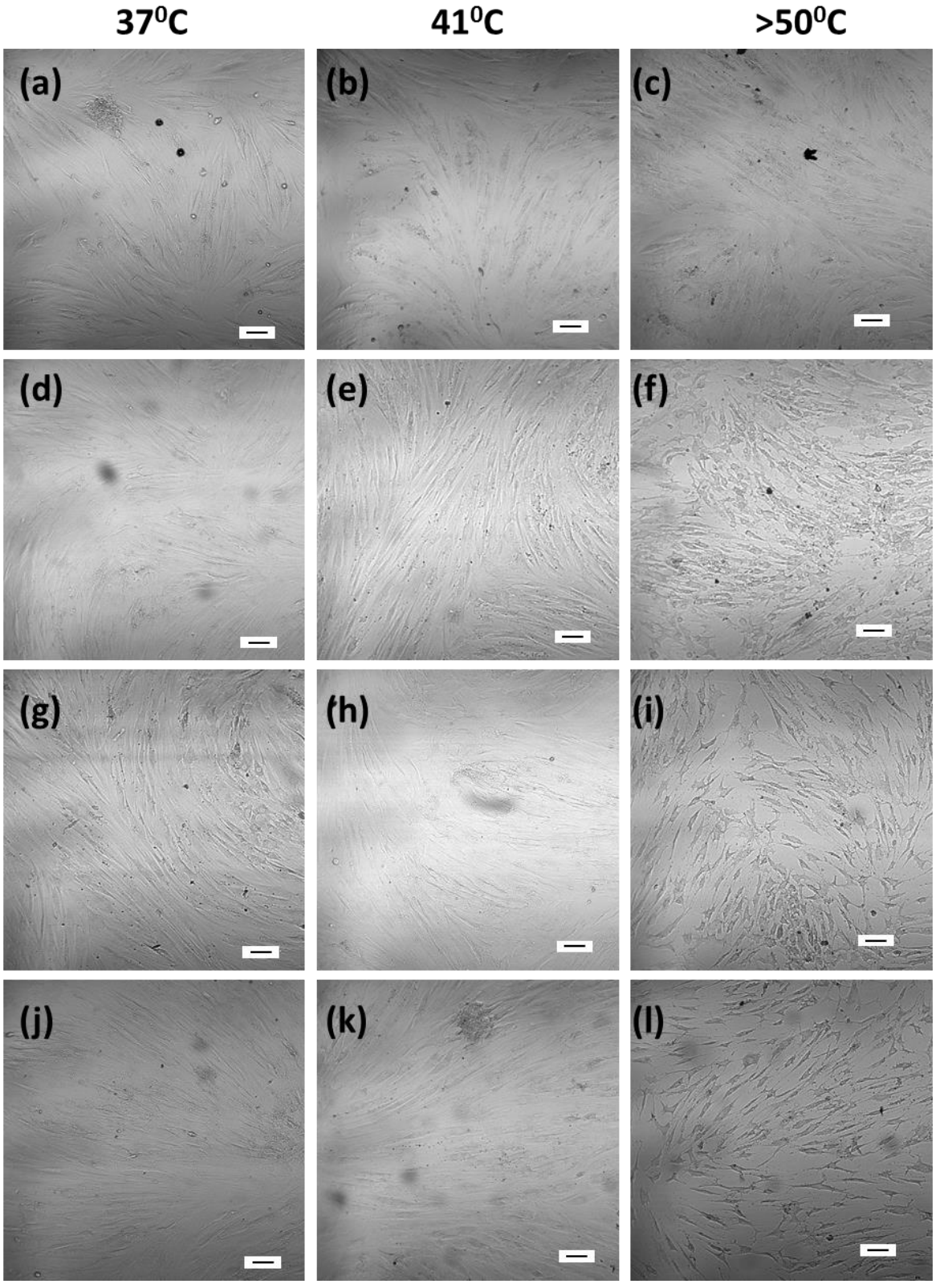

Fig 4.3.8 Bright field images of hMSCs exposed to multiple HS treatments (Experiment 04) cultured in expansion medium: Images show changes in morphology of hMSCs exposed to different temperatures (37, 41 and >50^{0}C for 60min on day 1, 3, 5, 7) imaged on days 2 (a-c), 3 (d-f), 6 (g-i) and 7 (j-l). (Scale bars represent 100μm)

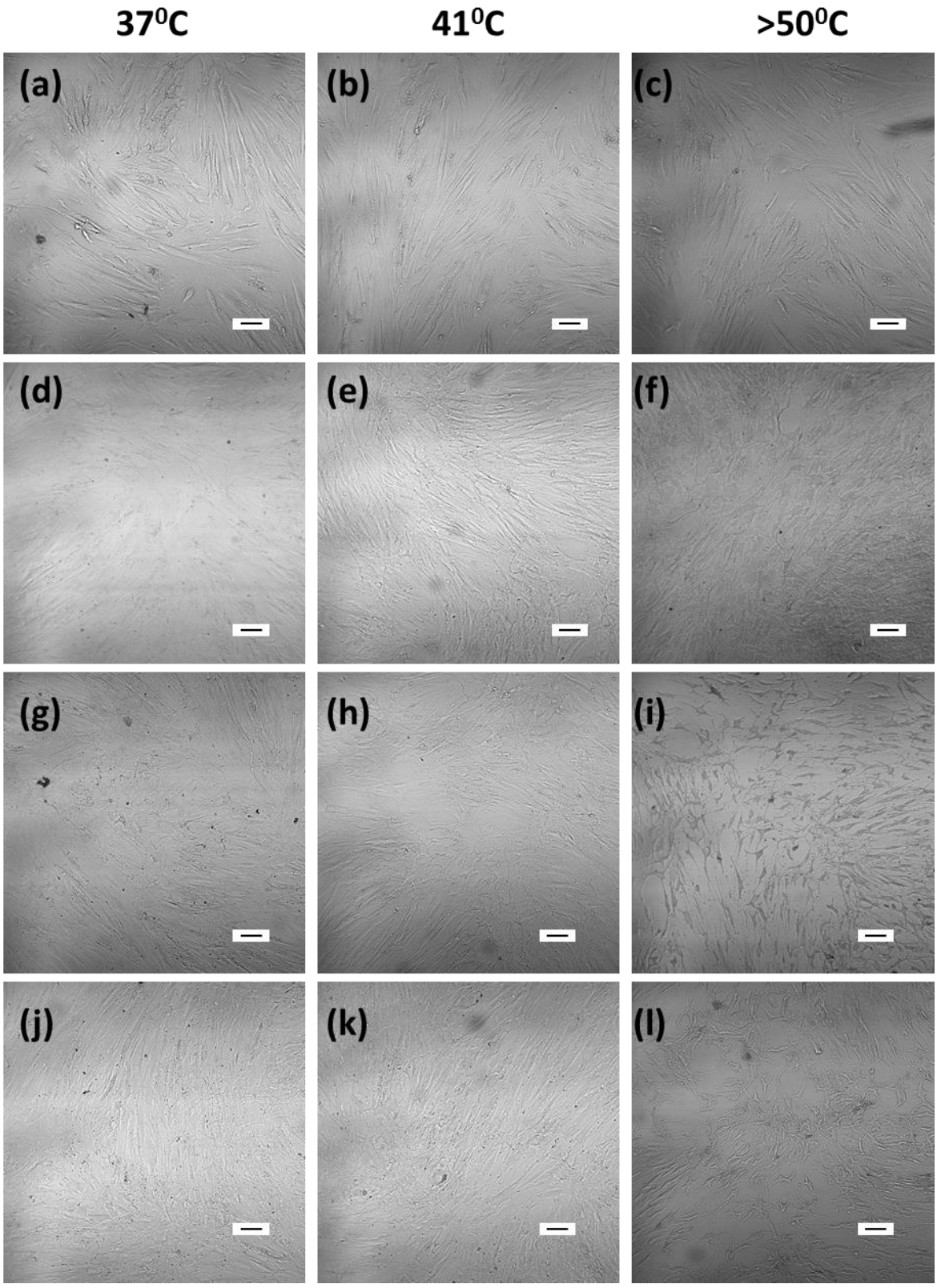

Fig 4.3.9 Bright field images of hMSCs exposed to multiple HS treatments (Experiment 04) cultured in osteogenic medium: Images show changes in morphology of hMSCs exposed to different temperatures (37, 41 and >50^{0}C for 60min on day 1, 3, 5, 7) imaged on days 2 (a-c), 3 (d-f), 6 (g-i) and 7 (j-l). (Scale bars represent 100μm)

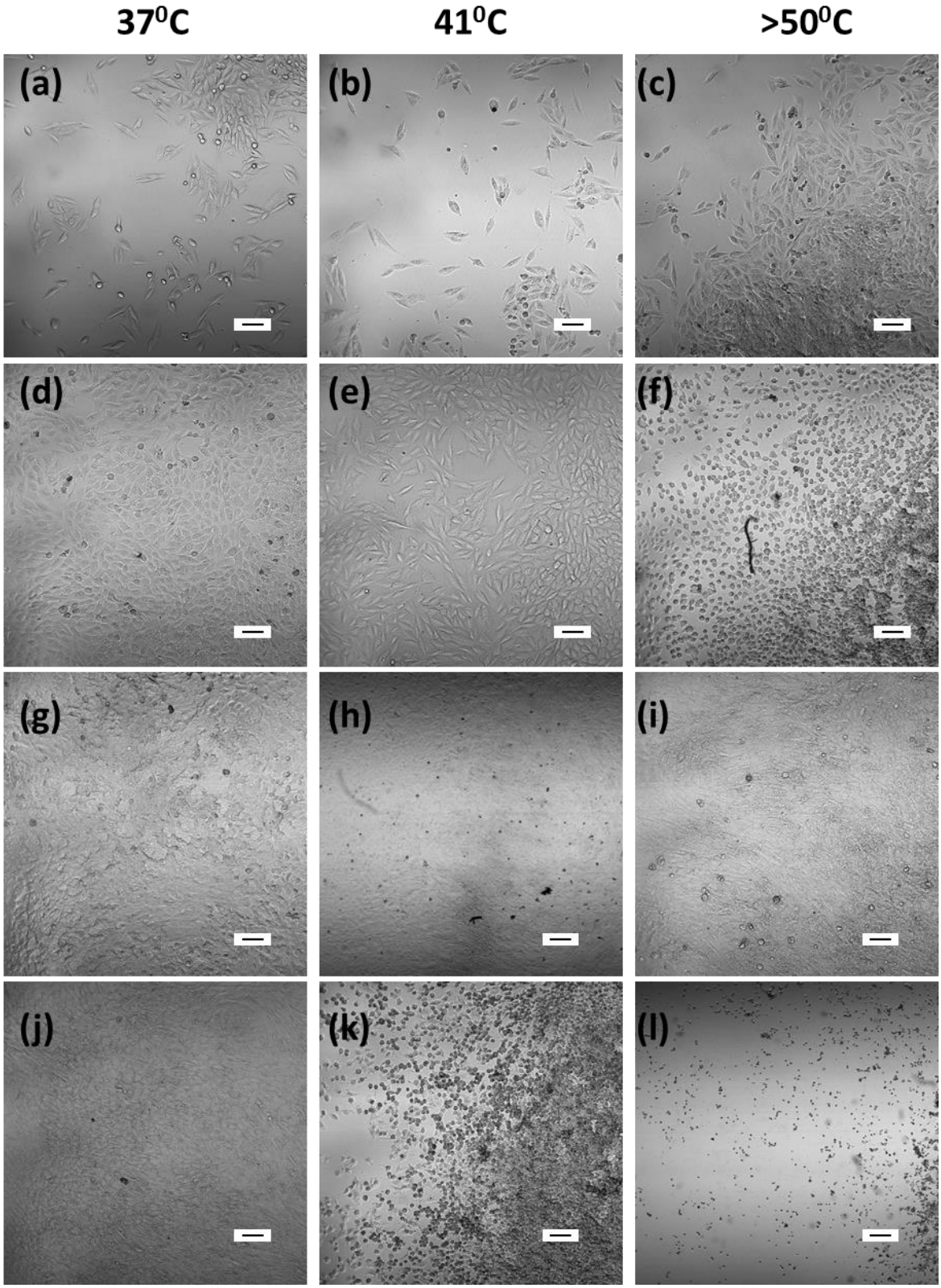

Fig 4.3.10 Bright field images of MG-63 cells exposed to multiple HS treatments (Experiment 05) cultured in expansion medium: Images show changes in morphology of MG-63 cells exposed to different temperatures (37, 41 and >50^{0}C for 60min on day 1, 3, 5, 7) imaged on days 2 (a-c), 3 (d-f), 6 (g-i) and 7 (j-l). (Scale bars represent 100μm except for l where it corresponds to 200μm)

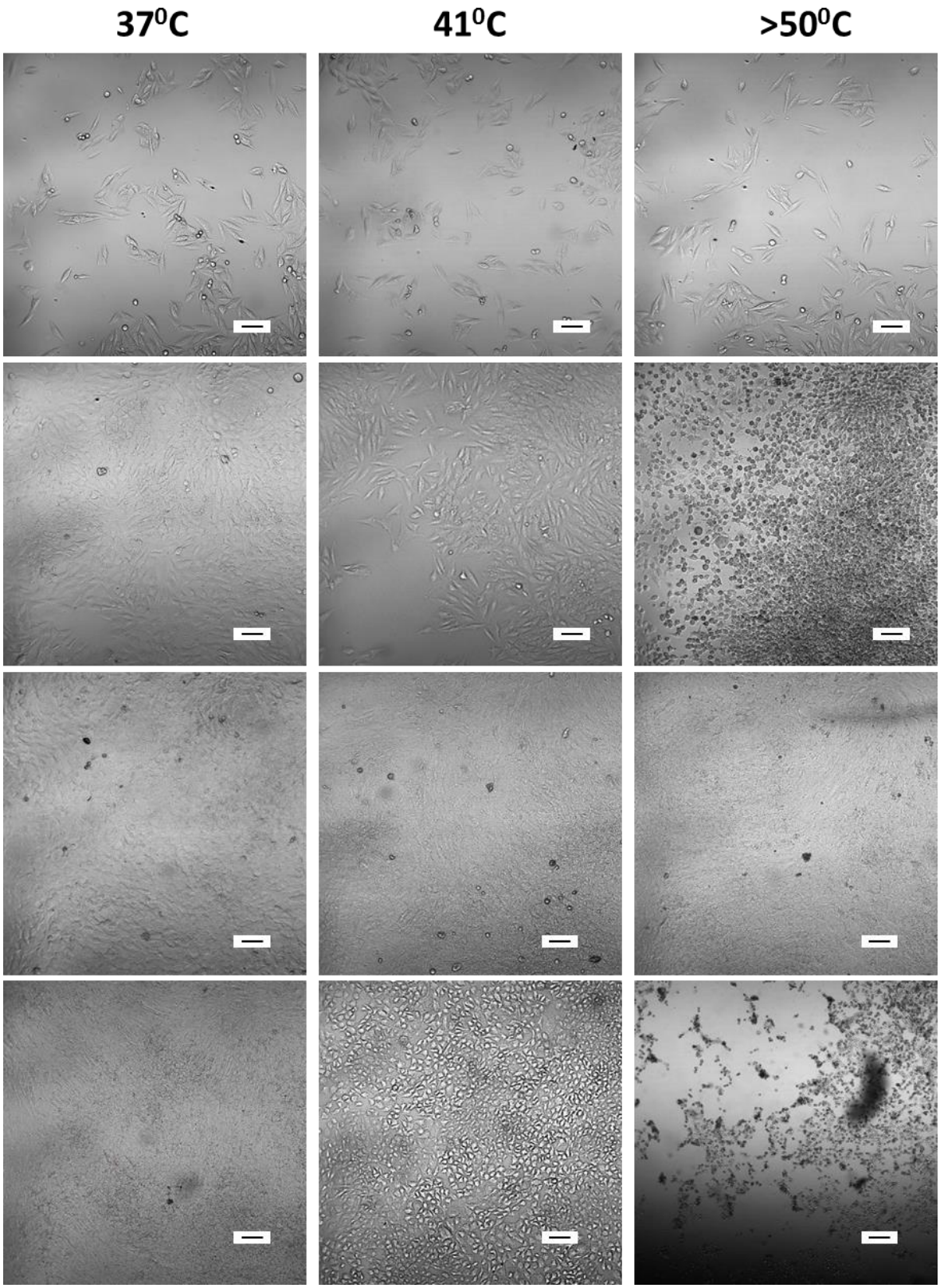

Fig 4.3.11 Bright field images of MG-63 cells exposed to multiple HS treatments (Experiment 05) cultured in osteogenic medium: Images show changes in morphology of MG-63 cells exposed to different temperatures (37, 41 and >50^{0}C for 60min on day 1, 3, 5, 7) imaged on days 2 (a-c), 3 (d-f), 6 (g-i) and 7 (j-l). (Scale bars represent 100μm except for l where it corresponds to 200μm)

The viability and osteogenesis were quantified by measuring the DNA (Fig 4.3.12a, 13a) and ALP content (Fig 4.3.12b, 13b) of the hMSCs and MG-63 cells respectively. For the hMSCs, as observed earlier (Fig 4.3.4-5), the cell numbers (DNA) are higher in osteogenic medium than expansion medium for untreated samples (day 4 and 6; Fig 4.3.12a). For mild heat shock, viability is not significantly affected until after the fourth treatment for cells in expansion medium alone (Fig 4.3.12a, D8 EXP). On the other hand, severe heat shock seems to strongly affect viability which decreased with every treatment for cells in both media types. These results confirm the observations of loss in viability detected by changes in cell morphology (Fig 4.3.8, 9).

In the case of MG-63 cells, except for a minor increase at day 4, no significant difference in cell numbers was observed between cells in either medium (Fig 4.3.13a). In the previous experiment (Experiment 03), cell numbers were constant between day 4 and 6 with higher cell numbers in expansion medium compared to osteogenic medium (Fig. 4.3.7a). In contrast, in this experiment cell numbers progressively increased with time for both media types (Fig. 4.3.13a). The mild- heat shock did not affect viability at any of the time points assayed in either medium except for a transient decrease for cells in osteogenic medium at day 4. On the other hand, the severe heat shock caused a significant loss in viability beyond day 2. Data is not available for the MG-63s exposed to severe heat shock on day 8 as the cells had died and detached by this point and so were not available for assaying. Once again, these results match the observations from the bright field images (Fig 4.3.10, 11).

For the hMSCs, the total ALP content (Fig 4.3.12b) and ALP/cell (Fig 4.3.12c) were enhanced in osteogenic media, confirming onset of osteogenesis. Mild heat shock did not

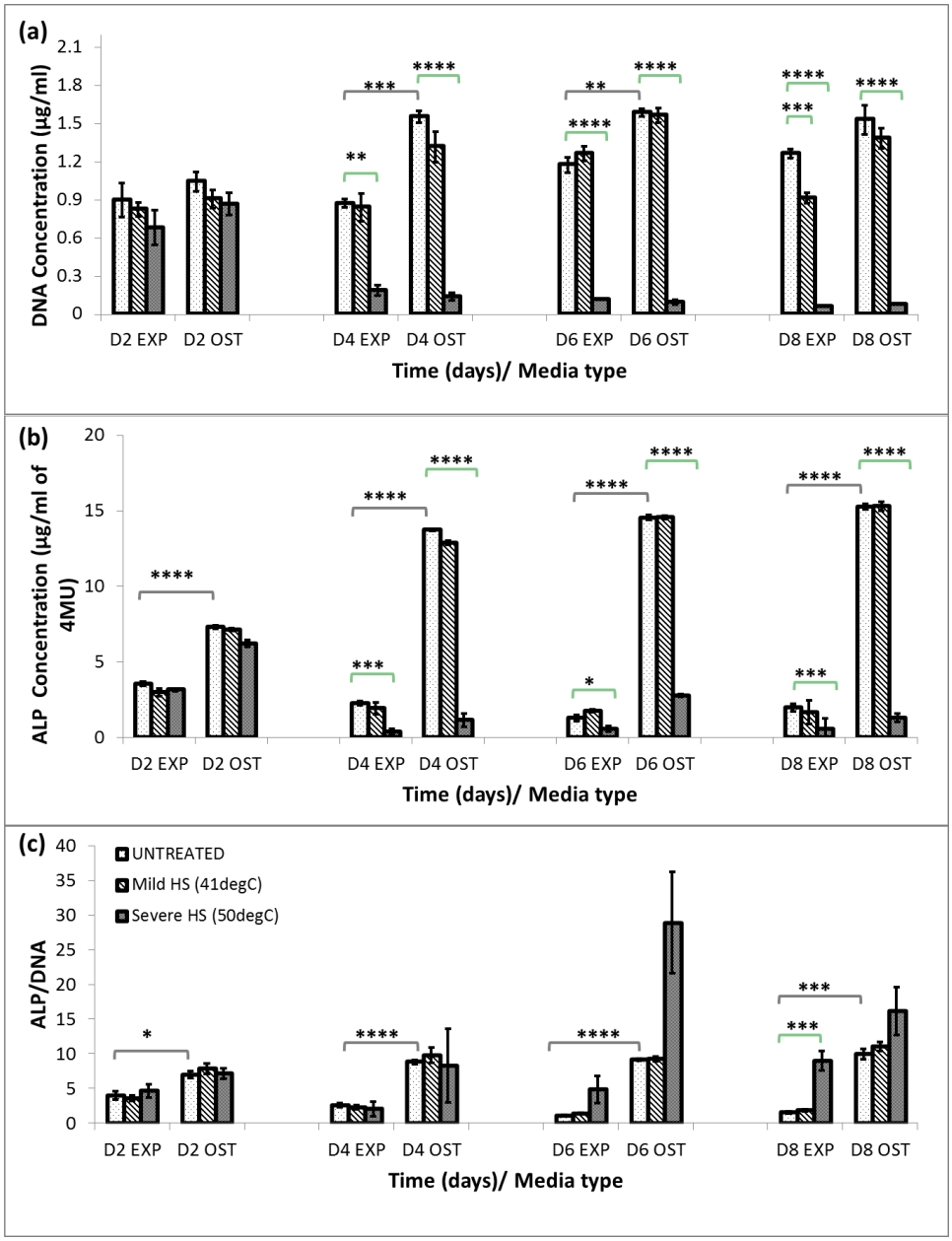

*Fig 4.3.12 Effect of mild HS on cell numbers and ALP production of hMSCs (Experiment 04): Total DNA content (a), total ALP expression (b) and the ALP/ cell (Normalized to DNA content; c) of cells exposed to repetitive bulk heat shock (40^0C or $>50^0$C for 60min every 2^{nd} day) at day 2, 4, 6 and 8 in expansion (EXP) and osteogenic (OST) media. Error bars represent standard error of the mean for n=3 and line over columns indicates groups that were significantly different from each other (unpaired student t-test between samples in the same media type and for untreated controls across media type. $p< 0.05$ with * indicating level of significance. No comparison was made between treated and untreated samples across media types or for any of the samples across different time points).*

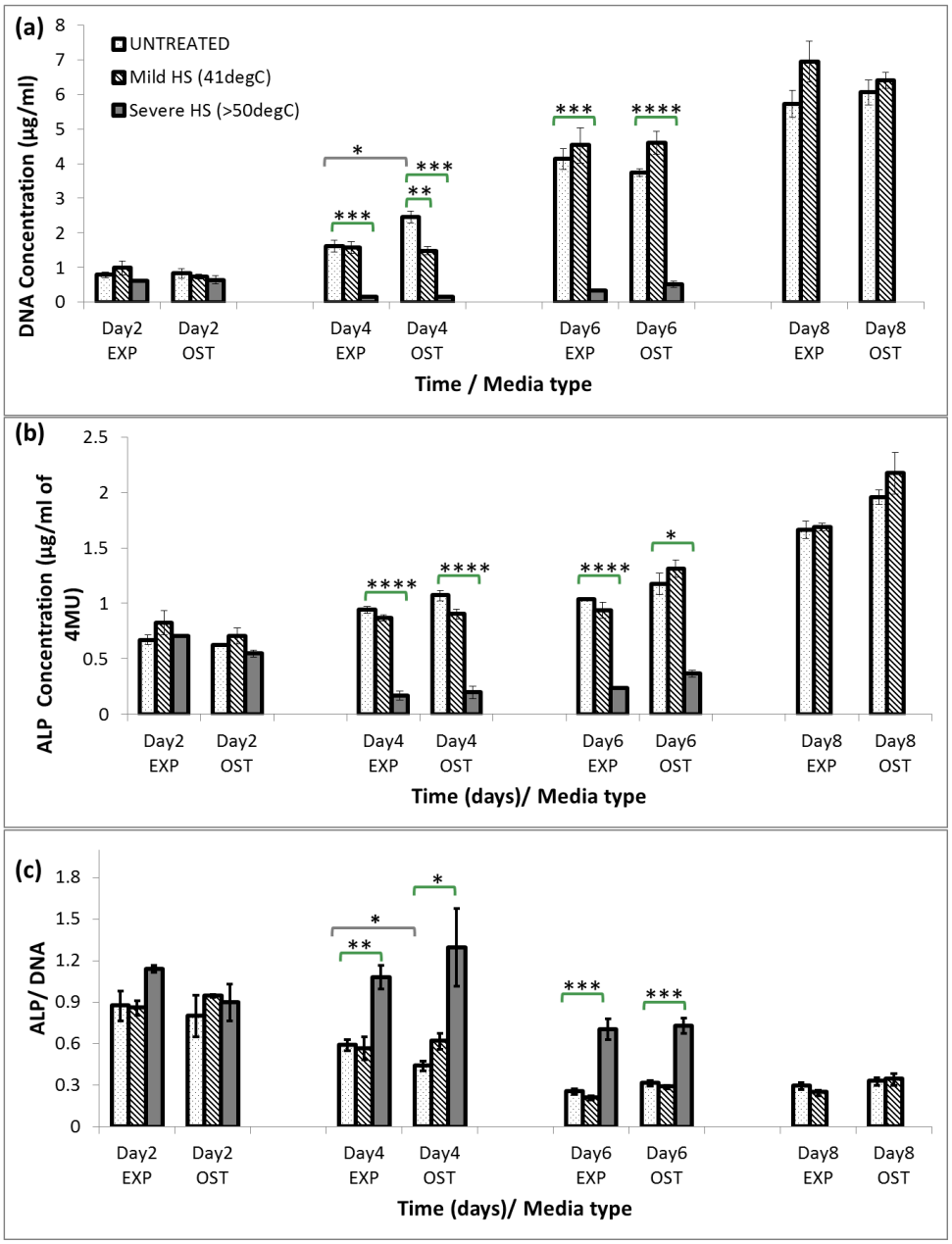

*Fig 4.3.13 Effect of mild HS on cell numbers and ALP production of MG-63 cells (Experiment 04): Total DNA content (a), total ALP expression (b) and the ALP/ cell (Normalized to DNA content; c) of cells exposed to repetitive bulk heat shock (Experiment 05: 40^0C or $>50^0$C for 60min every 2^{nd} day) at day 2, 4, 6 and 8 in expansion (EXP) and osteogenic (OST) media. Error bars represent standard error of the mean for n=3 and line over columns indicates groups that were significantly different from each other (unpaired student t-test between samples in the same media type and for untreated controls across media type. $p< 0.05$ with * indicating level of significance. No comparison was made between treated and untreated samples across media types or for any of the samples across different time points)*

affected the total ALP or ALP/cell expression compared to the untreated samples in the same medium. A small but not significant increase in the ALP/cell expression was observed with heat treatment in both media types, similar to the previous experiment of mild heat shock in hMSCs (Experiment 01, 02; Fig 4.3.4b, 5b). Whilst severe heat shock strongly reduced total ALP, the ALP/cell values were similar to the untreated controls. On day 8, a strong upregulation of ALP/cell (Fig 4.3.12c) was observed in expansion medium alone. At day 6 in both media types and at day 8 in osteogenic media, again a minor but non-significant increase in the ALP/cell expression was observed but due to the large error the data cannot be accurately interpreted.

In MG-63 cells, neither the total ALP (Fig 4.3.13b) nor the ALP/cell (Fig 4.3.13c) was significantly different between the two media types for the untreated cells at all time points. Previously, a difference between the ALP content of cells in expansion and osteogenic media could be detected by day 4 (Fig 4.3.7b, c) but the absolute amounts were lower compared to those in this experiment especially the total ALP. It is not clear why this was the case but being osteoblastic in nature, MG-63 cells even without a chemical stimulus (osteogenic media) could actively express ALP thus negating any chemically induced enhancement in the cells in osteogenic media. Mild heat shock does not show an increase in total ALP or ALP/cell in either medium type at all time points similar to the observations from the previous experiment (Experiment 03; Fig 4.3.7b. c). In the case of the severe heat shock, the total ALP (Fig 4.3.13b) decreased (similar to hMSCs) at day 4 and 6 (no data available for day 8) in both media types. On the other hand, the ALP/cell was significantly higher for both media types compared to the untreated on day 4 and 6 (no data available for day 8), in contrast to hMSCs where an enhancement was only found in expansion medium (Fig. 4.3.13c).

4.3.4 Assessing heat shock protein expression and its role in osteogenesis

To further evaluate the effect of heat shock on hMSCs, the expression of heat shock protein was investigated. To assess the expression of heat shock protein 70 (HSP70), one of the highly expressed HSPs during heat shock and other forms of stress in hMSCs[37,44,65], a chemical inducer of HSP70, geranylgeranylacetone[180] (GGA) was added to cells. In addition, the effect of passage number on ability of hMSCs to express HSPs was also investigated.

At all concentrations of the heat shock inducer GGA, cells at passage 1 (Fig 4.3.14 a-h) displayed higher HSP70 staining than cells at passage 5 (Fig 4.3.14 i-p) indicating that hMSCs lose their tolerance for stress, in terms of HSP production with increasing age (as measured by higher passage number).[181] Hence for all future experiments (Chapter 5), hMSCs were used only up to their second passage.

Basal levels of HSP70 expression are seen for cells not exposed to GGA (0μM; Fig 4.3.14. a, e, i, m). With increasing concentration of GGA (from 0 to 100μM) an increasing staining for HSP70 can be observed clearly in cells at passage 1. For cells at passage 5, this trend is observed till 50μM GGA but not very clearly and with little staining is observed at 100μM.

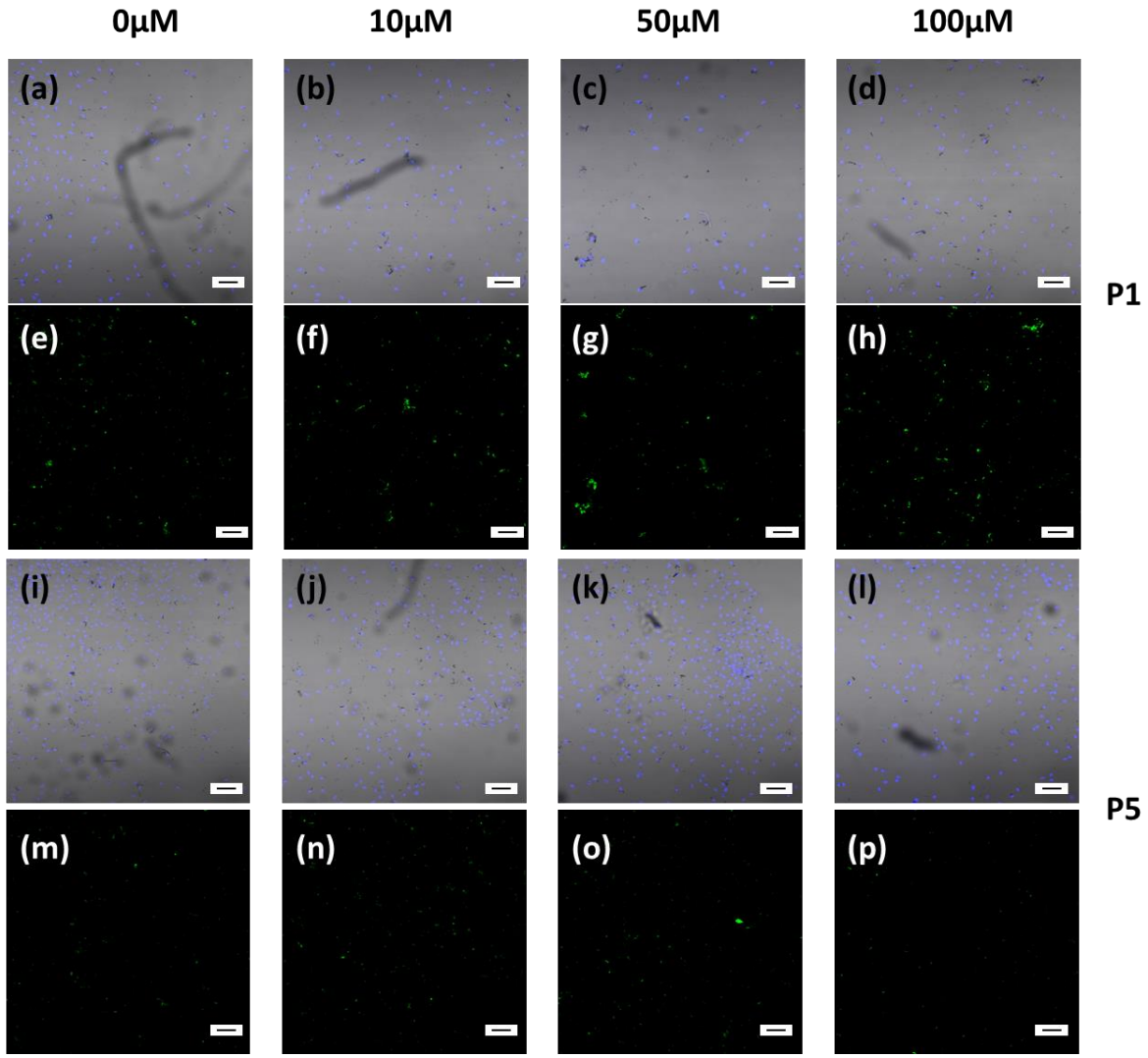

Fig 4.3.14 Effect of passage number on the HSP70 production capacity in hMSCs: The chemical inducer of HSP70, GGA was added to hMSCs at passage 1 (P1; a-h) and passage 5 (P5; i-p) for 1h at 0 (a, e, i, m), 10 (b, f, j, n), 50 (c, g, k, o) and 100µM (d, h, l, p) for 1h. After 24h, cells were stained for nuclei (DAPI, a-d and i-l) and HSP70 (e-h and m-p) to assess HSP70 expression. (Scale bars represent 100µm)

In the same experiment, one set of cells were exposed to mild heat shock (~42^0C in a water bath; Fig 4.3.15 top) for 40min. Their HSP70 expression for cells at passage 1 and 5 is shown after a 24h recovery period (Fig 4.3.15 a-d). Once again a stronger expression was observed for cells at passage 1 than 5. Qualitatively, the levels are comparable to that of cells exposed to high concentrations of GGA (50 or 100µM) indicting that the short exposure to mild heat shock increased HSP70 expression.

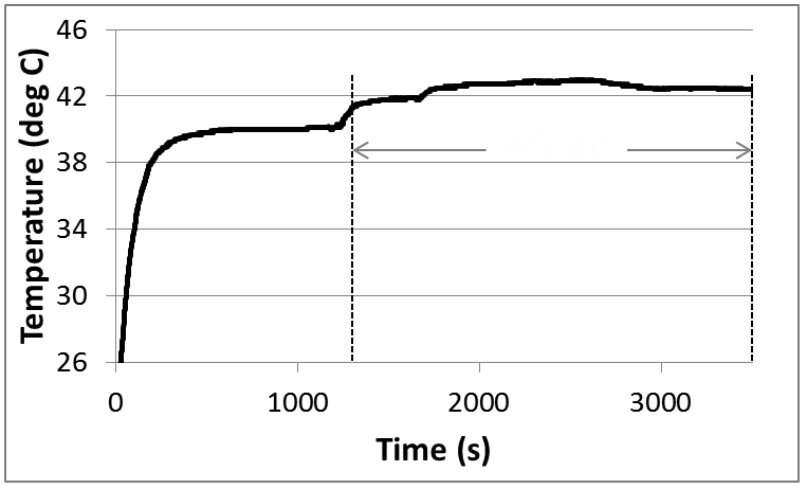

Fig 4.3.15 Effect of bulk heat shock on HSP70 protein production in hMSCs: Graph showing temperature of a cell-free well in the sample well plate placed in a water bath set at 43^0C as measured using an optical temperature probe. The staining for DAPI (blue) and HSP70 (green) for cells at passage 1 (a, b) and passage 5 (c, d) 24h after exposure to the heat shock treatment is shown. (Scale bars represent 100μm)

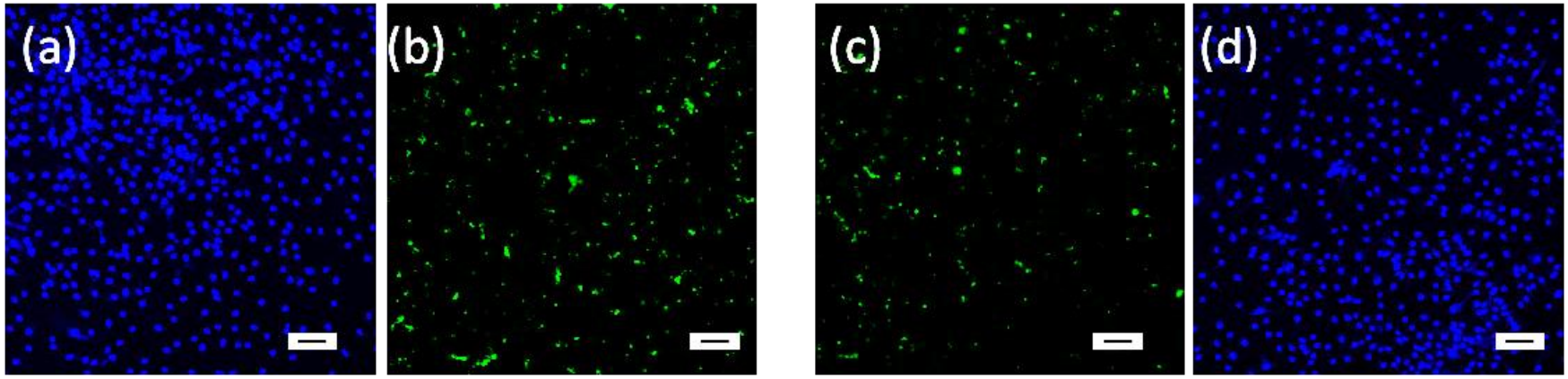

To explore the role of HSP70 in osteogenic differentiation, hMSCs can be treated with GGA and analysed for gene expression using the real-time quantitative PCR (Polymerase Chain Reaction) technique. The approach when carried out thoroughly in terms of assessing other housekeeping genes, and other analysis time points following treatment, can help shed light on the causal role between HSPs and differentiation of stem cells. Such an analysis was attempted in this work by exploring hMSCs in expansion medium alone, expansion medium with 100μM of GGA for 1h, and in osteogenic medium alone. The cells were assessed for the expression of the housekeeping gene β-Actin, early osteogenic marker gene RUNX2, and the HSP70 gene to see if the cells exposed to GGA showed a similar expression profile for RUNX2 to that of the cells in osteogenic medium. Cells were exposed to GGA in expansion medium for 1h once every three days (after treatment wells were washed and fresh expansion media added) and gene expression analysed on day 7 and 14. However, no clear result in terms of the upregulation of HSP70 in GGA-induced cells or RUNX2 for cells in osteogenic medium was observed, and so the data is not included here.

4.4 Discussion

Exposure to mild heat shock temperatures did not show any strong evidence of a positive effect on the osteogenic differentiation potential of human bone-marrow derived mesenchymal stem cells (hMSCs). Various time durations ranging from 30min to an hour as single or cyclic treatment (every second day) were investigated with moderate temperatures ranging from between 40 to 42^0C. Although there was some possible indication of a positive effect of mild-heat shock enhancing chemically stimulated (osteogenic media) differentiation in hMSCs (but not MG-63 cells), no such effect was observed in expansion media.

In one of the first studies on the effect of heat shock on osteogenesis, iliac crest- derived hMSCs were established into a telomeres immortalized cell line (hMSCs-TERT; seeding density of 10,000 cells/cm^2) and exposed to a single shock of 41.5^0C.[47] Cells were placed in a water bath for 1h. The treatment caused an upregulation of ALP (nM/min/10^4 cells) and mineralization (Alizarin red stain μmol/10^4 cells) on day 8 for cells in osteogenic medium supplemented with vitamin D (10^{-8}M 1α,25-dihydroxy-vitamin-D3). This is typically a very early time point to observe mineralization for hMSCs grown in osteogenic media.[182] In the work by Chen *et al*.[45], increased ALP activity (nmol/min/10^4 seeded hMSCs) was observed at day 6 between untreated and 41^0C treated iliac crest-derived hMSCs in osteogenic media. However, this effect was lost by day 12. Mineralization, in terms of calcium mass (μg/10^4 seeded cells) was also higher for the heat shock treated samples at day 19 and 27 in 2D culture.

In another study, adipose derived hMSCs placed in a water bath at 41^0C for 60min once weekly showed higher viability and proliferative potential.[43] Their extracellular matrix deposition levels were also found to be higher than the untreated counterparts in osteogenic media. In the work by Shiu *et al*.,[44] hMSCs derived from the ribs and MG-63 cells (seeding density of ~10,000 cells/cm^2) were exposed to a range of temperatures (up to 45^0C) for 1h or 96h using a water bath (placed in an incubator only for the 96h study). The ALP/cell production on day 4 in expansion medium was found to increase linearly with temperature (37-45^0C for 1h and at 39 and 41^0C for 96h) in both cell types. When cells were grown in vitamin D3 containing media, at 42.5^0C enhanced ALP/cell production was observed which linearly increased with the vitamin D3 concentration. Mineralization was not observed for the single 1h treated samples (in contrast to the work by Nørgaard et a, 2006)[47], but for repeated treatments (1h per 72h once), at 39 and 41^0C enhanced

mineralization was observed at day 21. A continuous exposure for 10 days at 39^0C greatly increased calcium deposition with and without vitamin D3.

All the above studies have results in contradiction to the results obtained in this chapter. The various mild heat shock treatments of 40-42^0C for exposure durations of 15-60min as single or multiple treatments have not shown a strong effect on viability, ALP production, or changes in morphology of cells in expansion media indicating onset of osteogenesis in either cell types. Different seeding densities used in the various studies were also tested and did not show a different trend in terms of the heat shock treatment. The main difference between these previous studies and my experiments are the lack of *in situ* temperature measurements during the heat treatment in the former. This is important because my results show there could be discrepancies between the temperature set-point in the instruments and actual temperature of media in the cell-seeded wells, by as much as a few degrees. Such variations in achieved temperature could have a varying impact on activation of heat sensitive ion channels or production of HSPs. Also, for the prior studies discussed above, where heat shock was applied in a water bath, the untreated controls were placed in the incubator where the pH and O_2 were not regulated. It could be possible that the difference in pH and possibly oxygen concentrations in the heat shocked samples could have increased the stress on cells in addition to the elevated temperatures, therefore increasing the proclivity of cells to differentiate. Hence, the difference in contribution of more than one parameter between treated and control samples could possibly add uncertainty regarding the veracity of the observations in these prior studies.

The osteogenic differentiation of stem cells and MG-63s follows three stages:[182,183] (1) Proliferation typically occurring for the first 4 days, followed by (2) an early differentiation stage characterized by ALP production and expression of collagen matrix. This typically

occurs between 5 to 14 days in the case of hMSCs and from day 1 to 12 for MG-63 cells and in most experimental designs ALP production is assessed once every 7 days. In the final stage, the matrix is mineralized by calcium deposition which occurs day 14-28 for hMSCs and beyond day 12 for MG-63 cells where the alizarin red staining for calcium is performed at end of 3 weeks. The effect of heat shock was expected to manifest either as an enhancement in osteogenesis by increasing ALP production or an earlier onset by temporally shifting the ALP peak to an earlier time point. Hence, in this work, the initial experimental design assessed ALP production once every ten days. As some of the effect of heat shock was observed at the earliest time point (day 10), in the later experiments ALP production was assessed at shorter intervals until day 8 in order to pick up any temporal shifts in the peak. However, despite these changes in the experimental design the results showed no clear indication of an ALP peak. This suggests that for experiments involving mild heat shock conditions, a different osteogenic marker that is more sensitive to differentiation would be more accurate.

Although the mild heat shock results did not show an obvious effect, the severe heat shock treatment showed strong evidence of upregulation of ALP/cell especially in MG-63 cells with multiple treatments. On the other hand, repeated exposures to such high temperatures ($>50^0$C) had an adverse effect on cell viability. It appears that cells that were extremely heat- stressed but managed to survive, produce higher ALP after the heat treatment. This could be linked to the level of HSP protein expression if it does play a role in mediating the effect. While a mild- heat shock causes a transient expression of HSPs a severe heat shock would cause a strong and sustained HSP expression, where the latter might be criteria for regulating expression of osteogenic genes. This also highlights the need to dissect the pathway and the cellular and molecular components by which heat affects differentiation.

4.5 Conclusions and implications for future work

In this study it was apparent that mild heat shock did not strongly influence osteogenesis for both hMSCs and MG-63 cells. However there was evidence for a positive effect of severe heat shock on differentiation in both cell types, though it also had a strong negative impact on cell viability. It appears that an optimal temperature range might exist between 42^0C and 50^0C where a positive effect on differentiation can be achieved without affecting cellular viability. Bulk heat shock suffers from the disadvantage of having to expose entire cells to elevated temperature. In the next chapter, magnetic nanoparticles can be used as more targeted sources of heat and hence it might be possible to achieve higher target temperatures at certain regions of the cell without negatively impacting the viability of the cell as whole. Also, the findings from this chapter can be compared to the effect of magnetic nanoparticle-mediated heat shock on cellular behaviour (Chapter 5).

CHAPTER 5 Effect of magnetic nanoparticle mediated heat stress on cellular behaviour

5.1 Introduction

Various studies have shown that heat shock can enhance proliferative or differentiation behaviour of stem cells. [38,44–46] By understanding the effect of important parameters, in this case heat shock, on stem cell behaviour, more efficient cell-based therapies can be designed. For this purpose, the ability of magnetic nanoparticles (MNPs) to transduce external field energy to thermal energy could be exploited. MNP based heating (also known as magnetic hyperthermia) has been successfully used to trigger cellular processes such as activation of heat sensitive membrane ion channels[139,140] or apoptosis in the case of cancerous cells.[184,185] Apart from these applications, MNPs might be an ideal source of thermal cues to also control stem cell fate.

The mechanism underlying the heat shock induced changes in cellular behaviour is not clear. Theoretically, two main components might play a role in the response, namely, heat shock proteins or heat-sensitive membrane ion channels, or both. HSP expression increases with heat shock as does that of genes implicated in differentiation.[45,46,66] Whether the concurrent upregulation has a causal relationship has not been established. Also, no studies have looked at the effect of the activation of heat-sensitive ion channels on differentiation behaviour of stem cells. This is because a bulk heat shock approach where the temperature of the entire system is elevated makes it difficult to compare the effect of heat on individual component or regions within the cell.

The questions that need to be addressed are: how does the heat-shock stimulus regulate stem cell behaviour, and what are the ideal conditions in terms of temperature, duration of heat shock and frequency of application to elicit the necessary cell response? To answer these questions a different approach to bulk heating could be employed. Specifically,

MNPs could be used as a source of thermal energy and targeted to different cellular regions. This would enable the application of a localized heating effect in a controlled manner. Two key properties of MNPs make this possible: (1) their size and (2) their heat dissipation profile. MNPs have comparable size scales to different cellular organelles and biomolecules such as the proteins that form the membrane receptors. This permits efficient interaction between the MNPs and sub-cellular components and enables precise targeting at a sub-cellular scale. Also, the heat they generate dissipates with distance[140] and hence is localized at cellular scales (few tens of μm). By careful consideration of the magnetic and heating properties of the MNPs, as well as choosing suitable external magnetic field conditions, the heat dissipated could be controlled. Also, by identifying key components involved in the heat shock response and targeting them, the MNP approach would avoid the systemic nature of a bulk heating approach, combining the additional advantages of a targeted therapy.

This chapter discusses experiments with different bacterially synthesized MNPs in order to assess their magnetic and heating properties, and thus to identify the best candidates for cellular heating. Following this, strategies developed for targeting different cellular regions will be discussed. Finally, the effect of MNP- mediated heating of different cellular regions on cell behaviour will be compared.

As in previous chapters, experiments were performed using both primary stem cells: human bone marrow derived mesenchymal stem cells (hMSCs) and osteoblast-like cancerous cell line, MG-63s. In addition to previously discussed methodologies, the Electrical-Cell Impedance Sensing technique (ECIS) was employed to monitor changes in cellular behaviour, especially the onset of osteogenesis, by indirectly probing cell morphology using impedance measurements. A particular benefit of this technique is that it

allows continuous monitoring of the cells, rather than sampling cell behaviour at specific time points. It could therefore prove to be a more effective probe of osteogenic induction than relying solely on the various assays used in the previous chapter. The theory behind this technique is explained in detail in the following section.

Electrical-cell impedance sensing- Theory

Changes in the functioning of cells can be monitored by studying changes in gene expression, protein production or changes in morphology, metabolic activity, and structure of cellular components. For example, decrease in mitochondrial metabolic activity, increase in membrane permeability, or detachment and a spherical morphology are indicative of loss in cell viability. The differentiation of stem cells can be evaluated by measuring expression of the lineage-related genes using PCR (Polymerase chain reaction), protein production using ELISA (Enzyme-Linked Immunosorbent Assay), western blotting or histological staining. Although these assays give crucial information of specific biological changes in cells, they all are invasive and hence end-point assays. Hence, the information gained is only a snapshot of cellular behaviour at a specific time point during the course of the experiment. A majority of information is lost when studying gene and protein expression at fixed time points alone as they are temporal events. On the other hand, conducting experiments with a higher number of time-points is cumbersome as many of these assays are labour-intensive and expensive. A technique that is non-invasive, relatively more economical, less labour-intensive and continuous could give a better insight into the changes in cellular behaviour with time.

Electrical cell-substrate Impedance Sensing (ECIS) is a technique that measures the impedance to current flow across an adherent layer of cells.[186] It is a label-free, non-

invasive continuous monitoring technique to measure changes in cellular activity. The non-invasive nature of the technique allows real-time monitoring with the technology optimized for *in situ* measurements of cellular behaviour.

For the ECIS technique cells are cultured in special well plate arrays. A set of planar gold-film electrodes (Fig 5.1.1a) is deposited on the base of each well of the array. [186] On top of the gold layer a photosensitive non-conductive layer is deposited. The electrode pattern is generated using a mask through which light is shone to remove necessary areas of the photosensitive layer. The remaining photosensitive layer is deactivated by further processing and acts as an insulating film. The cell-culture medium or other suitable buffer acts as the electrolyte (Fig 5.1.1a). Current passes through the exposed electrode surface and when cells are present on the electrode, they alter the current flowing across (Fig 5.1.1b, c). The ECIS system measures the potential (V) developed across the electrodes when a small alternating current (I) is applied. Based on Ohm's Law, the impedance (Z) is calculated by the expression $\bar{Z} = \frac{\bar{V}}{\bar{I}}$.

Cells impede the flow of current and by growing the cells onto the electrodes (Fig 5.1.2) any changes in cell numbers (electrode coverage), morphology or nature of cellular attachment can be monitored by the ECIS impedance measurements.[187–191] At lower frequencies (<2kHz) of the applied current, the current flows around the cells beneath the cell layer and through cell-cell junctions (barrier function; solid arrows in Fig 5.1.1c) as the cell membranes act as insulators. The impedance is hence a function of the space under and between cells and the tightness of these junctions.[186] At higher frequencies, the current can capacitively couple (transfer energy through capacitance) through the insulating cell membrane and impedance depends on the confluency of the cell layer. Changes in cellular

function are implicated with changes in the above mentioned parameter such as cell numbers, morphology and barrier function (strength of tight junctions between cells). For example, when stem cells lose viability they become more spherical and eventually lift-off unlike viable cells which have an attached well-spread morphology.[9] By exposing the cells to various chemical, physical or biological stimuli or stresses, it would be possible to measure the effect of these stimuli on the cellular functioning by measuring changes in their impedance.

< *copyrighted image* >

Fig 5.1.1 Schematic explaining theory behind ECIS measurements: Current flow through cell-free electrode (a) and cell attached electrode (b; c- magnified)[192]

In the ECIS system, cells are grown on electrode well arrays and depending on the type of study, a suitable array-type is chosen. Some examples of different electrode layout are shown in Fig 5.1.2. The right choice of electrode layout is determined based on the sensitivity necessary for the cellular parameter being studied. The 8W1E system (Fig 5.1.2a) has a single working electrode of 250μm^2 (Fig 5.1.2f) (total surface area of well bottom is 0.8 cm^2) and a counter electrode of ten times the surface area of the working electrode. Hence the working electrode is the most sensitive to changes in impedance due to cellular activity. The counter electrode can be assumed to be constant due to its

relatively large surface area. In the 8W10E+ system (Fig 5.1.2c), there are forty electrodes (4 sets in parallel of 10 electrodes in series, Fig 5.1.2e) each of 250μm^2 surface area. The number of cells attached to the electrode is higher in the 8W10E+ array than the 8W1E array. Hence the changes in cellular parameters such as their morphology and micromotion will be averaged out over the population of cells directly on the electrode. It is necessary to have a smaller sample population for experiments which need a higher time resolution as a higher number of cells could mean that the different cells within the population could be at different phases and the overall reading is averaged out over the entire population and small nuances in the reading are lost. For example, when the effect of a drug or toxic agent on cell viability is studied, the electrode coverage in terms of overall impedance and the micromotion (motility of cells which is affected when cells lose viability) of the cells in terms of the level of oscillation of the impedance measurement for the cells can be compared. In such cases, the 8W1E system would be more suitable.

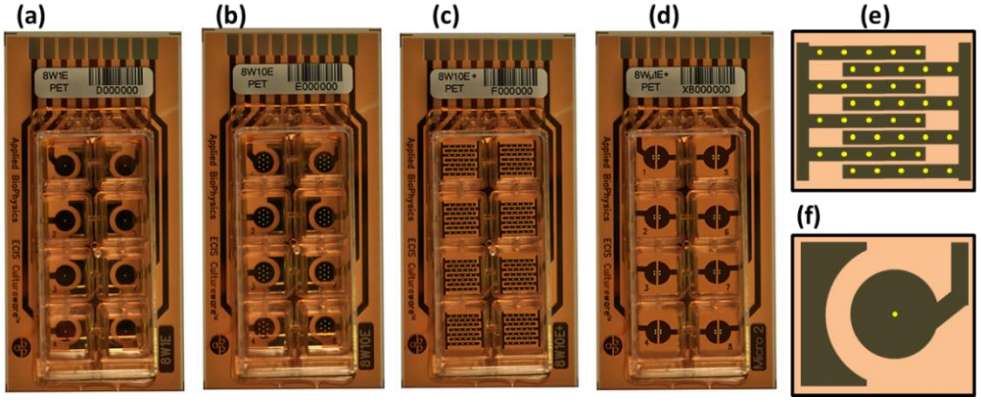

Fig 5.1.2 ECIS array types: (a) 8 wells with 1 electrode in each (8W1E), (b) 8 wells with 10 electrodes in each (8W10E), (c) 8 wells with 4 sets of 10 electrodes in series (8W10E+) and (d) has 8 wells with 4 electrodes each (8Wμ1E+). The layout of the circular electrodes in each well of a 8W10E+ (e) and 8W1E (f) is also shown (adapted from Applied Biophysics)[193]

ECIS has found applications in assessing cytotoxicity of drugs, in wound healing studies, to assess effect of additives on cellular behaviour such as their motility.[194] It has also been used to monitor differentiation of stem cells where a clear difference in the magnitude and the temporal trend of impedance varied for proliferating cells, cells undergoing osteogenesis or adipogenesis.[187] This shows promise for using the ECIS technique to assess changes in cellular behaviour especially viability and differentiation upon heat shock.

5.2 Materials and methods

5.2.1 Nanoparticle characterization

MNPs fabricated chemically (Sigma, UK) and bacterially were coated with citric acid (see section 2.1.1). Citric acid coated MNPs were used in all experiments unless otherwise mentioned. The size measurements were performed using the dynamic light scattering technique. ACS measurements were performed in water or glycerol. For suspending the MNPs in glycerol the required volume of glycerol (up to 200µl for ACS measurements) was added to the aqueous suspensions of the MNPs already placed in the ACS sample-holder vials. The water was evaporated in a hot plate overnight at temperatures not exceeding 80^0C (so as to not damage the citric acid coating).

For samples with a very high concentration of magnetic materials, the instrument overloaded and gave fluctuations at specific frequencies. For these, the measurement was corrected based on the values flanking the rogue point.

5.2.2 RGD biofunctionalization of MNPS and assessment of cell membrane binding

Citric acid coated particles were further functionalised by grafting RGD peptide, as described here. In brief, the carboxyl groups of the citric acid coated MNPs were activated using N-(3-Dimethylaminopropyl)-N′-ethylcarbodiimide hydrochloride (EDC; Sigma, UK)) and N-Hydroxysuccinimide (NHS; Sigma, UK). This was done by mixing 0.1-1mg (0.3ml) of citric acid coated MNP solution with a fresh sterile solution EDC/NHS (31mM of EDC and 0.1mM NHS prepared in 0.5M MES (2-(N-morpholino)ethanesulfonic acid; Sigma UK) buffer pH 6.3. For 1mg (0.1ml) of MNP solution, 20µl of EDC/NHS solution was added. The sample was incubated at room temperature for 1 hour in the dark. Following this step, the MNPs were washed via magnetic separation with 0.1M MES, pH 6.3 to remove excess EDC/NHS. For 1mg of MNP, 25µg of RGD was added in 0.3ml of 0.1M MES buffer and mixed gently by pipetting up and down. Samples were incubated overnight at 4^0C in the dark. Following incubation, excess RGD was washed off with 0.1M MES buffer (twice) and the functionalized MNPs were resuspended in sterile water.

For assessing membrane binding capacity of RGD functionalized MNPs, synthetic magnetite MNPs with and without RGD coating were incubated with cells for 1.5 or 3h in serum-free media. Serum-free medium was used because the presence of serum is known to cause protein corona formation on MNPs[144,195] which would hinder the efficient interaction of RGD with membrane receptors. As a control, citric acid coated MNPs were added to cells. Following incubation, the cells were washed to remove unbound NMPs with PBS prior to Prussian blue staining. Care was taken to wash the side of the wells where MNPs have a tendency to settle down more than in the centre of the wells. For iron quantification using Ferrozine, the cell-culture medium was pipetted a few times in each

well to re-suspend unbound MNPs and the medium was collected. The cells were trypsinized with 1x trypsin-EDTA in PBS and transferred to 1.5ml centrifuge tubes. The volume of medium and the trypsinized samples were kept identical to make comparisons valid. The samples were acid digested and processed for Ferrozine measurements (see Chapter 2, section 23.2).

5.2.3 Measurement and application of magnetic hyperthermia

To quantify the heating properties of the nanoparticles, MNP suspensions were transferred to 1.5ml centrifuge tubes and placed in the centre of a magnetic hyperthermia system comprising a temperature-regulated coil capable of generating high-frequency (50-1000 kHz) AC magnetic fields of up to 30 mT. By using different coil-capacitor combinations, different field strengths were attained. A list of the available combinations is shown in Table 5.1. Water at a pre-set temperature was circulated through the coil to prevent the coil from over-heating and to regulate the non-magnetic heating of the sample. The temperature was recorded in the sample space at the centre of the coil by inserting an optical probe into the sample, connected to a data-logging computer where the values were recorded.

The heating power produced by the MNPS depends on the applied field as demonstrated by Fig 5.2.1 where the same $Zn_{0.2}$ was exposed to same frequency but with differing field strength. The field strength has a linear dependence on power supply unit (PSU) voltage and hence by setting the PSU voltage parameter (20, 25 and 29V), the field strength can be modified.

	Coil (Turns/ Coil diameter)	Capacitor (nF)	Max. applied V (p-p)	Frequency (kHz)	Max Field strength (mT)
1.	17/ 25mm	187	1,000	184	24.3
2.	24/ 25mm	33	2,500	362	29.4
3.	17/ 25mm	15	3,000	654	32.5
4.	17/ 25mm	9	3,000	843	20.4

Table 5.1 Coil-capacitor combinations available in the magnetic hyperthermia device

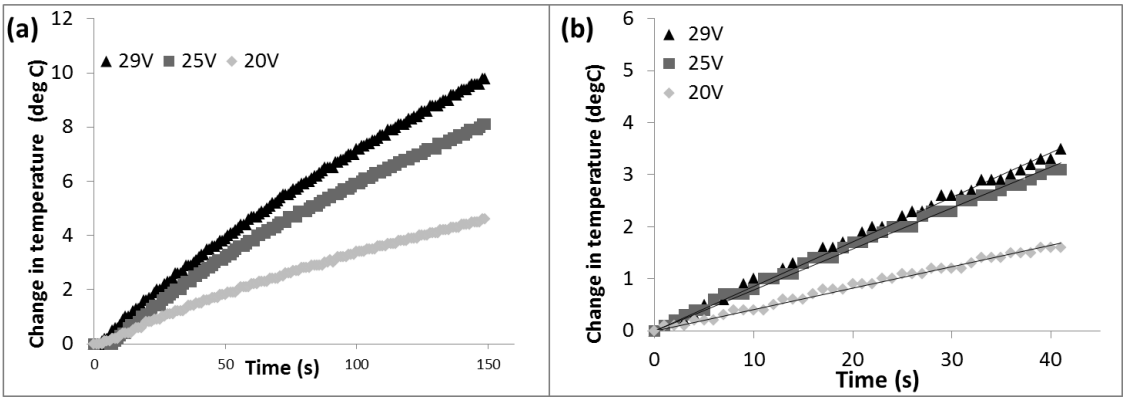

*Fig 5.2.1 Rate of heating for an aqueous suspension of $Zn_{0.2}$ at a set frequency of 165kHz and varying voltages (a). A trend line of the form y= (slope*x) has been fitted to the initial linear region (b) of the curves readings. SLP is calculated (Eq 5.1) using this slope which is the rate of heating (dT/dt).*

The heating efficiency of nanoparticles is measured by what is known as their specific loss power (SLP), given by the expression

$$SLP = \frac{CV_s}{m}\frac{dT}{dt} \qquad (5.1)$$

where C is the volumetric specific heat capacity of the sample (C_{water} = 4185 $JL^{-1}K^{-1}$), V_s is the sample volume, and m is the mass of magnetic material in the sample.[196] A plot of temperature (T) vs time (sec) was plotted and the slope of the initial linear region of the heating curve, dT/dt (Fig 5.2.1) was used to calculate the SLP values based on equation 5.1.

5.2.4 Electrical-Cell substrate Impedance Measurements

Commercially available sterile arrays were bought from Ibidi (Germany). Serum containing medium was added to the well and incubated overnight to improve attachment of cells. Before all experiments, measurements for 400µl of medium without cells were taken to ensure the wells were not faulty (leaks) and that they had comparable background impedance. Cells were concentrated in 200µL to achieve seeding densities of 25,000 cells/cm^2 for hMSCs and 50,000 cells/cm^2 for MG-63s (unless otherwise mentioned). Scans were performed in Multi-frequency time scan mode (MFT) where impedance is measured within a range of set frequencies from 60 to 64,000Hz. Media change was performed once every 3-4 days.

5.2.5 Cellular heat shock experiments using magnetic hyperthermia

For cellular based hyperthermia experiments, cells were seeded on PLA films. The films were cut out as 1cm^2 squares, rinsed in 70% ethanol, PBS and finally UV sterilized (thrice for 90s each). They were incubated with serum containing cell-culture medium overnight at 37^0C for protein binding to improve cell attachment.

The PLA films in sets of 4 (Fig 5.2.2) were transferred to bijou tubes, cell-culture medium was added and the tubes placed within the coil of the magnetic hyperthermia instrument or the incubator. After treatment, the PLA films were transferred to new wells and topped up with cell-culture media. The water cooling in the magnetic hyperthermia system coil was set at a temperature that allowed the solution placed within the coil to be maintained at 37^0C in the absence of MNP induced heating.

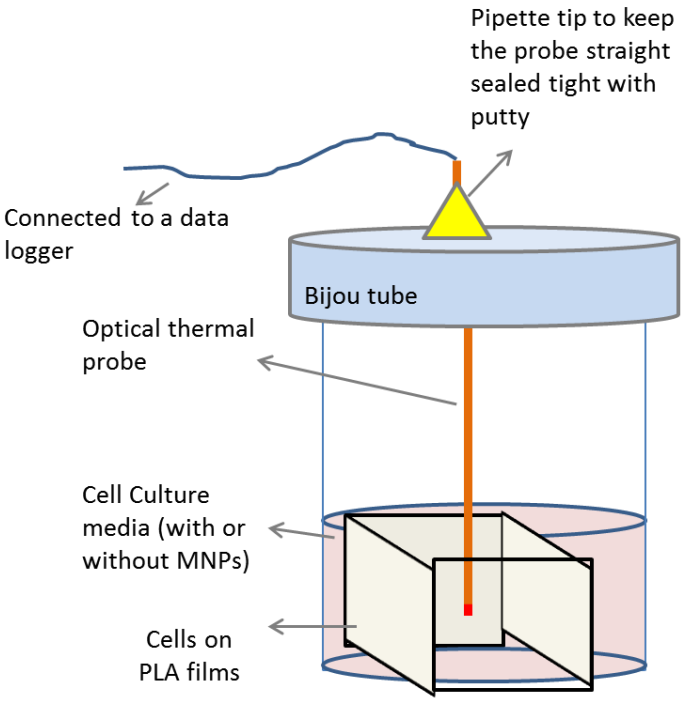

Fig 5.2.2 Schematic showing the set-up for applying magnetic hyperthermia to cells: PLA films on which cells were seeded were placed within a bijou tube in sets of 4 (they keep each other in place). The thermal probe was passed through a pipette tip attached to the cap of the bijou and then through a hole in the cap: this helped keep the probe at the centre of the tube without disturbing the films. To maintain sterile conditions the probe was disinfected with 70% ethanol and rinsed in PBS before insertion into tube, all in a sterile environment. Putty was used to seal the gaps formed due to the hole in the cap as well as keep the pipette tip in place.

Intracellular heating experiments

For intracellular experiments, an appropriate concentration of MNPs ($Zn_{0.2}$ or $Zn_{0.4}$ biogenic nanoparticles) was incubated with cells seeded on PLA films for specific periods of time (24-72h). Following this the wells were washed to remove excess MNPs and PLA/cell films transferred to 7ml bijou tubes with 1-2ml of DMEM containing 10% FBS, 1% antibiotics/antimycotics and 1% L-glutamine, for treatment in the magnetic hyperthermia system.

MG-63 cells (lower than passage 30) (40,000 cells/cm^2) were incubated with 500μM of synthetic magnetite MNPs for 24h. These MNPs were previously assessed for the heating power as aqueous suspensions and had an SLP of 24.7W/g at 112.53 kHz and 12.9mT field conditions. Following incubation with MNPs, cells were trypsinized and resuspended in cell-culture media. They were exposed to the external magnetic field (Field parameters: 112.53 kHz, 12.9mT) for 10min (Experiment 01) and re-seeded for further studies. For experiment 02, cells grown on 1cm^2 PLA films were incubated with 100μM of biogenic magnetite for 72h and exposed to magnetic field conditions of 362 kHz, 29.4 mT for 5 min.

Extracellular heating experiments

In the case of extracellular heating, after cell attachment (24h after seeding), the PLA films were transferred to 7ml Bijou tubes. In initial extracellular heating experiments, the same medium composition as described for the intracellular experiments was used. Upon finding that cells were stressed due to long durations of being outside the incubator (i.e. without pH control or gas regulation) a new medium was used which was more optimal for cell survival. It was composed of CO_2-independent basal medium (pH stable without gas regulation) containing 20% FBS, 2% antibiotics/antimycotics, 1% L-glutamine and 1% Non-essential amino acids. A stable aqueous suspension of $Zn_{0.2}$ or $Zn_{0.4}$ biogenic MNPS was then added to the media. Each experiment had 4 main sample conditions as shown in table 5.2.

The cells were exposed to different fields for different durations. Following the treatment, the PLA films were transferred to well plates or the cells were trypsinized and re-seeded in

the ECIS arrays. Various assays including live/dead staining, XTT or Alizarin red staining for mineralization were performed (see chapter 2, section 2.6).

Sample	**Location**	**Additive**
No MNP/ No magnetic field (MF)	Incubator	ddH2O
No MNP/ MF	Magnetic heating coil	ddH2O
MNP/ No MF	Incubator	MNPs
MNP/ MF	Magnetic heating coil	MNPs

Table 5.2 List of the different samples for extracellular the heat shock experiments and the conditions of treatment.

For extracellular experiments, hMSCs up to passage 2 were used. They were seeded on 1cm^2 PLA films and allowed to attach overnight. For applying the alternating field, the cells on the films were transferred to bijou tubes in sets of 4, cell-culture media with or without MNPs were added and the tubes and placed within the coil of the instrument. For all experiments, sterile suspension of $Zn_{0.4}$ in 1.5ml medium (0.3mg/ml; 10% v/v) was used for the heating. For the no MNP controls, water was added instead (10% v/v). They were exposed to extracellular heating with $Zn_{0.4}$ suspension in medium for different durations (Table 5.3) at 362 kHz and varying field strength to achieve the target temperature. Temperature was measured using an optical temperature probe immersed in the medium within the tube. Following treatment, the cells on the PLA films were transferred to fresh well plates and incubated in expansion or osteogenic media for further assays.

	Cell type (Seeding density in cells/cm^2)	Treatment/ MNP type/ Temperature(^{0}C)/ Duration (min)	Assays
01	MG-63 (40,000)	Intracellular/synthetic magnetite /10	Bright field images(24h)
02	MG-63 (40,000)	Intracellular/Biogenic magnetite /5	Bright field and Live/dead Images (4, 24h) DNA and Mitochondrial metabolic activity (4, 24h)
03	hMSCs (5000)	Extracellular/$Zn_{0.4}$ 47/50	Bright field Images(2h)
04	hMSCs (25,000)	Extracellular/$Zn_{0.4}$ 42/10	DNA and ALP (day 7, 14) Mineralization (Day 21)
05	hMSCs (25,000)	Extracellular/$Zn_{0.4}$ 42/30	Bright field images(0, 24h)
06	hMSCs (25,000)	Extracellular/$Zn_{0.4}$ 42/30	Bright field images(0h, 12 days) ECIS DNA and ALP (day 14)
07	hMSCs (25,000)	Extracellular/$Zn_{0.4}$ 42/60	Bright field images(day 13) ECIS DNA and ALP (day 21)

Table 5.3 Details of the various MNP-mediated heat shock experiments

A summary of the all the cellular based hyperthermia experiments is given in Table 5.3.

For ECIS measurements, cells were trypsinized and reseeded in the ECIS array wells. Alkaline phosphatase (ALP) was measured using the 4-MUP method, DNA via the Picogreen method and mineralization via Alizarin red staining technique as described in detail in Chapter 2, section 2.6. Calcein-AM and Ethidium homodimer dyes were used to differentially stain viable and compromised cells (see Chapter 3 section 3.2.4).

5.3 Results

5.3.1 Nanoparticle characterization for magnetic field heating experiments

For all cellular experiments, stable suspensions of nanoparticles were prepared by citric acid coating of the MNPs. The hydrodynamic size of the particles was found to increase when added to cell-culture media. For example, synthetic magnetite nanoparticles which measure ~70nm in water formed aggregates of around 500nm in cell-culture medium (DMEM) containing serum (Fig 5.3.1a). On the other hand, further aggregation after addition to media, did not occur as evidenced by the time series of size measurements shown in Fig 5.3.1a for synthetic magnetite. The ACS measurements in media for biogenic magnetite, up to 48h are shown in Fig 5.3.1b. The overlap of the χ" peak at all time points (this peak being an indirect measure of the hydrodynamic size) indicates that no further clustering occurred in media. Hence, apart from the initial clustering, citric acid coated MNPs maintained their hydrodynamic sizes in cell-culture media with further incubation.

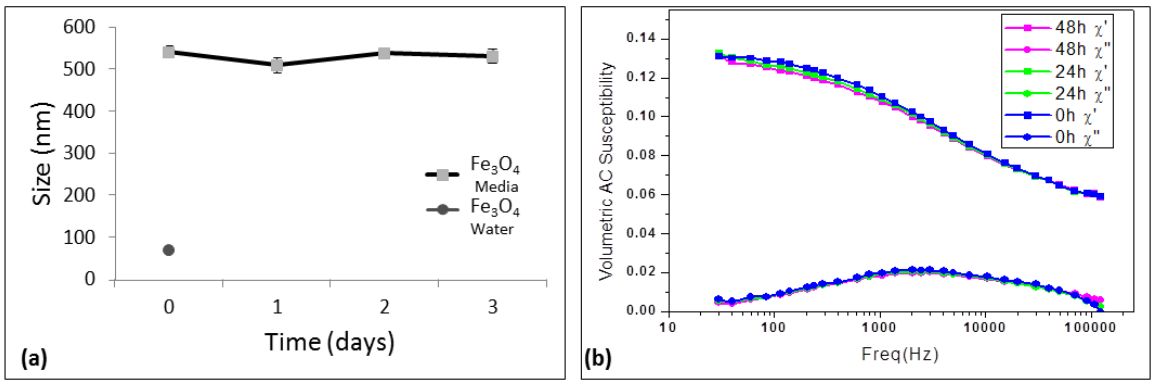

Fig 5.3.1 Stability of citric acid coated MNPs with time in cell-culture medium: Size measurement via dynamic light scattering for of synthetic Fe_3O_4 in water and cell-culture medium (a). ACS measurements for biogenic Fe_3O_4 in cell-culture medium between 0-48h showing the overlap of the measurements at all time points indicating the absence of size changes with time (b).

The citric acid coated nanoparticles were studied with regard to their magnetic properties as both stable aqueous suspensions and when internalized by cells, as discussed earlier (see Chapter 3 section 3.3.3). Further to this, Fig 5.3.2a shows the ACS curves obtained for $Zn_{0.4}$ MNPs in water. The characteristic Brownian relaxation peak was observed at the higher frequencies. Previously, in cells, the MNPs were found to lose their Brownian component due to immobilization or further clustering (Chapter 3 section 3.3.3). This was found to be the case for $Zn_{0.4}$ MNPs as well (Fig 5.3.2b). When the MNPs ($Zn_{0.4}$) were suspended in glycerol (Fig 5.3.2c), they lost their Brownian component in a similar fashion

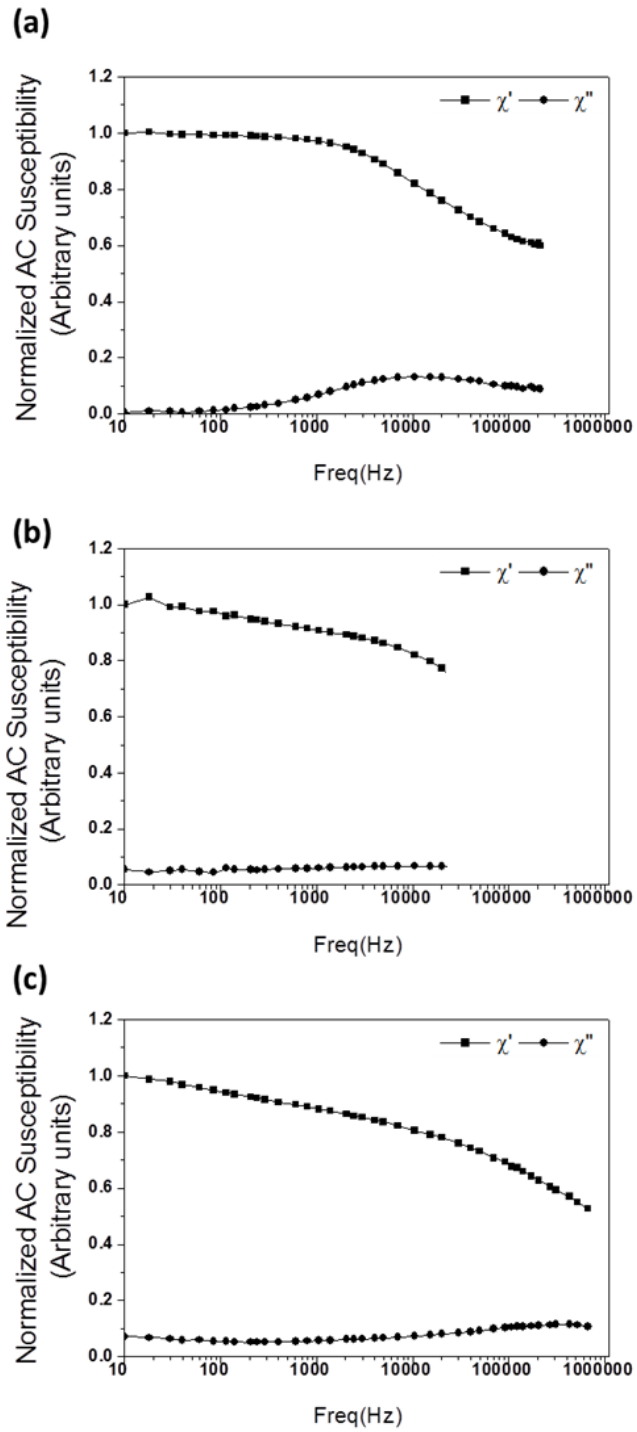

Fig 5.3.2 Comparison of the magnetic behaviour of MNPs in different biological environments: ACS measurements of MNPs in water (a), cells (b) and glycerol (c) following 72 incubation with MG-63 cells. All values were normalized to the value of χ' at 10 Hz. The frequency range was truncated in (b) due to the reduced signal obtained from MNPs in cells.

to the condition when they were internalized by cells. The shape of the χ' and χ" were very similar to that of MNPs in cells as seen in Fig 5.3.2. This is explained by the high viscosity of glycerol that immobilizes the particles preventing them from physically rotating and hence displaying Brownian relaxation. Therefore the glycerol system is the closest to mimic cellular conditions and is ideal for predicting the magnetic response of MNPS in cells.

Since MNPs' ACS measurements in glycerol are representative of their behaviour in cells, the ACS measurements of the various zinc–doped MNPs in glycerol were compared (Fig 5.3.3) to identify the best candidates for cellular applications. As seen earlier, the zinc doping imparted the strongest Neél component to the MNPs and hence they gave a strong signal when immobilized in cells (see Chapter 3 section 3.3.3). The ACS measurements show that biogenic magnetite (Fig 5.3.3a), $Zn_{0.2}$ (Fig 5.3.3b) and $Zn_{0.4}$ (Fig 5.3.3c) MNPs all have a strong magnetic response in glycerol. The strong response of biogenic magnetite which has no zinc doping, indicates that it also shows a strong Néel relaxation. This is probably due to its biogenic origin that gave rise to MNPs of small core sizes with highly ordered crystalline structure that results in well-defined anisotropy and hence a more visible Néel component.

For all the samples, the χ' and χ" curves neither overlap nor reduce to zero, implying that the Néel peak occurs at frequencies beyond the experimental range. This can be demonstrated by calculating the expected behaviour at higher frequencies using model simulations as shown in Fig 5.3.4b.[114] The experimental data agrees quite well with the simulated data at the lower frequencies as seen in Fig 5.3.4 a, b, respectively. The Néel peak can be observed in the simulated curves at around 10^7 kHz (Fig. 5.3.4a). The

frequency at which the relaxation peak occurs is where relaxation-associated heating for MNPs will be close to maximum.

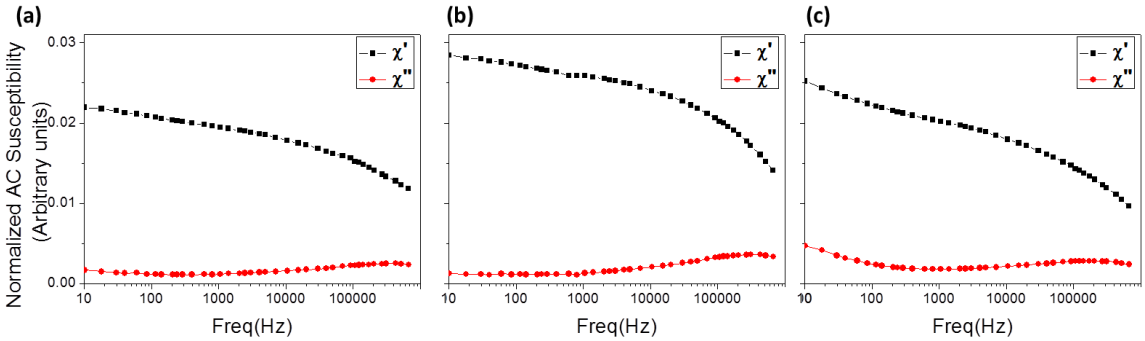

Fig 5.3.3 Comparing ACS behaviour between different Zn-doped MNPs: ACS measurements of Fe_3O_4 (a) $Zn_{0.2}$ (b) and $Zn_{0.4}$ (c) in glycerol. All values normalized to the concentration of the MNP suspension as measured via the Ferrozine assay.

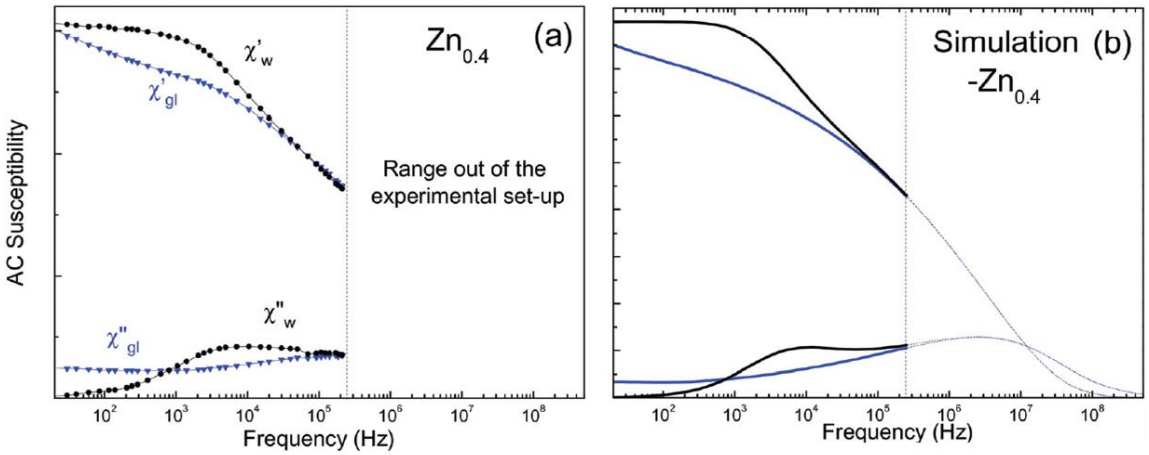

Fig 5.3.4 Predicting the resonant frequency for MNPs: Comparing the experimental ACS measurements for $Zn_{0.4}$ in water and glycerol (a) to the simulated curve (b). The simulation also predicts the shape of the ACS curves beyond the range of the experimental values where a clear Néel relaxation peak can be observed. [114]

Following the confirmation of their strong magnetic signal in glycerol, the heating power of the biogenic MNPs was measured under different field conditions (Fig 5.3.5). The strongest heating was at 362 kHz in water for all the MNPs (Fig 5.3.5 a) with $Zn_{0.4}$ showing the highest specific loss power (SLP) of >400W/g. SLP increased between 184

and 362 kHz. This result could be due to the increase in frequency and field strength as heating driven purely by relaxation mechanisms would increase SLP linearly with frequency, and would show a squared dependence with field strength. On the contrary, a further increase in frequency did not cause a corresponding increase in the SLP value, suggesting that the overall heating effect depends on a complex interplay of Néel and Brownian relaxation as well as hysteresis losses.

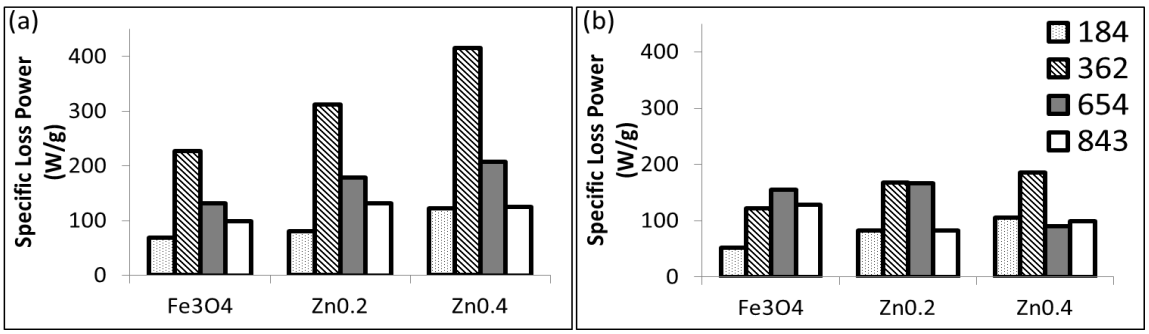

Fig 5.3.5 Heating power of Zn-doped MNPs under different magnetic field conditions: Biogenic magnetite, $Zn_{0.2}$ and $Zn_{0.4}$ in water (a) and glycerol (b) are exposed to different frequencies (184 - 843kHz) of AC magnetic field and their SLP measured calculated.

The SLP values for all MNPs were lower in glycerol (Fig 5.3.5b) compared to in water. This is because the Brownian contribution was lost due to the immobilization. However as evidence of Néel relaxation can be seen for all the biogenic MNPs (Fig. 5.3.3), a heating effect was preserved even in the absence of Brownian relaxation. Similar to the trend in water, $Zn_{0.4}$ showed the highest SLP at 362 kHz of 182W/g, $Zn_{0.2}$ intermediate with 168W/g and biogenic magnetite showing the lowest of 122W/g. A high SLP was also observed at 654 kHz for biogenic magnetite (155W/g) and $Zn_{0.2}$ (167W/g) though not for $Zn_{0.4}$ (90W/g). SLP was lower for all MNPs at the highest frequency 843 kHz, probably due to the lower maximum field that could be applied at this frequency (table 5.1). The differences in the SLP measured between particle types reflect their different particle sizes and magnetic anisotropy constants.

5.3.2 Strategies for cellular level scale targeting of MNPs

To test the effect of different heat stress delivery approaches on cells, multiple strategies were developed to target MNPS to specific cellular locations. The main approaches to deliver the heat stress were: (1) extracellular heating and (2) intracellular heating. For extracellular heating, the MNPs were re-suspended in the cell-culture media and exposed to the external field. The external field parameters were tuned to achieve the target temperature. For example, in Fig 5.3.6, the rise in temperature of the cells immersed in cell-culture medium containing MNPs is shown.

To target attachment of MNPs to the membrane (via integrin receptors), it was aimed to functionalize the surface of the MNPs with RGD peptide. ACS measurements were used to assess changes in the hydrodynamic size of the MNPS caused by the additional surface binding of the RGD. The Brownian peak for the citric acid coated MNPs prior to RGD attachment was observed at around 6000 Hz (Fig 5.3.7). MNPs which were treated with the activator groups (EDC/NHS) alone showed a shift from the untreated MNPs closer to 2000 Hz. Finally, the MNPs which were activated with EDC/NHS and subsequently functionalized with RGD showed an even further shift closer to 1000 Hz. The size change, as indicated by the shift in the peaks, is higher from the untreated to the activation step compared to between the activated MNPs to RGD-bound MNPs. This is because the attachment of the activators causes a considerable increase in the hydrodynamic size and hence a large shift in peak position. When the RGD binds, it replaces the activator (zero-length crosslinking agent).[197] Probably the activator molecule and the peptide have comparable size scales, and hence the replacement of the activator by the RGD does not cause a major change in the hydrodynamic size of the MNPs.

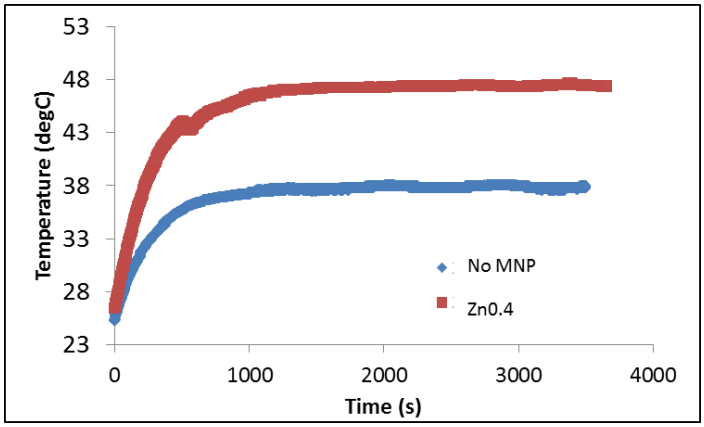

Fig 5.3.6 Heating rates of solutions with and without MNPs (Experiment 03): The increase in temperature of the cell-culture medium (1ml) containing $Zn_{0.4}$ MNPs (200µl) compared to MNP-free cell-culture medium (1ml + 200µl water) is shown as measured via an optical temperature probe.

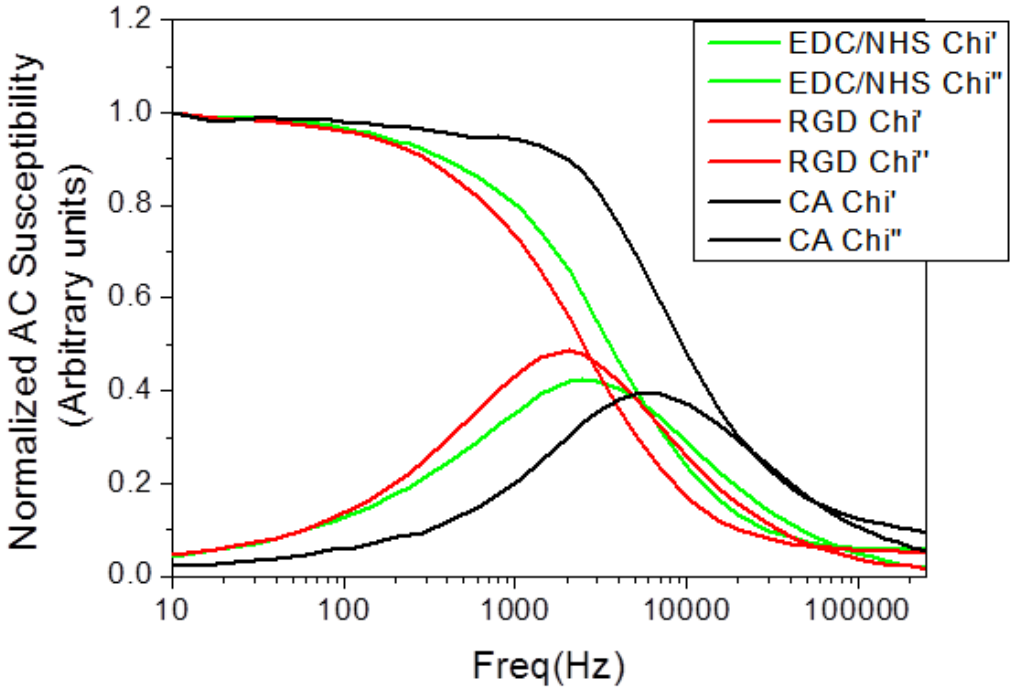

Fig 5.3.7 Changes in ACS signal with bio-functionalization: The ACS curves for non-functionalized magnetite (CA) are compared to that of RGD-functionalized MNPs (RGD). The RGD binding to the MNP surface was performed using the EDC-NHS activator which binds to the carboxyl groups of citric acid. RGD then replaces the activator. ACS curves for MNPs which have been activated but not bound to RGD (EDC/NHS) are also shown. All values are normalized to the value of χ' at 10 Hz frequency

One interesting feature to note from the ACS curves is the increase in the overlap of χ' and χ" for the RGD coated $Zn_{0.4}$ MNPs compared to the citric acid coated ones. The curves for the RGD coated samples are typical of a blocked particle (see fig 1.2.7 and fig 3.3.21c) This could be because the steps involved in the RGD coating, especially the magnetic separation of particles during washing, have caused a loss of the smaller superparamagnetic fraction of MNPs due to an effective filtering process. The significance of this change in behaviour is that the heating power of the MNP suspension may also be altered necessitating reassessment of these MNPs to predict suitable field condition parameters for the desired heating.

The membrane-binding efficiency of MNPs ($Zn_{0.4}$) following RGD functionalization was then assessed. Bright field images of hMSCs incubated with non-functionalized and RGD functionalized MNPs stained for iron (Prussian blue) are shown in Fig 5.3.8 a-d. The dark spots correspond to the iron staining. The wells were not confluent and hence have some non-specific binding of the MNPs to the well bottom. Since the seeding densities were equivalent between the different conditions, the error arising from this would also be equivalent between the conditions. More confluent wells will reduce the error arising from this non-specific binding of MNPs to the well bottom. For the MNPs associated with cells, as expected, no peri-nuclear localization of MNPs was observed as an incubation time of 1.5-3h is not sufficient for significant uptake of MNPs by the cells. So any MNPs that become associated with the cells have a higher probability of being membrane bound rather than internalized. Qualitatively, there was no difference between the two particle groups (i.e. those with and without RGD functionalization) following 1.5h or 3h incubation with cells.

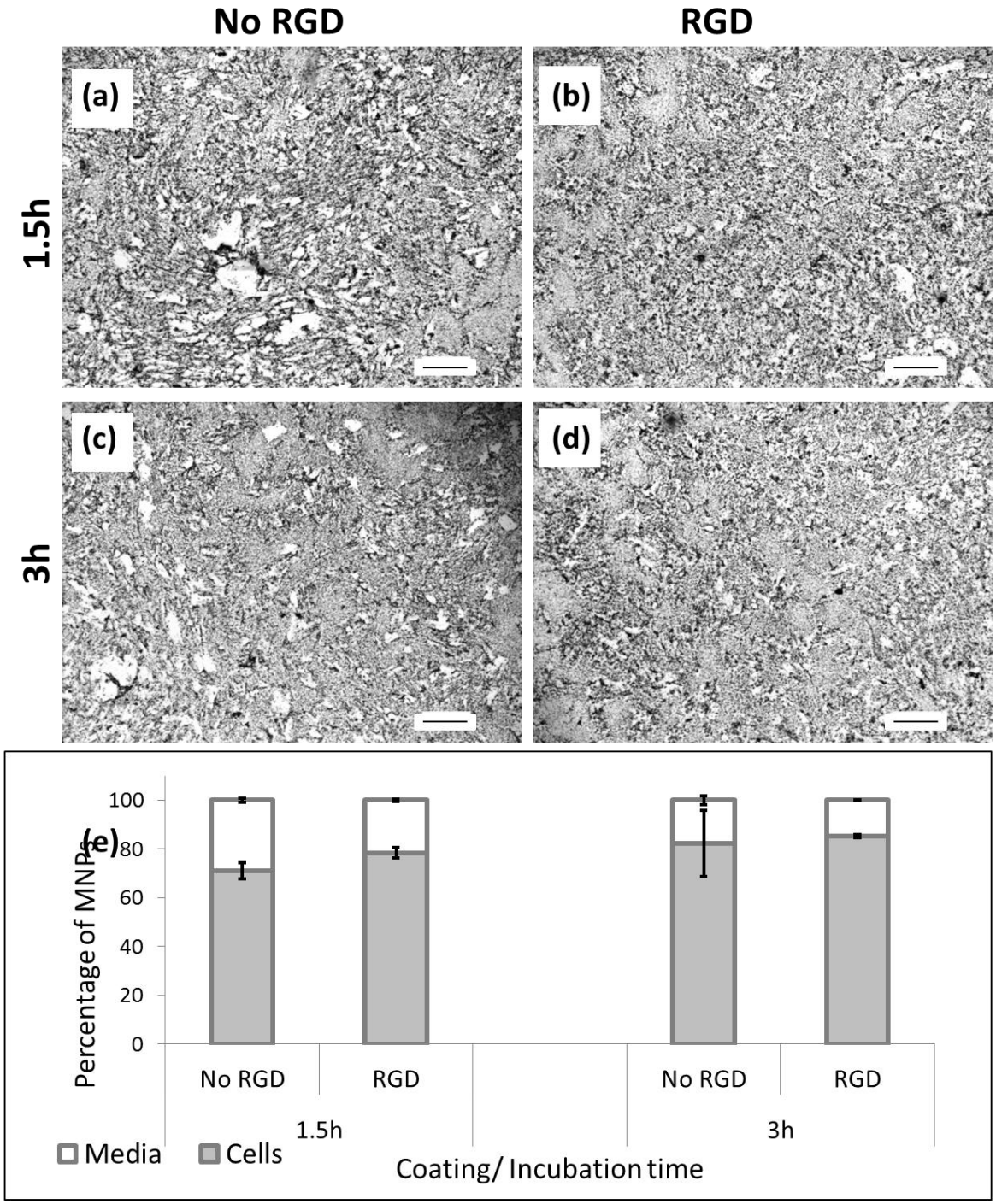

Fig 5.3.8 Effect of RGD coating and time on cell-membrane association of MNPs: Cells were stained for iron (Prussian blue staining) following incubation with $Zn_{0.4}$ MNPs either not functionalized (a, c) or functionalized with RGD functionalized (b. d) following 1.5h (a, b) or 3h (c, d) incubation.(Scale bars correspond to 200μM). MNP association was assessed by quantifying iron (Ferrozine assay) present in the cells and remaining in the media. Error bars represent standard error of the means and no significant difference was found between the groups. (Scale bars correspond to 100μm)

The MNP binding was quantified via the Ferrozine assay for iron by measuring on both the cells and the media added to the cells (Fig 5.3.8e). Between 1.5h and 3h, the percentage concentration of MNPs in cells had increased while in the media added to cells, it has proportionately decreased (Fig 5.3.8e). Between the RGD-functionalized and non-functionalized MNPs, percentage concentration in cells was higher for the former, though only by a small amount for both incubation periods (by 7% at 1.5h and 3% by 3h) while an inverted trend was observed for the media added to cells. The decrease in the difference of the concentration from 1.5 h to 3h between the MNPs with and without RGD indicate that by 3h even without membrane receptor binding, the MNPs can form strong enough attachments to the cell membrane to withstand washing steps performed (with an aim to remove the unbound MNPs).

5.3.3 ECIS for monitoring changes in cellular behaviour

Prior to using the ECIS technique for studying the effect of MNP-mediated heat stress on cellular behaviour, it was necessary to perform optimization studies as described below. All experiments were initially compared between two array types namely, 8W1E and 8W10E+. Bright field images of MG-63 cells attached to the arrays are shown in Fig 5.3.9. The circles observed are the boundaries of the electrodes. A single electrode for the 8W1E array type (Fig 5.3.9a) and multiple electrodes for 8W10E+ type (Fig 5.3.9b) can be seen. Since the 8W1E has only a single working electrode it has a smaller sample size but a higher sensitivity (Fig 5.1.2f). For example, as seen in Fig 5.3.10 the impedance values fluctuated rapidly for hMSCs (Fig 5.3.10a) and MG-63 cells (Fig 5.3.10b) seeded on an 8W1E array while the signal was more stable with time for cells on 8W10E+ array.

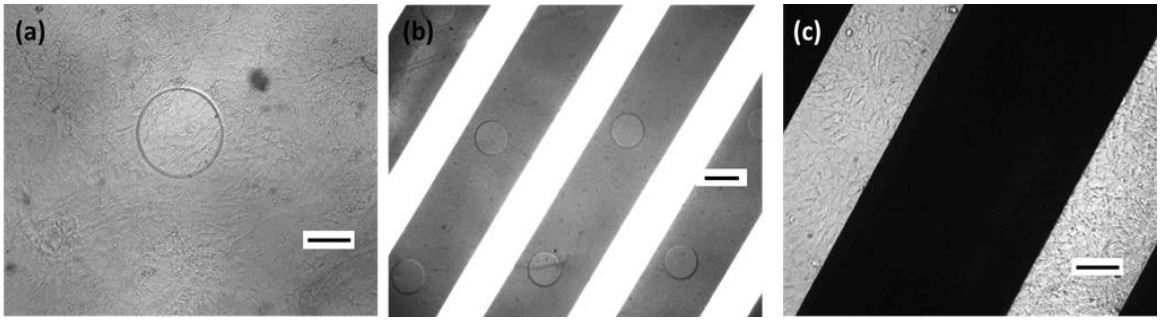

Fig 5.3.9 MG-63 cells attached to different ECIS arrays: 8W1E (a) and the 8W10E+ arrays (b, c). The electrodes can be seen as circular regions in (a) and (b). A magnified and different contrast of the 8W10E+ arrays is shown in (c) for a clearer observation of the cells. (Scale bars in a, c correspond to 100μm and in b corresponds to 200μm)

If the cells are motile, their morphology and attachment sites constantly change (micromotion) which would cause constant fluctuations in the impedance to current flow. These manifest as a time-dependent oscillating impedance measurement. In the 8W10E+ electrode layout, due to the larger number of cells present on the electrodes, the impedance changes average out, reducing individual cell-associated fluctuations. It is interesting to note that the magnitude and frequency of the oscillations are higher for the hMSCs than MG-63 cells, at all seeding densities, indicating the stem cells have higher micromotion than the more mature osteoblastic cell type (MG-63 cells; Fig 5.3.10 a, b).

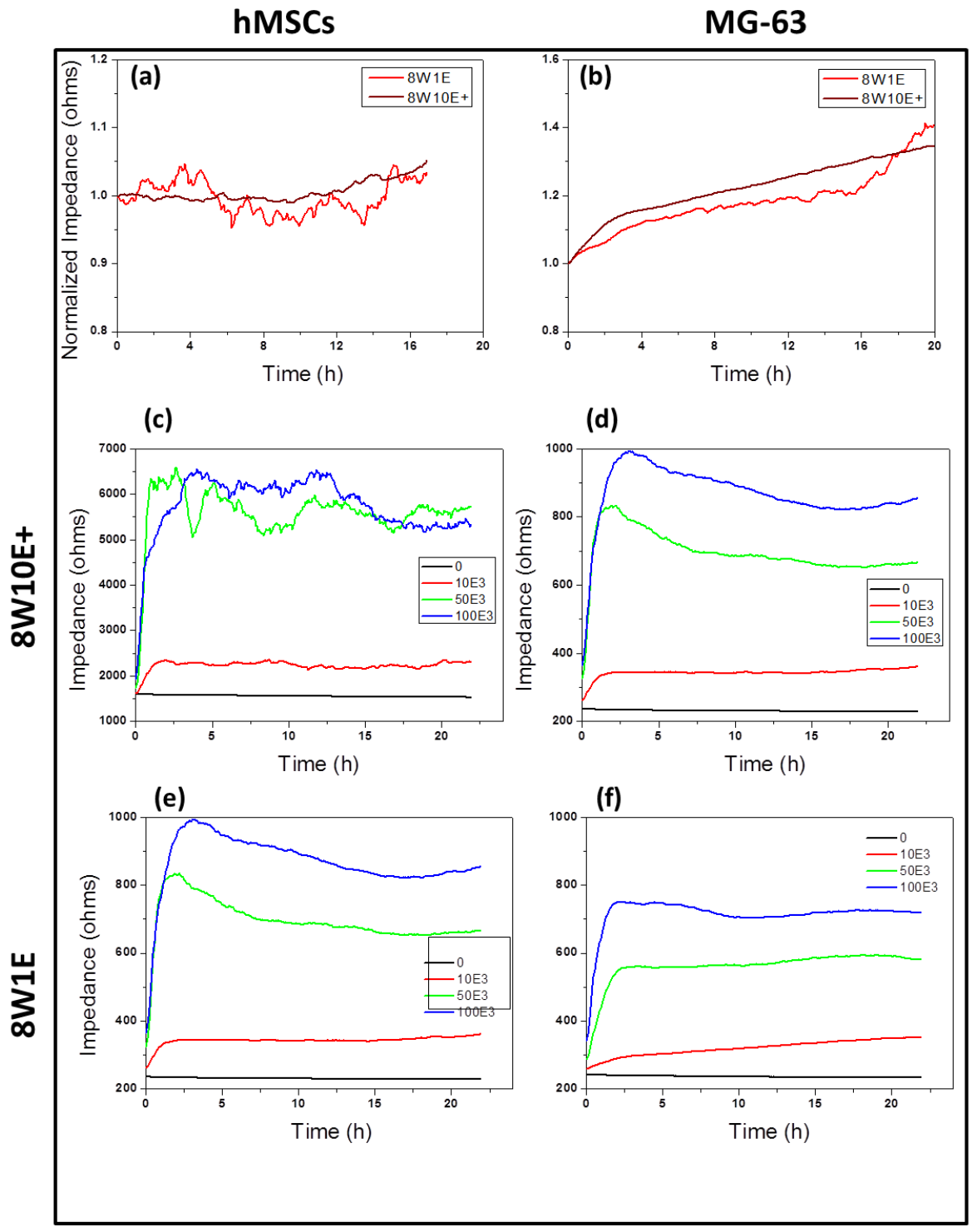

Fig 5.3.10 Cells on 8W1E and 8W10E+ arrays at 10E3 cells/cm^2 seeding density immediately following attachment [hMSCs (a), MG-63 (b)]. hMSCs at varying seeding densities (legend units: cells/cm^2) on 8W1E (c) and 8W10E+ (e) arrays. MG-63 cells in 8W1E (d) and 8W10E+ (f).

To optimize the seeding density for the different cell types, different cell concentrations were seeded in both arrays for hMSCs and MG-63 cells (Fig 5.3.10 c-f; Fig 5.3.11). Bright

field images show the increasing number of cells attached on the electrode for MG-63 cells (Fig 5.3.11 a-d) and hMSCs (Fig 5.3.11 e-f) with increasing seeding density. For all seeding densities, the impedance increased exponentially for up to 5 hours beyond which it plateaued (see for e.g. Fig. 5.3.10c). The initial increase in signal occurs as the cells settle down and adhere to the electrode surface and the later plateauing indicates complete cell attachment and no further increase in cell-coverage. On the other hand, for wells seeded at 10,000 cells/cm^2, the signal did not plateau and instead increased at a more gradual rate after the initial exponential increase (see for e.g. Fig. 5.3.10d, f). This is because the wells were not completely confluent after complete attachment following which the cells proliferated (increased electrode coverage) leading to a further but more gradual rise in impedance. When the different seeding densities (0, 10,000, 50,000 and 100,000 cells/cm^2) are compared, it can be seen that for the 8W10E+ system (Fig 5.3.9 e, f), the impedance directly correlates with the cell numbers in contrast to the 8W1E system (Fig 5.3.9 c, d). In the 8W1E system there was no observable difference between the 50 and 100,000 cells/cm^2. This could be due to the inhomogeneous distribution of cells on the well bottom, an effect that will be more obvious with a single and smaller centrally located sampling space. For all further experimental work, an intermediate cell seeding density of 25,000 cells/cm^2 was chosen for hMSCs (due to constraints in availability of cells) and 50,000 cells/cm^2 for MG-63s to achieve near-confluent wells.

The impedance measurement is a function of the frequency of the electric field applied. Depending on the frequencies (below or higher than 2kHz) the contribution of different cellular parameters (barrier function, membrane capacitance) to the impedance of current flow varies (see section 5.1). Hence, the most sensitive frequency needs to be identified for

each cell type. This was done by comparing the difference in impedance measurements of cell-free media to cell-covered electrodes at different frequencies (Fig 5.3.12).

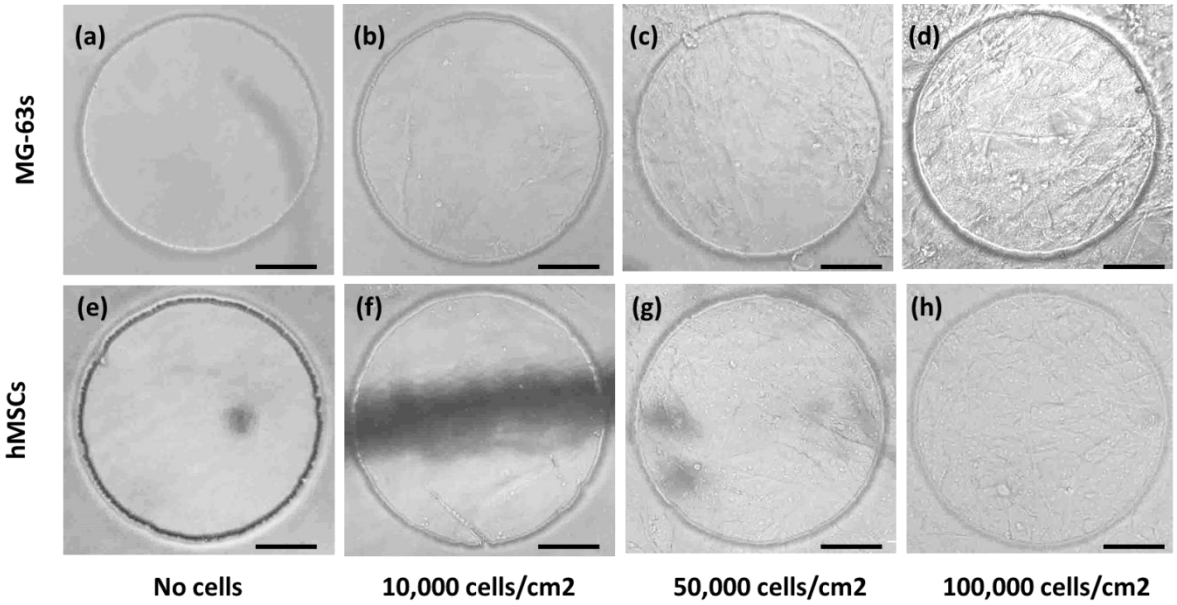

Fig 5.3.11 Bright field images of cells on ECIS well plates: MG-63s cells (a-d) and hMSCs (e-h) seeded on 8W1E array at varying cell densities of 0 (a, e), 10,000 (b, f), 50,000 (c, g) and 100,000 cells/cm^2 (d, h) the circular region is the working electrode and cells can be seen growing across it. hMSCs are very flat cells and hence do not have a strong contrast in bright field images making it hard to delineate them compared to MG-63 cells.(Scale bars correspond to 50µm)

The most sensitive frequency can be identified by doing a Multi-Frequency Time (MFT) scan on the ECIS system. In this mode, the impedance was measured in chosen wells at a range of pre-set frequencies and the impedance versus frequency graph for cell-free media and cell covered electrodes were plotted. Fig 5.3.12 shows the impedance measurements at 0h and 10h following cell seeding. At 0h (Fig 5.3.12a, c) when the cells had not yet attached to the electrodes the cell-free and cell-containing samples show similar impedance values at all frequencies. Cells attached within 5h following seeding as seen in Fig 5.3.10 c-f in both arrays for both cell types. Hence by 10h, when cell attachment was completed, a difference in the impedance between the cell-free and cell-containing samples was

observed at frequencies beyond 4 kHz for all the different cell and array types. The maximum difference was at 32 kHz and 64 kHz, (most sensitive frequencies) hence 32 kHz was the frequency studied for all future experiments.

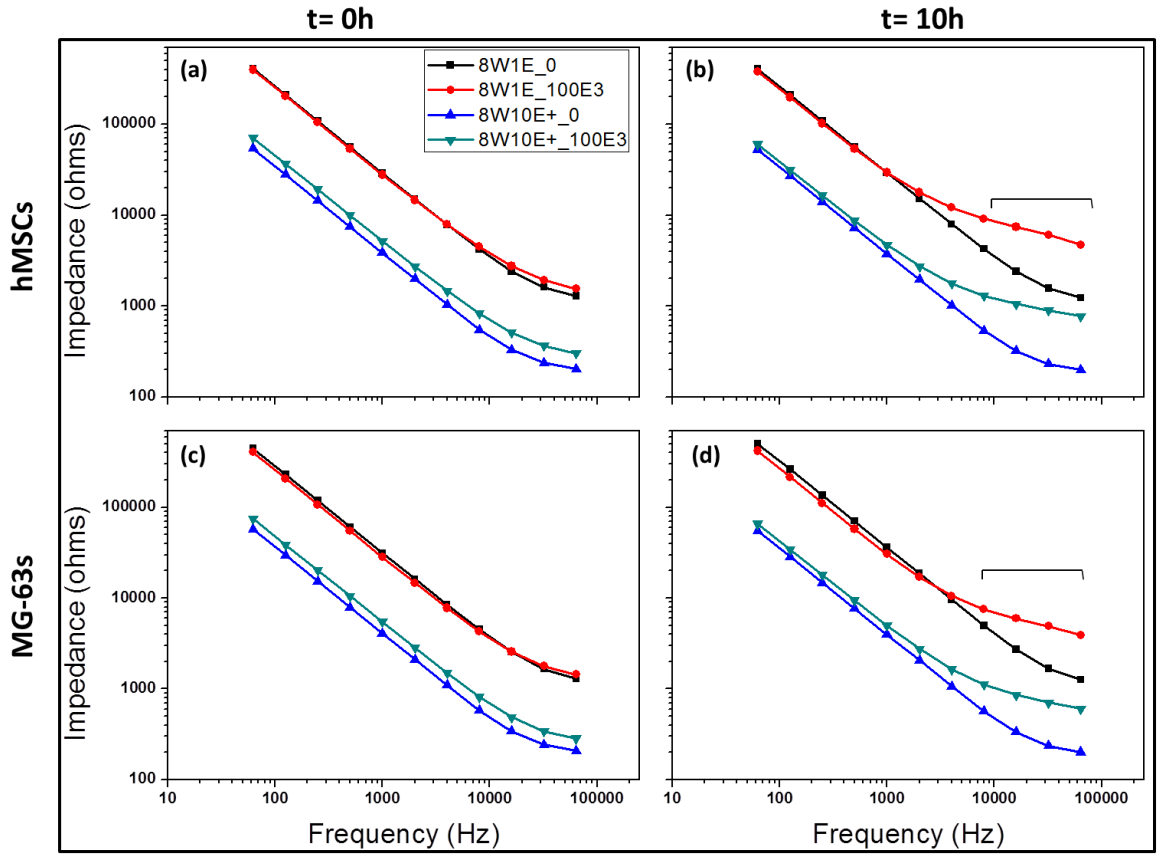

Fig 5.3.12 Identification of optimum frequency of measurement: Cells were seeded at 100,000 cells/cm^2 (100E3) and impedance measured at 0h for hMSCs (a) and MG-63s (c) and at 10h (b- hMSCs, d- MG-63s). Measurements were done in 8W1E and 8W10E+ arrays for cells and cell-free media. The most sensitive frequencies are marked in plot (d).

Based on the optimization assays, the 8W10E+ array was chosen as the ideal array type for all further experiments as it samples a larger number of cells, hence being more representative of the population. Sensitivity to single cell-changes was not the primary concern for the viability and differentiation experiments. Also impedance was analysed at 32 kHz where maximum sensitivity was obtained.

Following this, the suitability of impedance measurements to detect osteogenesis of cells was investigated (Fig 5.3.13). Initially, all the cells were seeded in expansion medium and hence showed similar impedance values. At 45h, in some wells, the expansion medium was replaced by osteogenic medium to induce differentiation. The cell-free osteogenic and expansion media had similar very low impedance levels indicating that all measurements came from cells and any change is due to a change in cellular parameters. An obvious difference in the measured impedance between hMSCs cultured in expansion and osteogenic media emerged beyond 24h post-induction (e.g. Fig. 5.3.13a).

As observed previously, the impedance plateaued-off for the cells in expansion medium with any fluctuations occurring only during media change or when the wells were removed from the incubator for imaging (marked by the broken lines at 45, 140, 170 and 240h). The system is very sensitive to changes in temperature which manifested as sharp spikes (also seen in the cell-free media wells) in the impedance values when the arrays were removed from the incubator causing a change in the solution temperature. These artefacts are short-lived (until the system attains equilibrium) and did not cause too much information loss in long-term experiments (spanning over days).

For the cells in osteogenic medium, the impedance increased between 75-140h at which point the medium was replaced. Following the media change, the impedance temporarily decreased for cells in osteogenic medium while for the cells in expansion medium impedance plateaued after an initial moderate rise. The falling impedance values for the hMSCs in osteogenic medium, started rising again around 30 hours after the media change, and this rise-and-fall trend is also observed after the second media change at 240 hours. Clear differences can be observed in the plots for individual wells containing cells in expansion and osteogenic media (Fig 5.3.13 b-d). The change in impedance is consistent

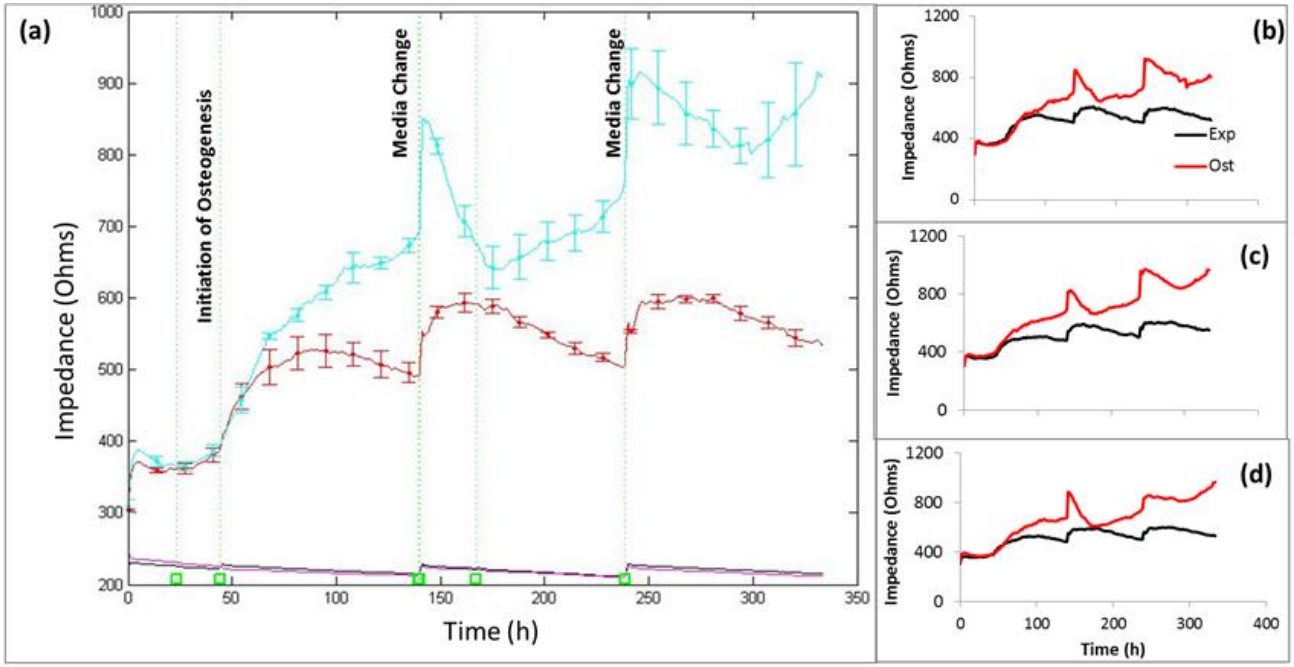

Fig 5.3.13 ECIS measurements for detecting osteogenesis in hMSCs: hMSCs were seeded in expansion medium at 0h in 8W10E+ arrays and the average impedance measurements (n=3) are shown in (a) using 32 kHz AC current. At 45h, expansion medium (red curve) was replaced by osteogenic medium (blue curve) in half the wells. Cell free wells containing expansion and osteogenic media were also measured (pink and black curves). Media were changed for all wells once every 4 days at 45h, 140h and 240h (marked by dashed lines). Cells were checked during every media change as well as at 170h (marked by dashed lines) using bright field microscopy. To highlight the reproducibility in the trend for cells in expansion and osteogenic media, individual impedance measurements (i.e. n=1) from randomly paired wells containing osteogenic (OST) and expansion media (EXP) are plotted in b, c and d.

The clear difference in the trend of differentiating cells to proliferating cells confirms the suitability of impedance measurements for identifying early stages of osteogenesis in hMSCs (up to 12 days in this experiment). Unlike traditional assays, where differentiation markers are not significantly up-regulated until after about a week, the ECIS measurement technique allows identification of the onset of differentiation within 48 hours in the case of hMSCs. In addition, although absolute impedance values may vary, the overall trend of the impedance as a function of cellular morphology is very reproducible, as can be seen by comparing impedance measurements from individual cell populations (i.e. individual wells) (Fig. 5.3.13 b-d).

In the case of MG-63 cells, similar impedance values were observed for all cells initially cultured in expansion medium until 48h (Fig 5.3.14). After 48h, when the expansion medium in half the wells had been replaced with the osteogenic medium, the impedance measurements were found to decrease for these wells. In contrast, for the wells maintained in expansion medium, after an initial dip the impedance values returned to their original magnitude (Fig 5.3.14). A clear difference in the trend of the impedance changes between the media types is observed, especially in the individual plots for wells containing cells in expansion or osteogenic media (Fig 5.3.14 b-d). Although, the difference in the magnitude of the impedance value decreases beyond 100h post-induction, the trend of the curves are distinct from each other.

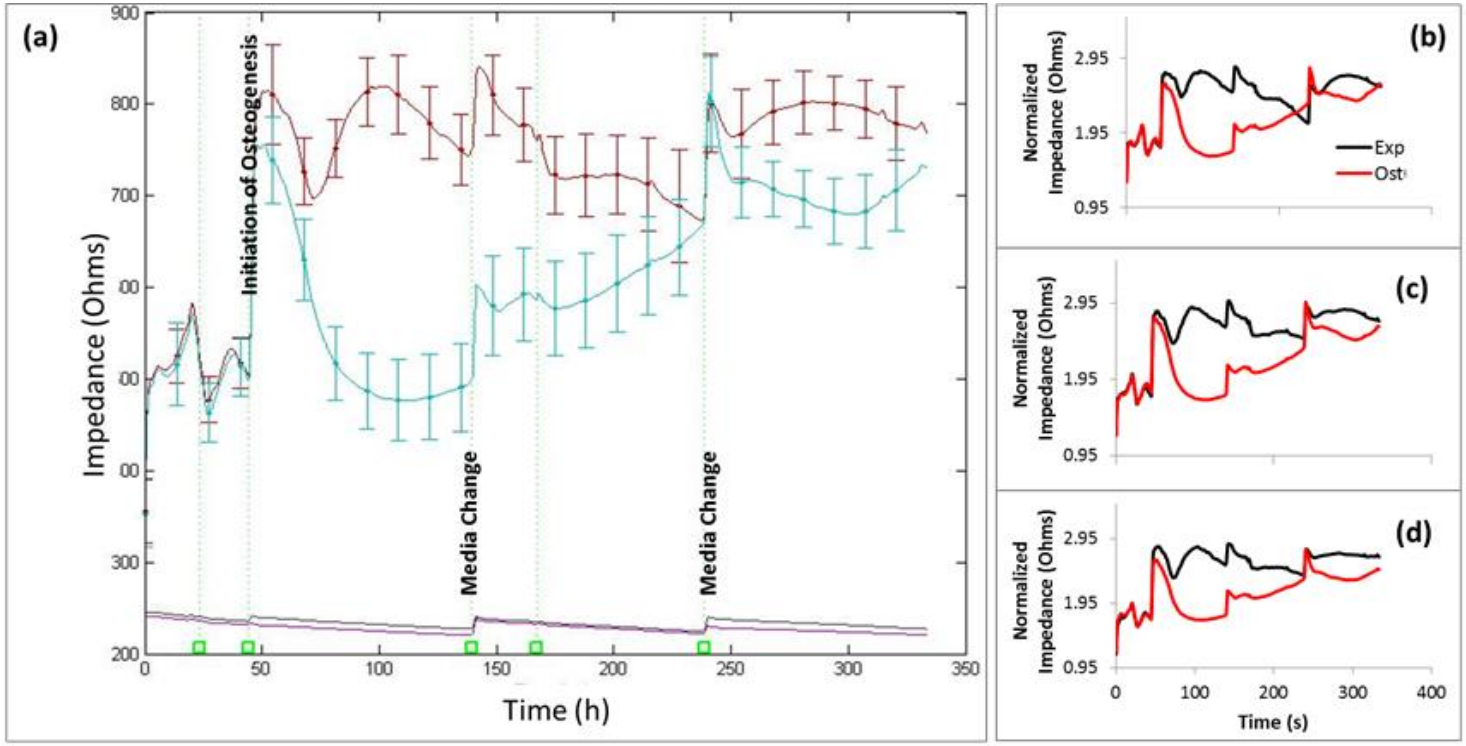

Fig 5.3.14 ECIS measurements for detecting osteogenesis in MG-63 cells: MG-63 cells were seeded in expansion medium at 0h in 8W10E+ arrays and the average impedance measurements (n=3) are shown in (a) using 32 kHz AC current. At 45h, expansion medium (red curve) was replaced by osteogenic medium (blue curve) in half the wells. Cell free wells containing expansion and osteogenic media were also measured (pink and black curves). Media were changed for all wells once every 4 days at 45h, 140h and 240h (marked by dashed lines). Cells were checked during every media change as well as at 170h (marked by dashed lines) using bright field microscopy. To highlight the reproducibility in the trend for cells in expansion and osteogenic media, individual impedance measurements (i.e. n=1) from randomly paired wells containing osteogenic (OST) and expansion media (EXP) are plotted in b, c and d

After 21 days in culture, the impedance for the cells in expansion and osteogenic media were measured to see if they still showed a similar trend as during the early onset of osteogenesis. Though the magnitude of impedance was higher for differentiating hMSCs compared to the cells in expansion medium, the values were almost constant with time (Fig 5.3.15 a). The media were changed to see if the replenishment of nutrients had an effect on cellular behaviour and hence impedance, but apart from an initial increase just after the media change, no change in the overall baseline was observed. The trend for individual wells can be observed in Fig 5.3.15b, c. A similar stable impedance measurement that wasn't affected by a media change was observed for MG-63 cells (Fig 5.3.15e-h). Unlike the hMSCs, impedance of MG-63 cells in expansion medium were higher than for cells in osteogenic medium (Fig 5.3.15 e) as also observed during the initial stages of differentiation (Fig 5.3.14). The trend for individual wells are shown in Fig 5.3.15 f, g, h. Osteogenesis was confirmed by staining with alizarin red in both cell types (Fig 5.3.15 d, i) at day 24, where a clear red staining in the osteogenic wells can be observed, indicative of mineralization. However, it was not possible to obtain clear microscopy images from these plates due to the presence of the electrodes (difficulties in setting the contrast and obtaining focus).

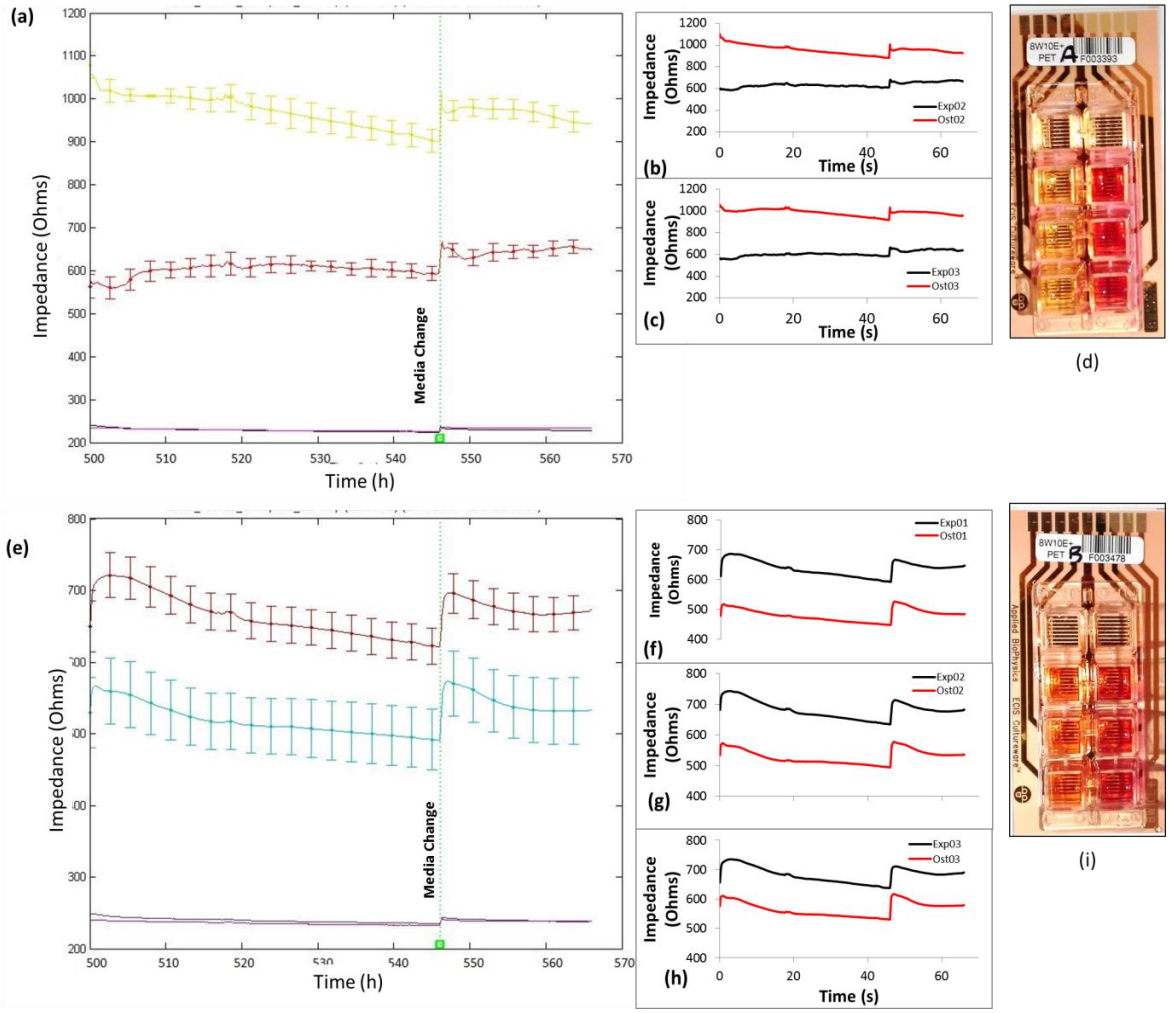

Fig 5.3.15 ECIS measurements during later stages of osteogenesis in both cell types: Impedance measurements for hMSCs (a-c) and MG-63 cells (e-h) as average (n=3) and as couples of individual wells of cells in expansions and osteogenic media (randomly coupled; b-c; f-g) between day 21 to 24. The samples were assessed for mineralization via the alizarin red staining for calcium (hMSCs- d; MG-63- i). The top 2 wells contained cell-free media. In the remaining wells, the ones on the left had cells in expansion medium and on the right in osteogenic medium.

5.3.4 Effect of MNP-mediated heat shock on cellular behaviour

Intracellular Heat Shock Experiments

For the intracellular heat shock experiments, the initial aim was to apply a strong MNP-mediated heating to affect cell viability. This was to confirm that the MNPs were dissipating heat and affecting the cells. Preliminary experiments were performed as described below.

In a preliminary experiment, MG-63 cells were exposed to intracellular heat shock for 10 mins using synthetic magnetite MNPs (Experiment 01). Following incubation of the cells with the MNPs for 24 hours a perinuclear localization of MNPs in the cells can be seen (Fig 5.3.16 c, d, and e). There was no change in the morphology of cells between the controls (Fig 5.3.16 a, b, c) and the treated cells (Fig 5.3.16 d) indicating the 10min treatment had no effect on cell viability. This could probably be because the treatment duration was too short to generate sufficient cellular heating. Also, synthetic magnetite does not have a strong SLP compared to the biogenic magnetite or the zinc-doped samples. The SLP of these MNPs in water was found to be only 24.7W/g for the field conditions used in the above treatment which reduces even further when in cells as these MNPs lose their Brownian relaxation, a major contributor to their heating (decrease in the ACS signal in cells due to loss of Brownian motion can be seen in Fig 3.3.22).

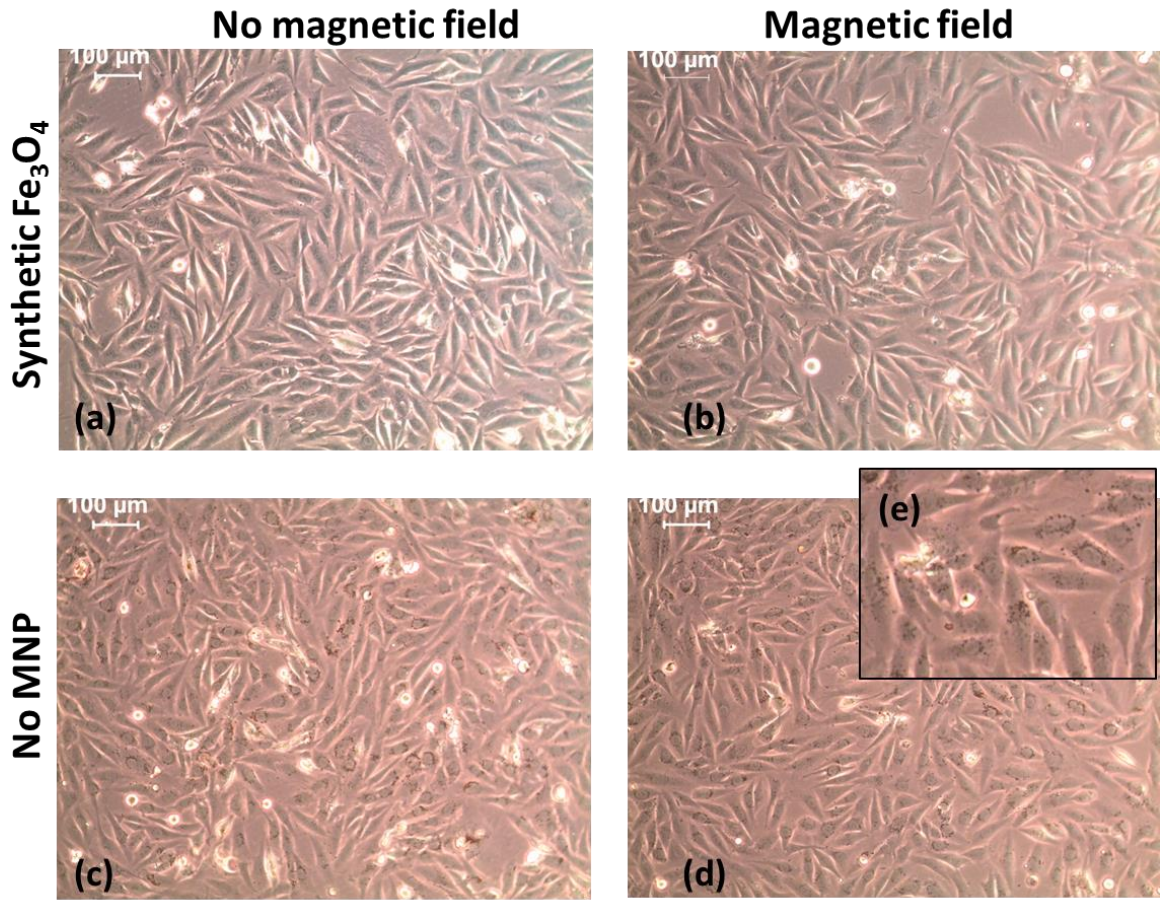

Fig 5.3.16 Effect of MNP-mediated heat shock on cellular morphology (Experiment 01): Bright field images of MG-63 cells 24h following exposure (b, d) or no exposure (a, c) to a 10min alternating field (112kHz, 0.15mT; SLP_{water}=24.7W/g) Cells were loaded with MNPs (c, d) or not loaded (a, b). MNPs were incubated with cells for 24h for intracellular uptake (Magnified image showing perinuclear localization confirming intracellular uptake – inset e). (Scale bars correspond to 100µm)

In the next experiment, MNPs with a stronger heating profile were investigated for their effect on cell viability (Fig 5.3.17; Experiment 02). Cells loaded with biogenic magnetite (SLP_{water}=226 W/g; $SLP_{glycerol}$=122 W/g at 362kHz and 29.4mT; Fig 5.3.5) which has a much stronger SLP than synthetic magnetite, were exposed to stronger field conditions (362kHz, 29.4mT) for 5min. The perinuclear localization of the MNPs was observed in the cells incubated with MNPs confirming uptake (Fig 5.3.17 c, e). The morphology of the cells in the treatment samples (Fig 5.3.17g) shortly after the treatment (4h; Fig 5.3.17 top)

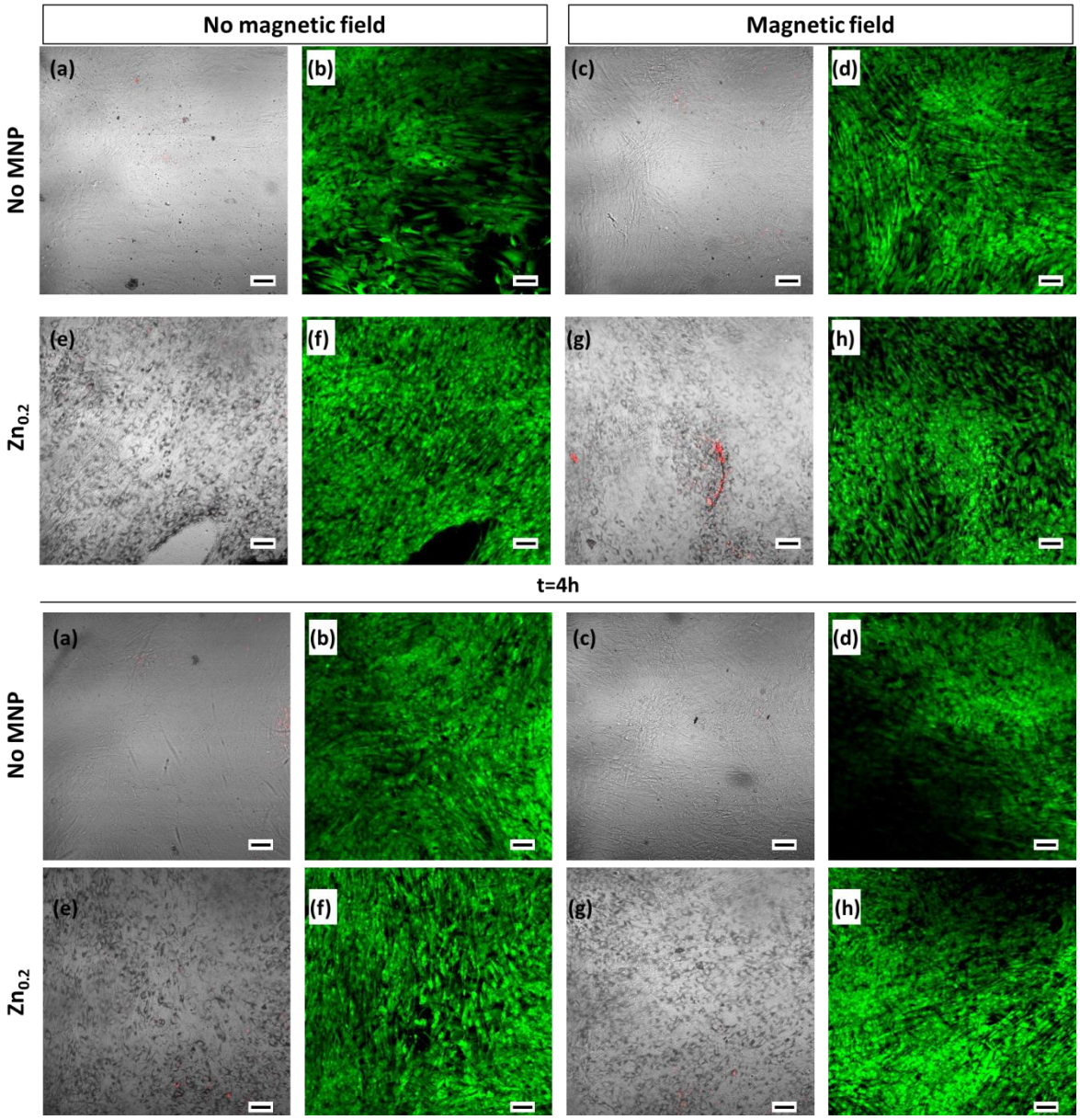

Fig 5.3.17 Morphology and cellular viability of MG-63 cells exposed to MNP-mediated heat shock (Experiment 02): Cells after a 4h (top) and 24h (bottom) recovery period with (e-h) or without $Zn_{0.2}$ (a-d) were exposed to 10min heat shock treatment (c, d, g, h) (Controls not exposed to magnetic field include a, b, e and f). Cells were stained for Calcein-AM and Ethidium homodimer. The bright field images merged with images of Ethidium stained cells and another set of Calcein stained cells are shown above. Perinuclear localization of cells with MNPs can also be observed in the bright field images (e, g). (Scale bars correspond to 100µm)

and after a 24h (Fig 5.3.17 bottom) recovery period are both comparable to the controls (Fig 5.3.17 a, c, e). The wells largely consisted of Calcein-stained cells (Live) in all the controls (Fig 5.3.17 b, d, f) and the treated sample (Fig 5.3.17h). Very few compromised

cells (Red staining for compromised cells merged with the bright field images) were observed (Fig 5.3.17 a, c, e, g). The DNA content and mitochondrial metabolic activity were also assessed as shown in Fig 5.3.18. No significant changes in cell numbers (DNA) or metabolic activity were observed between the treated and untreated controls at 4h or 24h following treatment. These results show that even with stronger intracellular heating, there is no significant loss in viability.

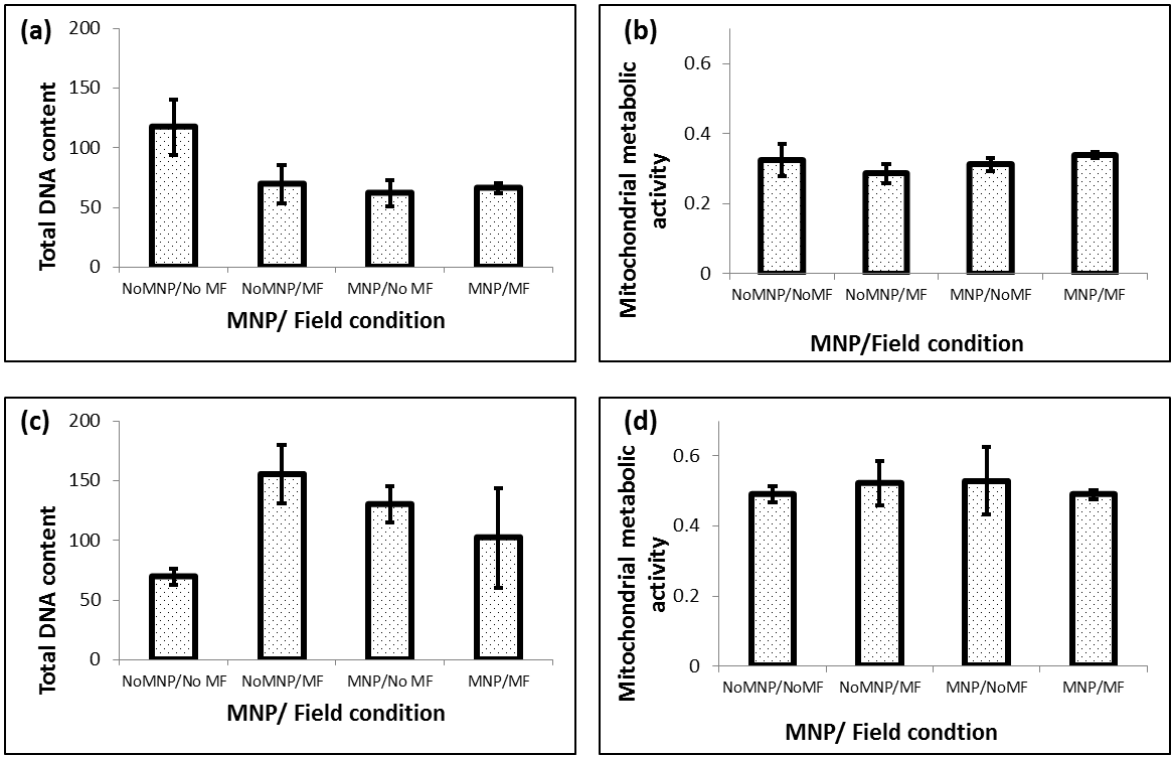

Fig 5.3.18 Mitochondrial metabolic activity and cellular viability of MG-63 cells exposed to MNP-mediated heat shock (Experiment 02): Cells after a 4h (a, b) and 24h (c, d) recovery period with $Zn_{0.2}$ (MNP) or without $Zn_{0.2}$ (No MNP) were exposed to 10min heat shock treatment (MF) (Controls not exposed to magnetic field: No MF). Mitochondrial metabolic activity was measured using the XTT assay and the total DNA content using the Picogreen assay. Error bars represent standard error of the mean for n=3. No significant difference was found between any of the groups for both measurements (Tukey's HSD, $p< 0.05$).

Extracellular Heat shock Experiments

In order to achieve temperatures in the extracellular MNP-mediated heating experiments consistent with those used in the bulk heating experiments, $Zn_{0.4}$ was used as it had the highest SLP (at 362 kHz, 29.4 mT; Fig 5.3.5). In the first experiment (experiment 03), to confirm the effect of magnetic nanoparticle heating on cells, strong field conditions (362 kHz and 29.4 mT) were used to generate maximum heating. The MNP-media suspension in which cells were immersed reached temperatures of around 47^0C for 50min (Fig 5.3.6). Bright field images show cells having the expected morphology of viable hMSCs for: the untreated cells (Fig 5.3.19 a), cells with MNPs not exposed to an external field (Fig 5.3.19 c) and cells without MNPs exposed to the external field (Fig 5.3.19c). However the cells which were exposed to the external field in the presence of particles alone, showed a change in morphology due to the heat shock stress. They appeared more rounded; typical of cells observed shortly before detachment and eventual death (Fig 5.3.19d). This experiment confirms the effectiveness of the approach of using MNPs to heat cells and hence affect their behaviour, in this case their viability, and that temperatures capable of inducing severe heat shock effects can be applied to cells using MNPs as a local heat-source.

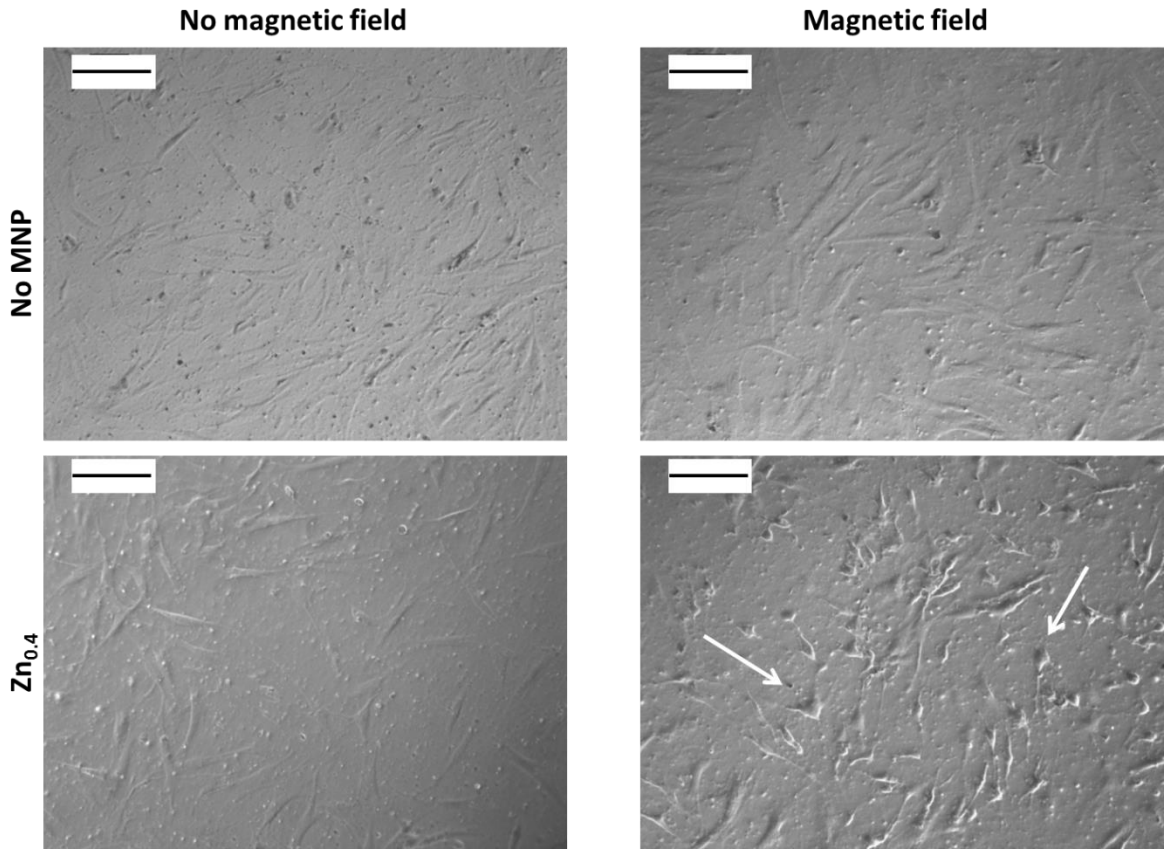

Fig 5.3.19 Effect of MNP-mediated severe heat shock on cellular morphology (Experiment 03): Untreated hMSCs (a), cells without MNPs exposed to field (b), with MNPS not exposed to an external field (c) and with MNPs exposed to an external field [362kHz, 29.4mT for 1h maintained at 47^0C for 50min] (d) after a 2h recovery period. (Scale bars correspond to 100μm)

In the next experiment (Experiment 04), cells were exposed to a milder heat treatment of 41^0C using the same MNP-media suspension. The target temperature of 41^0C (Fig 5.3.20) was achieved and maintained for 10min by adjusting the external magnetic field parameters by altering the PSU voltage which determines the field strength. The controls were maintained at 37^0C. As for the bulk heat shock experiments discussed in Chapter 4, measurements of ALP to assess osteogenesis, and DNA content to assess viability were performed at different time points (Fig 5.3.21).

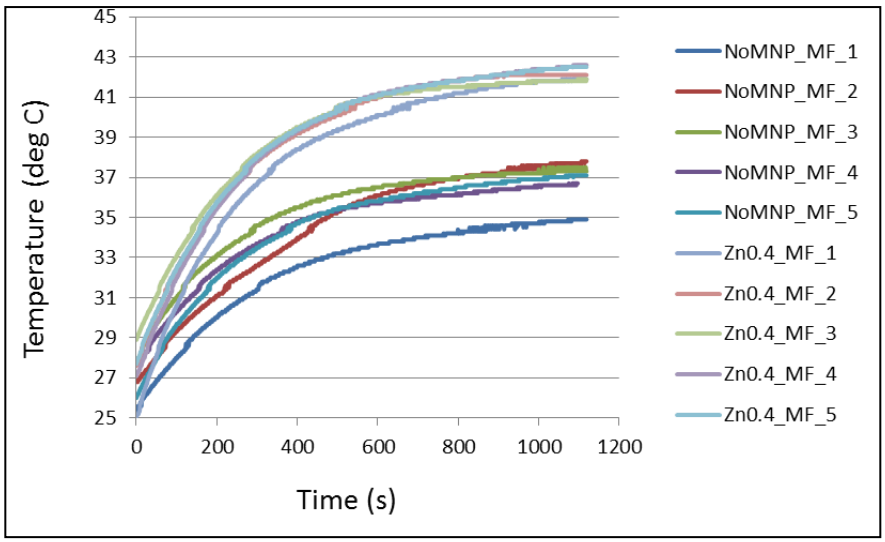

Fig 5.3.20 Temperature measurements during extracellular MNP-mediated heating of cells (Experiment 04): hMSCs seeded on PLA films were immersed in media with or without MNPs under the influence of an external magnetic field. Treated cells were exposed to temperatures around 42^0C for 10min. The different curves marked by increasing number (1 to 5) show subsequent treatments of all the replicates for each condition.

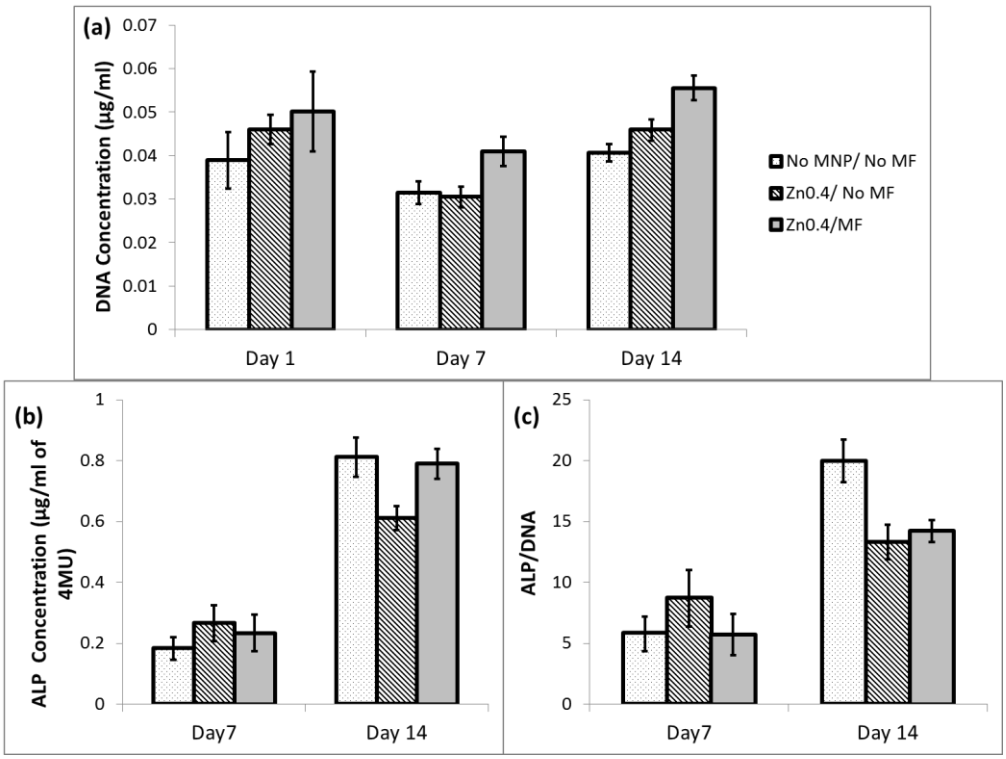

Fig 5.3.21 Effect of MNP-mediated mild HS on DNA content and ALP production of hMSCs (Experiment 04): The total DNA (a), ALP (b) and ALP/DNA (c) for hMSCs exposed to a single treatment of $Zn_{0.4}$ mediated heat stress (42^0C for 10min) on day 7 and 14. All cells were cultured in osteogenic medium. Error bars represent standard error of the mean for n=3 and no significant

difference was found between any of the groups for both measurements (One way ANOVA, $p < 0.05$).

Osteogenesis was confirmed by staining for mineralization at day 21 for the MNP-mediated heat shocked hMSCs (Fig 5.3.22).

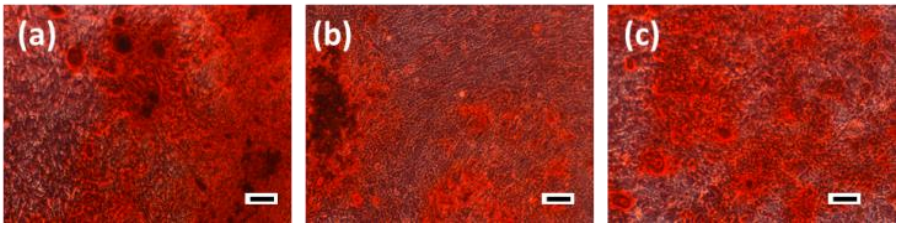

Fig 5.3.22 Mineralization of hMSCs exposed to $Zn_{0.4}$ - MNP mediated heat shock (Experiment 04): Cells were stained with alizarin red for calcium to visualize mineralization at day 21. Images show untreated cells (a), cells with MNPs not exposed (b) or exposed to an external magnetic field (c). (Scale bars correspond to 100µm)

In the next attempt (experiment 05), hMSCs were treated to heat shock for a longer duration and maintained at the target temperature of 42^0C for 30min (with the whole system kept outside the incubator for almost an hour; Fig 5.3.23). The cells appeared extremely stressed (including the controls) after treatment as observed by the shrunken appearance of the cells in the bright field images (Fig 5.3.24 a-e). This did not happen in the previous attempt (Experiment 03) and hence it is not clear why the same conditions for the controls were suddenly unfavourable to the cells. One possible explanation is that without an option for gas exchange across the air-tight bijou tubes, the pH in the media was not regulated. However, although they appeared stressed immediately after treatment, 24h later all samples had recovered (Fig 5.3.24 f-h, j), with the notable exception of the heat-shock treated cells (Fig 5.3.24i). This is probably because, while for the controls the stress levels they had endured were within levels where the damage was reversible, in the

heat-treated samples the additional thermal stress might have caused irreversible damage to the cells.

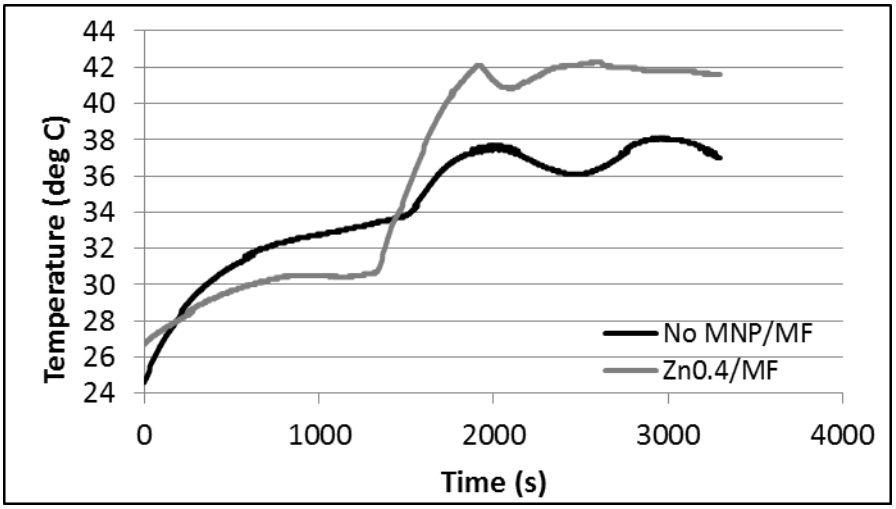

Fig 5.3.23 Temperature measurements during extracellular MNP-mediated heating of hMSCs (Experiment 05): Measurements of temperature for hMSCs on PLA films immersed in media with or without MNPs during magnetic heating. Treated cells were exposed to temperatures around 42^0C for 30min.

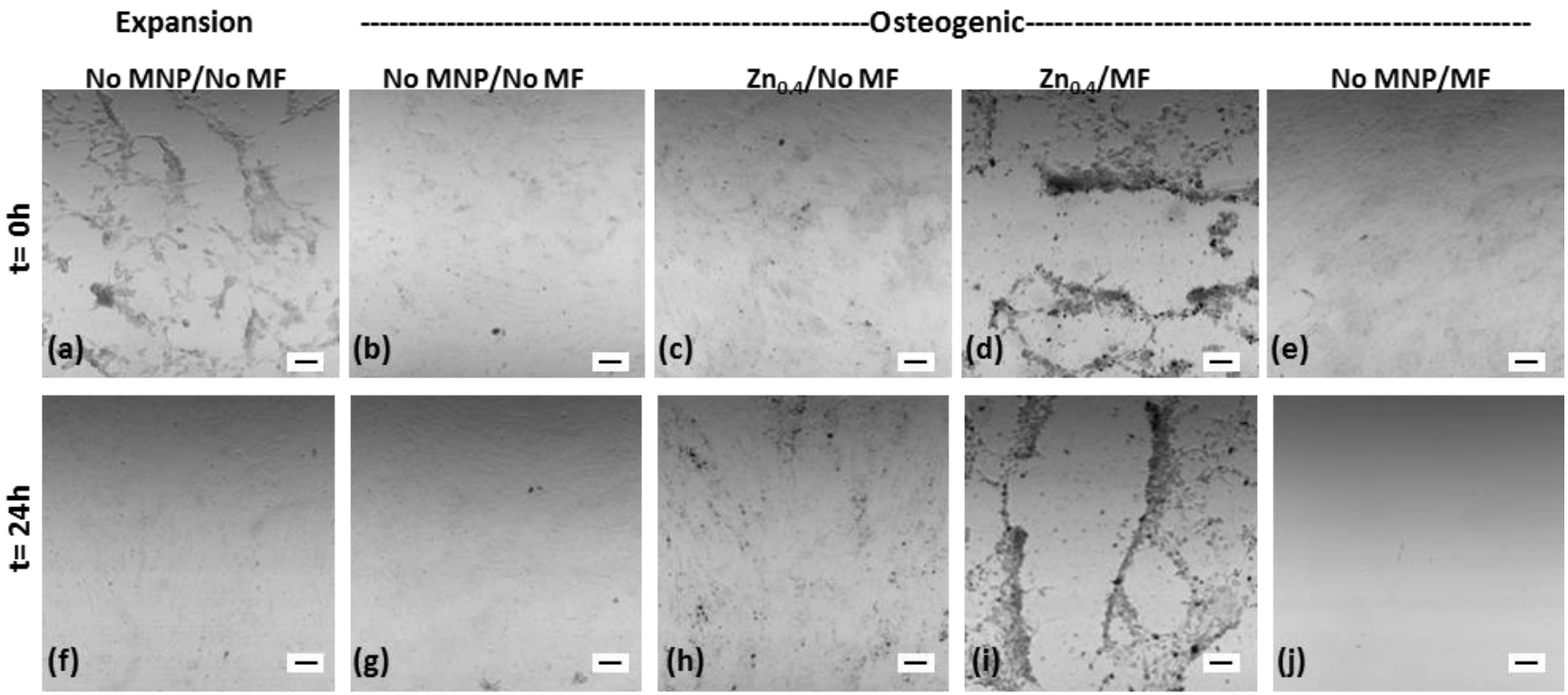

Fig 5.3.24 Effect of MNP-mediated heat treatment on morphology hMSCs (Experiment 05): Bright field images of cells immediately following MNP-mediated heat treatment (top row; t= 0h) and 24h later (bottom row; t= 24h). Immediately after the treatment (42^0C for 30min), changes in morphology indicative of cellular stress are observed. 24h following MHT cells show normal morphology and hence recovery for all conditions except for the cells with MNPs exposed to the external magnetic field. Untreated controls in expansion (a, f) and osteogenic (b, g) media, cells with MNPs not exposed (c, h) and exposed (d, i) to a magnetic field. Cells without MNPs exposed to an external magnetic field (e, j). (Scale bars correspond to 100μm)

As a method to reduce stress, the pH was regulated using CO2 independent medium. The previous experiment (Experiment 05) was repeated using the CO_2-independent medium (serum content was also increased from 10 to 20%) and the temperature measurements during treatment are shown in Fig 5.3.25. Cells were maintained at 42^0C for around 30min while the controls were kept at 37^0C.

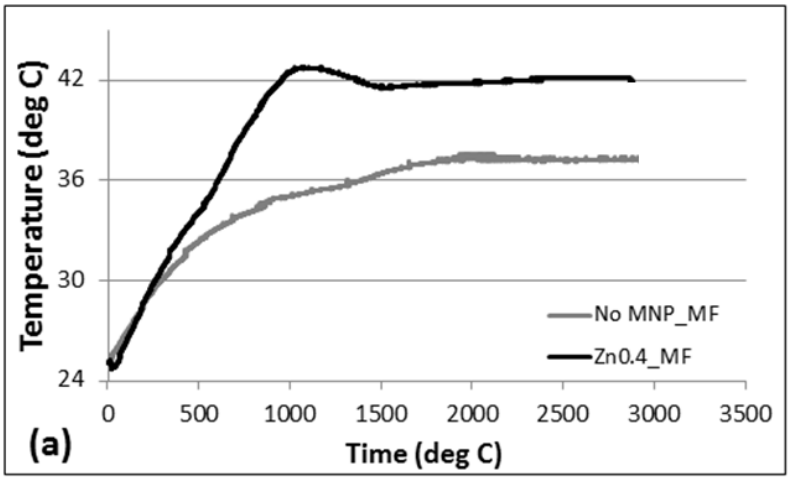

Fig 5.3.25 Temperature measurements during extracellular MNP-mediated heating of hMSCs (Experiment 06): Measurements of temperature hMSCs on PLA films were immersed in media with or without MNPs during magnetic heating. Treated cells were exposed to temperatures around 42^0C for 30min.

The control cells had healthy morphology in this experiment as observed in bright field images taken immediately and 12 days (images of cells seeded in the ECIS arrays) following a single ~1h treatment (Fig 5.3.26 a-d) . The treated cells also appear healthy at both time points. For the untreated controls in osteogenic medium some evidence of extracellular matrix deposition can be observed at day 12 (dark spots in Fig 5.3.26 g) indicating osteogenesis.

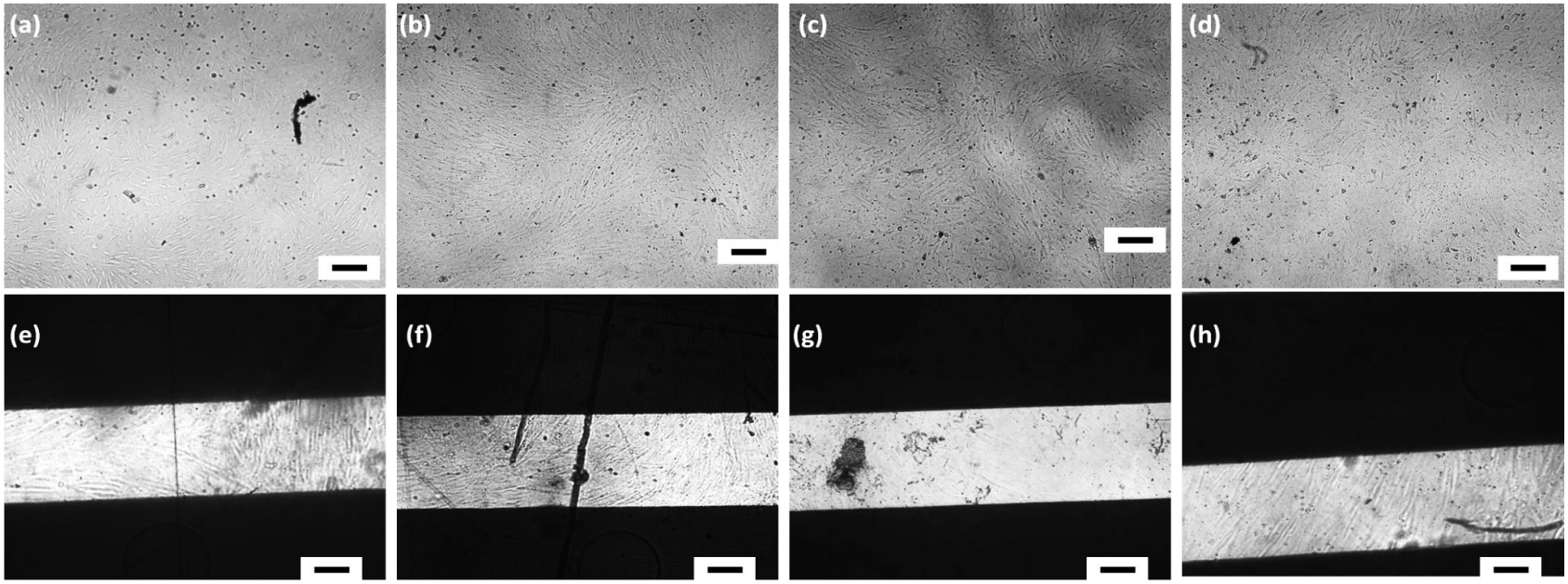

Fig 5.3.26 Effect of MNP-mediated heat shock on hMSC morphology (Experiment 06): Bright field images of hMSCs immediately following a single MNP-mediated heat treatment (42^0C for 30min; a-d) and after 12 days (e-h) following attachment to ECIS well plates. Cells exposed to $Zn_{0.4}$ -MNP mediated HS (d, h). Controls included cells not exposed to heat treatment in expansion medium (a, e), exposed to magnetic field without MNPs in expansion medium (b, f) and untreated cells in osteogenic medium (c, g). (Scale bars correspond to 200μm)

In this and later experiments, initial investigations were performed for treated cells in only one medium type (expansion medium) due to restrictions in the number of samples that could be assessed simultaneously in the ECIS instrument (maximum of 16 wells). However untreated cells in osteogenic medium were also investigated, as a positive control for osteogenesis. The impedance measurements for this experiment are shown in Fig 5.3.27. Between the untreated cells in expansion (Fig 5.3.27a) and osteogenic media (Fig 5.3.27b) a clear difference was observed with the impedance of the cells in osteogenic medium increasing. On the other hand for the rest of the samples including the controls (Fig 5.3.27 c, d) and the heat shock treated sample (Fig 5.3.27 e), while some samples appeared to be the proliferating cells others had higher impedance suggesting onset of osteogenesis. With such a low number of replicates, nothing conclusive could be drawn from the ECIS results of these samples.

The DNA, total ALP and ALP/cell measured on day 21 (when the ECIS measurement was terminated) are shown in Fig 5.3.28. Cell numbers, as shown by the DNA content are not significantly different between the controls and the treated sample (Fig 5.3.28a), showing that the cells eventually recovered from any stress during the experiment. The total ALP and ALP/cell content (normalized to DNA content) are higher for cells in the osteogenic medium confirming onset of differentiation. The total ALP (Fig 5.3.28b) and ALP/cell (Fig 5.3.28c) for the treated samples were not different to the expansion controls implying that the treatment did not affect ALP production and hence osteogenesis.

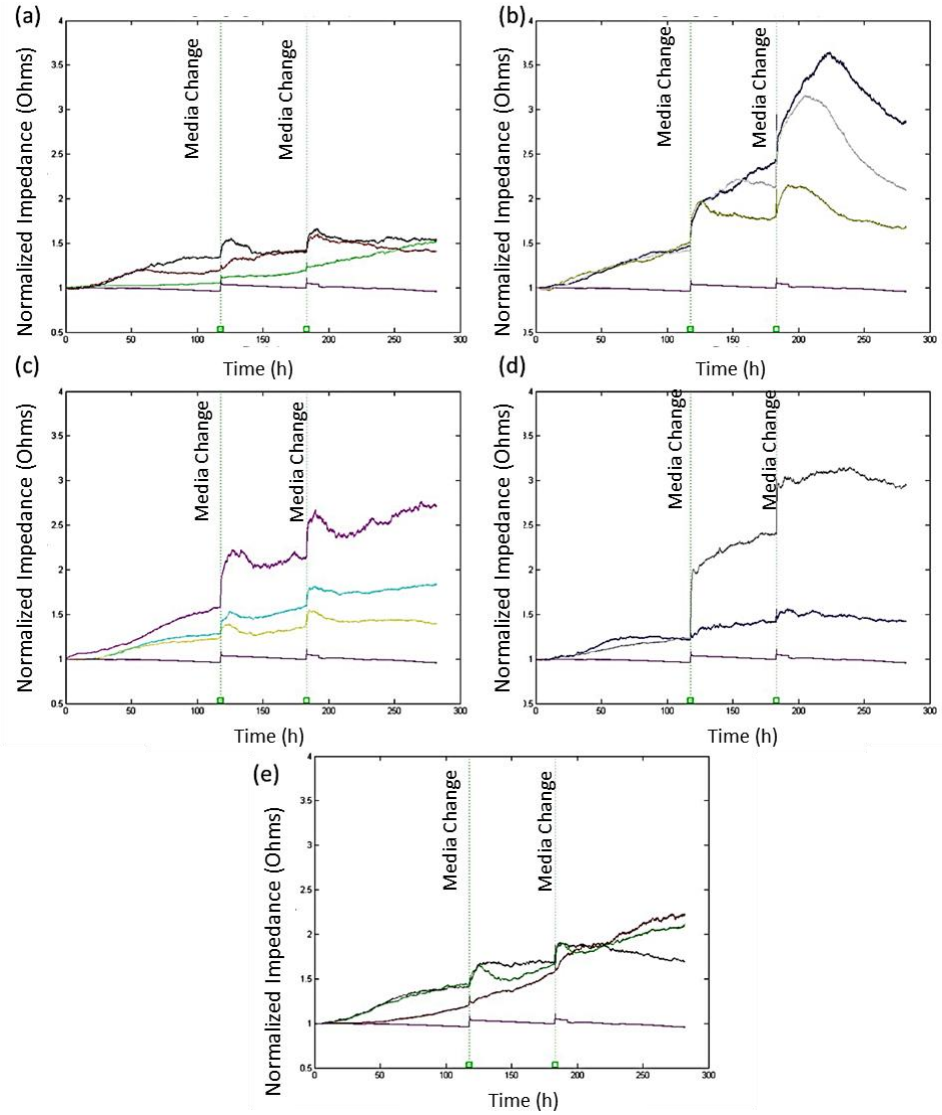

Fig 5.3.27 ECIS measurements showing the effect of MNP-mediated heat shock on hMSCs (Experiment 06: 42^0C for 30min): Impedance measurements for cells exposed to $Zn_{0.4}$ mediated extracellular HS are shown as individual replicates and compared to the control samples in the experiment. All cells were cultured in expansion medium except the osteogenic control. Graphs show untreated cells in expansion (a) and osteogenic media (b), cells exposed to magnetic field in the absence of MNPs (c), cells in the presence of $Zn_{0.4}$ not exposed to magnetic field (d), and cells exposed to magnetic field (single 1h treatment) in the presence of MNPs (e). Green dashed lines indicate points where the measurement was pauses for media change.

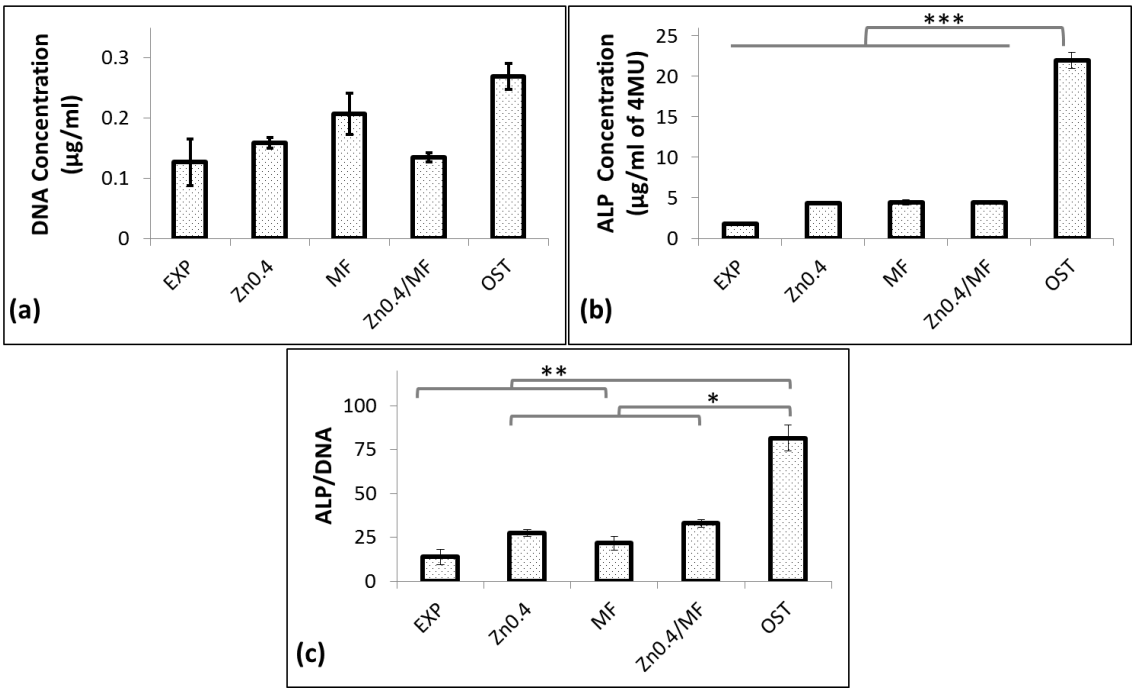

Fig 5.3.28 Effect of MNP-mediated mild HS on DNA content and ALP production of hMSCs (Experiment 06): Total DNA content (a), total ALP expression (b) and the ALP/ cell (Normalized to DNA content; c) of hMSCs 14 days after exposure to mild heat shock (42^{0}C for 30min; EXP: Untreated cells in expansion medium; Zn0.4: Cells with MNPs without field; MF: Cells without MNPs exposed to magnetic field; Zn0.4/M: Cells exposed to magnetic field in the presence of $Zn_{0.4}$ MNPs and OST: untreated cells in osteogenic medium). Error bars represent standard error of the mean for n=3 and line over columns indicates groups that were significantly different from each other (One way ANOVA, p< 0.05)

As only a maximum of 16 wells can be read at any one point in the ECIS system, to increase the replicates (from n=3 to 5), two of the controls were not included in the next experiment (Experiment 07). In this experiment, the same treatment to the previous one was carried out. However in this case the temperature of the treated samples was maintained at 42^{0}C for 60min (Fig 5.3.29). The temperature was not monitored for the controls but they were kept in the incubator and so were maintained at 37^{0}C (usually the temperature for the control kept in the magnetic hyperthermia instrument is measured to ensure it is at 37^{0}C but this control was not present for the current experiment). The morphology of the cells appear healthy for all samples immediately after treatment

(Fig5.3.30 a, d g). By day 13, extensive mineralization (dark regions in Fig 5.3.30 e, f) was observed in the osteogenic controls while the treated (Fig 5.3.30 b, c) and untreated cells (Fig 5.3.30 h, i) in expansion medium appear clear without any deposits.

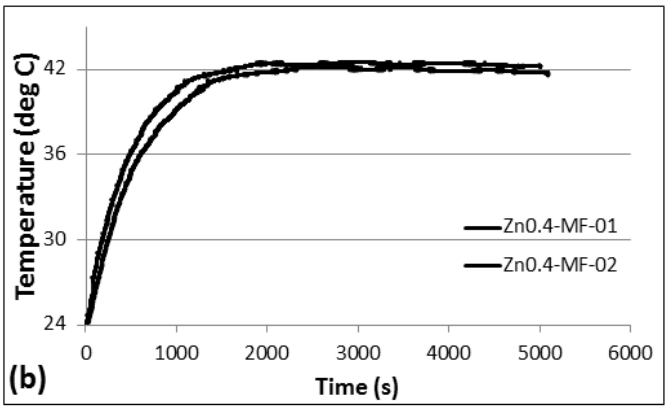

Fig 5.3.29 Temperature measurement during extracellular MNP-mediated heating of hMSCs (Experiment 07): Measurements of temperature on two different runs is shown. hMSCs on PLA films were immersed in medium with MNPs and exposed to an external magnetic field (362kHz, ~32V). Treated cells were exposed to temperatures around 42^0C for 60min while untreated controls were kept in the incubator at 37^0C.

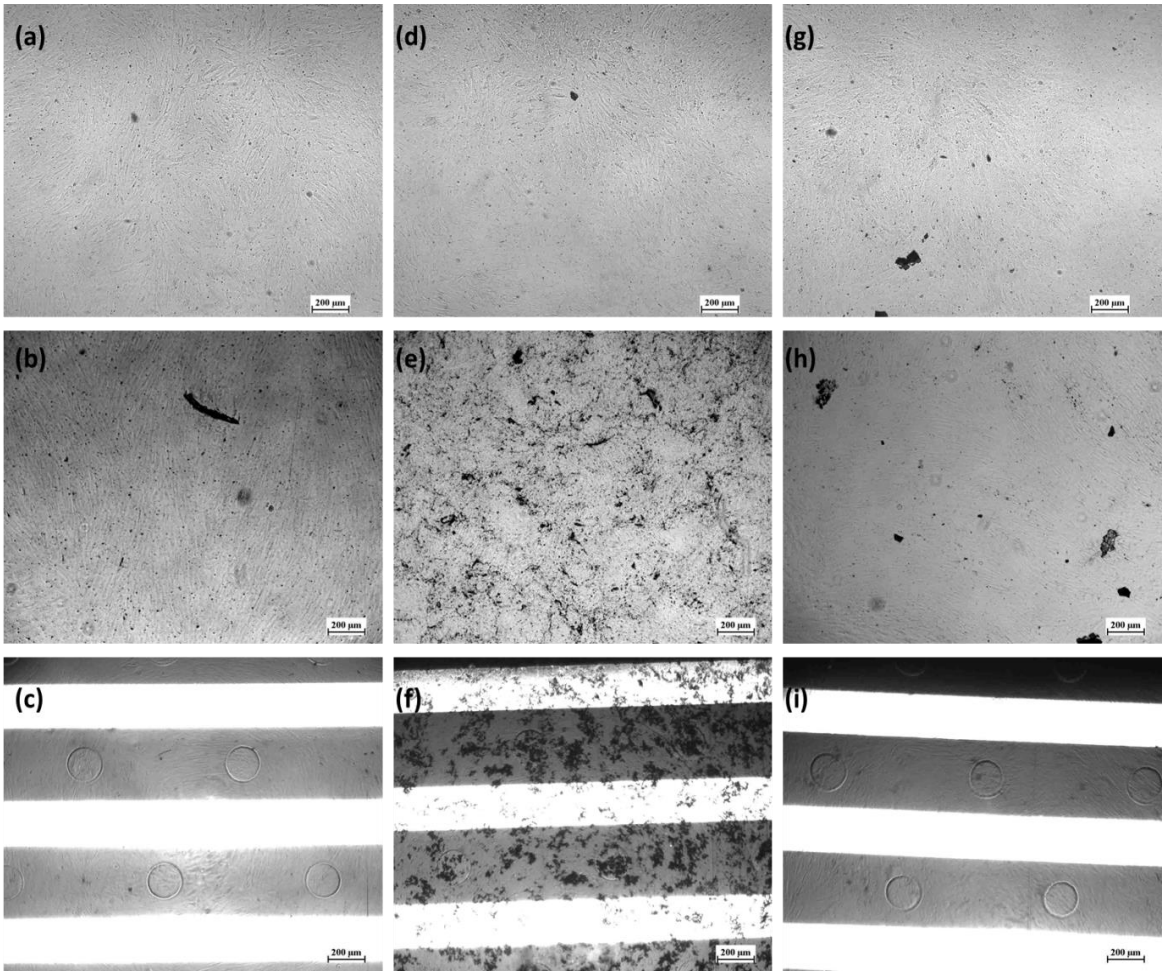

Fig 5.3.30 Effect of MNP-mediated heat shock hMSC morphology (Experiment 07): Bright field images of hMSCs immediately following a single MNP-mediated heat treatment (42^0C for 60min; a-c) and after 13 days on PLA films (b, e, h) and in the ECIS array (c, f, i) cultured in expansion medium following attachment to ECIS well plates. The controls included cells not exposed to the external field cultured in expansion (a-c) and osteogenic media (d-f). (Scale bars correspond to 200µm)

The impedance measurements for the average of the replicates (Fig 5.3.31a) and for randomly coupled individual well for each group (Fig 5.3.31 b, c, d) are shown. The impedance for the cells in osteogenic medium was lower than for those in expansion medium. This is in contrast to all the previous measurements. Also the oscillations in the signal were lower for cells in osteogenic medium compared to the cells in expansion medium. This could probably be explained by the unusually early deposition of extracellular matrix in the differentiating wells (Fig 5.3.31 e, f). The reduction in the oscillation could possibly be because of decreased micromotion of cells which might have been caused by the presence of the extracellular matrix deposited around the cells. In terms of the trend of the impedance, the heat-shock treated cells appear very similar to cells in expansion medium indicating that the treatment did not induce significant differentiation-related morphology changes. However the absolute impedance appears slightly higher in the heat treated cells compared to the controls in expansion medium (Fig. 5.3.31 b-d).

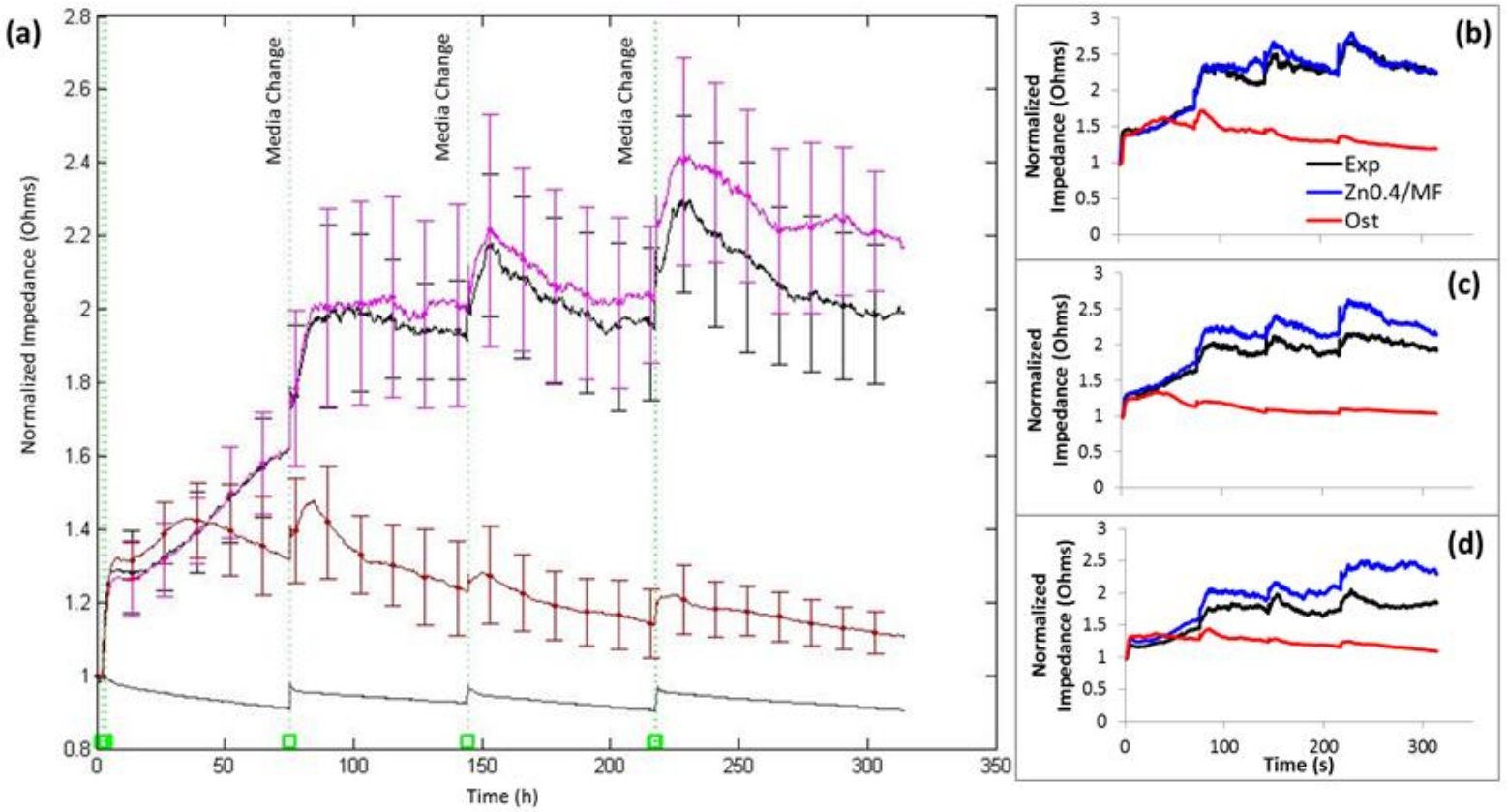

Fig 5.3.31 ECIS measurements showing the effect of MNP-mediated HS on cellular behaviour (Experiment 07): Average impedance measurements of untreated hMSCs cultured in expansion and osteogenic media compared to cells exposed to $Zn_{0.4}$ mediated HS (42^0C for 60min) cultured in expansion medium (a). To highlight the difference in the trend of cells in expansion to osteogenic media, wells were randomly coupled and their individual impedance measurements are plotted in b, c and d.

The total DNA content was similar between the untreated controls in the two media types and the treated sample (Fig 5.3.32a) indicating no long term loss in viability of the cells with mild heat shock. The total ALP value at day 21 (when the experiment was terminated) was significantly higher for the cells in osteogenic medium (Fig 5.3.32b). The less pronounced enhancement in ALP in this experiment compared with previous time points is not surprising as ALP is an early marker and its production starts decreasing with onset of mineralization. There was no difference in the total ALP between the untreated cells in expansion and osteogenic media as well as the treated sample (Fig 5.3.32c). Therefore, in summary, no clear evidence for a positive effect of MNP-mediated extracellular heat shock on osteogenic differentiation of hMSCs was found.

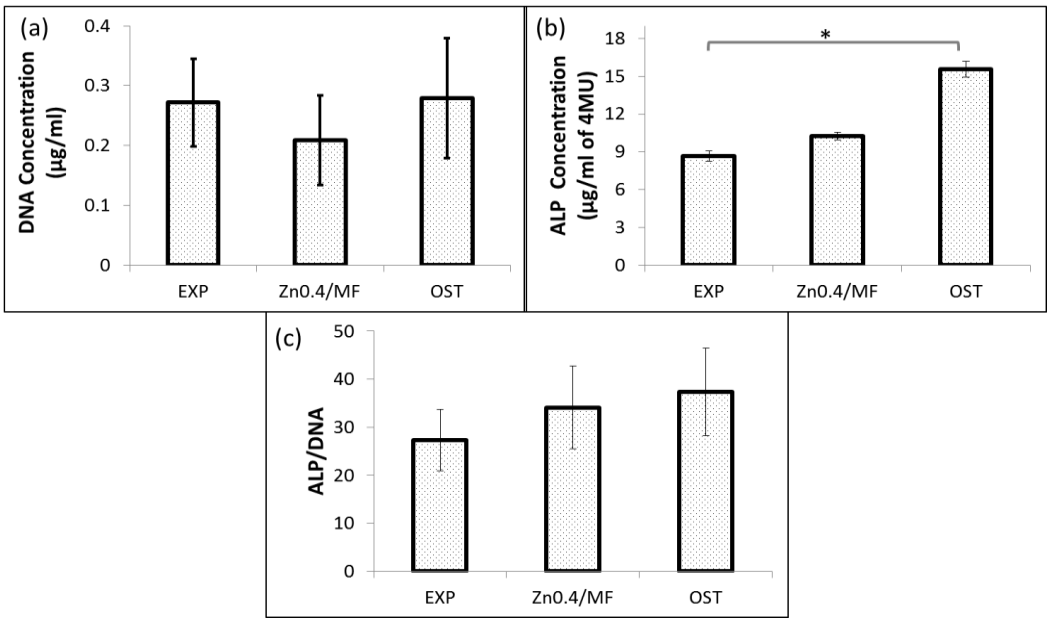

Fig 5.3.32 Effect of MNP-mediated HS on DNA content and ALP production of hMSCs (Experiment 07): The total DNA (a) , total ALP (b) and ALP/cell (c) content of hMSCs exposed to a single MNP-mediated HS treatment for ~1h (42^0C) after 21 days.(One way ANOVA, $p<0.05$)

5.4 Discussion

The MNPs best suited for the purpose of applying heat shock to cells were identified by comparing their heating powers. The zinc doped biogenic MNPs which were found to be promising for cellular applications (see Chapter 3) showed a strong heating power (SLP) in glycerol, a system that mimics the cellular conditions for the MNPs. With their strong Néel relaxation component they had a strong heating response as only this relaxation mechanism persists in cells. The field conditions, especially the frequency needs to match the MNP and for the zinc-doped MNPs under investigation the optimum field conditions to obtain maximum heating fell near clinically relevant limits (Clinical limit[103,104] is 5×10^9 $Am^{-1}s^{-1}$ and field conditions in this study gives 8.5×10^9 $Am^{-1}s^{-1}$ (for 362kHz and 29.4mT), which is only just larger than the clinical limit. This is encouraging as they could be potentially used for *in vivo* heating (hyperthermia) applications.

Experimental approaches for targeting different regions of the cells to understand the mechanism of heat shock were successfully developed. Cells were heated (1) intracellularly, (2) extracellularly in a fashion similar to bulk heating. Preliminary work for targeting the plasma membrane was performed. For this purpose, the citric acid coated MNPs were functionalized with the RGD peptide. Similar binding methodology for other ligands can be developed to target heat sensitive-ion channels. The MNPs also showed strong heating in cell-culture medium which is promising for applying severe heat shock to cells if necessary. Also, the extracellular heating approach is especially advantageous compared to bulk heating for *in vivo* applications where more localized temperature rise can be achieved by injecting and targeting MNPs with an external field to the region of

interest. This is already being exploited for magnetic hyperthermia –based *in vivo* cancer therapies.[185,198]

The MNP-mediated mild extracellular heat shock (similar to the bulk heat shock) caused a minor but not significant increase in the total ALP of treated hMSCs in expansion medium (Fig 5.3.32 and Fig 5.3.36) compared to untreated cells in expansion medium. This effect had also been observed in the bulk heat shock treatment (Fig 4.3.5). Because ALP is a temporal process and these time point assays could be missing crucial and subtle changes in cells with minor treatments as a single heat shock, the ECIS technique for continuous monitoring was adopted. The technique proved extremely suitable for assessing osteogenesis, but the presence of the metallic electrodes in the ECIS arrays prevented in-situ application of the AC fields required for magnetic hyperthermia treatments. Thus it was necessary to introduce additional cell culturing procedures using transportable PLA films. Unfortunately this was found to increase stress levels to the cells. Although methods were found to maintain cell viability despite these additional stresses, inevitably these effects increased variability between the different cells and treatment conditions, which may have masked subtle changes due to the MNP-mediated heat shock. In addition, it was necessary to provide only single heat shock treatments in order to avoid multiple trypsinization steps which in themselves can be an additional stress factor.

Only preliminary proof-of-concept experiments were performed for investigating the effect of intracellular heat shock on osteogenesis. These experiments did not show much evidence of a positive effect. In the case of the intracellular heating, this could probably be because of the localization of MNPs within the cells. Being tightly packed within lysosomes, the dissipation might not have reached the cellular temperature-sensory mechanism. Recent theories suggests that when MNPs are closely packed their individual

stray magnetic fields can interact with each other which can increase or decrease the overall heating efficiency provided by the external magnetic field.[199,200] The methodology developed in this work can help pave way to future experiments investigating the hypothesis in more detail.

5.5 Conclusions

Different bacterially synthesized MNPs were assessed in terms of their magnetic and heating properties to identify the best candidates for cellular heating. The zinc -doped MNPs that have a strong Néel relaxation contribution also showed the strongest heating effect under the conditions tested. Following this, to apply heat to the cells using these particles three strategies were successfully defined, each one targeting a different region of the cell. Using the MNPs the cells were heated either extracellularly (i.e. a localised version of the bulk heating discussed in Chapter 4 but with heat generation occurring in the vicinity of the cells), and intracellularly where the MNPs were localized within lysosomes. To measure the effect of this heating on osteogenic differentiation behaviour of the cells, in addition to the ALP assay, another continuous monitoring non-invasive technique known as ECIS was adopted.

The effect of extracellular MNP-mediated heat shock as measured via ECIS and changes in ALP production did not show any significant evidence for onset of osteogenic differentiation in hMSCs. The treatment temperatures and durations were similar to the bulk heat shock experiments and these studies taken together suggest that there is little proof for the effect of mild heat shock (up to 42^0C) on osteogenic differentiation of cells. Further work looking at the effect of more severe MNP-mediated heat shock, both

extracellularly and especially using membrane-targeted heat shock, could provide further insight into the applicability of heat as a stimulus for osteogenic differentiation.

CHAPTER 6 Conclusions and future work

The hypothesis that exposing cells to elevated temperatures can affect their cellular behaviour was addressed in this thesis. The first set of experiments aimed at testing this hypothesis adopted methods that had proven successful in published literature.[43,44,46,47] However in the work of this thesis, improvements in the experimental design such as the duration of treatment, frequency and the magnitude of temperature rise (mild and severe heat shock) showed that mild heat shock had a minor effect on viability as well as osteogenic differentiation for both human mesenchymal (bone marrow derived) primary stem cells (hMSCs) and MG-63 cancerous cells (human bone cancer cell line). Surprisingly, repeated exposures to higher temperatures (> greater than 50^0C) showed a strong positive effect on the upregulation of the osteogenic marker, ALP, when considered on a per cell basis, but an equally negative effect on viability in both cell types.

Extending this work beyond bulk heating methods, it was aimed to use magnetic nanoparticles to provide a more localised application of the heat stress. The suitability of bacterially synthesized zinc and cobalt doped iron oxide MNPs for cellular applications was assessed. These MNPs were coated with citric acid and tested for cytotoxicity. It was found that all the biogenic magnetite nanoparticles showed minimal cytotoxicity *in vitro* in both hMSCs and MG-63 cells after 72h of exposure. This was true except for the MNP with the highest levels of zinc: $Zn_{0.9}$. This issue can be addressed by testing various types of coating materials, especially polymers that form a more stable and thicker surface coating on the MNPs and will therefore reduce the interaction of the metallic core with the surroundings. In any case the high-content Zn doped MNPs had less useful magnetic properties and were not required for the heating experiments. The biogenic MNPs were also found not to interfere with the osteogenic differentiation of hMSCs. These results

strongly suggest the biocompatible nature of these biogenic doped magnetite based particles for *in vitro* applications.

Assessing the interaction of the MNPs with cells showed that a short incubation period (up to 3h) of cells with MNPs with or without RGD functionalization (targeting membrane integrin receptors) showed strong membrane binding. On the other hand, by 24h the nanoparticles were endocytosed and localized in the peri-nuclear region. Consistent with this uptake mechanism, the magnetic behaviour of the MNPs was also found to be different when associated with cells. Magnetization relaxation measurements using a novel application of AC magnetic susceptibility showed that the nanoparticles were immobilized once associated with cells and hence lost their Brownian relaxation component, while the Néel relaxation was not affected. The zinc-doped MNPs, which have a strong Néel relaxation component, showed a strong heating response under both mobile (water suspensions) and immobile (glycerol suspensions) conditions. As the latter mimics cellular conditions, these nanoparticles were the candidate of choice for cellular heating experiments.

Following the characterization of the interaction between cells and MNPs, the effect of MNP-mediated heating on cells was assessed. Different strategies for providing either extracellular heat shock, or heating the cells intracellularly were developed and tested in hMSCs and MG-63 cells. To measure the effect of this heating on osteogenic differentiation behaviour of the cells, ALP expression at specific time points and continuous impedance (ECIS) measurements were performed. The impedance measurements proved suitable for detecting osteogenic differentiation through associated changes in cellular morphology, and were especially effective in hMSCs. However the experiments with extracellular MNP-mediated heat shock did not show any evidence for

the onset of osteogenic differentiation in hMSCs. This extracellular treatment *in* vitro is similar to the bulk-heat shock treatment and the experimental results from both indicate that elevating the temperature of the medium to around 42^0C might not be effective to affect differentiation.

Further work in case of intracellular heating and also investigating membrane heating are necessary to confirm the best method to heat shock cells and the role of heat-sensitive ion channels (membrane heating) in improving differentiation. Cells could be transfected to express modified heat sensitive ion channels that express a binding domain for a specific ligand. By functionalizing the MNPs with these ligands, they could be targeted to the receptor[201] for selective activation. Also, the role of heat shock proteins can be investigated by stimulating their expression thermally and non-thermally (chemical inducer) and co-relating the effect on differentiation-related gene and protein expression profiles.

An important aspect that the approach in this work addressed is the measurement of the actual temperature in the wells containing cells, which showed disparities with the target temperature. Being such a crucial factor, heat shock experiments need to measure the temperatures cells experience as accurately as possible. For a bulk heating method or for nanoparticle mediated extracellular heating, simply immersing a probe into the medium within the wells as implemented in this work, can give a good measurement of the temperatures. On the other hand, it is more challenging in the case of localized heating at subcellular scales, as in the case of lysosomal heating after nanoparticle internalization or plasma membrane heating by targeting nanoparticles to membrane receptors. The dependence of the fluorescent intensity of certain fluorophores can be exploited to give information about the heating. The concept was demonstrated in the work by Huang *et al.*[140] where fluorescently tagged nanoparticles targeted to the plasma membrane were

exposed to an external magnetic field. When the field was switched on, the heat dissipated by the particle decreased the fluorescent intensity of the fluorophore bound to the nanoparticle (observed via fluorescence microscopy).

One of the biggest limitations of the bulk heat shock studies in this work are the sole dependence of measuring osteogenesis through ALP expression. A temporal process being studied discontinuously might not be the most sensitive method of detecting changes, especially subtle ones. Protein and gene expression in general are temporal events and the only way to confidently identify a difference is by using large number of time points. As different temperature exposure profiles need to be assessed (magnitude, duration, frequency) using other traditional assays such as PCR, ELISA or western blotting for protein and gene expression will be extremely time-consuming and expensive.

This issue was addressed in later experiments (magnetic nanoparticle-mediated heating) by adopting a continuous monitoring of cell impedance using ECIS: a technique that proved suitable for detecting osteogenesis. The ECIS technique measures impedance values continuously to provide a wealth of information about the viability and behaviour of cells. For bulk heating, it is possible to perform *in situ* impedance measurements during the heat shock treatment. Although the impedance is temperature dependant, this can be corrected for in the experimental methodology.

It is more challenging to extend *in situ* ECIS measurements to magnetic nanoparticle based heating. The metallic components of the base of the ECIS instrument and of the array (gold electrodes) will consequently be heated up in an external magnetic field. Hence for studies involving repeated magnetic hyperthermia treatments, cells may need to be reseeded after every treatment leading to additional stresses which is thus not ideal. However, other non-

invasive methods could be adopted. One example is detecting changes in morphology using two-photon microscopic imaging[65] where the images can be further processed to obtain quantitative data. This method again is not continuous but is non-invasive as well as suitable for the magnetic heating process.

In addition to the above, the recent technology of fluorescent probes that can detect RNA and protein expression in real time (SmartlfareTM, Merck Millipore) would provide a quicker and more accurate pre-screening approach for determining optimum temperature range for a positive response. By targeting the probes to RNA transcription of osteogenic or other differentiation marker genes and as well as heat shock factors (transcription factors for HSPs),[36,202] where the translocation of the latter can be monitored as well, further insights into the intracellular processes involved with the influence of heat shock can be dissected.

In conclusion, this thesis delivers insights on the role of temperature in determining osteogenic differentiation behaviour of primary stem cells and a cancerous cell line. It provides a methodology for using magnetic nanoparticle mediated heating for investigating the effect of temperature in a more systematic manner by identifying ideal MNP types, methods to deliver them to the region of interest within the cells and conditions to generate the desired heating. Based on the recommendations for future work, the role of temperature in defining the ideal stem cell niche can be answered.

REFERENCES

1. Buckminster Fuller, R. *Operating manual for spaceship earth*. (1969). doi:10.2307/812959

2. Smith, A. A glossary for stem-cell biology. *Nature* **441,** 1060–1060 (2006).

3. Toma, J. G. *et al.* Isolation of multipotent adult stem cells from the dermis of mammalian skin. *Nat. Cell Biol.* **3,** 778–784 (2001).

4. Friedenstein, A. J., Gorskaja, J. F. & Kulagina, N. N. Fibroblast precursors in normal and irradiated mouse hematopoietic organs. *Exp. Hematol.* **4,** 267–74 (1976).

5. Zuk, P. A. *et al.* Human adipose tissue is a source of multipotent stem cells. *Mol. Biol. Cell* **13,** 4279–95 (2002).

6. Johansson, C. B., Svensson, M., Wallstedt, L., Janson, A. M. & Frisén, J. Neural Stem Cells in the Adult Human Brain. *Exp. Cell Res.* **253,** 733–736 (1999).

7. Huang, G. T.-J., Gronthos, S. & Shi, S. Mesenchymal stem cells derived from dental tissues vs. those from other sources: their biology and role in regenerative medicine. *J. Dent. Res.* **88,** 792–806 (2009).

8. Fraser, J. K., Wulur, I., Alfonso, Z. & Hedrick, M. H. Fat tissue: an underappreciated source of stem cells for biotechnology. *Trends Biotechnol.* **24,** 150–4 (2006).

9. Pittenger, M. F. Multilineage Potential of Adult Human Mesenchymal Stem Cells. *Science (80-.).* **284,** 143–147 (1999).

10. Wei, X. *et al.* Mesenchymal stem cells: a new trend for cell therapy. *Acta Pharmacol. Sin.* **34,** 747–54 (2013).

11. Wang, S., Qu, X. & Zhao, R. C. Clinical applications of mesenchymal stem cells. *J. Hematol. Oncol.* **5,** 19 (2012).

12. Fehrer, C. & Lepperdinger, G. Mesenchymal stem cell aging. *Exp. Gerontol.* **40,** 926–30 (2005).

13. Jaiswal, N., Haynesworth, S. E., Caplan, a I. & Bruder, S. P. Osteogenic differentiation of purified, culture-expanded human mesenchymal stem cells in vitro. *J. Cell. Biochem.* **64,** 295–312 (1997).

14. Solchaga, L. A., Penick, K. J. & Welter, J. F. Chondrogenic differentiation of bone marrow-derived mesenchymal stem cells: tips and tricks. *Methods Mol. Biol.* **698,** 253–78 (2011).

15. Fink, T. & Zachar, V. Adipogenic differentiation of human mesenchymal stem cells. *Methods Mol. Biol.* **698,** 243–51 (2011).

16. Murphy, C. M., Matsiko, A., Haugh, M. G., Gleeson, J. P. & O'Brien, F. J. Mesenchymal stem cell fate is regulated by the composition and mechanical properties of collagen-glycosaminoglycan scaffolds. *J. Mech. Behav. Biomed. Mater.* **11,** 53–62 (2012).

17. Sun, Y., Chen, C. S. & Fu, J. Forcing stem cells to behave: a biophysical perspective of the cellular microenvironment. *Annu. Rev. Biophys.* **41,** 519–42 (2012).

18. Wang, L. D. & Wagers, A. J. Dynamic niches in the origination and differentiation of haematopoietic stem cells. *Nat. Rev. Mol. Cell Biol.* **12,** 643–55 (2011).

19. Guilak, F. *et al.* Control of stem cell fate by physical interactions with the extracellular matrix. *Cell Stem Cell* **5,** 17–26 (2009).

20. Davies, P. F., Remuzzi, A., Gordon, E. J., Dewey, C. F. & Gimbrone, M. A. Turbulent fluid shear stress induces vascular endothelial cell turnover in vitro. *Proc. Natl. Acad. Sci. U. S. A.* **83,** 2114–7 (1986).

21. Kannan, R. Y., Salacinski, H. J., Sales, K., Butler, P. & Seifalian, A. M. The roles of tissue engineering and vascularisation in the development of micro-vascular networks: a review. *Biomaterials* **26,** 1857–75 (2005).

22. Han, Y., Cowin, S. C., Schaffler, M. B. & Weinbaum, S. Mechanotransduction and strain amplification in osteocyte cell processes. *Proc. Natl. Acad. Sci. U. S. A.* **101,** 16689–94 (2004).

23. Weinbaum, S., Cowin, S. C. & Zeng, Y. A model for the excitation of osteocytes by mechanical loading-induced bone fluid shear stresses. *J. Biomech.* **27,** 339–360 (1994).

24. Cohen, D. M. & Chen, C. S. Mechanical control of stem cell differentiation. (2008). at <http://www.ncbi.nlm.nih.gov/books/NBK27063/>

25. Sachs, F. Stretch-Activated Ion Channels: What Are They? *Physiology* **25,** 50–56 (2010).

26. Hamill, O. P. & Martinac, B. Molecular basis of mechanotransduction in living cells. *Physiol. Rev.* **81,** 685–740 (2001).

27. Chen, C. S. & Ingber, D. E. Tensegrity and mechanoregulation: from skeleton to cytoskeleton. *Osteoarthritis Cartilage* **7,** 81–94 (1999).

28. Lu, Z., Roohani-Esfahani, S.-I., Wang, G. & Zreiqat, H. Bone biomimetic microenvironment induces osteogenic differentiation of adipose tissue-derived mesenchymal stem cells. *Nanomedicine* **8,** 507–15 (2012).

29. Lu, Z., Roohani-Esfahani, S.-I. & Zreiqat, H. Mimicking bone microenvironment for directing adipose tissue-derived mesenchymal stem cells into osteogenic differentiation. *Methods Mol. Biol.* **1202,** 161–71 (2014).

30. Wagers, A. J. The stem cell niche in regenerative medicine. *Cell Stem Cell* **10,** 362–9 (2012).

31. Mauney, J. R. *et al.* Mechanical stimulation promotes osteogenic differentiation of human bone marrow stromal cells on 3-D partially demineralized bone scaffolds in vitro. *Calcif. Tissue Int.* **74,** 458–68 (2004).

32. Heng, B. C., Haider, H. K., Sim, E. K.-W., Cao, T. & Ng, S. C. Strategies for directing the differentiation of stem cells into the cardiomyogenic lineage in vitro. *Cardiovasc. Res.* **62,** 34–42 (2004).

33. Guan, M. *et al.* Directing mesenchymal stem cells to bone to augment bone formation and increase bone mass. *Nat. Med.* **18,** 456–62 (2012).

34. Puscheck, E. E., Awonuga, A. O., Yang, Y., Jiang, Z. & Rappolee, D. A. Molecular biology of the stress response in the early embryo and its stem cells. *Adv. Exp. Med. Biol.* **843,** 77–128 (2015).

35. Mansouri, L., Xie, Y. & Rappolee, D. A. Adaptive and Pathogenic Responses to Stress by Stem Cells during Development. *Cells* **1,** 1197–224 (2012).

36. Byun, K. *et al.* Heat shock instructs hESCs to exit from the self-renewal program through negative regulation of OCT4 by SAPK/JNK and HSF1 pathway. *Stem Cell Res.* **11,** 1323–34 (2013).

37. Prinsloo, E., Setati, M. M., Longshaw, V. M. & Blatch, G. L. Chaperoning stem cells: a role for heat shock proteins in the modulation of stem cell self-renewal and differentiation? *Bioessays* **31,** 370–7 (2009).

38. Yao, S. *et al.* Proliferation of dental follicle-derived cell populations in heat-stress conditions. *Cell Prolif.* **44,** 486–93 (2011).

39. Saretzki, G., Armstrong, L., Leake, A., Lako, M. & von Zglinicki, T. Stress defense in murine embryonic stem cells is superior to that of various differentiated murine cells. *Stem Cells* **22,** 962–71 (2004).

40. Arai, F. & Suda, T. *Quiescent stem cells in the niche. Stembook [Internet] Cambridge (MA): Harvard Stem Cell Institute* (2008). at <http://www.ncbi.nlm.nih.gov/pubmed/20614597>

41. Li, L. & Clevers, H. Coexistence of quiescent and active adult stem cells in mammals. *Science* **327,** 542–5 (2010).

42. Cheshier, S. H., Morrison, S. J., Liao, X. & Weissman, I. L. In vivo proliferation and cell cycle kinetics of long-term self-renewing hematopoietic stem cells. *Proc. Natl. Acad. Sci. U. S. A.* **96,** 3120–5 (1999).

43. Choudhery, M. S., Badowski, M., Muise, A. & Harris, D. T. Effect of mild heat stress on the proliferative and differentiative ability of human mesenchymal stromal cells. *Cytotherapy* **17,** 359–68 (2015).

44. Shui, C. & Scutt, A. Mild heat shock induces proliferation, alkaline phosphatase activity, and mineralization in human bone marrow stromal cells and Mg-63 cells in vitro. *J. Bone Miner. Res.* **16,** 731–41 (2001).

45. Chen, J. *et al.* Enhanced osteogenesis of human mesenchymal stem cells by periodic heat shock in self-assembling peptide hydrogel. *Tissue Eng. Part A* **19,** 716–28 (2013).

46. Chen, J., Li, C. & Wang, S. Periodic heat shock accelerated the chondrogenic differentiation of human mesenchymal stem cells in pellet culture. *PLoS One* **9,** e91561 (2014).

47. Nørgaard, R., Kassem, M. & Rattan, S. I. S. Heat shock-induced enhancement of osteoblastic differentiation of hTERT-immortalized mesenchymal stem cells. *Ann. N. Y. Acad. Sci.* **1067,** 443–7 (2006).

48. Kim, Y. H., Yoon, D. S., Kim, H. O. & Lee, J. W. Characterization of different subpopulations from bone marrow-derived mesenchymal stromal cells by alkaline phosphatase expression. *Stem Cells Dev.* **21,** 2958–68 (2012).

49. Štefková, K., Procházková, J. & Pacherník, J. Alkaline phosphatase in stem cells. *Stem Cells International* **Article ID,** 11 pages (2015).

50. Golub, E. E. & Boesze-Battaglia, K. The role of alkaline phosphatase in mineralization. *Curr. Opin. Orthop.* **18,** 444–448 (2007).

51. Flanders, K. C., Winokur, T. S., Holder, M. G. & Sporn, M. B. Hyperthermia induces expression of transforming growth factor-beta s in rat cardiac cells in vitro and in vivo. *J. Clin. Invest.* **92,** 404–10 (1993).

52. Goumans, M.-J. *et al.* TGF-beta1 induces efficient differentiation of human cardiomyocyte progenitor cells into functional cardiomyocytes in vitro. *Stem Cell Res.* **1,** 138–49 (2007).

53. Zhang, M. *et al.* Cardiomyocyte grafting for cardiac repair: graft cell death and anti-death strategies. *J. Mol. Cell. Cardiol.* **33,** 907–21 (2001).

54. Suzuki, K. *et al.* Heat shock treatment enhances graft cell survival in skeletal myoblast transplantation to the heart. *Circulation* **102,** III216–21 (2000).

55. Lindquist, S. The heat-shock response. *Annu. Rev. Biochem.* **55,** 1151–91 (1986).

56. Ritossa, F. A new puffing pattern induced by temperature shock and DNP in drosophila. *Experientia* **18,** 571–573 (1962).

57. Lindquist, S. Translational efficiency of heat-induced messages in Drosophila melanogaster cells. *J. Mol. Biol.* **137,** 151–8 (1980).

58. Berendes, H. D. Factors involved in the expression of gene activity in polytene chromosomes. *Chromosoma* **24,** (1968).

59. Lindquist, S. Regulation of protein synthesis during heat shock. *Nature* **293,** 311–314 (1981).

60. Yamamori, T., Ito, K., Nakamura, Y. & Yura, T. Transient regulation of protein synthesis in Escherichia coli upon shift-up of growth temperature. *J. Bacteriol.* **134,** 1133–40 (1978).

61. Lemaux, P. G., Herendeen, S. L., Bloch, P. L. & Neidhardt, F. C. Transient rates of synthesis of individual polypeptides in E. coli following temperature shifts. *Cell* **13,** 427–434 (1978).

62. Neidhardt, F. C., VanBogelen, R. A. & Vaughn, V. The genetics and regulation of heat-shock proteins. *Annu. Rev. Genet.* **18,** 295–329 (1984).

63. Lindquist, S. Heat shock--a comparison of Drosophila and yeast. *J. Embryol. Exp. Morphol.* **83 Suppl,** 147–61 (1984).

64. Li, G. C. & Werb, Z. Correlation between synthesis of heat shock proteins and development of thermotolerance in Chinese hamster fibroblasts. *Proc. Natl. Acad. Sci. U. S. A.* **79,** 3218–22 (1982).

65. Hronik-Tupaj, M., Rice, W. L., Cronin-Golomb, M., Kaplan, D. L. & Georgakoudi, I. Osteoblastic differentiation and stress response of human mesenchymal stem cells exposed to alternating current electric fields. *Biomed. Eng. Online* **10,** 9 (2011).

66. Afzal, E., Ebrahimi, M., Najafi, S. M. A., Daryadel, A. & Baharvand, H. Potential role of heat shock proteins in neural differentiation of murine embryonal carcinoma stem cells (P19). *Cell Biol. Int.* **35,** 713–20 (2011).

67. Kolch, W. Meaningful relationships : the regulation of the Ras/Raf/MEK/ERK pathway by protein interactions. *Biochem. J.* **351,** 289–305 (2000).

68. Jaiswal, R. K. *et al.* Adult Human Mesenchymal Stem Cell Differentiation to the Osteogenic or Adipogenic Lineage Is Regulated by Mitogen-activated Protein Kinase *. **275,** 9645–9652 (2000).

69. Honoré, E. The neuronal background K2P channels: focus on TREK1. *Nat. Rev. Neurosci.* **8,** 251–61 (2007).

70. Köttgen, M. *et al.* TRPP2 and TRPV4 form a polymodal sensory channel complex. *J. Cell Biol.* **182,** 437–47 (2008).

71. Clapham, D. E. TRP channels as cellular sensors. **426,** 517–524 (2003).

72. Benham, C. D., Gunthorpe, M. J. & Davis, J. B. TRPV channels as temperature sensors. *Cell Calcium* **33,** 479–487 (2003).

73. Xu, H. *et al.* TRPV3 is a calcium-permeable temperature-sensitive cation channel. *Nature* **418,** 181–6 (2002).

74. Peier, A. M. A Heat-Sensitive TRP Channel Expressed in Keratinocytes. *Science (80-.).* **296,** 2046–2049 (2002).

75. Smith, G. D. *et al.* TRPV3 is a temperature-sensitive vanilloid receptor-like protein. *Nature* **418,** 186–190 (2002).

76. Watanabe, H. *et al.* Heat-evoked activation of TRPV4 channels in a HEK293 cell expression system and in native mouse aorta endothelial cells. *J. Biol. Chem.* **277,** 47044–51 (2002).

77. Güler, A. D. *et al.* Heat-evoked activation of the ion channel, TRPV4. *J. Neurosci.* **22,** 6408–14 (2002).

78. Maingret, F. *et al.* TREK-1 is a heat-activated background K(+) channel. *EMBO J.* **19,** 2483–91 (2000).

79. McKemy, D. D., Neuhausser, W. M. & Julius, D. Identification of a cold receptor reveals a general role for TRP channels in thermosensation. *Nature* **416,** 52–8 (2002).

80. Muramatsu, S. *et al.* Functional gene screening system identified TRPV4 as a regulator of chondrogenic differentiation. *J. Biol. Chem.* **282,** 32158–67 (2007).

81. Rossi, F. *et al.* The endovanilloid/endocannabinoid system in human osteoclasts: possible involvement in bone formation and resorption. *Bone* **44,** 476–84 (2009).

82. Hughes, S., Dobson, J. & El Haj, A. J. Magnetic targeting of mechanosensors in bone cells for tissue engineering applications. *J. Biomech.* **40 Suppl 1,** S96–104 (2007).

83. Bromberg, Z., Goloubinoff, P., Saidi, Y. & Weiss, Y. G. The Membrane-Associated Transient Receptor Potential Vanilloid Channel Is the Central Heat Shock Receptor Controlling the Cellular Heat Shock Response in Epithelial Cells. *PLoS One* **8,** e57149 (2013).

84. Tartaj, P., Morales, M. a D. P., Veintemillas-Verdaguer, S., Gonz lez-Carre o, T. & Serna, C. J. The preparation of magnetic nanoparticles for applications in biomedicine. *J. Phys. D. Appl. Phys.* **36,** R182–R197 (2003).

85. Béalle, G. *et al.* Ultra magnetic liposomes for MR imaging, targeting, and hyperthermia. *Langmuir* **28,** 11834–42 (2012).

86. Krishnan, K. M. Biomedical Nanomagnetics: A Spin Through Possibilities in Imaging, Diagnostics, and Therapy. *IEEE Trans. Magn.* **46,** 2523–2558 (2010).

87. Jun, Y.-W., Seo, J.-W. & Cheon, J. Nanoscaling laws of magnetic nanoparticles and their applicabilities in biomedical sciences. *Acc. Chem. Res.* **41,** 179–89 (2008).

88. Rousseau, V., Denizot, B., Pouliquen, D., Jallet, P. & Le Jeune, J. J. Investigation of blood-brain barrier permeability to magnetite-dextran nanoparticles (MD3) after osmotic disruption in rats. *MAGMA* **5,** 213–22 (1997).

89. Rosensweig, R. E. Heating magnetic fluid with alternating magnetic field. *J. Magn. Magn. Mater.* **252,** 370–374 (2002).

90. Wang, X., Zhou, L., Ma, Y., Li, X. & Gu, H. Control of aggregate size of polyethyleneimine-coated magnetic nanoparticles for magnetofection. *Nano Res.* **2,** 365–372 (2010).

91. Kirschvink, J. L., Kobayashi-Kirschvink, A. & Woodford, B. J. Magnetite biomineralization in the human brain. *Proc. Natl. Acad. Sci. U. S. A.* **89,** 7683–7 (1992).

92. Coker, V. S. *et al.* Harnessing the extracellular bacterial production of nanoscale cobalt ferrite with exploitable magnetic properties. *ACS Nano* **3,** 1922–8 (2009).

93. Schüler, D. & Frankel, R. B. Bacterial magnetosomes: microbiology, biomineralization and biotechnological applications. *Appl. Microbiol. Biotechnol.* **52,** 464–73 (1999).

94. Blakemore, R. Magnetotactic bacteria. *Science* **190,** 377–9 (1975).

95. Bazylinski, D. A. & Frankel, R. B. Magnetosome formation in prokaryotes. *Nat. Rev. Microbiol.* **2,** 217–30 (2004).

96. Thomas-Keprta, K. L. *et al.* Elongated prismatic magnetite crystals in ALH84001 carbonate globules: potential Martian magnetofossils. *Geochim. Cosmochim. Acta* **64,** 4049–81

(2000).

97. Yoza, B., Arakaki, A., Maruyama, K., Takeyama, H. & Matsunaga, T. Fully automated DNA extraction from blood using magnetic particles modified with a hyperbranched polyamidoamine dendrimer. *J. Biosci. Bioeng.* **95,** 21–26 (2003).

98. Sode, K., Kudo, S., Sakaguchi, T., Nakamura, N. & Matsunaga, T. Application of bacterial magnetic particles for highly selective mRNA recovery system. *Biotechnol. Tech.* **7,** 688–694 (1993).

99. Matsunaga, T., Nakayama, H., Okochi, M. & Takeyama, H. Fluorescent detection of cyanobacterial DNA using bacterial magnetic particles on a MAG-microarray. *Biotechnol. Bioeng.* **73,** 400–5 (2001).

100. Tanaka, T. & Matsunaga, T. Fully automated chemiluminescence immunoassay of insulin using antibody-protein A-bacterial magnetic particle complexes. *Anal. Chem.* **72,** 3518–22 (2000).

101. Yoshino, T. *et al.* Assembly of G protein-coupled receptors onto nanosized bacterial magnetic particles using Mms16 as an anchor molecule. *Appl. Environ. Microbiol.* **70,** 2880–5 (2004).

102. I.A, B. Low frequency hyperthermia: Capacitive and ferromagnetic thermoseed methods. *Med. Phys. Monogr.* **16,** 82–111 (1988).

103. Hergt, R. & Dutz, S. Magnetic particle hyperthermia—biophysical limitations of a visionary tumour therapy. *J. Magn. Magn. Mater.* **311,** 187–192 (2007).

104. Hugounenq, P. *et al.* Iron Oxide Monocrystalline Nanoflowers for Highly Efficient Magnetic Hyperthermia. *J. Phys. Chem. C* **116,** 15702–15712 (2012).

105. Tung, L. D. *et al.* Magnetic properties of ultrafine cobalt ferrite particles. *J. Appl. Phys.* **93,** 7486 (2003).

106. Giri, J., Pradhan, P., Sriharsha, T. & Bahadur, D. Preparation and investigation of potentiality of different soft ferrites for hyperthermia applications. *J. Appl. Phys.* **97,** 10Q916 (2005).

107. Staniland, S. *et al.* Controlled cobalt doping of magnetosomes in vivo. *Nat. Nanotechnol.* **3,** 158–62 (2008).

108. Baldi, G. *et al.* Synthesis and coating of cobalt ferrite nanoparticles: a first step toward the obtainment of new magnetic nanocarriers. *Langmuir* **23,** 4026–8 (2007).

109. Byrne, J. M. *et al.* Controlled cobalt doping in biogenic magnetite nanoparticles. *J. R. Soc.*

Interface **10,** 20130314 (2013).

110. Byrne, J. M. *et al.* Biosynthesis of Zinc Substituted Magnetite Nanoparticles with Enhanced Magnetic Properties. *Adv. Funct. Mater.* **24,** 2518–2529 (2014).

111. Brown, W. F. Thermal Fluctuations of a Single-Domain Particle. *Phys. Rev.* **130,** 1677–1686 (1963).

112. Néel, L. Théorie du trainage magnétique des ferromagnétiques au grains fin avec applications aux terres cuites. *Ann. Géophys* **5,** 99–136 (1949).

113. Connolly, J. & St Pierre, T. G. Proposed biosensors based on time-dependent properties of magnetic fluids. *J. Magn. Magn. Mater.* **225,** 156–160 (2001).

114. Céspedes, E. *et al.* Bacterially synthesized ferrite nanoparticles for magnetic hyperthermia applications. *Nanoscale* **6,** 12958–70 (2014).

115. Kötitz, R., Weitschies, W., Trahms, L., Brewer, W. & Semmler, W. Determination of the binding reaction between avidin and biotin by relaxation measurements of magnetic nanoparticles. *J. Magn. Magn. Mater.* **194,** 62–68 (1999).

116. Kriz, C. B., Rådevik, K. & Kriz, D. Magnetic permeability measurements in bioanalysis and biosensors. *Anal. Chem.* **68,** 1966–70 (1996).

117. Hergt, R., Dutz, S. & Zeisberger, M. Validity limits of the Néel relaxation model of magnetic nanoparticles for hyperthermia. *Nanotechnology* **21,** 015706 (2010).

118. HEATH, J. C. The effect of cobalt on mitosis in tissue culture. *Exp. Cell Res.* **6,** 311–20 (1954).

119. Daniel, M., Dingle, J. T., Webb, M. & Heath, J. C. THE BIOLOGICAL ACTION OF COBALT AND OTHER METALS I. The effect of cobalt on the morphology and metabolism of rat fibroblasts in vitro. (1962).

120. Rae, T. The toxicity of metals used in orthopaedic prostheses. An experimental study using cultured human synovial fibroblasts. *J. Bone Joint Surg. Br.* **63-B,** 435–40 (1981).

121. Yang, H., Liu, C., Yang, D., Zhang, H. & Xi, Z. Comparative study of cytotoxicity, oxidative stress and genotoxicity induced by four typical nanomaterials: the role of particle size, shape and composition. *J. Appl. Toxicol.* **29,** 69–78 (2009).

122. Monteiro-Riviere, N. a, Inman, a O. & Zhang, L. W. Limitations and relative utility of screening assays to assess engineered nanoparticle toxicity in a human cell line. *Toxicol. Appl. Pharmacol.* **234,** 222–35 (2009).

123. Weaver, J. L. Estimation of cell viability by flow cytometry. *Methods Mol. Biol.* **91,** 77–83 (1998).

124. Suzuki, H., Toyooka, T. & Ibuki, Y. Simple and Easy Method to Evaluate Uptake Potential of Nanoparticles in Mammalian Cells Using a Flow Cytometric Light Scatter Analysis. *Environ. Sci. Technol.* **41,** 3018–3024 (2007).

125. Wolff, J. *The Law of Bone Remodelling*. (Springer-Verlag, 1986). at <http://www.springer.com/us/book/9783642710339>

126. Turner, C. H., Forwood, M. R. & Otter, M. W. Mechanotransduction in bone: do bone cells act as sensors of fluid flow? *FASEB J.* **8,** 875–8 (1994).

127. Wang, Y., McNamara, L. M., Schaffler, M. B. & Weinbaum, S. A model for the role of integrins in flow induced mechanotransduction in osteocytes. *Proc. Natl. Acad. Sci. U. S. A.* **104,** 15941–6 (2007).

128. Geiger, B., Bershadsky, A., Pankov, R. & Yamada, K. M. Transmembrane crosstalk between the extracellular matrix--cytoskeleton crosstalk. *Nat. Rev. Mol. Cell Biol.* **2,** 793–805 (2001).

129. Sniadecki, N. J. Minireview: A Tiny Touch: Activation of Cell Signaling Pathways with Magnetic Nanoparticles. *Endocrinology* **151,** 451–457 (2010).

130. Wang, N. & Ingber, D. E. Probing transmembrane mechanical coupling and cytomechanics using magnetic twisting cytometry. *Biochem. Cell Biol.* **73,** 327–35

131. Dobson, J. Remote control of cellular behaviour with magnetic nanoparticles. *Nat. Nanotechnol.* **3,** 139–43 (2008).

132. Pankhurst, Q. a, Connolly, J., Jones, S. K. & Dobson, J. Applications of magnetic nanoparticles in biomedicine. *J. Phys. D. Appl. Phys.* **36,** R167–R181 (2003).

133. Pommerenke, H. *et al.* Stimulation of integrin receptors using a magnetic drag force device induces an intracellular free calcium response. *Eur. J. Cell Biol.* **70,** 157–64 (1996).

134. Bausch, A. R., Möller, W. & Sackmann, E. Measurement of local viscoelasticity and forces in living cells by magnetic tweezers. *Biophys. J.* **76,** 573–9 (1999).

135. Kanczler, J. M. *et al.* Controlled differentiation of human bone marrow stromal cells using magnetic nanoparticle technology. *Tissue Eng. Part A* **16,** 3241–50 (2010).

136. Frank, O. *et al.* Real-time quantitative RT-PCR analysis of human bone marrow stromal cells during osteogenic differentiation in vitro. *J. Cell. Biochem.* **85,** 737–46 (2002).

137. Liedert, A., Kaspar, D., Blakytny, R., Claes, L. & Ignatius, A. Signal transduction pathways involved in mechanotransduction in bone cells. *Biochem. Biophys. Res. Commun.* **349,** 1–5 (2006).

138. Huang, H., Delikanli, S., Zeng, H., Ferkey, D. M. & Pralle, A. Remote control of ion channels and neurons through magnetic-field heating of nanoparticles. *Nat. Nanotechnol.* **5,** 602–6 (2010).

139. Stanley, S. A. *et al.* Radio-wave heating of iron oxide nanoparticles can regulate plasma glucose in mice. *Science* **336,** 604–8 (2012).

140. Huang, H., Delikanli, S., Zeng, H., Ferkey, D. M. & Pralle, A. Remote control of ion channels and neurons through magnetic-field heating of nanoparticles. *Nat Nano* **5,** 602–606 (2010).

141. Wimpenny, I., Markides, H. & El Haj, A. J. Orthopaedic applications of nanoparticle-based stem cell therapies. *Stem Cell Res. Ther.* **3,** 13 (2012).

142. Zhang, H., Kay, A., Forsyth, N. R., Liu, K.-K. & El Haj, A. J. Gene expression of single human mesenchymal stem cell in response to fluid shear. *J. Tissue Eng.* **3,** 2041731412451988 (2012).

143. D'Ippolito, G. *et al.* Marrow-isolated adult multilineage inducible (MIAMI) cells, a unique population of postnatal young and old human cells with extensive expansion and differentiation potential. *J. Cell Sci.* **117,** 2971–81 (2004).

144. Safi, M., Courtois, J., Seigneuret, M., Conjeaud, H. & Berret, J. The effects of aggregation and protein corona on the cellular internalization of iron oxide nanoparticles I – Introduction. 1–21 (2011).

145. Schweiger, C. *et al.* Quantification of the internalization patterns of superparamagnetic iron oxide nanoparticles with opposite charge. *J. Nanobiotechnology* **10,** 28 (2012).

146. Zhang, Y., Kohler, N. & Zhang, M. Surface modification of superparamagnetic magnetite nanoparticles and their intracellular uptake. *Biomaterials* **23,** 1553–1561 (2002).

147. Wang, Y. X., Hussain, S. M. & Krestin, G. P. Superparamagnetic iron oxide contrast agents: physicochemical characteristics and applications in MR imaging. *Eur. Radiol.* **11,** 2319–31 (2001).

148. DANIEL, M., DINGLE, J. T., WEEB, M. & HEATH, J. C. The biological action of cobalt and other metals. I. The effect of cobalt on the morphology and metabolism of rat fibroblasts in vitro. *Br. J. Exp. Pathol.* **44,** 163–76 (1963).

149. Borovanský, J. & Riley, P. A. Cytotoxicity of zinc in vitro. *Chem. Biol. Interact.* **69,** 279–91 (1989).

150. Gault, N. *et al.* Cobalt toxicity: chemical and radiological combined effects on HaCaT keratinocyte cell line. *Toxicol. In Vitro* **24,** 92–8 (2010).

151. Papageorgiou, I. *et al.* The effect of nano- and micron-sized particles of cobalt-chromium alloy on human fibroblasts in vitro. *Biomaterials* **28,** 2946–58 (2007).

152. Kwon, Y.-M. *et al.* Dose-dependent cytotoxicity of clinically relevant cobalt nanoparticles and ions on macrophages in vitro. *Biomed. Mater.* **4,** 025018 (2009).

153. Giri, J. *et al.* Synthesis and characterizations of water-based ferrofluids of substituted ferrites [Fe1−xBxFe2O4, B=Mn, Co (x=0–1)] for biomedical applications. *J. Magn. Magn. Mater.* **320,** 724–730 (2008).

154. Beji, Z. *et al.* Magnetic properties of Zn-substituted MnFe 2 O 4 nanoparticles synthesized in polyol as potential heating agents for hyperthermia. Evaluation of their toxicity on Endothelial cells. *Chem. Mater.* **22,** 5420–5429 (2010).

155. Kim, D.-H. *et al.* Cytotoxicity of ferrite particles by MTT and agar diffusion methods for hyperthermic application. *J. Magn. Magn. Mater.* **293,** 287–292 (2005).

156. Kostura, L., Kraitchman, D. L., Mackay, A. M., Pittenger, M. F. & Bulte, J. W. M. Feridex labeling of mesenchymal stem cells inhibits chondrogenesis but not adipogenesis or osteogenesis. *NMR Biomed.* **17,** 513–7 (2004).

157. Farrell, E. *et al.* Effects of iron oxide incorporation for long term cell tracking on MSC differentiation in vitro and in vivo. *Biochem. Biophys. Res. Commun.* **369,** 1076–81 (2008).

158. Arbab, A. S. *et al.* Labeling of cells with ferumoxides-protamine sulfate complexes does not inhibit function or differentiation capacity of hematopoietic or mesenchymal stem cells. *NMR Biomed.* **18,** 553–9 (2005).

159. Allen, M. J., Myer, B. J., Millett, P. J. & Rushton, N. The effects of particulate cobalt, chromium and cobalt-chromium alloy on human osteoblast-like cells in vitro. *J. Bone Joint Surg. Br.* **79,** 475–482 (1997).

160. Trounson, A., Thakar, R. G., Lomax, G. & Gibbons, D. Clinical trials for stem cell therapies. *BMC Med.* **9,** 52 (2011).

161. Mizuno, H., Tobita, M. & Uysal, A. C. Concise review: Adipose-derived stem cells as a novel tool for future regenerative medicine. *Stem Cells* **30,** 804–10 (2012).

162. Steinert, A. F., Rackwitz, L., Gilbert, F., Nöth, U. & Tuan, R. S. Concise review: the

clinical application of mesenchymal stem cells for musculoskeletal regeneration: current status and perspectives. *Stem Cells Transl. Med.* **1,** 237–47 (2012).

163. Wu, S. M. & Hochedlinger, K. Harnessing the potential of induced pluripotent stem cells for regenerative medicine. *Nat. Cell Biol.* **13,** 497–505 (2011).

164. Byrne, J. M. *et al.* Control of nanoparticle size, reactivity and magnetic properties during the bioproduction of magnetite by Geobacter sulfurreducens. *Nanotechnology* **22,** 455709 (2011).

165. Di Corato, R. *et al.* Magnetic hyperthermia efficiency in the cellular environment for different nanoparticle designs. *Biomaterials* **35,** 6400–11 (2014).

166. Jeun, M., Kim, Y. J., Park, K. H., Paek, S. H. & Bae, S. Physical contribution of Néel and Brown relaxation to interpreting intracellular hyperthermia characteristics using superparamagnetic nanofluids. *J. Nanosci. Nanotechnol.* **13,** 5719–25 (2013).

167. Lévy, M., Gazeau, F., Bacri, J.-C., Wilhelm, C. & Devaud, M. Modeling magnetic nanoparticle dipole-dipole interactions inside living cells. *Phys. Rev. B* **84,** 075480 (2011).

168. Connolly, J. & Pierre, T. G. S. Proposed biosensors based on time-dependent properties of magnetic # uids. **225,** 156–160 (2001).

169. Gutiérrez, L. *et al.* Ac magnetic susceptibility study of in vivo nanoparticle biodistribution. *J. Phys. D. Appl. Phys.* **44,** 255002 (2011).

170. Soukup, D., Moise, S., Céspedes, E., Dobson, J. & Telling, N. D. In Situ Measurement of Magnetization Relaxation of Internalized Nanoparticles in Live Cells. *ACS Nano* (2015). doi:10.1021/nn503888j

171. Breuer, W., Epsztejn, S., Millgram, P. & Cabantchik, I. Z. Transport of iron and other transition metals into cells as revealed by a fluorescent probe. *Am J Physiol Cell Physiol* **268,** C1354–1361 (1995).

172. Krause, U., Seckinger, A. & Gregory, C. A. Assays of osteogenic differentiation by cultured human mesenchymal stem cells. *Methods Mol. Biol.* **698,** 215–30 (2011).

173. Campelj, S., Makovec, D. & Drofenik, M. Preparation and properties of water-based magnetic fluids. *J. Phys. Condens. Matter* **20,** 204101 (2008).

174. Teeguarden, J. G., Hinderliter, P. M., Orr, G., Thrall, B. D. & Pounds, J. G. Particokinetics in vitro: dosimetry considerations for in vitro nanoparticle toxicity assessments. *Toxicol. Sci.* **95,** 300–12 (2007).

175. Albanese, A. & Chan, W. C. W. Effect of gold nanoparticle aggregation on cell uptake and

toxicity. *ACS Nano* **5,** 5478–89 (2011).

176. Mudunkotuwa, I. A., Rupasinghe, T., Wu, C.-M. & Grassian, V. H. Dissolution of ZnO nanoparticles at circumneutral pH: a study of size effects in the presence and absence of citric acid. *Langmuir* **28,** 396–403 (2012).

177. Collier, C. G., Pearce, M. J., Hodgson, A. & Ball, A. Factors affecting the in vitro dissolution of cobalt oxide. *Environ. Health Perspect.* **97,** 109–13 (1992).

178. Davisson, T., Kunig, S., Chen, A., Sah, R. & Ratcliffe, A. Static and dynamic compression modulate matrix metabolism in tissue engineered cartilage. *J. Orthop. Res.* **20,** 842–8 (2002).

179. Altman, G. H. *et al.* Cell differentiation by mechanical stress. *FASEB J.* **16,** 270–2 (2002).

180. Suzuki, S. *et al.* Geranylgeranylacetone ameliorates ischemic acute renal failure via induction of Hsp70. *Kidney Int* **67,** 2210–2220 (2005).

181. Stolzing, A., Sethe, S. & Scutt, A. M. Issues in Development Stressed Stem Cells : Temperature Response in Aged Mesenchymal Stem Cells. *Stem Cells Dev.* **15,** 478–487 (2006).

182. Birmingham, E. *et al.* Osteogenic differentiation of mesenchymal stem cells is regulated by osteocyte and osteoblast cells in a simplified bone niche. *Eur. Cells Mater.* **23,** 13–27 (2012).

183. Luo, X. H., Liao, E. Y. & Zhou, H. D. [Differentiation and gene expression of human osteosarcoma cell line MG-63]. *Hunan Yi Ke Da Xue Xue Bao* **26,** 107–10 (2001).

184. Jordan, A., Scholz, R., Wust, P. & Fähling, H. Magnetic fluid hyperthermia (MFH): Cancer treatment with AC magnetic field induced excitation of biocompatible superparamagnetic nanoparticles. *J. Magn. Magn. Mater.* **201,** 413–419 (1999).

185. Johannsen, M. *et al.* Clinical hyperthermia of prostate cancer using magnetic nanoparticles: Presentation of a new interstitial technique. *Int. J. Hyperth.* **21,** 637–647 (2005).

186. Lo, C. M., Keese, C. R. & Giaever, I. Impedance analysis of MDCK cells measured by electric cell-substrate impedance sensing. *Biophys. J.* **69,** 2800–7 (1995).

187. Angstmann, M., Brinkmann, I., Bieback, K., Breitkreutz, D. & Maercker, C. Monitoring human mesenchymal stromal cell differentiation by electrochemical impedance sensing. *Cytotherapy* **13,** 1074–89 (2011).

188. Bagnaninchi, P. O. & Drummond, N. Real-time label-free monitoring of adipose-derived stem cell differentiation with electric cell-substrate impedance sensing. *Proc. Natl. Acad.*

Sci. U. S. A. **108,** 6462–7 (2011).

189. Hofmann, U., Michaelis, S., Winckler, T., Wegener, J. & Feller, K.-H. A whole-cell biosensor as in vitro alternative to skin irritation tests. *Biosens. Bioelectron.* **39,** 156–62 (2013).

190. Mouras. Label-free assessment of adipose-derived stem cell differentiation using coherent anti-Stokes Raman scattering and multiphoton microscopy. (2012).

191. Park, H. E. *et al.* Real-time monitoring of neural differentiation of human mesenchymal stem cells by electric cell-substrate impedance sensing. *J. Biomed. Biotechnol.* **2011,** 485173 (2011).

192. Applied Biophysics. at <http://www.biophysics.com/ecis-theory.php>

193. Applied Biophysics. at <http://www.biophysics.com/cultureware.php>

194. Lukic, S. & Wegener, J. Impedimetric Monitoring of Cell-Based Assays. *eLS* 1–8 (2015). at <http://www.els.net/WileyCDA/ElsArticle/refId-a0025710.html>

195. Treuel, L., Jiang, X. & Nienhaus, G. U. New views on cellular uptake and trafficking of manufactured nanoparticles. *J. R. Soc. Interface* **10,** 20120939 (2013).

196. Fortin, J.-P. *et al.* Size-sorted anionic iron oxide nanomagnets as colloidal mediators for magnetic hyperthermia. *J. Am. Chem. Soc.* **129,** 2628–35 (2007).

197. Hermanson, G. T. *Bioconjugate Techniques*. (Academic Press, 2013). at <https://books.google.com/books?id=6aO-207lhdgC&pgis=1>

198. Kobayashi, T. Cancer hyperthermia using magnetic nanoparticles. *Biotechnol. J.* **6,** 1342–7 (2011).

199. Urtizberea, A., Natividad, E., Arizaga, A., Castro, M. & Mediano, A. Specific Absorption Rates and Magnetic Properties of Ferrofluids with Interaction Effects at Low Concentrations. *J. Phys. Chem. C* **114,** 4916–4922 (2010).

200. Tan, R. P., Carrey, J. & Respaud, M. Magnetic hyperthermia properties of nanoparticles inside lysosomes using kinetic Monte Carlo simulations: Influence of key parameters and dipolar interactions, and evidence for strong spatial variation of heating power. *Phys. Rev. B* **90,** 214421 (2014).

201. Hughes, S., McBain, S., Dobson, J. & El Haj, A. J. Selective activation of mechanosensitive ion channels using magnetic particles. *J. R. Soc. Interface* **5,** 855–63 (2008).

202. Goodman, R. *et al.* Extremely low frequency electromagnetic fields activate the ERK

cascade, increase hsp70 protein levels and promote regeneration in Planaria. *Int. J. Radiat. Biol*. **85,** 851–9 (2009).

203. Dominici, M. *et al.* Minimal criteria for defining multipotent mesenchymal stromal cells. The International Society for Cellular Therapy position statement. *Cytotherapy* **8,** 315–7 (2006).

APPENDIX

Characterization of primary bone marrow-derived human mesenchymal stem cells (hMSCs)

The International Society of Cellular Therapy defined hMSCs based on the following three criteria: firstly, human MSCs must be able to adhere to plastic surface under standard tissue culture conditions; secondly, human MSCs must express certain markers, including CD73, CD90, and CD105, and lack the expression of markers, such as CD45, CD34, CD14, CD79 alpha, or CD19 and HLA-DR surface molecules; and, finally, the cells must be capable for differentiation into osteoblasts, chondroblasts, and adipocytes under appropriate *in vitro* conditions.[203]

hMSCs used in this study were adherence selected from bone-marrow aspirates after 14 days in culture. Fluorescent micrographs of hMSCs stained CD14, CD19, CD31, CD 34, CD45, CD73, CD90, CD105, HLA – DR, IgG1, IgG2a is shown in Fig A1. The nuclei stained with DAPI appear blue. The cells stained positive only for MSC markers CD 73, 90 and 105 whilst not staining for hematopoietic markers including CD14 (expressed on monocytes and macrophages), CD19 (marker of B cells), CD31, CD 34 (specific for primitive hematopoietic progenitors and endothelial cells), CD45 (pan-leukocyte marker), HLA – DR (should not be expressed on hMSCs unless stimulated by IFN-γ), or the isotype control antibodies including IgG1, IgG2a. This was also confirmed via flow cytometry (Fig A2, A3). Population of cells negatively stained for the markers showed very low fluorescence intensity (in the FL2 channel for assessing red fluorescence; Fig A2 d, e; A3). On the other hand, for the MSC markers, cells show high fluorescence intensity and the entire population is shifted to higher values (Fig A2 a-c).

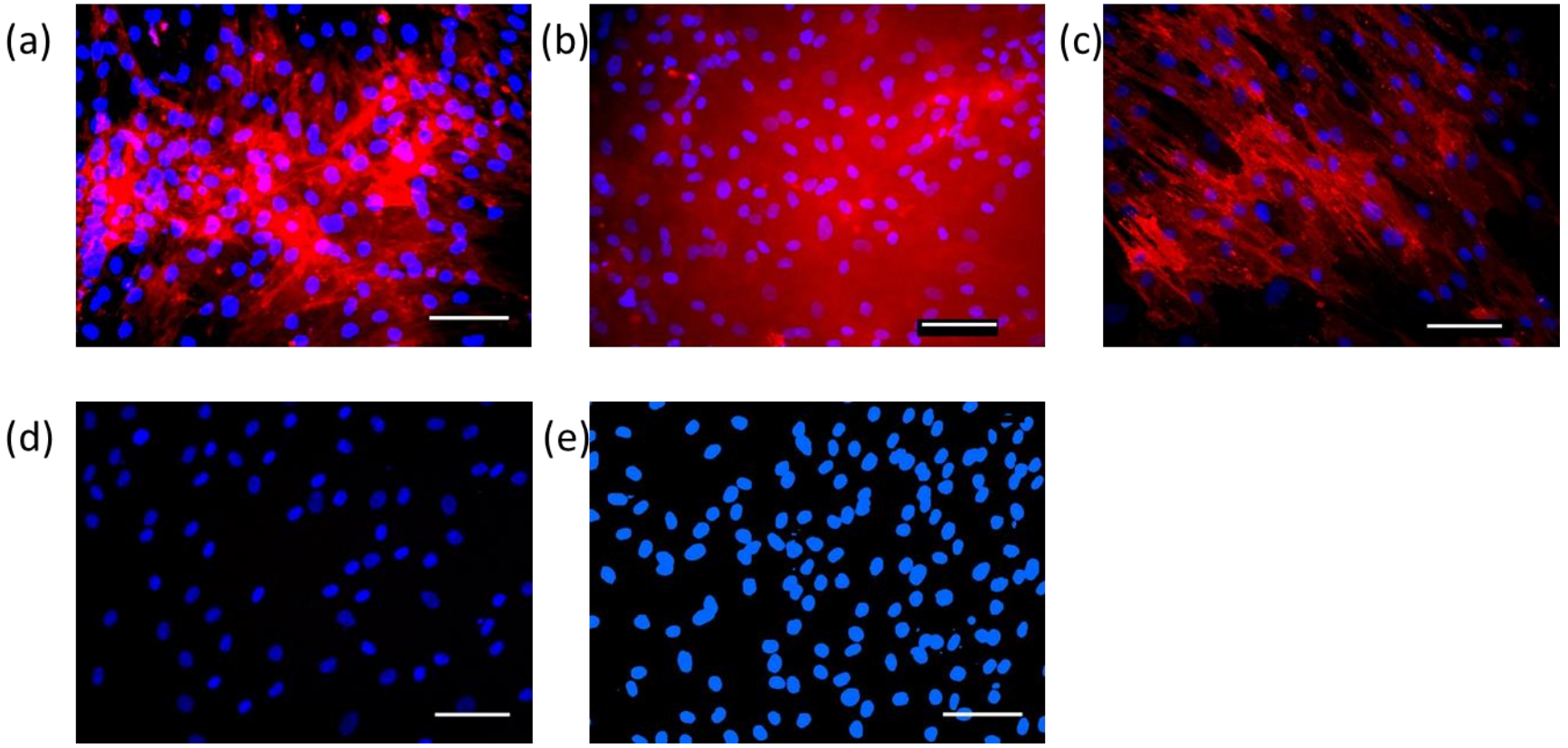

Fig A1: hMSC staining for CD markers: Fluorescent micrographs of hMSC stained for the nuclei with DAPI and for CD markers CD73 (a), CD90 (b), CD105 (c), mixture of IgG1 and IgG2a (d) and a mixture of CD14, CD19, CD31, CD34, CD45and HLA-DR (e).(Scale bars correspond to 100µm)

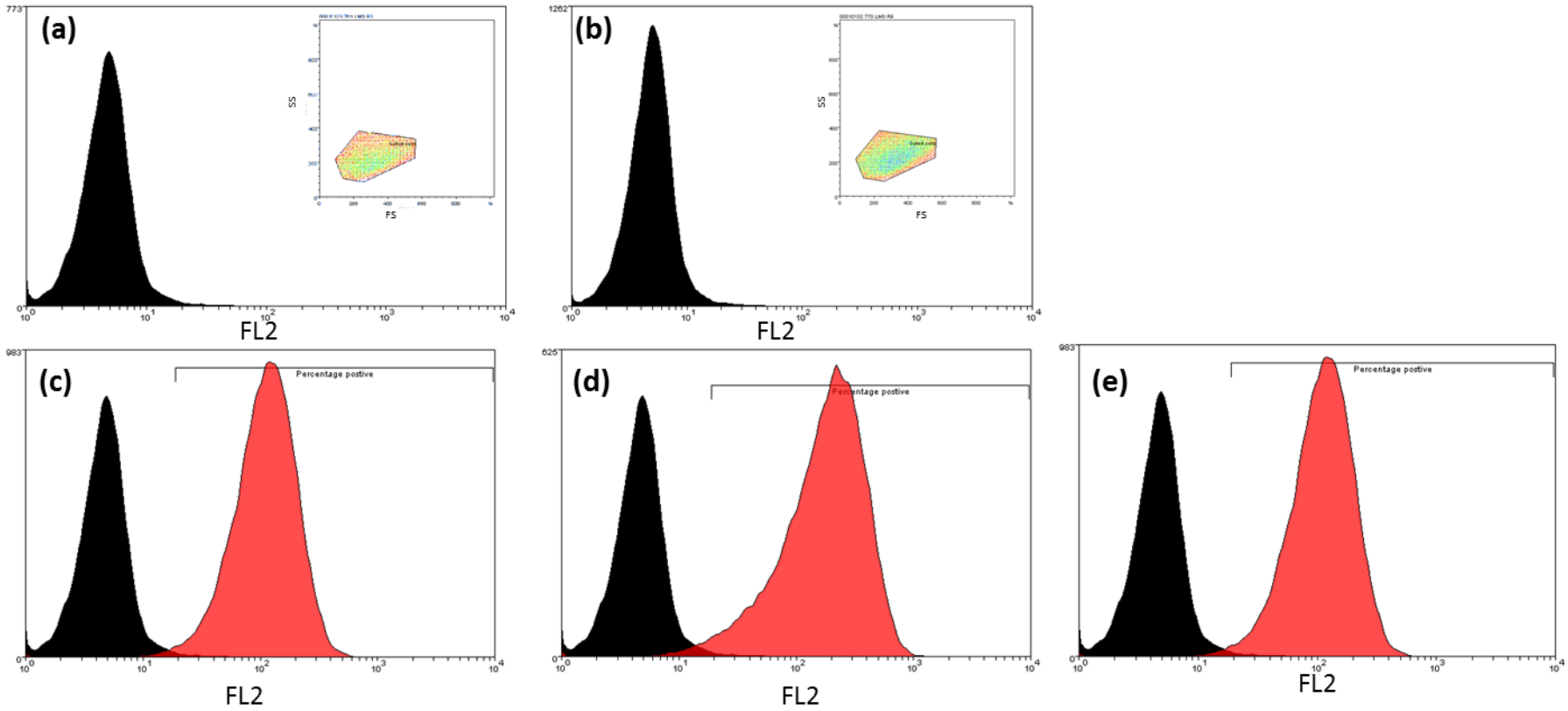

Fig A2: Quantification of CD marker expression in hMSCs: Flow cytometry data showing the intensity of fluorescence for the fluorophore tagged isotypes IgG1, IgG2a (b) (a) and hMSC markers, CD73 (c), CD90 (d), CD105 (e). While the isotype controls show very low intensity of staining (shaded black) the cells stained for the hMSCs markers show a strong fluorescence (shaded red) indicating positive staining. [Inset shows the gating of the population in forward (FS) vs side scatter (SS) plots for the isotype controls] (Re-printed with permission from J.C. Price)

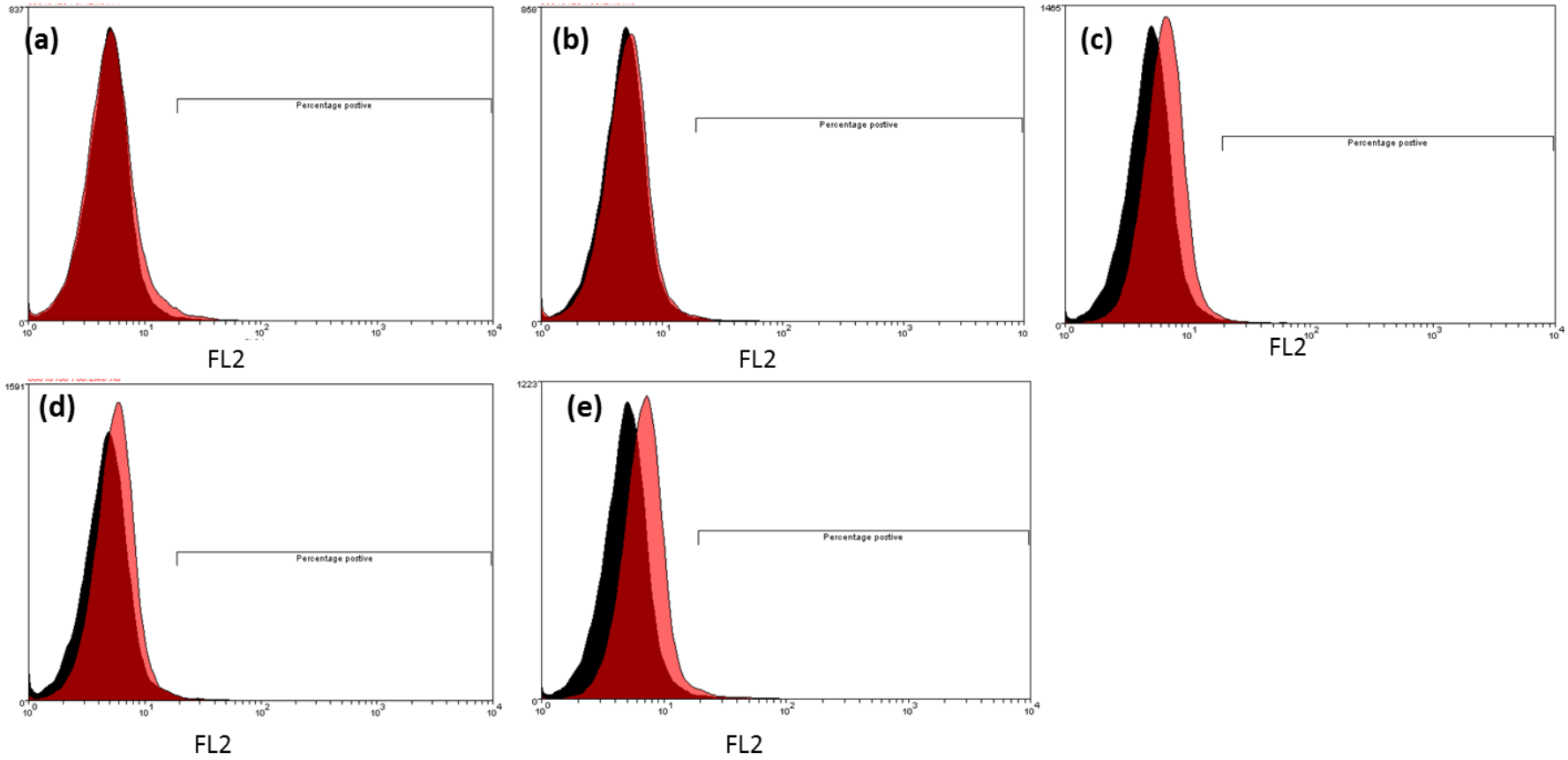

Fig A3: Quantification of CD marker expression in hMSCs: Flow cytometry data showing the low intensity of fluorescence indicating negative staining for CD markers (shaded pink) CD14(a), CD34 (b), CD45 (c), CD19 (d) and HLA-DR (e) overlapping with the isotype controls (shaded black) the fluorophore tagged isotypes and CD markers. (Re-printed with permission from J.C. Price)

The cells were also tested for their multilineage differentiation potential by culturing them for 21 days in relevant differentiation media (Fig A4). Cells grown only in osteogenic medium showed staining only for calcium (Alizarin red; Fig A4 d) and not for chondrogenesis (Alcian blue; Fig A4 e) or adipogenesis (Oil red ‘O’; Fig A4 f). Similar results were observed for cells in chondrogenic medium (only stained for sulphated glycosaminoglycans with Alcian blue for cells grown only in chondrogenic medium; Fig A4 h) and in adipogenic medium (only stained for lipid droplets with oil red ‘O’ for cells grown only in adipogenic medium; Fig A4 c). Cells grown in expansion medium did not stain for any of the dyes indicating cells had not differentiated without stimulation (Fig A4 j-l). These results confirm that the cells obtained from the bone-marrow aspirate were hMSCs.

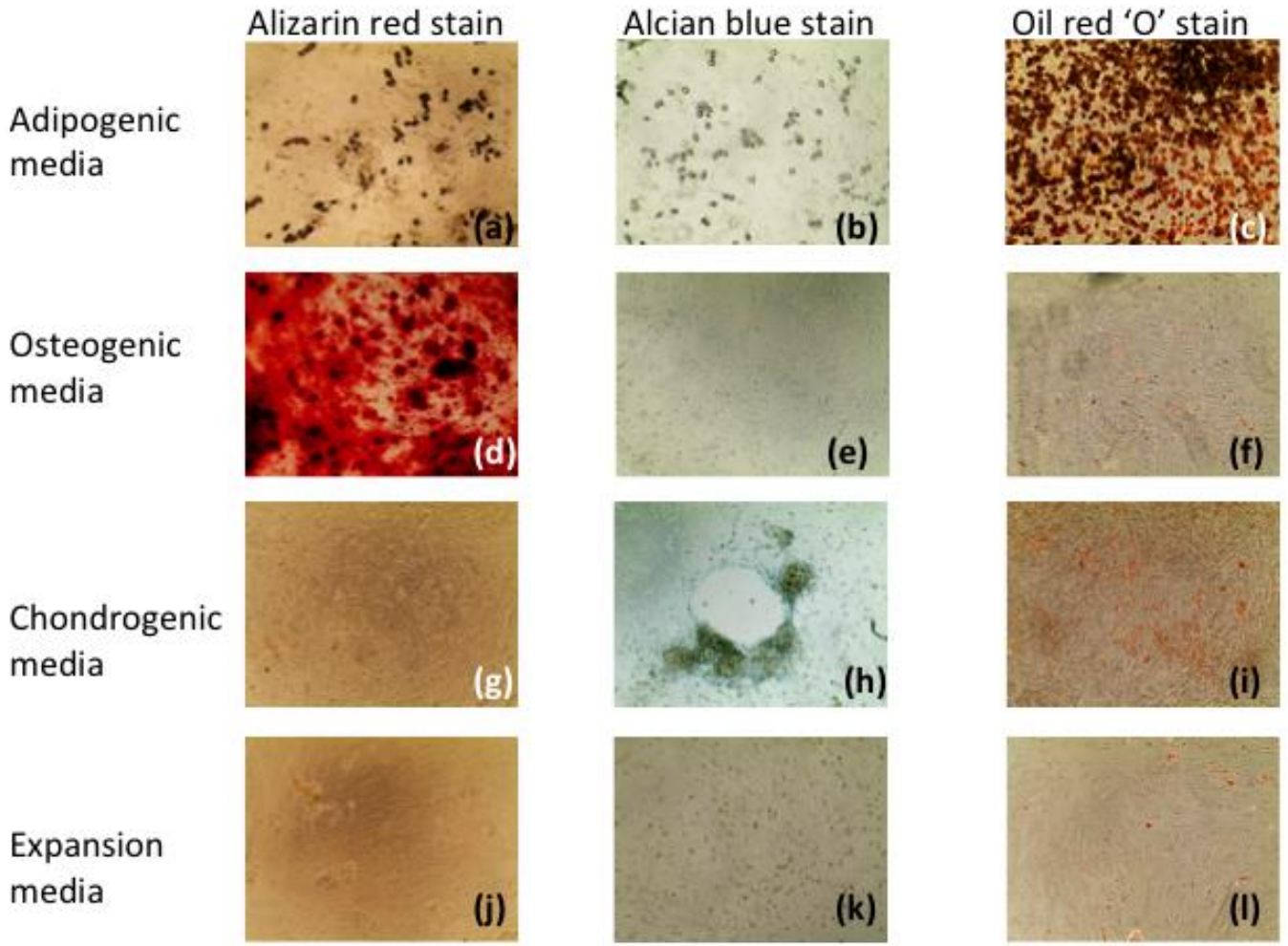

Fig A4 Multilineage potential of hMSCs: hMSCs stained for Alizarin red, Alcian blue and oil red 'O' after 21 days of culture in expansion, osteogenic, chondrogenic and adipogenic media. *(Re-printed with permission from J.C. Price)*